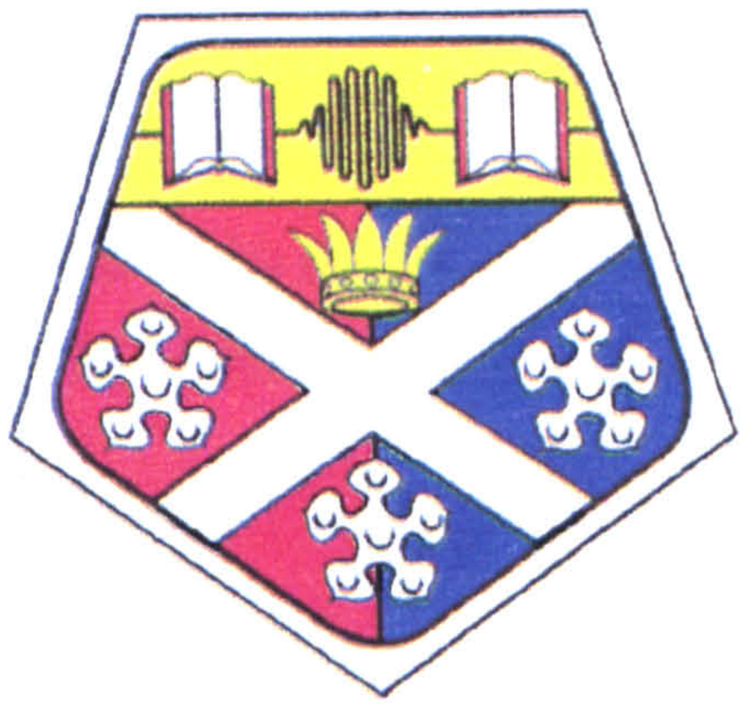

UNIVERSITY OF STRATHCLYDE

Department of Chemical and Process Engineering

"The Condensation of Hydrocarbons in a Vertical Reflux Condenser Tube"

Alan Bartleman

PhD

Declaration

This thesis, "The Condensation of Hydrocarbons in a Vertical Reflux Condenser Tube", is submitted for the award of the degree of Doctor of Philosophy in Chemical and Process Engineering from the University of Strathclyde.

A Bartleman

Acknowledgements

I wish to express my gratitude to the following individuals and organisations:

My Industrial Supervisor Mr Jim M McNaught, and my Academic Supervisor Prof. Colin D Grant, for their support and encouragement during this research.

The technical staff at the National Engineering Laboratory (NEL) who assisted during the project.

The Heat Transfer and Fluid Flow Service (HTFS), for providing me with the opportunity to work on this research project.

The Postgraduate Training Partnership (PTP) scheme for affording me with the opportunity to participate in the scheme, especially Mr Jim T R Watson, PTP Co-ordinator at NEL.

The UK's Department of Trade and Industry (DTI), the Engineering & Physical Sciences Research Council (EPSRC), and NEL for providing funding.

A Bartleman

Abstract

A new test facility, with a vertical reflux condenser of 1500mm overall length and 45mm internal diameter, has been commissioned and tested and methods developed for measuring key process parameters. An experimental study of reflux condensation in a single tube using n-pentane and iso-octane and binary mixtures of these single component hydrocarbons has been undertaken.

Using water as the cooling medium, a correlation was developed for determining the coolant-side heat transfer coefficient in the reflux condenser based on the Wilson plot method. The composition of binary liquid mixture samples from the test facility was determined using an empirical correlation developed using density measurements from a vibrating u-tube densitometer.

The single components were condensed in the range 32.0-48.4°C and 0.106-1.515bara by adjusting the test condenser heat load for fixed conditions on the coolant side to investigate how the condensate-film heat transfer coefficient varied with the condensate film Reynolds number. The results show good agreement with the method recommended by HTFS for correcting the Nusselt theory for the effects of waves. A further small correction was made to improve the fit to the data.

The binary hydrocarbon mixtures were condensed across the range 65.9-90.1°C and 0.729-1.531bara by conducting similar experiments where the feed vapour contained 50% and 70% n-pentane. Composition measurements of the condensate and vapour leaving the test condenser were made to examine the separation of components during partial reflux condensation. The results suggest that this separation is influenced by heat flux and that it would be improved if the test condenser were

operated at a lower heat flux. Further experimental work is needed to verify this, and to investigate how this influences the number of thermodynamic stages, which was found to be less than one with the conditions reported here.

Analysis of the heat transfer resistances on the vapour side showed that the standard procedure of using a dry-gas heat transfer coefficient, with or without a mass transfer correction term based on the film theory, poorly predicted the experimental values. These predictions were improved by the use of an enhancement factor, which may be more relevant in counter-current than co-current condensing situations. The results indicate that use of a dry-gas heat transfer coefficient with the film theory correction factor, over-predicts the mass transfer resistance.

Comparison was made between the data and predictions based on the integral condensation curve, as might be used in Silver's method for condenser thermal design. It was shown that this method poorly predicted the surface area and the separation achieved in the test condenser. The results indicate that the heat and mass transfer coefficients obtained in a plain tube are significantly higher than those based on using a dry-gas heat transfer coefficient corrected by film theory. Implications for the design of reflux condensers have been presented.

Contents

List of Nomenclature

Upper Case Symbols

A Heat Transfer Surface Area (m^2).

C Constant defined by (3.316) (-).

Cp Specific heat capacity (J/kg°C).

$\tilde{C}p$ Molar specific heat capacity (J/kmol°C).

D Diffusion coefficient (m^2/s).

F_e Enhancement factor (-)

I_e Electrical current (amperes).

K Numerical constant (-).

K' Constant defined by (5.2.13) ($W/m^2°C$).

$\tilde{K}$ Equilibrium constant (moles/mole).

K_v Vapour Kutateladze number (-).

L Length (m).

M Mass (kg).

$\dot{M}$ Mass flow rate (kg/s).

$\tilde{M}$ Molecular weight (kg/kmol).

$\dot{N}$ Molar flow rate (kmols/s).

N_r Number of turns in a coil (-).

Nu Nusselt number (-).

P Pressure (bar).

Pr Prandtl number (-).

$\dot{Q}$ Rate of heat transfer (W).

R Reflux ratio (-).

R_e Electrical resistance (ohms).

Re Reynolds number (-).

S Cross-sectional Area (m^2).

T Temperature (°C).

$\overline{T}$ Mean temperature (°C).

U Local overall heat transfer coefficient ($W/m^2°C$).

$\overline{U}$ Mean overall heat transfer coefficient ($W/m^2°C$).

V Volume (m^3).

$\dot{V}$ Volumetric flow rate (m^3/s).

V_e Electrical voltage (volts).

Y Constant defined by (5.2.7) ($m^2°C/W$).

Z Ratio of vapour sensible heat flux to total heat flux (-).

Lower Case Symbols

a Constant defined by (5.1.4a) (-).

b Constant defined by (5.1.4b) (-).

c Elasticity constant (kg/s^2).

$\tilde{c}$ Molar concentration (moles/mole).

d Tube diameter (m).

f Function (-).

f Frequency (Hz).

g Gradient of line ($m^2°C/W$).

g_n Acceleration due to gravity (m/s^2).

h Channel height (m).

Δh_v Specific latent heat of vapourisation (J/kg).

m Mass (kg).

$\dot{m}$ Mass flux (kg/m^2s).

n Numerical value (-).

$\dot{n}$ Molar flux (mol/m^{2}s).

p Perimeter (m).

$\dot{q}$ Heat flux (W/m^2).

s Coil pitch (m^{-1}).

t Period of vibration (s).

$\dot{u}$ Velocity (m/s).

$\dot{v}$ Flooding velocity (m/s).

w Channel width (m).

x Thickness (m).

x_v Quality or vapour mass flow fraction (kg/kg).

$\dot{x}$ Liquid mass fraction (kg/kg).

$\tilde{x}$ Liquid mole fraction (moles/mole).

y Distance (m).

$\dot{y}$ Vapour mass fraction (kg/kg).

$\tilde{y}$ Vapour mole fraction (moles/mole).

$\tilde{y}^*$ Equilibrium vapour mole fraction (moles/mole).

z Vertical distance (m).

$\tilde{z}$ Ratio of vapour condensing molar flux to total condensing molar flux (-).

Greek Symbols

α Local film heat transfer coefficient (W/m^2°C).

α' Combined local film heat transfer coefficient for condensate-film (W/m^2°C).

$\overline{\alpha}$ Mean film heat transfer coefficient (W/m^2°C).

α^* Corrected film heat transfer coefficient (W/m^2°C).

β Mass transfer coefficient (m/s).

Γ Condensate mass flow rate per unit tube periphery (kg/ms).

δ Film thickness (m).

Δ Difference operator (-).

ε Number of thermodynamic stages (-).

ν Kinematic viscosity (m^2/s).

ρ Density (kg/m^3).

σ Surface tension (N/m).

η Dynamic viscosity (Ns/m^2).

θ Mass transfer correction term defined by (3.4.4) (-).

λ Thermal conductivity (W/m°C).

τ Shear stress (N/m^2).

ϕ Rate factor for heat transfer defined by (3.4.5) (-).

Sub-scripts

a Air.

A Ackermann correction factor.

b Bulk.

c Coolant.

cs Condensing side.

DC Dump condenser.

eff Effective.

eh Equivalent hydraulic.

f Condensate film.

flow Flow channel.

hc Hydrocarbon.

heat Heated.

H_2O	Water (purified).
HTFS	Calculated by the method of HTFS.
i	Inner.
in	Inlet.
I	Interface.
l	Liquid.
L	Latent heat.
mean	Mean.
mix	Mixture.
o	Outer.
out	Outlet.
O	Iso-octane.
P	n-Pentane.
s	Sensible cooling.
sb	Sensible cooling of bulk mixture.
sc	Sub-cooled.
scf	Sensible cooling of condensing flux.
T	Total.
TC	Test condenser.
TS	Test section.
v	Vapour.
v1	First vapour component in mixture.
v2	Second vapour component in mixture.
w	Tube wall.
z	Vertical position.
ρ	Densitometer.

List of Figures

List of Tables

1.0 Introduction

This chapter describes the background to the research work carried out and documented in this thesis. Introductions to the Heat Transfer and Fluid Flow Service (HTFS) and the Postgraduate Training Partnership (PTP) scheme are given, followed by the reasons for undertaking this research and an outline of the main objectives of the work. The chapter ends by outlining the remainder of the thesis.

1.1 Background to the Research Work

The Heat Transfer and Fluid Flow Service (HTFS) was established in 1968 to advance the science and practice of heat transfer engineering. It is an association of users, designers and manufacturers of heat exchangers, which has now gained the reputation for being a source of advanced technology throughout the world. HTFS is now a major international heat transfer research and software business.

HTFS has a number of guiding principles:

- Research is essential both to validate HTFS methods but also to understand fully the processes and mechanisms in heat transfer equipment.

- The close relationship between HTFS and its Member companies provides a valued additional resource of guidance and expertise to ensure the relevance of the work.

- Heat transfer is a broad subject, which should not be confined to one type of exchanger or transfer process. HTFS has therefore concerned itself with fired heaters and compact exchangers as well as the trusty shell-and-tube exchangers.

- HTFS must be at the forefront of science and engineering and hence not just content to follow trends as they develop.

- HTFS researchers and developers must be recognised leaders in their field and must be given their head to drive the subject forward.

The HTFS research philosophy has always been to study the basics in order to develop understanding and hence produce prediction models and software. These models are then tested in combination with other models and with overall performance tests.

This research project was initiated by HTFS who sought funding from the UK's Department of Trade and Industry (DTI). It was decided that the project be run through the Postgraduate Training Partnership (PTP) scheme. The DTI and the Engineering & Physical Sciences Research Council (EPSRC) introduced the PTP schemes in 1992.

The PTP scheme involved a PTP Associate undertaking a research project for a PhD degree by carrying out practical work in a Research & Technology Organisation (RTO) in partnership with a Higher Education Institute (HEI). Each partnership involves a single RTO with a single HEI at which the PTP Associate was registered for a PhD.

An important feature of the scheme was that the PTP Associate spent much of their time in the RTO rather than in the HEI. The commercial environment of the RTO was designed to accelerate progress towards research goals and help the Associate to adapt more rapidly to work in an industrial environment.

The PTP scheme aimed to increase the industrial relevance of PhD training, and to create a mechanism to produce high quality postgraduate researchers whose training had included elements of practical technology transfer and management skills. The structured business training meant that the PTP Associate received a good grounding in the core competencies for an industrial career, and was commercially aware with knowledge of exploitable technologies and techniques.

The author was registered for a PhD at the University of Strathclyde, Glasgow between 1996 and 1999, and was based at the National Engineering Laboratory (NEL), East Kilbride, working as a PTP Research Associate during this time.

1.2 Justification for the Research Work

Effective use of heat exchangers is vital to the success of the UK's power and process industries, which contribute significantly to the UK's Gross Domestic Product (GDP). The achievement of these industries is interdependent with the success of the UK contract engineering industry, which remains strong although facing stiffer competition with US, Far Eastern and European contractors.

The unit operations of heat and mass transfer are usually treated separately in a process plant. However, by operating a condenser in the reflux mode, condensation and fractionation can take place together with possible substantial energy and

equipment savings. Despite this, the area is still one of considerable technical difficulty, where very little experimental data and no reliable design procedures are available.

As industry is unable to benefit from these possible savings, HTFS plans to develop thermal design technology to handle condensation with reflux, to meet the anticipated increase in the use of combined heat and mass transfer devices. At present, some basic obstacles to the application of HTFS design technology to reflux condensers exist:

- The absence of a computational model that takes into account the effects of liquid-phase and gas-phase resistances in limiting the separation achieved.

- There are no data available for use in developing and testing models.

- Flooding velocity predictions, which have been derived from data taken often under artificial, usually adiabatic, conditions, have not been properly validated in condensing conditions.

A research programme was therefore required to develop a new thermal design technology in this area, that extends the existing HTFS design methods in the area of combined heat and mass transfer processes, and produces the results in a form that can and will be taken up by industry.

1.3 Objectives of the Research Work

The objective of the author's research project was to initiate development of HTFS thermal design technology for partial reflux condensation by:

- Commissioning a new research facility for the experimental work, the main components of which were an electrically heated evaporator, a single tube test section and an after condenser.

- Carry out experimental work, firstly using two single component hydrocarbons, and then binary mixtures of these hydrocarbons to gather test data on the heat and mass transfer aspects of the process.

- Analyse this test data to provide information on the heat and mass transfer aspects of the process, which could then be validated by further experimental work in the facility, perhaps using different test fluids.

There were several factors to consider when choosing the fluids to be used in this new facility, although the author was not involved in this process. From the point of view of data analysis, it was important that the properties and the vapour/liquid equilibrium of both liquids were well known. It was also important that the properties were sufficiently different so that they could be used as a means of measuring composition.

From the point of view of operation, it was required that one of the components had a normal boiling point in the range 35-50°C, and that the other had a normal boiling

point in the range 80-120°C. This ensured that the liquids were capable of operating within the upper limits of the test facility. Furthermore, it was necessary that the liquids were not unacceptably dangerous, and that they were miscible in one another. The two single component hydrocarbons chosen were n-pentane and iso-octane (2,2,4 trimethylpentane), and various properties for these liquids are provided in Appendix A1 at the end of this thesis.

Commissioning the new Reflux Condensation Facility at NEL involved calibrating some of the instrumentation used and ensuring that the measurement systems functioned as intended. Owing to the unique nature of the test condenser outer surface geometry, it was necessary to carry out work to determine a suitable expression for accurately evaluating the coolant-side heat transfer coefficient.

An on-line sampling system was designed, installed and commissioned, which was used to withdraw and analyse liquid samples in order to determine the composition of the exit streams from the test condenser. Some laboratory and off-line analysis work was carried out to derive a reliable correlation that related the composition of these samples to some suitable measurement.

Initial test work was carried out using single component hydrocarbon fluids. The purpose of these tests was to provide a benchmark for later test work using the binary hydrocarbon mixtures. In addition to this, these tests were used to verify the measurement systems, correct any further technical difficulties, and to develop the data analysis systems.

The main area of research was test work using binary hydrocarbon mixtures. As well as the heat transfer measurements, it was hoped to obtain additional information

about the mass transfer processes from the composition measurements of the exit vapour and condensate streams from the test condenser.

All test data were used to determine the heat transfer coefficients on the condensing side of the test condenser. Also, the change in composition of the vapour stream during test work with the binary hydrocarbon mixtures was measured. These measurements formed the basis for the discussions and conclusions contained in this thesis.

1.4 Layout of the Thesis

In Chapter 2, the condensation process is defined and a description of the ways in which condensation may occur is given. A discussion on the basics of condenser design follows this, and is concluded by an introduction to the methods available for the thermal design of industrial condensers.

The reflux condensation process is described in Chapter 3, as is the design of reflux condensers. The shortcomings of previous studies on condensation are highlighted with respect to condensation with reflux, and the implications of these to the thermal design methods presently employed for condensers discussed.

A description of the new research facility, the instrumentation and the method of operating are contained in Chapter 4. The methods used to carry out the data analysis are also presented in this chapter.

Following on from this, Chapter 5 contains the results of the main areas of the research work. Firstly, findings from the work carried out to investigate the measurement of composition are presented. Secondly, work carried out to accurately measure the coolant-side heat transfer coefficient in the test condenser is described. The results of test work with single component hydrocarbons and then with binary hydrocarbon mixtures conclude this chapter.

The conclusions of this research work along with the recommendations for future work are given in Chapter 6. The References are then followed by a series of appendices that contain additional material relevant to the main body of the thesis, test data and data analysis calculations. These appendices are referred to at the appropriate points of the thesis.

2.0 Condensation and Condenser Design

This chapter defines and describes the condensation process and the mechanisms by which condensation occurs. The remainder of the chapter provides an outline of the basic features of condenser design, and an introduction to the methods for condenser thermal design.

2.1 Definition of the Condensation Process

Condensation is the change from vapour to liquid. This change can occur when vapour comes into contact with a surface or fluid at a temperature below the saturation temperature of the vapour. In some circumstances, the vapour condenses straight away, in others the vapour cools down first before it condenses.

During condensation, molecules change state by passing from the vapour to the liquid state. This is accompanied by a release of energy, known as the latent heat of condensation. Therefore condensation is both a heat transfer and a mass transfer process.

Condensation can occur by two distinct modes, filmwise and dropwise, as shown in Figure 2.1 [p.10]. As the vapour is condensed, small drops of liquid begin to appear on the cold surface in contact with the vapour. As the condensation continues, the number of drops increases until they completely cover the surface. The condensate drops join to form a continuous sheet of liquid that flows with the properties of a liquid film. This is known as filmwise condensation.

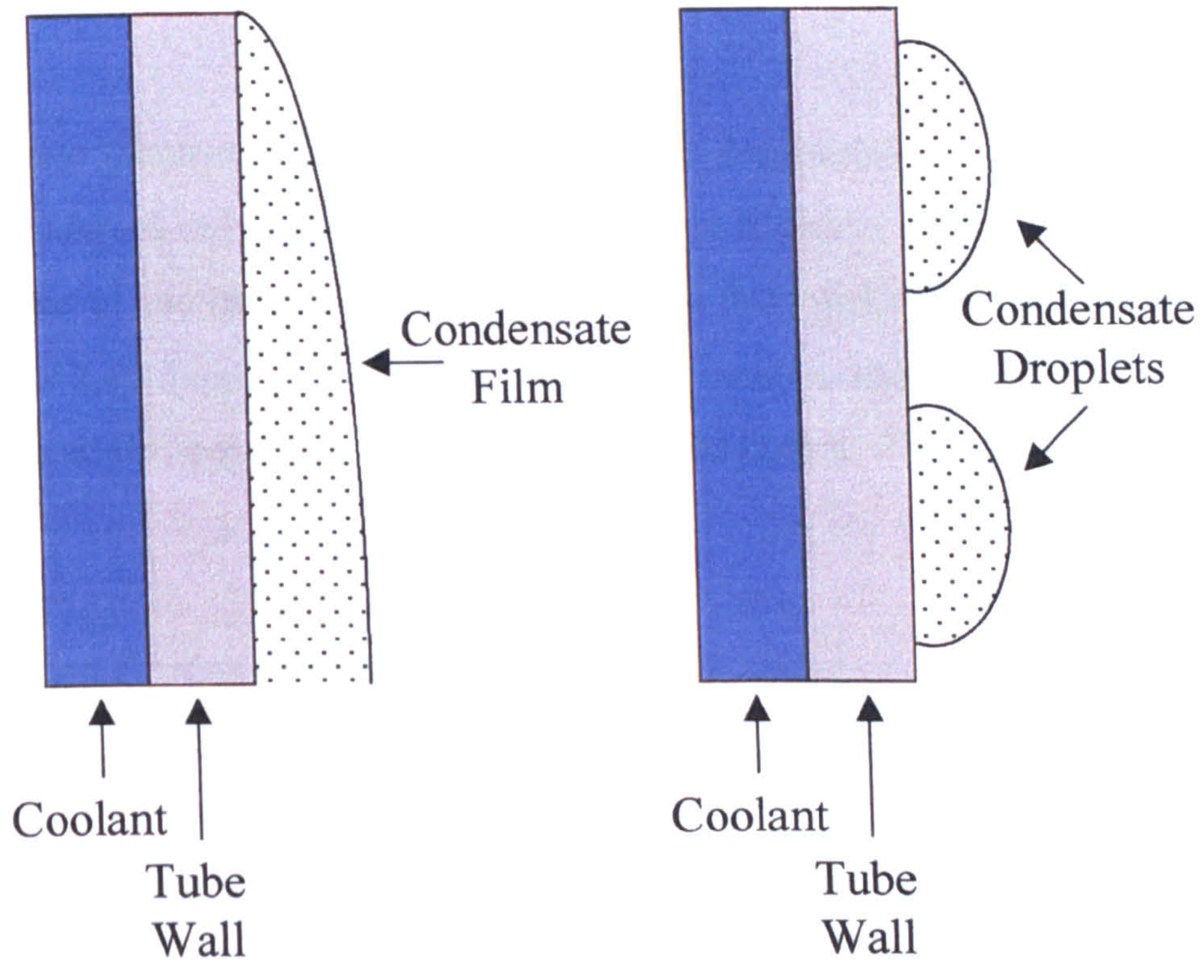

Figure 2.1. The filmwise and dropwise modes of condensation.

In dropwise condensation, the condensate exists as patches of liquid on the surface where it forms. As with filmwise condensation, the condensate that forms exists as droplets. Although these droplets may grow in size as condensation proceeds, they do not join together. This method of condensation may be sustained by coating the surface on which the condensate forms, or by doping the vapour with additives to promote the dropwise mechanism. However it is extremely difficult to maintain this mode of condensation in industrial condensers.

As no steps were taken to sustain the formation of droplets, it was assumed that condensation occurred only by the filmwise mode. In addition, it was assumed that the entire surface of the test condenser remained free from dirt and thus suitable for the formation of a continuous liquid film. Dropwise condensation was therefore not considered beyond this point, and will not be discussed further.

2.2 Condensation Process for a Single Component Vapour

A single component vapour in contact with a flat, solid surface whose temperature is maintained below that of the vapour will condense, and assuming filmwise condensation, the condensate produced will form a film of liquid on the solid surface.

The pressure difference between the bulk vapour and the condensate on the surface of the solid means that the condensing vapour molecules are transported by molecular diffusion to the vapour-liquid interface. Vapour molecules are also transported to the vapour-liquid interface by convective motion of the vapour itself. The vapour-liquid interface represents a resistance to the condensation process.

At this interface, the vapour molecules pass into the liquid phase by releasing their latent heat. At the same time, liquid molecules absorb this latent heat to evaporate and pass back across the interface. Under equilibrium conditions, the rates of arrival and departure of vapour and liquid molecules would be exactly equal. However, during condensation, the rate of arrival is much greater than the rate of departure and hence a liquid film is produced and maintained.

The liquid phase itself also represents some resistance to the condensation process, and this resistance is much greater than that represented by the vapour-liquid interface. Therefore, the resistance due to the condensate film is taken to be the controlling resistance during condensation of a single component vapour.

As well as a difference in pressure between the bulk vapour and the condensate surface, there is also a temperature difference. This difference is so small that it is often ignored. Condensation of a single component vapour is therefore regarded as taking place at constant temperature, and this temperature is known as the pure vapour saturation temperature.

For condensation to continue to form on the surface of any existing liquid film, a temperature difference must exist between the vapour-liquid interface and the condensate film. The condensate film is therefore regarded as being sub-cooled below the saturation temperature corresponding to the pressure of the system. This process is illustrated in Figure 2.2 [p.13].

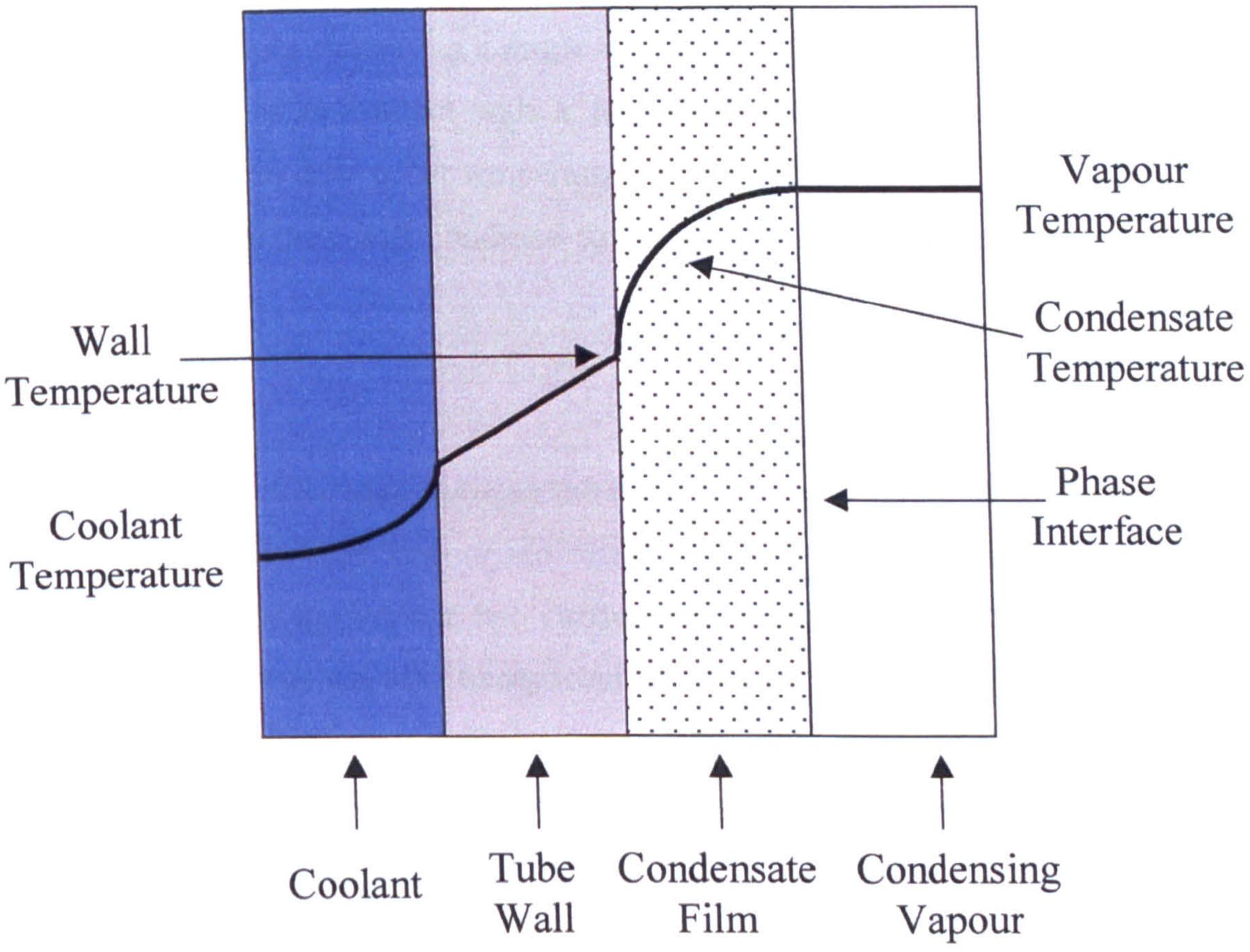

Figure 2.2. The single component condensation process.

2.3 Condensation Process for a Vapour Mixture

A mixture of vapours can mean several things: a mixture containing a vapour and a noncondensable gas, a mixture of two condensable vapours, or a mixture of more than two vapours, which might include noncondensable gases.

Consider first a mixture containing a single component vapour and a noncondensable gas. This mixture is in contact with a flat, solid surface whose temperature is maintained below the dew point temperature of the mixture. Assuming filmwise condensation, the mixture will condense to form a thin layer of condensate on the surface.

The partial pressure difference between the bulk vapour-gas mixture and the vapour-liquid interface means that vapour molecules diffuse towards the interface. The convective motion of the vapour also carries vapour molecules to the interface. In addition, gas molecules are also transported towards the interface as a result of the pressure difference. However, as the gas molecules are noncondensable, the vapour-liquid interface is impermeable to them and they accumulate next to the interface. This is illustrated in Figure 2.3 [p.15].

This accumulation of noncondensable molecules adjacent to the interface creates an additional resistance to the condensing vapour molecules. This layer of noncondensable gas is often referred to as the diffusion layer, as vapour molecules must diffuse through it to reach the vapour-liquid interface. This resistance is greater than that presented by the liquid condensate film, and so is taken to be the controlling resistance during the condensation of vapour mixtures.

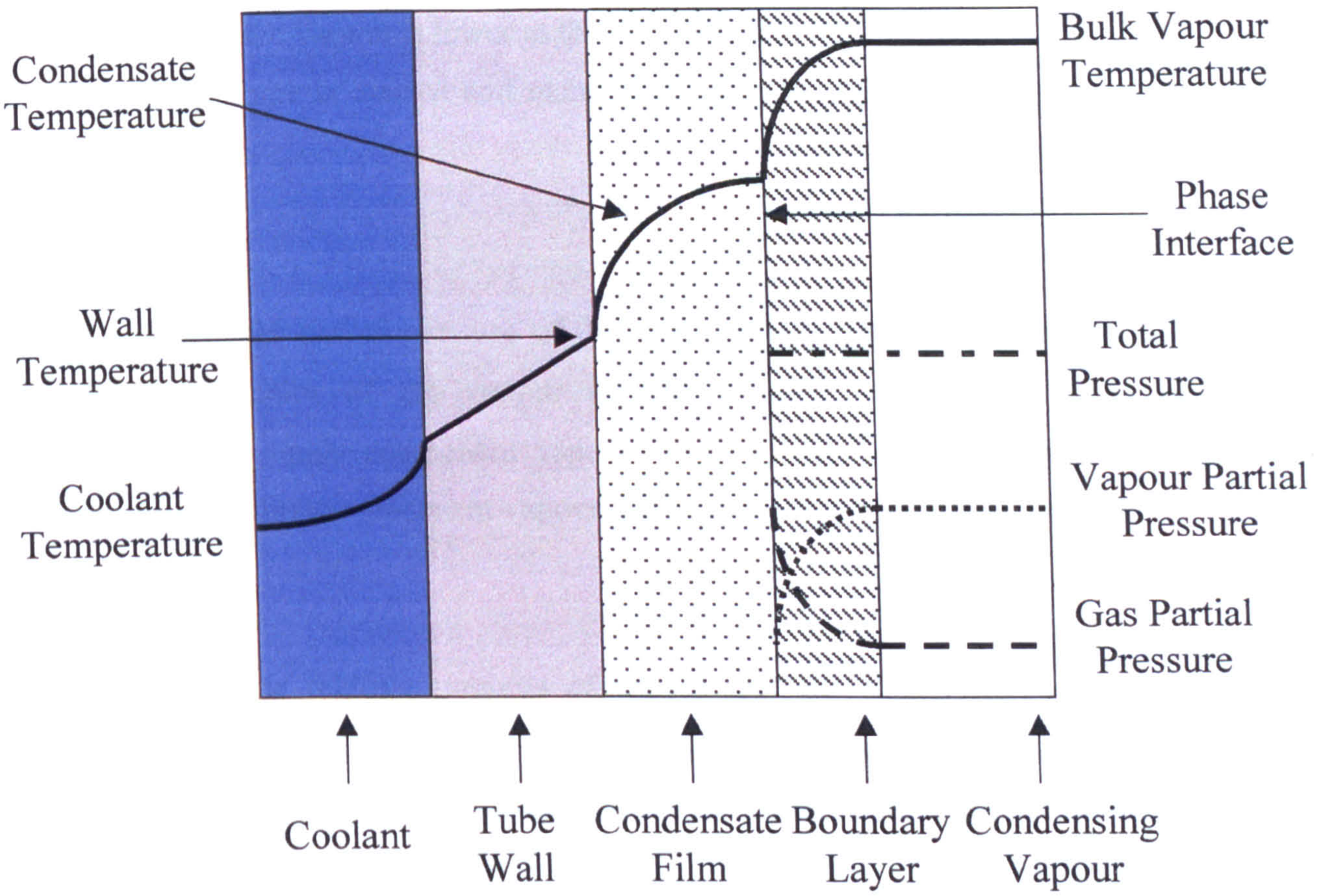

Figure 2.3. The multicomponent condensation process.

The accumulation of gas molecules means that the partial pressure of the gas is higher in the diffusion layer than in the bulk vapour-gas mixture. This produces a driving force for gas diffusion back into the bulk of the mixture, which is balanced by the diffusion of the vapour-gas mixture towards the diffusion layer.

Similarly, the molecular diffusion of vapour towards the interface means that the partial pressure of the vapour is lower at the interface than in the bulk of the mixture, and so a driving force is created and maintained. The total pressure of the system remains constant.

The reduction in the partial pressure of the vapour at the interface means that the saturation temperature of the vapour is also reduced. Compared with the condensation of a single component vapour, the temperature driving force during condensation of a single component vapour and a noncondensable gas is lower.

Furthermore, as the relative amounts of vapour and gas change throughout the condenser, the partial pressure of the vapour at the interface and hence the saturation temperature change throughout. As the vapour condenses, the number of molecules decreases and so its partial pressure is subsequently reduced. It follows therefore, that the dew point temperature decreases as condensation occurs.

Now consider a mixture containing two condensable vapours, a light (low boiling point) component and a heavy (high boiling point) component. This mixture is in contact with a flat, solid surface whose temperature is maintained below the dew point temperature of the mixture. Assuming filmwise condensation, the mixture will condense to form a thin layer of condensate on the surface.

Unlike the situation for the single vapour and noncondensable gas, both components are capable of being condensed but do so at different rates. In general, the heavy component condenses preferentially while the light component accumulates at the interface. A diffusion layer, made up of the light component, exists adjacent to the vapour-liquid interface, and the heavy component must diffuse through this layer to reach the interface.

The accumulation of light component molecules means that the partial pressure of the light component is higher in the diffusion layer than in the bulk vapour mixture. This produces a driving force for diffusion back into the bulk of the mixture, which is balanced by the diffusion of the vapour mixture towards the diffusion layer.

Similarly, the molecular diffusion of heavy component molecules towards the interface means that the partial pressure of the heavy component is lower at the interface than in the bulk of the mixture, and so a driving force is created and maintained. The total pressure of the system remains constant.

As the heavy component condenses, the number of molecules decreases and so its partial pressure is subsequently reduced. It follows therefore, that the dew point temperature decreases as condensation occurs.

2.4 Basic Design of Condensers

The aim in designing any heat exchanger is to transfer heat from one fluid to another within the allowable pressure drops of the two fluids, and without risking the plant or the safety of the plant operators. The design must be capable of withstanding both the process conditions and those of its surrounding environment, and should be

maintainable during its expected operational life. In addition to all of these, the design must be economical.

With condensers, this transfer of heat is accompanied by vapour changing to liquid, and the condensation can be total or partial depending on the process requirements. It is normal for the condensing and coolant streams to be kept separate, the heat being transferred through a surface upon which the liquid condensate will form. However, some occasions exist when both streams are brought into direct contact to produce condensation.

The first stage in the design process is to fully specify the design problem. Information on the operating conditions and any initial details of the condenser must be given. This includes details on the flow rates, compositions, inlet temperatures and pressures, corrosiveness, and fouling characteristics of the process streams as well as any likely fluctuations in all of these. The required heat duty and the maximum allowable pressure drops must also be specified. Information on the overall size, weight, materials, costs and alternative condenser types plus information on the flow arrangement, surface characteristics and allocation of process streams to sides of the condenser should be included.

Once the design problem has been fully specified, a thermal and hydraulic design is attempted, followed by a mechanical design. The thermal and hydraulic design calculations estimate the heat transfer and pressure drops involved in the condensation. The thermophysical properties of the process streams and of the condenser materials have to be known to perform these calculations, as well as surface heat transfer and fluid friction characteristics, and all geometrical parameters of the condenser. The mechanical design of the condenser is where the structural, thermal and vibration analyses are performed. The operating temperatures, pressures

and stream velocities must be known, along with the corrosiveness and fouling characteristics of these streams.

The condenser design has to meet a number of basic requirements to ensure that the thermal performance is not inhibited. The thermal performance of the condenser must be achieved, and the allowable pressure drops in both streams should be fully utilised. Noncondensable gases have to be removed through suitable vents to avoid gas blanketing, and the condensate produced drained from the exchanger, thus maintaining the same available heat transfer surface area. The removal of noncondensable gases must be achieved despite the reduction in vapour volumetric flow rate and subsequent changes in the vapour velocity.

When the thermal and mechanical designs are complete, it is likely that several condenser designs will have been produced. At this stage, serious consideration is given to the manufacturing and cost of each of these designs, and trade-off factors are employed to establish which design is the optimum. It is here that the real art of design comes into play. As well as making decisions based on the results of the calculations, some decisions will have to be made based on experience or understanding of the condensation process, or of the physical design. The design process is therefore based on quantitative and qualitative decisions.

2.5 Condenser Thermal Design Methods

The vapour stream entering the condenser might be a single component vapour, a binary mixture of vapours, a vapour and a noncondensable gas, or a multicomponent mixture of vapours, which may or may not contain noncondensable gases. The complexity of the situation increases as the number of components within the vapour

phase increases, and becomes further complicated if there are noncondensables present.

The simplest design would be for condensing a single component vapour, but industrial condensers rarely handle single component vapours. It is more likely to be a mixture of vapours, possibly containing noncondensable gases. The purpose of the condenser might be to partially condense the vapour mixture to recover one of the components, or to reduce or remove the amount of noncondensable gas present.

The two most commonly used methods for the thermal design of condensers are the film-theory and the equilibrium (or approximate) methods and they are outlined briefly below.

2.5.1 The Film-theory Method

This is the most physically realistic model of the condensation process that has been incorporated into a design procedure used in industry. The method assumes that there is a thin, laminar film next to the phase interface. Within this film, concentration, temperature and pressure gradients exist, and all changes in these occur in this film. Outside the film, the concentration, temperature and pressure are assumed to be at the conditions of the bulk mixture.

The emphasis in this approach is on the heat and mass transfer in the vapour phase. Mass is transferred through this film by molecular diffusion and convective transport. Heat and mass transfer rates are evaluated through the use of heat transfer coefficients and heat and mass transfer analogies. The effect of mass transfer on heat transfer is taken into account.

2.5.2 The Equilibrium Method

In this method, the mass transfer resistance is estimated using the resistance to the sensible heat transfer in the vapour phase. This means that there is no need for mass diffusivity data. It is also assumed that the condensing vapour and condensate are in local equilibrium at every point in the condenser, so therefore, the condensation process is assumed to follow a pre-determined equilibrium condensation curve. The method has been improved to allow for the effect of mass transfer during condensation.

3.0 Reflux Condensation and Reflux Condensers

This chapter deals with the reflux condensation process and the design features of reflux condensers.

A description of the heat and mass transfer processes that take place during reflux condensation is provided to give the reader an appreciation for the subject area. The available subject literature has been reviewed to present the existing knowledge for reflux condensation, and to highlight the areas where the understanding of the processes involved is limited.

The basic design features of the reflux condenser are also outlined in this chapter, examining the advantages and disadvantages for this type of condenser. The applications for reflux condensers in the chemical and process industries are briefly discussed.

A detailed review of the methods used for industrial condenser thermal design is included in this chapter, with attention focused on how these methods might be applied to the design of a reflux condenser.

3.1 The Reflux Condensation Process

A diagram showing the basic features of the reflux condensation process is given in Figure 3.1 [p.23].

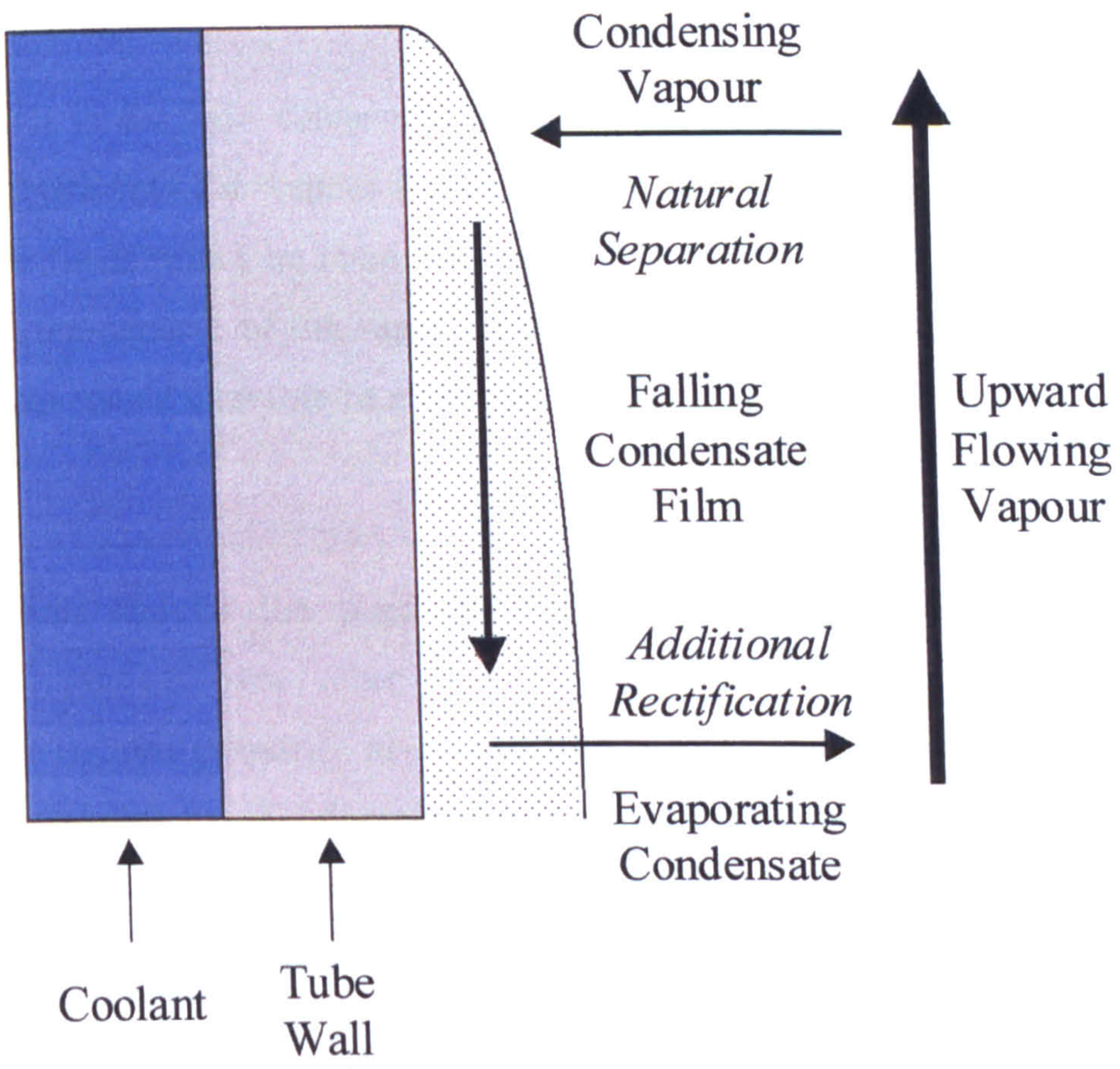

Figure 3.1. The reflux condensation process.

The process is characterised by the current-current flow of the condensing vapour and liquid condensate streams. In reflux condensation, the hot vapour mixture flows upward and the condensate flows (or drains) downward under the influence of gravity. It is this unique feature that gives rise to the difficulties in describing both the heat and mass transfer processes taking place. Normally, the vapour mixture would be on the tube-side and the coolant on the shell-side.

This can result in the light component in the condensate phase being re-vaporised and passing back into the vapour stream. The condensate that drains out of the bottom of the tubes would be more concentrated in the heavy component, and will approach the temperature of the vapour entering the tubes. The vapour leaving the top of the tubes would therefore be more concentrated in the light component.

This separation can be the major advantage offered by utilising the reflux condensation process over other types of condensation process. Although condensation is seen primarily as a heat transfer process, the process of reflux condensation is mass transfer dominated. Thus, the operation of a reflux condenser would be improved if it were operated under those conditions that are most favourable for the transfer of mass across a phase boundary.

Mass transfer from a condensing vapour is improved if the rates of heat transfer in the condenser are low. This can be explained by examining the equation used to describe mass transfer in condensing systems.

$$\dot{n}_P = \beta\left(\tilde{y}_{P,b} - \tilde{y}_{P,I}\right) + \dot{n}_T \tilde{y}_{P,b} \qquad (3.1.1)$$

The first term on the right-hand side of (3.1.1) represents the transfer of mass by diffusion, which results from the concentration gradient between the bulk of the mixture and that at the interface. The second term represents the transfer of mass due to convective motion of the condensing vapour toward the interface.

At high rates of heat transfer, the convective term in (3.1.1) will dominate the mass transfer process, as the motion of the vapour will sweep the molecules towards the interface at high velocities. This means that the concentrations of the condensing molecules in the bulk and at the interface are virtually identical, and hence a small concentration gradient exists. Therefore, the diffusive term in (3.1.1) becomes very small in comparison to the convective term.

At low rates of heat transfer, the convective term is much smaller as the vapour travels much slower at low rates of heat transfer. In this case, the concentrations of the condensing molecules in the bulk and at the interface are very different, and hence a large concentration gradient exists. Thus, the diffusive term in (3.1.1) becomes dominant, and the concentration gradient means that a separation of the components in the vapour mixture can occur.

An important feature of the reflux condensation process is mass transfer in the liquid film, the behaviour of which is characterised in one of two ways, either as a well mixed film or an unmixed film. A film of condensate on a vertical condensing surface will initially be unmixed but as it flows downward it will become more mixed due to the increased flow rate and turbulence in the film. In a reflux condenser, this effect is likely to be exaggerated by the fact that as the film reaches the bottom of the tube, the flow rate of vapour is higher, and hence more likely to produce surface turbulence on the film. This will in turn be expected to promote good liquid mixing within the film.

The mass transfer of components within the condensate film will depend upon which of these models is assumed for the film behaviour. If the film is described as being well mixed, all of the condensate formed on the surface is in contact with all of the condensing vapour and is involved in continuous mass transfer between the phases. Thus it is possible to enhance the mass transfer caused by the condensation of some of the vapour. If the film is unmixed, only the freshly formed condensate is assumed to be in contact with the bulk vapour. Hence the potential for mass transfer is reduced and the separation achievable with an unmixed film is smaller than with a mixed film. A well mixed condensate film corresponds to a very high liquid-side mass transfer coefficient, and hence a low resistance to mass transfer. This is important in aiding the rectification effect, caused by re-evaporation of the more volatile component back across the phase interface.

The major drawback to reflux condensation concerns the stability of the vapour and condensate phases flowing counter-currently to one another. Under certain conditions, the upward flow of vapour may prevent condensate drainage, and the condensate will either be held up within the tubes, or will be carried upwards and out of the condenser by the vapour.

Flooding is a complicated physical phenomenon, which has received a great deal of attention in the open literature on two-phase flow. However, it is still a poorly understood subject with regard to reflux condensation, and is therefore a major obstacle to the application of reflux condensers in the modern chemical processing industries. Most studies on flooding have been carried out either under adiabatic conditions, or where the test section geometries do not accurately reflect the geometry of industrial reflux condensers. It is unclear whether the results from such work can be applied to reflux condensing situations with any real accuracy.

3.2 The Reflux Condenser

Reflux, or knock-back condensers, sometimes known as dephlegmators, have been used in the chemical and process industries for the control of chemical reactors or for separating the components in a vapour mixture. Reflux condensers can also be used as air-cooled heat exchangers. The principles have also been applied to the design of emergency core cooling systems in nuclear reactors, but this is beyond the scope of this particular study.

The most common configuration for a reflux condenser is the vertical shell-and-tube exchanger. In this arrangement, the vapour flows upwards inside the tubes and condenses on the tube walls, while the coolant stream flows on the shell-side. The condensate drains downward under the influence of gravity, counter-current to the rising vapour. Any noncondensable gas present is carried up and out of the exchanger by the rising vapour. A typical reflux condenser is shown in Figure 3.2 [p.28].

Other common arrangements for reflux condensers are for the condensation to take place inside the inclined surface of a shell-and-tube heat exchanger, inside the vertical passages of a plate-fin heat exchanger, outside a helical coil bundle, or through the vertically orientated passages of a spiral heat exchanger. Horizontal shell-side reflux condensation is also possible.

The reflux condenser can be mounted on top of, or internal to, a distillation column to produce further separation of the vapour. The tops product from the column enters the reflux condenser where it is partially or totally condensed. This condensation helps to remove some of the light components from the vapour stream, and the final vapour product leaving the top of the condenser is richer in the more volatile

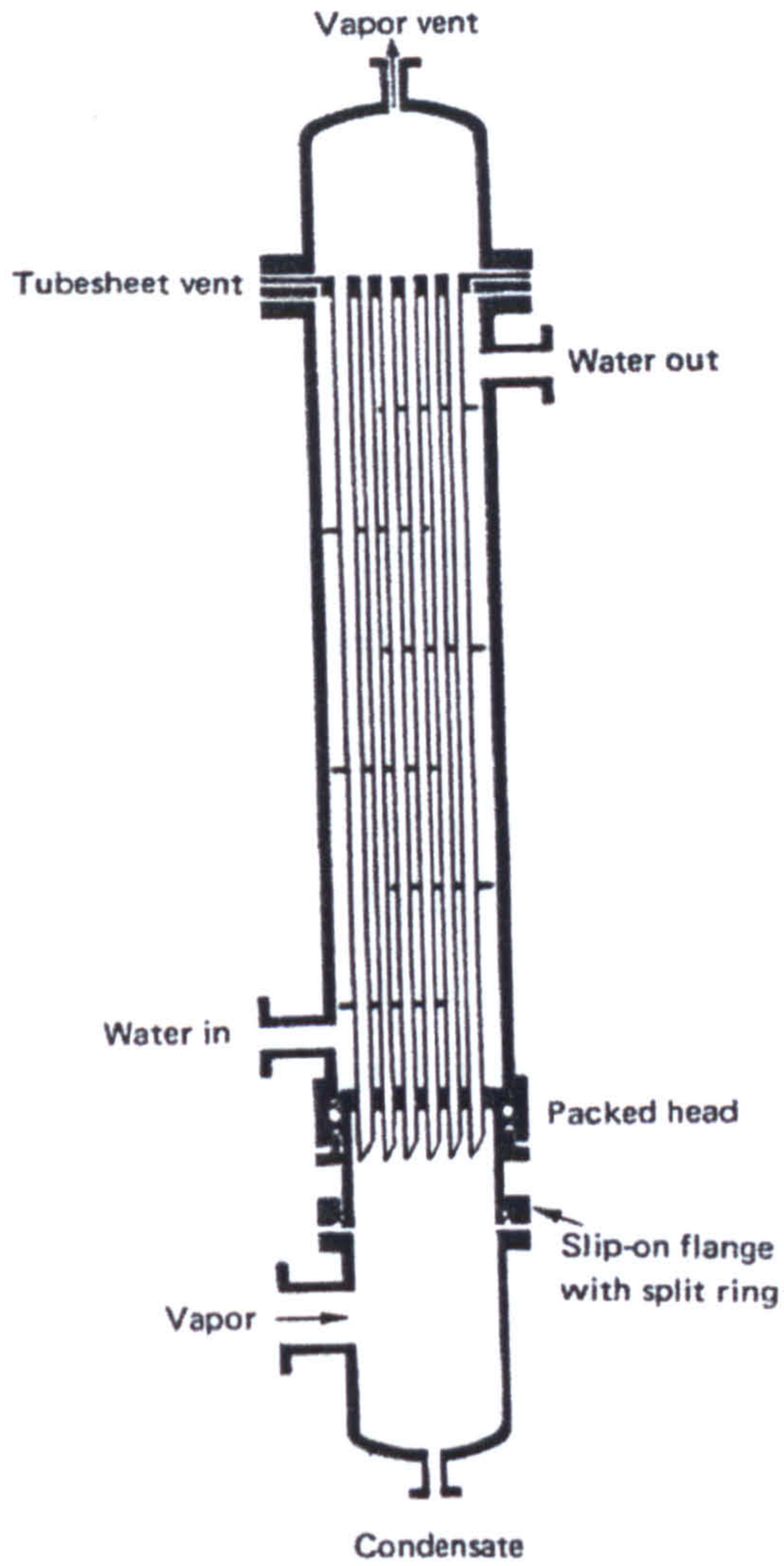

Figure 3.2. A typical reflux condenser.

components than it was leaving the top of the column. The separation achieved in the reflux condenser has been likened to a number of additional theoretical plates in the column.

A reflux condenser used on its own to produce this sort of separation by partially condensing a vapour mixture is known as a dephlegmator, and it has found wide use in the hydrocarbon processing industries. These units combine the mass transfer and heat exchange to achieve the desired separation, and the units are found to work well and be economical (Chiu (1990)). Typical applications of dephlegmators include the recovery of ethylene from cracked gas, olefins recovery from fluid catalytic cracking off-gas, and methane recovery from hydrogen-carbon monoxide synthesis gases (Bernhard, Goodwin and Rowles (1986) and Bernhard and Rowles (1988)).

A further use of reflux condensers is in the control of exothermic chemical reactors. As with distillation columns, the condenser can be positioned directly on top of, or internal to, the reactor. The boiling solvent from the reactor will enter the condenser tubes and flow upwards, along with any noncondensable gas present. The solvent will be condensed and returned to the reactor and the noncondensable gas vented from the system. The condensate return acts like additional material that has been added to the reactor, at or near to the reaction temperature. The condensate is therefore capable of absorbing the heat of reaction, causing it to be vaporised, but only to be condensed and returned back to the reactor. As this means that the pressure losses will be very small, the temperature and pressure of the reactor can be easily controlled.

Despite no rigorous design procedures for reflux condensers, they do still find use in industry, as illustrated above. As units they offer some distinct advantages that the design engineer and process operator might be willing to trade-off against the disadvantages faced in using such a unit. These advantages and disadvantages are

summarised below, using information provided from ESDU (1989) and Chunangad (1994).

Advantages of Reflux Condensers

1. Mounting condensers directly on top of columns or reactors reduces the piping requirements and number of joints. This reduces or eliminates leakage problems and helps to minimise pressure losses. It also removes the need for a reflux pump and its associated costs, and makes a saving on the space required.

2. Reflux condensers are self-venting. Light components and noncondensables gases are swept up and out of the condenser by the vapour flow.

3. When used in conjunction with distillation columns, reflux condensation is accompanied by additional separation of the components in the vapour and liquid phases. This separation is equivalent to several additional separation stages.

4. In a reflux condenser, the rising hot vapour will be cooled by the condensate flowing down the tube walls. This heat transfer minimises cooling of the condensate. A hot condensate return reduces the heat input requirement of the vessel or column, representing an energy saving.

5. A further consequence of a hot condensate return is that condensation of unwanted light (low boiling) components is prevented. They are discharged at the top of the condenser together with any noncondensable gases present.

6. Reflux condensers are operated at low vapour velocities, and so pressure losses in the system are small. Combined with the fact that the condensate is returned at the hottest temperature in the system, reflux condensers provide excellent thermal and mechanical stability of the system, and require very few controls.

7. With dirty vapours, a reflux condenser acts as a scrubber.

Disadvantages of Reflux Condensers

1. Flooding limits the maximum design vapour velocity at the tube inlet. A higher number of tubes are needed for the same flow throughput than would be required with co-current vapour and condensate flow. Consequently, the shell diameter will be larger and the condenser more expensive. Furthermore, the predictive accuracy of flooding correlations is such that a significant safety margin has to be applied to any calculated flooding velocity.

2. The possibility of flooding the condenser tubes implies that vertical in-tube reflux condensers are not normally appropriate where large amounts of noncondensable gases are present.

3. The possibility of poor flow distribution between tubes, or groups of tubes exists with attendant parallel path instability, occasioned by the very low tube-side pressure drop inherent with in-tube reflux condensation.

4. Reflux condensation in tubes requires a single tube-side pass, and in the case of a shell-and-tube heat exchanger, the insertion of expansion bellows or a packed

head to relieve the resultant tube stresses may be required. These may be unacceptable to the process operator.

As mentioned previously, the design of reflux condensers is not based on rigorous procedures. The critical features that need to be considered may be summarised as follows:

1. *Heat transfer in the condensate film.* Previous studies on condensation heat transfer have examined and quantified the effects of surface waves, turbulent films and interfacial shear forces at high vapour velocities. However, no study has aimed at addressing the problem of condensation heat transfer in vertical counter-current vapour-liquid flow, where the vapour velocities may be relatively low.

2. *Heat and mass transfer in the vapour and condensate phases.* The processes of combined heat and mass transfer during condensation of vapour mixtures has been studied intensively, and rigorous design procedures now exist for calculating the rates of heat and mass transfer. Mass transfer behaviour in the liquid film is just as important in reflux condensation because it is crucial in describing the additional rectification effect that takes place. Despite this fact, condensate mixing is paid little attention to in the literature.

3. *Prediction of condenser flooding velocities.* Numerous studies have been carried out, experimental and analytical, on the subject of flooding in vertical tubes, for both adiabatic and condensing situations. As a result, there are a large number of correlations available for predicting the flooding velocity. Unfortunately, there is vast disagreement amongst these correlations under similar operating parameters. No single correlation has yet been identified which can predict the flooding

velocity without having to introduce significant safety margins for a wide range of operating conditions.

As the heat and mass transfer processes were of most interest in this particular research, the first and second points highlighted above were examined in more detail by reviewing some of the open literature on condensation heat transfer, and the more specific literature on reflux condensation and reflux condensers. The remainder of this chapter examines the findings of this review.

3.3 Heat and Mass Transfer during Reflux Condensation

3.3.1 Heat Transfer during Reflux Condensation

During condensation inside tubes, heat is transferred from the condensing vapour across the phase interface, through the condensate film and the walls of the condensing surface area, before entering the coolant on the outer surface of the heat transfer area.

Each of these stages presents some resistance to the heat that is transferred, and these resistances can be quantified by individual heat transfer coefficients, which are related through an overall heat transfer coefficient. This overall heat transfer coefficient can also be calculated from the condenser heat load, the temperature driving force for condensation, and the condenser surface area.

$$\frac{1}{U_i} = \frac{1}{\alpha_i} + \left(\frac{A_i}{A_o}\right)\frac{x_w}{\lambda_w} + \left(\frac{A_i}{A_o}\right)\frac{1}{\alpha_o} \tag{3.3.1}$$

$$\dot{Q} = U\ A\ \Delta T_{mean} \tag{3.3.2}$$

The heat transfer resistance on the vapour side is evaluated using a heat transfer coefficient assuming that the vapour phase is on its own, which can then be corrected for the presence of a condensate film and the effects of condensation. The condensate-film heat transfer coefficient is calculated from a correlation that reflects the orientation of the condenser surface (horizontal or vertical), the mode of

condensation (filmwise or dropwise), and the mechanism controlling the condensation (gravity or shear).

The orientation of the condenser surface is obvious, and it is normal to assume that the condensation process will occur by the filmwise mode unless special steps have be taken to promote the formation of droplets rather than a continuous liquid film on the heat transfer surface.

The controlling mechanism will depend on the flow orientation of the vapour and condensate phases and their magnitude. Irrespective of the condenser orientation, gravity will influence the condensation process, by exerting some downward pull on the condensate film. Vapour shear forces become more dominant as the velocity of the vapour increases. For co-current flow of vapour and condensate, vapour shear has a tendency to thin the film, whilst for counter-current flow the film becomes slightly thicker.

In any condenser design, it is often convenient to know how much condensate has been produced by a particular exchange of heat across the surface. For a single component vapour condensing with sub-cooling of the film below the saturation temperature, the mass flow rate of condensate produced can be found using

$$\dot{M}_f = \frac{\dot{Q}}{\Delta h_v + Cp_f\left(T_v - T_f\right)} \tag{3.3.3}$$

A convenient alternative to the mass flow rate is the mass flow rate per unit width of surface, or the drainage rate, which is defined for condensation in a single tube by

$$\Gamma = \frac{\dot{M}_f}{\pi\, d_i} \tag{3.3.4}$$

This term is used to remove the expression for the temperature drop across the condensate film in equations for the condensate-film heat transfer coefficient. The condensate film Reynolds number, which is used to indicate whether the film flow is laminar or turbulent, or in transition to turbulent flow, is defined by

$$Re_f = \frac{4\Gamma}{\eta_f} \tag{3.3.5}$$

Nusselt (1916) carried out the first analytical study of condensation heat transfer based on a single component vapour condensing against a flat, vertical plate. It was assumed that the condensate film was purely laminar in nature, and that the vapour exerted no shear force on the surface of the film. Nusselt further assumed that subcooling was negligible, and that heat was transferred through the film by conduction, giving a linear temperature profile through the film.

Applying mass and energy balances to a unit volume of the condensate produced equations for the local and the mean condensate-film heat transfer coefficients. Nusselt's equation for the mean condensate-film heat transfer coefficient is shown below.

$$\overline{\alpha}_f = 0.924 \left[\frac{\lambda_f^3\, g_n\, \rho_f \left(\rho_f - \rho_v\right)}{\eta_f\, \Gamma} \right]^{1/3} \tag{3.3.6}$$

Substituting (3.3.5) into (3.3.6) allows Nusselt's equation for the mean condensate-film heat transfer coefficient to be expressed as a function of the condensate film Reynolds number.

$$\overline{\alpha}_f = 1.47\left[\frac{\lambda_f^3\, g_n\, \rho_f\left(\rho_f - \rho_v\right)}{\eta_f}\right]^{1/3} Re_f^{-1/3} \qquad (3.3.7)$$

Kutateladze (1963) suggested a modification to the Nusselt equation based on results at film Reynolds numbers in the range 40 to 1800. The observed values were higher than those predicted by Nusselt theory, and the difference was explained by the presence of waves on the film surface. Kutateladze's expression for use in this laminar-wavy region is shown in (3.3.8) below.

$$\overline{\alpha}_f = \left[\frac{\lambda_f^3\, g_n\, \rho_f\left(\rho_f - \rho_v\right)}{\eta_f^2}\right]^{1/3} \frac{Re_f}{1.08\, Re_f^{1.22} - 5.2} \qquad (3.3.8)$$

The form of the Nusselt equation given in (3.3.7) has been recommended for use up to a film Reynolds number of 30. Up to this point, the film can be taken to be purely laminar and free from surface waves. For a film Reynolds number greater than 30, the condensate film heat transfer coefficient should be determined using (3.3.8).

There have been many studies made on condensation with turbulent films, and it has been generally accepted that the transition from a laminar to a turbulent film occurs between the film Reynolds numbers of 1600 to 1800. Labuntsov (1957) suggested a semi-empirical correlation for use where the film Reynolds number was greater than

1600. Owing to its simple form, this equation has been easily incorporated into design methods for computer programs.

$$\overline{\alpha}_f = \left[\frac{\lambda_f^3 \, g_n \, \rho_f \left(\rho_f - \rho_v\right)}{\eta_f^2}\right]^{1/3} \frac{Re_f}{8750 + 58 \, Pr_f^{-0.5} \left(Re_f^{0.75} - 253\right)} \qquad (3.3.9)$$

These equations ((3.3.7) to (3.3.9)) were developed assuming that the dominant force in the condensation process was gravity. Any force exerted by the condensing vapour on the surface of the condensate film was so small that it had no measurable effect. Other studies have been carried out where the force exerted by the condensing vapour was much larger, and indeed became the dominant force. It is worthwhile highlighting just a few of these studies.

Kirkbride's (1933) studies on condensation on the outside of long vertical tubes found that the film Reynolds numbers were greater than those values which dictated the onset of turbulence, and that the film heat transfer coefficients were higher than the Nusselt predictions. Colburn (1933) extended the work of Kirkbride by using the analogy for the flow of liquids in pipes, where the liquid completely filled the pipe, and the pressure drop was due to gravitational forces.

The resulting equation for evaluating the local condensate-film heat transfer coefficient in turbulent flow was given as a function of the condensate film Reynolds and Prandtl numbers.

$$\alpha_f \left(\frac{\eta_f^2}{\lambda_f^3 \, \rho_f^2 \, g_n}\right)^{1/3} = 0.056 \left(\frac{Cp_f \, \eta_f}{\lambda_f}\right)^{1/3} \left(\frac{4\Gamma}{\eta_f}\right)^{0.2} \qquad (3.3.10)$$

Colburn also presented his results graphically, with a break in the graph at a film Reynolds number of 2100, which he had assumed was the critical value.

Carpenter and Colburn (1951) carried out condensation experiments with significant downward vapour velocities inside vertical tubes for a range of fluids. They found that the condensate-film heat transfer coefficients were much higher than those obtained for a stationary vapour. The results also showed that the critical film Reynolds number was lower at high vapour velocities, and they reported turbulence appearing at film Reynolds numbers of between 250 and 300. They presented an equation for the local condensate-film heat transfer coefficient that included a term for the shear stress at the outer edge of the laminar sub-layer, i.e. the wall shear stress.

$$\alpha_f = 0.043 \frac{\lambda_f \rho_f^{1/2}}{\eta_f} \left[\frac{Cp_f \eta_f}{\lambda_f} \right]^{1/2} \tau_w^{1/2} \qquad (3.3.11)$$

To evaluate this term, it was necessary to take into account interfacial shear and gravitational effects in the film. In addition, momentum changes in the condensing vapour and the influence of mass transfer on the interfacial shear had to be considered.

They suggested a simplified correlation for the mean film coefficient by neglecting the gravitational and momentum terms, and assuming that the wall shear stress was equal to the interfacial shear stress. The interfacial shear stress was calculated using an apparent interfacial friction factor evaluated as for single-phase flow at a mean vapour mass flow rate.

$$\bar{\alpha}_f = 0.065 \frac{\lambda_f \rho_f^{1/2}}{\eta_f} \left[\frac{Cp_f \eta_f}{\lambda_f} \right]^{1/2} \tau_I^{1/2} \qquad (3.3.12)$$

Dukler (1960) presented a more refined method of predicting the hydrodynamics and heat transfer in vertical filmwise condensation, for downward co-current vapour flow. Working from the definition of eddy viscosity and using the Deissler equation for its variation near a solid boundary, Dukler obtained velocity distributions in a liquid film as a function of interfacial shear stress and film thickness.

The results agreed with the predictions of the classic Nusselt theory at very low Reynolds numbers, and with the empirical correlations of Colburn in the turbulent region. Dukler presented an equation for the mean condensate-film heat transfer coefficient, based on the assumption of a constant wall-to-gas temperature difference.

$$\bar{\alpha}_f \left[\frac{\eta_f^2}{\rho_f^2 \lambda_f^3 g_n} \right]^{1/3} = \frac{Re_f}{\int_0^{Re_{f,out}} \frac{dRe_{fz}}{\alpha_f \left(\frac{\eta_f^2}{\rho_f^2 \lambda_f^3 g_n} \right)^{1/3}}} \qquad (3.3.13)$$

There were two main objections to this work. Firstly, the velocity distribution used was obtained from experimental work in pipes with a different shear stress distribution. Secondly, in defining the temperature profile at a certain distance from the surface, the molecular conductivity term was neglected with respect to eddy conductivity.

Lee (1964) and Kunz and Yerazunis (1967) repeated Dukler's analysis for the case of no interfacial shear stress, and for the case of positive interfacial shear stress, respectively. The results showed similar agreement with those in the original work of Dukler.

A simple approach for evaluating the condensate-film heat transfer coefficient for shear controlled condensation was proposed by Boyko and Kruzhilin (1967). This method related the film coefficient to the quality of the condensing vapour and to the heat transfer coefficient for the equivalent flow of liquid with the same saturated conditions. The liquid heat transfer coefficient was estimated by the correlation of Mikheev (1956).

$$\alpha_l = 0.021 \frac{\lambda_l}{L} Re_l^{0.8} \; Pr_l^{0.43} \tag{3.3.14}$$

The local condensate-film heat transfer coefficient was then found using Boyko and Kruzhilin's equation.

$$\alpha_f = \alpha_l \left[1 + x_v \left(\frac{\rho_f}{\rho_v} - 1 \right) \right]^{1/2} \tag{3.3.15}$$

The average film coefficient for a range of vapour quality conditions was calculated by taking the arithmetic mean of the end values.

With further experimental data, Soliman, Schuster and Berenson (1968) were able to improve the work of Carpenter and Colburn by modifying the equation for the local

condensate-film heat transfer coefficient. They defined the wall shear stress as being the sum of three terms: interfacial shear stress due to vapour phase friction, gravitational force in the liquid film, and momentum change in the vapour phase. The void fraction correlation of Zivi (1964) was used to derive the equation for momentum change in the condensing vapour. Their equation for the local condensate-film heat transfer coefficient is shown in (3.3.16) below.

$$\alpha_f = 0.036 \frac{\lambda_f \rho_f^{1/2}}{\eta_f} \left[\frac{Cp_f \eta_f}{\lambda_f} \right]^{0.65} \tau_w^{1/2} \qquad (3.3.16)$$

Unfortunately, these studies have concentrated on shear-controlled condensation with downward co-current vapour and condensate flow, but do not consider the counter-current flow present in a reflux condenser.

With vapour and condensate flowing counter-currently, the vapour exerts some shear force upon the surface of the condensate film, which might be expected to produce several effects on the film. The surface of the film could become wavy, and depending on the magnitude of the forces involved, some of the film could become entrained in the vapour core. Another consequence of upward vapour flow is that the thickness of the film might be greater than if the vapour were stationary, or flowing co-currently with the film. The overall effect experienced in reflux condensers is still not known exactly.

As reflux condensers have to operate well below the vapour flooding velocity in order for the condensate to drain from the tubes, it is likely that the condensation process is one where the forces due to gravity are still controlling. This suggests that a correlation based on gravity being the dominant force would be more appropriate for determining the condensate-film heat transfer coefficient.

An examination of the literature specifically on the subject of reflux condensation showed that no real attempt has been made at developing a unique correlation for evaluating the condensate-film heat transfer coefficient in a counter-current condenser. The problem is compounded by the fact that very little experimental data exists in the open literature with which to develop and validate such a correlation.

One of the earliest studies was that of Clements and Colver (1973), who carried out experiments on the condensation of various hydrocarbons in a vertical reflux condenser tube. They suggested an empirical equation, based on the work of Grigull (1942) on turbulent films, of the form

$$\frac{\alpha_f z}{\lambda_f} = K\left[\frac{z^3 g_n \rho_f^2 \Delta h_v}{\lambda_f \eta_f \Delta T}\right]^n \tag{3.3.17}$$

When experimenting with binary hydrocarbon mixtures, they assumed the mixture to be a pseudo pure component with the physical properties of the binary. The temperature driving force they used was taken to be the difference between the mixture bubble point and the surface temperature. They stated that this method of analysis was not applicable to the condensation of vapour mixtures where one of the components was a noncondensable gas, or if there were surface tension gradients within the condensate film.

The results of their work were correlated best where K was equal to 1.88×10^{-8}, and n to 0.75, although the scatter of the data was found to have an average absolute deviation of 35.7%. When their data was plotted on the same axes as the Nusselt predictions, it was seen to have a steeper gradient than Nusselt's values. They concluded from this that their data was in turbulent rather than laminar flow.

Subramanyam (1983) used the equations of Nusselt and Soliman et al. for evaluating local condensate-film heat transfer coefficients in an incremental analysis of a reflux condenser. They stated that where the condensing vapour flow rate was known to be very small (at the top of the tube), it was safer to use Nusselt's equation, but otherwise, the higher of the two predictions was normally taken.

Bell (1988) recommended the equation by Soliman et al. for calculating the local condensate-film heat transfer coefficients in several theoretical studies of reflux condensation. He stated that the condensate film in a reflux condenser operating near the flooding velocity was likely to be turbulent, and so the equations of Dukler, Carpenter and Colburn, and Soliman et al. were more applicable. No experimental evidence was provided to substantiate these claims.

Following the approach of Soliman et al., Chunangad (1994) performed an analysis of the frictional, gravity and momentum forces acting on the condensate film for the case of counter-current vapour and liquid flow. Neglecting momentum changes in the condensing vapour, they proposed a modified expression for the wall shear stress, and outlined a procedure for estimating local condensate-film heat transfer coefficients.

The first stage in this approach involved evaluating the forces due to gravity and friction. Based on the criteria of Carpenter and Colburn, if the frictional force was less than half that of the gravitational force, then the condensation was assumed to be gravity controlled. In this situation, the local condensate-film heat transfer coefficients were evaluated by the equations of Nusselt, Kutateladze, or Labuntsov, depending on the value of the film Reynolds number. Otherwise, the local condensate-film heat transfer coefficients were found by the equation of Soliman et al. using their modified expression for the wall shear stress.

As Chunangad states, the success in predicting the local condensate-film heat transfer coefficient will ultimately depend on the applicability of the Soliman et al. equation for counter-current condensing systems. This has not yet been investigated due to a lack of suitable data.

Abdelmessih, Rabas, and Panchal (1997) carried out a study on the use of reflux condensers. In this paper, the authors used the equation of Chen, Gerner and Tien (1987) for calculating the condensate-film heat transfer coefficient. This equation was based on counter-current condensation of a single component vapour.

$$Nu_f = \left\{ \left[\left(\frac{0.31}{Re_f^{1.32}} \right) + \left(\frac{Re_f^{2.4}\, Pr_f^{3.9}}{2.37 \times 10^{14}} \right) \right]^{1/3} - \frac{C\, Re_f^{1.8}\, Pr_f^{1.3}}{771.6} \right\}^{1/2} \qquad (3.3.18)$$

The condensate film Nusselt number was defined in this paper as

$$Nu_f = \frac{\alpha_f}{\lambda_f} \left(\frac{\nu_f^2}{g_n} \right)^{1/3} \qquad (3.3.19)$$

The parameter C was used in determining the interfacial shear stress as given by Chen et al., and was defined as

$$C = 0.023 \left[\frac{\eta_f^{1.133}\, \eta_v^{0.2}}{d_i^2\, g_n^{0.667}\, \rho_v\, \rho_f^{0.333}} \right] \qquad (3.3.20)$$

Abdelmesih et al.'s preference for the correlation of Chen et al. was that it was readily available in the open literature. Their results showed, however, that reasonable agreement existed between the correlation of Chen et al. and the method of Chunangad. In their comparison, they state that the conditions simulated inside the condenser were below that necessary to cause flooding, which suggested that the force due to friction was much smaller than that due to gravity (and is confirmed in their results). This meant that the procedure developed by Chunangad for evaluating the local condensate-film heat transfer coefficient when vapour shear was significant had not been tested in the paper by Abdelmessih et al..

In comparing their results to the predictions of Chunangad, Abdelmessih et al. were actually comparing their results to those of Nusselt, Kutateladze and Labuntsov. A more interesting comparison might have arisen had the simulated condition been one where vapour shear forces were more significant. This would have involved using the modified equations of Chunangad for determining the wall shear stress, which was then used in the equation of Soliman et al. for determining the local condensate-film heat transfer coefficient.

3.3.2 Mass Transfer during Reflux Condensation

The transfer of mass during reflux condensation is a feature that has made this particular operation attractive. Reflux condensers have been used in conjunction with distillation columns to further separate the components in a vapour mixture. They have also been used on their own to produce rough rectification of vapour mixtures, particularly in the hydrocarbon processing industries.

For the condensation of a binary vapour mixture containing a heavy component and a light component, the heavy component (less volatile) has a lower diffusivity but a

higher tendency to condense. The net effect is that the light component (more volatile) accumulates at the phase interface, hindering the condensation of the heavy component.

During condensation of such a mixture in a co-current condenser, a separation of the components would take place. Mass would be transferred from the bulk vapour mixture, across the phase interface and into the liquid condensate. As the two streams would leave the condenser at the same end, they would be in phase equilibrium with one another corresponding to the least efficient separation of the mixture components.

In reflux condensation, there can be additional mass transfer from the liquid condensate back across the phase interface and into the condensing vapour. This additional mass transfer takes place as a result of the warm rising vapour evaporating the low boiling (light) component within the liquid condensate film. The component is vaporised and returns back across the phase interface into the condensing vapour. The net effect is that the condensate film becomes richer in the less volatile (heavy) component and the vapour richer in the more volatile component. It is possible that the reflux condensate stream may be in phase equilibrium with the feed vapour, and the exit vapour will be much more concentrated in the light component.

It is this additional mass transfer effect that makes expressing the process that occurs during reflux condensation difficult. No reliable methods for describing this transfer mechanism have been proposed or rigorously tested, and in addition, very little data exist to help develop such a method. A survey of the open literature on reflux condensation has confirmed that very little is known about this topic, and that no attempt has been made to incorporate this knowledge into a design procedure for reflux condensers.

Kent and Pigford (1956) carried out a study on the separation of a vapour mixture in a wetted-wall column, which was operated both as an adiabatic distillation column with an overhead condenser (conventional distillation apparatus), and as a partial counter-current condenser. In this study the Colburn-Drew (1937) equations were used to describe the rates of mass transfer across the phase interface. The authors introduced the concept of transfer units and related them to liquid-phase and gas-phase resistances, surface area, and amount of condensation. Their system of equations meant that it was impossible to specify independently the amount of separation, the heat load, and the coolant temperatures. Vapour-liquid equilibrium data were required in their approach.

They concluded that a reflux condenser would require a larger interfacial area in comparison to conventional distillation apparatus if the same separation were to be carried out at the same heat load. The reflux condenser would require a greater rate of heat removal in comparison to the overhead condenser associated with the distillation column if the same separation were to be carried out across the same interfacial area.

It appears that the experimental procedure adopted in this study for the condensation experiments involved condensing the exit vapour from the partial condenser in the overhead condenser, and returning this to the top of the partial condenser as liquid reflux. Thus total reflux operation involved the use of an external condenser, and an artificial reflux liquid flow rate was employed. As the reflux ratio was an important parameter in determining the capability of the unit to separate the components of a vapour mixture, it seems strange to have deliberately manipulated this value.

Tröster (1960) studied the capability of a reflux condenser to separate the components of vapour mixtures, and presented two different scenarios. The first case was for a constant condensate load across the condenser surface area, and the

outlet concentration of the vapour stream was to be determined. The second case was when the condensate load varied across the condenser surface area and the exit vapour composition was known, and the problem became one of determining the required surface area for achieving the stated separation. This second case required a much more involved solution.

The equation of Kirschbaum (1930) was used by Tröster to determine the composition of the exit vapour from the reflux condenser. Equilibrium data was also required for the solution, although in the second approach the equilibrium relationship was simplified by a linear relationship across the concentration range considered. Kirschbaum's equation as stated by Tröster is given in (3.3.21) below.

$$\ln(R+1)=\int_{\tilde{x}_{f,in}}^{\tilde{x}_{f,out}}\frac{d\tilde{x}}{\tilde{x}-\tilde{x}_f} \qquad (3.3.21)$$

For the assumption of a constant condensate load, Tröster concluded that the calculation to determine the separation possible in the condenser could be carried out independently of any heat transfer calculation. However, when the condensate load was no longer constant across the condenser surface, and the amount of surface was to be determined to achieve a desired separation, the heat transfer calculation was no longer independent.

An useful study by Di Cave, Mazzarotta, and Sebastiani (1987), examined the separation achieved in a vertical reflux condenser tube. They developed a model for the heat and mass transfer processes based on the film theory approach used by Colburn and Drew (1937), but adapted this to the case of a vapour and liquid moving counter-currently to one another. Using this approach, they produced equations for the composition changes in each phase as a function of the local condensation ratio.

Using experimental data from the condensation of two binary mixtures, they compared the measured separation of the more volatile component with the predictions of their own model and found reasonably good agreement. Furthermore, they compared their data with the predictions using the equation of Kirschbaum, presented in this paper in the form shown in (3.3.22) below, and which they stated was still used as a short-cut method in industry.

$$\ln(R+1)=\int_{\tilde{y}_{in}}^{\tilde{y}_{out}}\frac{d\tilde{y}}{\tilde{y}-\tilde{x}} \qquad (3.3.22)$$

These authors reported that the separations predicted by this equation were much greater than both the experimentally measured values and the values predicted by their own model. In this paper the authors stated that the separations predicted by (3.3.22) corresponded to between 2 and 4 theoretical stages, although they did not show how they arrived at these values. They also stated that this contradicted industrial practice, but gave no reference to support this claim.

More recently, Lintern and Haseler (1995) developed an approach to evaluate the number of thermodynamic stages within a reflux condenser. The number of stages was defined in terms of the tube length, tube diameter, the flow rate per tube, the thermodynamic state of the vapour, and the fraction of the vapour fed to the tube that is to be condensed.

The numerical method was based on previous work by these two authors (Lintern and Haseler (1994)). This earlier method calculated the flow rates, temperatures and compositions of the liquid and vapour at a predefined number of points in the tube. It was further assumed that the liquid was well mixed and hence at its bubble point,

while the bulk vapour could be above or below its dew point temperature corresponding to its composition.

The results of their work showed that the number of thermodynamic stages in a reflux condenser tube could be increased if the tube diameter, the heat flux, or the fraction of the inlet vapour condensed were decreased. Alternatively, the number of thermodynamic stages could be increased if the tube length was increased.

3.4 Thermal Design Methods for Condensers

As described in Chapter 2.5, two methods are available for the thermal design of industrial condensers, the Film-theory method and the Equilibrium method.

3.4.1 The Film-theory Method for Condenser Thermal Design

The film theory method is based on the work of Colburn and Drew (1937) for binary vapour mixtures, which was developed from work on the condensation of a single component vapour and noncondensable gas mixture by Colburn and Hougen (1934). It is assumed that a thin, laminar film exists next to the phase interface, and that within this film, concentration, temperature and pressure gradients exist. Outside the film, the concentration, temperature and pressure are assumed to be at the conditions of the bulk mixture. This was illustrated in Figure 2.3 [p.15].

Heat and mass transfer rates are evaluated using heat transfer coefficients, and heat and mass transfer analogies. The balancing equations of mass and energy are constructed across this laminar film, and solved for a variety of condensing situations.

The heat flux from the interface to the coolant was written in terms of an overall heat transfer coefficient and the appropriate temperature difference. This overall heat transfer coefficient included the resistances from the coolant, any dirt or fouling present, the tube wall and the condensate film.

$$\dot{q}_T = U(T_I - T_c) \tag{3.4.1}$$

Three individual heat fluxes contributed to this total heat flux. The first of these heat fluxes was the latent heat flux, found by summing the contributions of the condensation flux and the enthalpy of vapourisation of each component that was condensed.

$$\dot{q}_L = \sum \dot{m}\, \Delta h_v \tag{3.4.2}$$

The second heat flux, which was the sensible heat flux due to cooling of the vapour mixture from the bulk temperature to the interface temperature, was described in terms of the vapour convective heat transfer coefficient.

$$\dot{q}_{sb} = \alpha_v\, \theta\, (T_{bv} - T_I) \tag{3.4.3}$$

The vapour heat transfer coefficient was obtained from a standard single-phase heat transfer correlation using vapour flowrate, with no correction made for the presence of the condensate film. The factor θ was used to account for the flow of heat associated with the transfer of mass across the film, and was defined as

$$\theta = \frac{\phi}{(e^{\phi} - 1)} \tag{3.4.4}$$

$$\phi = \frac{(\sum \dot{m}\, Cp_v)}{\alpha_v} \tag{3.4.5}$$

The third heat flux, which was the sensible heat flux term due to cooling of the condensing vapour, was calculated by summing the contributions of each of the condensing components.

$$\dot{q}_{scf} = \sum \dot{m}\, Cp_v \left(T_{bv} - T_I\right) \tag{3.4.6}$$

The two sensible heat terms can be combined to give one equation for sensible heat flux using the correction factor proposed by Ackermann (1937). In the presence of a mass flux, the temperature profile between the phase interface and the boundary layer is altered, and an expression describing the heat flux in the presence of this mass flux can be written. Ackermann's correction factor is the ratio of the heat flux in the absence of mass transfer to that in the presence of mass transfer.

$$\dot{q}_s = \alpha_v \theta_A \left(T_{bv} - T_I\right) \tag{3.4.7}$$

$$\theta_A = \frac{\phi}{\left(1 - e^{-\phi}\right)} \tag{3.4.8}$$

It was assumed that the sensible heat flux term due to cooling of the condensate was negligible. The latent and sensible heat fluxes were combined to give the total heat flux. Thus

$$U\left(T_I - T_c\right) = \sum \dot{m}\, \Delta h_v + \alpha_v\, \theta \left(T_{bv} - T_I\right) + \sum \dot{m}\, Cp_v \left(T_{bv} - T_I\right) \tag{3.4.9}$$

Or, alternatively, using the Ackermann correction factor

$$U(T_I - T_c) = \sum \dot{m}\, \Delta h_v + \alpha_v\, \theta_A\, (T_{bv} - T_I) \qquad (3.4.10)$$

As this equation was to be satisfied at every location in the condenser, the interface temperature and the condensation fluxes for each component had to be determined. It was generally accepted that at the interface, the vapour and liquid were in equilibrium at the interface temperature and total system pressure. The vapour composition at the interface was found using the equilibrium relationship.

$$\tilde{y}_I = \tilde{K}\, \tilde{x}_I \qquad (3.4.11)$$

However, this required knowledge of the liquid composition at the interface, which was a result of the mass transfer behaviour within the condensate film. Two limiting cases have been suggested:

1. A completely mixed condensate film having an infinitely large mass transfer coefficient, and hence no resistance to mass transfer. The liquid composition at the interface was equal to that in the bulk of the mixture, and

2. A completely unmixed condensate film having zero mass transfer coefficient, and hence an infinitely large resistance to mass transfer. The liquid composition at the interface was a function of the molar flux of that condensing species to the total molar flux of all condensing species.

The condensation molar flux of any component was made up of a diffusive contribution and a convective contribution, and could be described by an equation of the form

$$\dot{n}_v = \dot{n}_T \, \tilde{y}_v + D \, \tilde{c} \, \frac{d\tilde{y}_v}{dy} \tag{3.4.12}$$

For a binary condensable vapour mixture, the condensation molar flux of one of the vapour components was expressed as

$$\tilde{z} = \frac{\dot{n}_{v1}}{\dot{n}_T} = \frac{\dot{n}_{v1}}{\dot{n}_{v1} + \dot{n}_{v2}} \tag{3.4.13}$$

From which it followed that

$$\dot{n}_{v1} = \dot{n}_T \, \tilde{y}_{v1} + D_{v1v2} \, \tilde{c} \, \frac{d\tilde{y}_{v1}}{dy} \tag{3.4.14}$$

Rearranging (3.4.14) gave

$$\dot{n}_T = \left[\frac{-D_{v1v2} \, \tilde{c}}{(\tilde{z} - \tilde{y}_{v1})} \right] \frac{d\tilde{y}_{v1}}{dy} \tag{3.4.15}$$

This equation was integrated across the laminar film to give

$$\dot{n}_T = \frac{D_{v1v2}\,\widetilde{c}}{\delta} \ln\left[\frac{\widetilde{z} - \widetilde{y}_{v1,b}}{\widetilde{z} - \widetilde{y}_{v1,I}}\right] \tag{3.4.16}$$

Or alternatively

$$\dot{n}_T = \beta \ln\left[\frac{\widetilde{z} - \widetilde{y}_{v1,b}}{\widetilde{z} - \widetilde{y}_{v1,I}}\right] \tag{3.4.17}$$

It was also possible for there to be more than two components in the vapour mixture, and in such cases the complexity of the situation was increased. The study of multicomponent condensation is beyond the scope of this present study, but a short discussion has been included here for completeness.

Two mass transfer models have been developed to describe the processes taking place if all the concentration changes took place across a thin film. The first of these models was an interactive model based on a generalisation of Fick's Law. Toor (1957) has shown that the diffusional behaviour of each species was dependent on all independent concentration gradients and that the interaction effects could affect the mass transfer behaviour in unexpected ways.

Two such interactive models have been proposed, the linearised theory of Toor (1964) and Stewart and Prober (1964), and the Krishna-Standart (1979) method, both of which required the solution of the Maxwell-Stefan equations.

The second model was a non-interactive model, also known as the effective diffusivity model, and was a simplification of the first type. The mass diffusion of any component in the mixture was dependent only on its own concentration gradient, and it was further assumed that each component had no interaction with any other component in the mixture. The mass diffusion rate of each component was determined by assuming it diffused alone through an arbitrary reference component.

3.4.2 The Equilibrium Method for Condenser Thermal Design

The equilibrium (or approximate) method is a less rigorous design method than the film-theory method. It was first developed by Silver (1947) and then later by Bell and Ghaly (1972). Ward (1960) proposed a similar method.

In all of these methods, the mass transfer resistance was estimated using the resistance to the sensible heat transfer in the vapour phase. This meant that there was no need for mass diffusivity data. Further, it was assumed that the condensing vapour and condensate were in local equilibrium at every point in the condenser. Thus the condensation process was assumed to follow a pre-determined equilibrium condensation curve.

For calculating the equilibrium condensation curve, it was necessary to make a simplifying assumption about the flow structure of the vapour and condensate. Two possibilities existed, producing two different types of curve. Examples of each type of curve are shown in Figure 3.3 [p59].

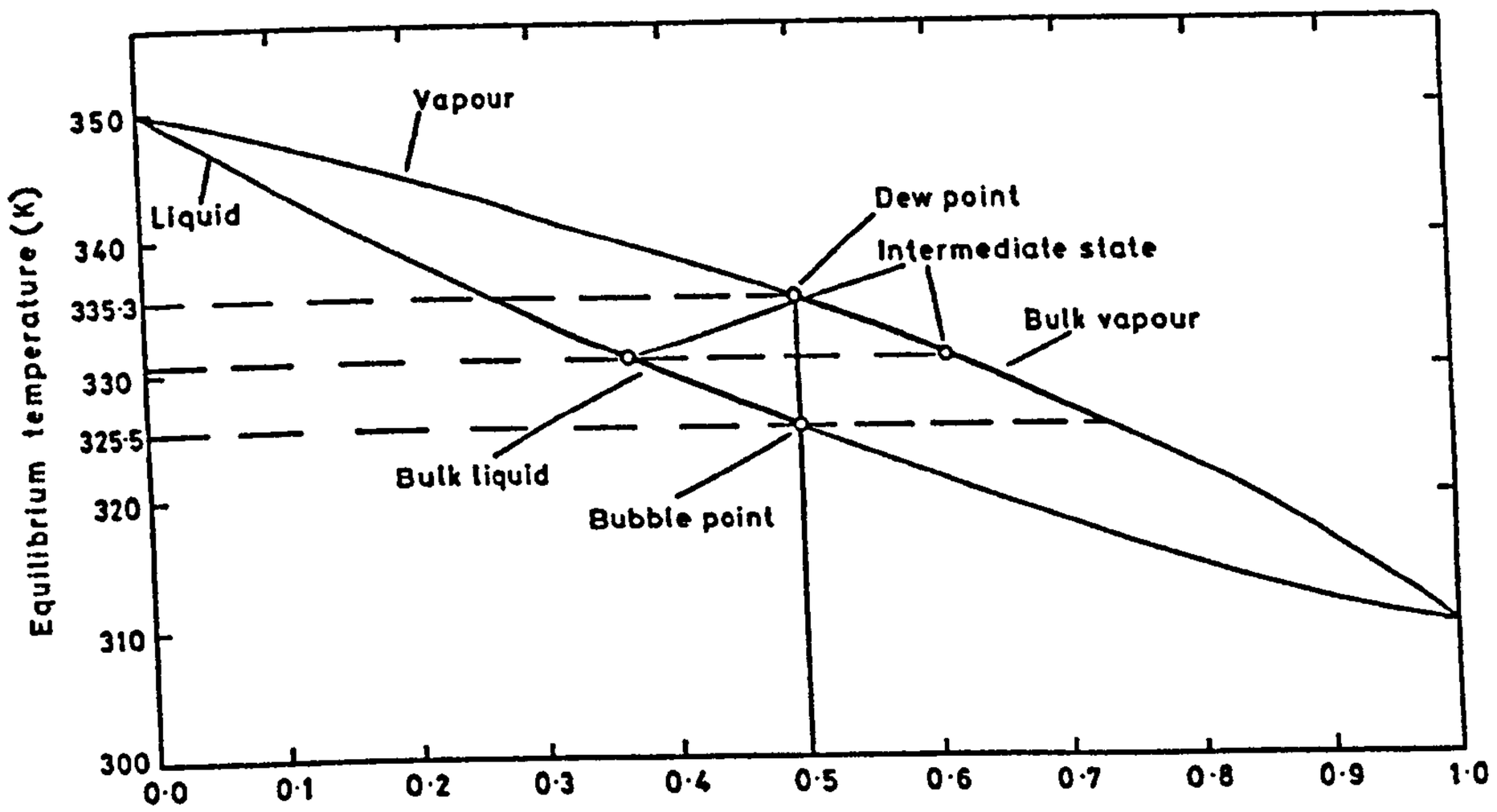

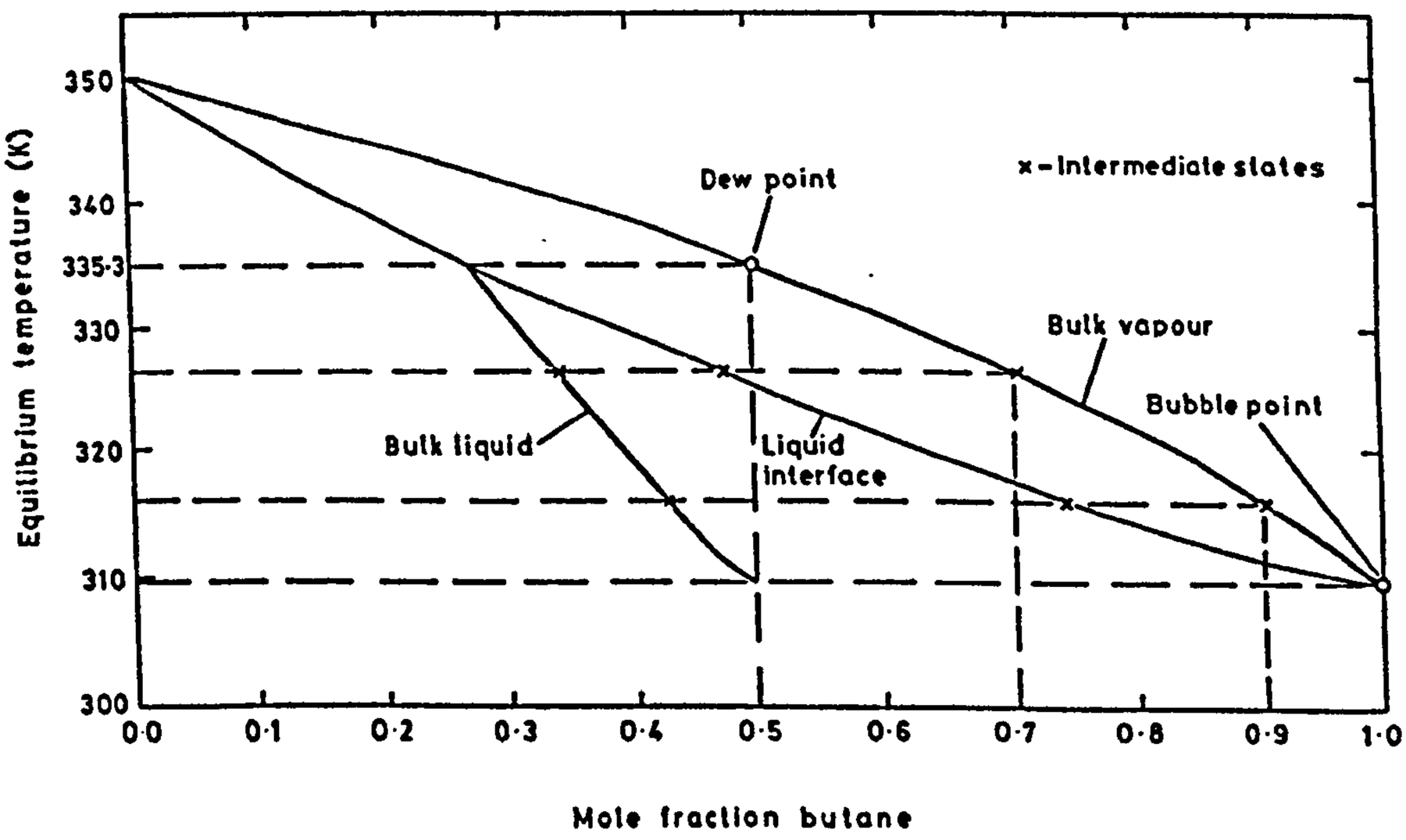

Figure 3.3. Examples of Integral (top) and differential (bottom) condensation diagrams for a mixture of butane and pentane (from HTFS Handbook Sheet CP13).

1. Integral Condensation. The bulk vapour at a point in the condenser is in equilibrium with all of the bulk mixed condensate previously formed. The bulk of the liquid on the condenser surface is therefore in equilibrium with the bulk of the vapour, and the condensate composition is the same as that at the interface.

2. Differential Condensation. The bulk vapour at a point in the condenser is in equilibrium with the newly formed condensate. All previously formed condensate is removed from contact with the bulk vapour. The bulk of the liquid is no longer in equilibrium with the bulk of the vapour, and so the condensate composition differs from that at the interface, and must be found by mass balance. This process is described by (3.3.22)

The total heat flux due to sensible cooling of vapour, sensible cooling of condensate and the latent enthalpy of condensation was described in terms of an overall heat transfer coefficient and the appropriate temperature difference. The overall heat transfer coefficient incorporated the resistances due to the coolant, fouling, the tube wall, and the condensate film.

$$\dot{q}_T = U(T_I - T_c) \tag{3.4.1}$$

The sensible heat flux due to the cooling of the bulk vapour mixture from the bulk vapour temperature to the interface temperature was given by

$$\dot{q}_v = \alpha_v(T_v - T_I) \tag{3.4.20}$$

As the interface temperature was not known, it was eliminated from these equations to give on rearrangement, an expression for the total heat flux.

$$\dot{q}_T = \frac{(T_v - T_c)}{\frac{1}{U} + \left(\frac{\dot{q}_v}{\dot{q}_T}\right)\frac{1}{\alpha_v}} \tag{3.4.21}$$

The parameter Z was defined as

$$Z = \frac{\dot{q}_v}{\dot{q}_T} \tag{3.4.22}$$

As this parameter varied with position along the condensing path, it was evaluated at several points on the heat release curve (a curve of cumulative heat load against temperature) before the required condenser surface area was determined.

McNaught (1979) and Sardesai, Palen and Taborek (1983) have improved the original method by allowing for the effect of mass transfer on the heat transfer that takes place during condensation. The mass transfer correction factor was applied to the sensible heat flux due to cooling of the bulk vapour mixture from the bulk vapour temperature to the interface temperature, thus modifying (3.4.20).

$$\dot{q}_v = \alpha_v \frac{\phi}{e^{\phi} - 1}(T_v - T_I) \tag{3.4.23}$$

Therefore the expression for the total heat flux was re-written as

$$\dot{q}_T = \frac{(T_v - T_c)}{\frac{1}{U} + \frac{Z}{\alpha_v^*}} \tag{3.4.24}$$

$$\alpha_v^* = \alpha_v \frac{\phi}{e^{\phi} - 1} \tag{3.4.25}$$

3.4.3 Application of the Film-theory and Equilibrium Condenser Thermal Design Methods to Reflux Condensers

There is no body of evidence available in the open literature that supports the use of either of these methods for designing reflux condensers. The lack of available experimental data to validate these methods is no doubt a major reason for the absence of clear guidelines, although suggestions have been made as to which model may be more appropriate.

In the equilibrium method, the flow of vapour and condensate was characterised in one of two ways, and was used as a basis for evaluating the condensation curve used in the thermal design. Of course, regardless of the flow orientation of the vapour and condensate, these assumptions are idealised situations, and the actual behaviour of the phases is likely to be somewhere in between.

One of these assumptions was that vapour and condensate remained in intimate contact with one another throughout the entire condensing length, a situation that

would be likely to occur in a vertical co-current condenser. The second assumption was that the vapour was only in contact with the condensate just formed on the surface, any previous condensate that had formed was removed from the condensing surface. This situation is likely to take place in a horizontal condenser, where the condensate that forms on the outside of a horizontal bundle, drips off the tubes and falls to the bottom of the condenser. The physical separation occurs due to the action of gravity.

In applying either of these assumptions, the rates of heat and mass transfer are pre-defined by the integral or differential condensation curve. These rates were then assumed to be those required to maintain equilibrium between all of the vapour and condensate, or the vapour and that part of the condensate still in contact with the condensing vapour. This meant that the outlet compositions of the vapour and condensate phases were decided only by equilibrium considerations.

The equilibrium method with an integral condensation curve is best suited for the design of total condensers handling vapour mixtures, because end conditions are forced to equilibrium conditions. Therefore, the temperatures and compositions of the vapour and condensate phases are more likely to approach the equilibrium values. Consequently, as reflux condensers are more frequently operated as partial condensers, the use of the equilibrium method with an integral condensation curve seems inappropriate.

It is interesting to see that ESDU (1986) recommends the use of the equilibrium method with a differential condensation curve for the design of reflux condensers. This is despite the danger of the differential curve over-estimating the composition of the condensate, and hence predicting a higher degree of separation than would actually be obtained in the condenser.

In addition, they recommend that Ward's method be used as opposed to the traditional Silver-Bell-Ghaly method used more frequently. The difference between these two methods was that Ward neglected the sensible heat transfer due to cooling of the condensate in his evaluation of the total heat flux. However, McNaught and Emerson (1977) argued that the Ward method inaccurately evaluated the liquid sub-cooling term, and so the Silver-Bell-Ghaly method was to be preferred.

Chunangad (1994) discussed the use of the equilibrium method for the design of a reflux condenser. Acknowledging that equilibrium curves calculated in the normal way could not be applied to reflux condensation, a method was proposed for calculating the incremental temperatures and compositions of the two phases through the reflux condenser, making the assumption that vapour and liquid leave each increment in equilibrium.

The success of the equilibrium method to predict the surface area, phase temperatures and compositions for a reflux condenser is, at this point in time, unclear. As it is an approach that does not permit the estimation of temperatures and compositions independently of the equilibrium conditions, and that these equilibrium conditions are dependent on the two phases flowing co-currently, it would suggest that this method is inappropriate for reflux condenser design.

The film theory method was one based on a limited understanding of the physical reality of the condensation process. Here the heat and mass transfer equations were combined to predict the surface area requirements, and the temperatures and compositions of the vapour and condensate were evaluated locally through the condenser, and were dependent on the calculated rates of heat and mass transfer.

In the absence of information about the mass transfer behaviour in the condensate film, it was necessary to make some assumption about the composition of the liquid condensate. The first assumption was that there was no resistance to mass transfer presented by the condensate, and the film was described as being well mixed. The second assumption was that the condensate presented an infinite resistance to mass transfer, and the film was described as being completely unmixed. With the first assumption, the composition of the condensate was the same as that at the interface. With the second assumption, the condensate composition was determined by the ratio of component condensing flux to total condensing flux.

As with transfer from the vapour to the condensate, a boundary layer model is used on the vapour side to describe the transfer of mass during condensation. In reflux condensation, the additional separation is due to the transfer of the more volatile component in the liquid film evaporating back across the phase interface. A boundary layer model to describe the transfer of mass during multicomponent evaporation might help in the development of a more complete film theory model applicable to reflux condensation.

As with the assumptions concerning integral and differential condensation, these two assumptions about the extent of mixing in the condensate film were extremes. It is not clear which of these is best applied to condensation with counter-current vapour and condensate. The situation where the condensate is well mixed is more likely to be achieved in a co-current vertical condenser. It might have been expected that an upward flow of vapour relative to the flow of condensate would promote good liquid mixing within the film.

The temperatures and compositions of the vapour and condensate were evaluated locally in the film theory method by the use of differential equations. In formulating these equations, the two phases were taken to be travelling co-currently in the

original work of Colburn and Drew. There is obviously some doubt about how well these equations would work for a condensing system where the two phases flow counter-currently, as in a reflux condenser.

Di Cave, Mazzarotta, and Sebastiani (1987) applied the theory of Colburn and Drew to a laboratory scale reflux condenser. They developed their own set of equations to describe the heat and mass transfer, and the composition changes of the vapour and condensate based on counter-current operation. Comparing their results with the values predicted from their model, they concluded that the model gave reasonable predictions.

Lintern and Haseler (1993) applied the film theory method to the case of a reflux condenser. In this work, they discuss modifying the heat transfer equation proposed by Colburn and Drew but use the same the mass transfer equations. The outcome of making simplifying assumptions about the extent of mixing in the condensate was discussed.

If the film was assumed completely unmixed, their calculations showed that the reflux condensate was heated to a non-equilibrium state as it flowed down the tube wall. On the other hand, if the film was assumed well mixed, the condensate could only remain in its equilibrium state if some of the more volatile component was re-vaporised while the less volatile component was condensing. This simultaneous condensation and evaporation meant that the condensing flux could have negative and positive values. The authors used this as a basis for redefining the latent heat term in the original Colburn and Drew analysis, and presented enthalpy balances for use in a stepwise calculation procedure.

Application of the film theory method for the design of reflux condensers is still some way off. Very little work has been done in assessing how successful the original method has been at determining the surface area requirements, and the temperature and composition profiles of both the vapour and condensate. Until such comparison work has been carried out, it is difficult to see how any modifications to the original theory will add value.

3.4.4 Conclusions about Reflux Condensation and Reflux Condenser Design

Having reviewed the literature to investigate the level of understanding in relation to condensation with reflux, and the design of condensers operating in this mode, the following conclusions can be made:

- Very little published information exists concerning reflux condensation in comparison to other modes of condensation presently employed in industry. There is also a lack of experimental data available in the open literature concerning this type of operation.

- Understanding of the mechanism involved in transferring heat through the condensate film during reflux condensation is limited, and no attempt has been made to develop a correlation for determining the heat transfer coefficient in the condensate film during condensation with reflux.

- The processes occurring in a reflux condenser during the condensation of vapour mixtures, with or without a noncondensable gas present, are less well understood in comparison to those occurring in co-current condensers. It is therefore unclear

which of the thermal design methods currently employed to design condensers is most applicable to the design of reflux condensers handling vapour mixtures.

- There is no general consensus on which methods should be applied to produce the most realistic design for a reflux condenser.

It was the intention of this research project to address these problems, and to provide information that would be of benefit to both the heat transfer and heat exchanger design communities.

4.0 Experimental Equipment and Methods

This chapter describes the new research facility used for the experimental work described in this thesis, and an outline of the experimental programme is provided for all test work carried out. A description of the data acquisition program is included in this chapter, as are descriptions of the data analysis calculations for the single component hydrocarbons and the binary hydrocarbon mixtures.

The author was not involved in the design of the test facility or in the specification of equipment for the facility. These stages had already been carried out prior to the author beginning work on the research project. Under the supervision of Dr Chris Chu, the author was acquainted with the test facility specifications and its control systems for the first part of the project.

The author then undertook the commissioning phase of the project, with the responsibility for identifying potential measurement problems, and proposing modifications to the original design to overcome these. In addition, the author drafted all operating procedures for the test facility and re-drafted original specifications where necessary.

A major piece of commissioning work undertaken by the author was the design and installation of an on-line composition measurement system. Based on using a vibrating cell densitometer for measurement purposes, the author designed a system for removing liquid samples from the test facility, measuring them, and then returning them back to the test facility. All ancillary equipment (except sampling loop pump) was specified by the author, who then supervised the installation, and carried out the commissioning.

4.1 Description of the Test Facility

A new research facility has been built to study the condensation of single component hydrocarbons and their mixtures in a single vertical tube utilising counter-current two-phase flow. The test rig is situated in a modular outhouse joined to the exterior wall of the main laboratory. It has a concrete floor to support the process fluid circuit. This outhouse is furnished with power points and lighting, and is supplied with mains water and compressed air. A photograph of the outhouse is shown in Figure 4.1 [p.71].

The operator's control console and the test facility control panels are located inside the main laboratory. Ducts have been provided through the existing rear wall to allow connection of all instrumentation in the test facility to these panels and the console, and for the delivery of electricity, mains water and compressed air. A hydrocarbon sensor has been positioned next to the operator's console and test facility control panels to detect the presence of process fluid in the main laboratory. Figure 4.2 [p.72] and Figure 4.3 [p.73] show the operator's control console and the test facility control panels respectively.

The test facility can be divided into three circuits: the process fluid circuit, the primary coolant circuit, and the secondary coolant circuit. The process fluid circuit contained the test fluid, which was either a single component hydrocarbon or a binary hydrocarbon mixture, the primary coolant circuit contained mains water, and the secondary coolant circuit contained a mixture of mains water and ethylene glycol. These three circuits are represented in the flow diagram shown in Figure 4.4 [p.74].

For safety, the process fluid circuit has been built within a metal containment cabinet, ventilated by a fan positioned on the front exterior wall of the outhouse.

Figure 4.1. The reflux condensation facility outhouse.

Figure 4.2. The reflux condensation facility operator's control console.

Figure 4.3. The reflux condensation facility control panels.

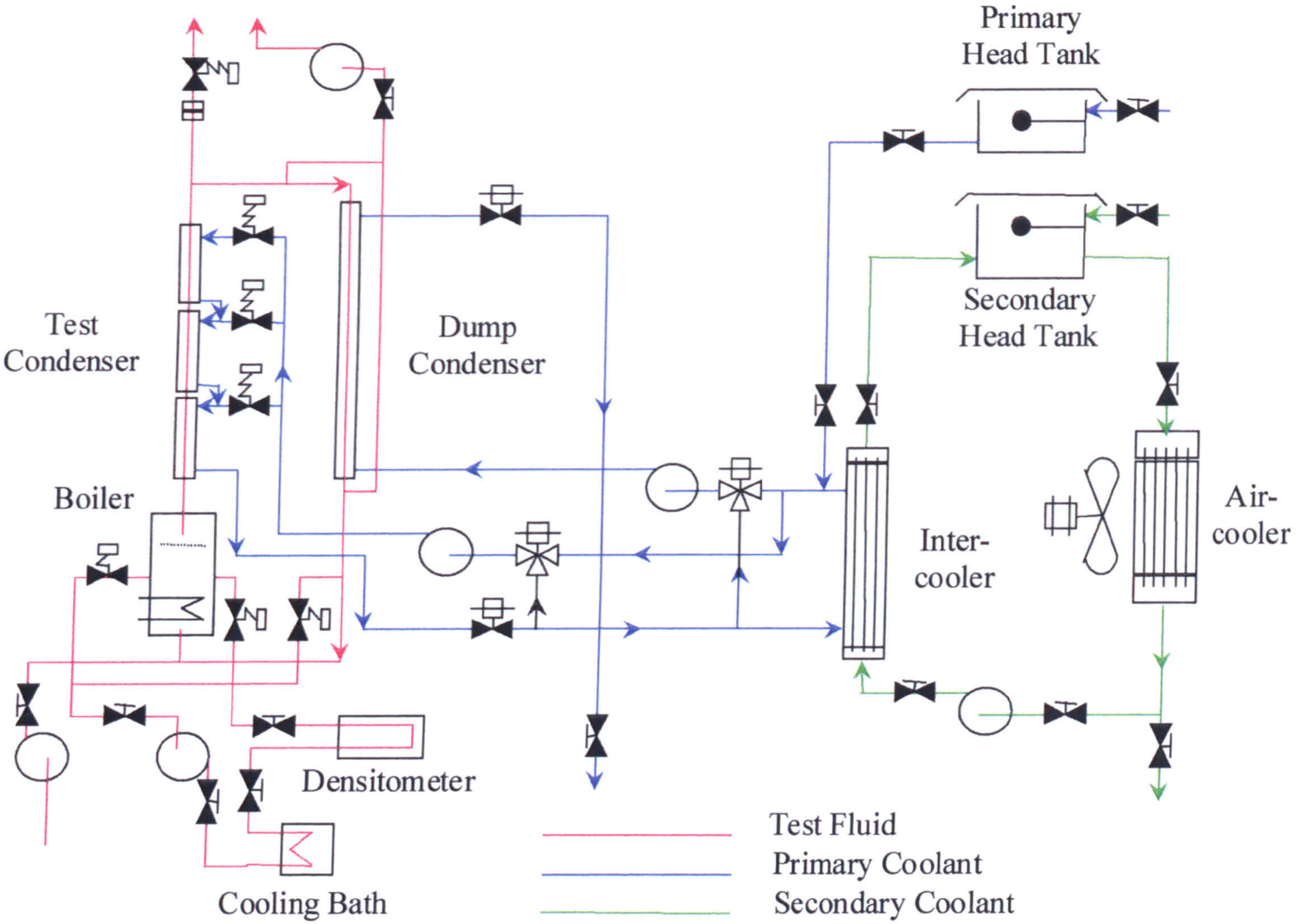

Figure 4.4. A line diagram of the reflux condensation facility.

This metal cabinet has been fabricated in sheet metal and constructed on a light metal frame. It has been sealed along the junction of adjacent plates to ensure it is a gas-tight structure. The base of the cabinet has been tilted at an angle to the floor to provide a drainage slope for any spilled liquid.

The ventilating fan drew air upward through a vertical cylindrical duct from low down in the cabinet and it was then discharged through the duct on the exterior wall to the atmosphere. Make-up air was drawn downwards through the opposite exterior wall and entered the cabinet high up. In this way, good downward ventilation of any heavy hydrocarbon vapour was ensured, the cabinet was therefore always at a negative pressure relative to atmosphere, and any leakage of air was into the cabinet.

A bursting disc and a pressure relief valve were positioned in a line directly above the top of the test condenser, which travelled up for a short distance before passing through the outhouse wall and into the atmosphere. Furthermore, the walls of the outhouse have been insulated and made fire proof, and a section of the wall has been fitted with a grill to act as a pressure relief. Hydrocarbon sensors have been positioned inside the containment cabinet and inside the outhouse to detect any leakage from the process fluid circuit. The containment cabinet is shown in Figure 4.5 [p.76].

The process fluid circuit comprised three main elements: the boiler, the test condenser, and the dump condenser. It was designed to operate up to a pressure of 6 bar absolute and a temperature of 120°C. The total internal volume of the process fluid circuit was 50 litres and the total inventory of process fluid was around 20 litres. The total volume of the boiler was around 35 litres. To prevent the escape of test fluid, the number of joints has been kept to a minimum, and all flanges have been sealed and earth-bonded to prevent against electrostatic build-up.

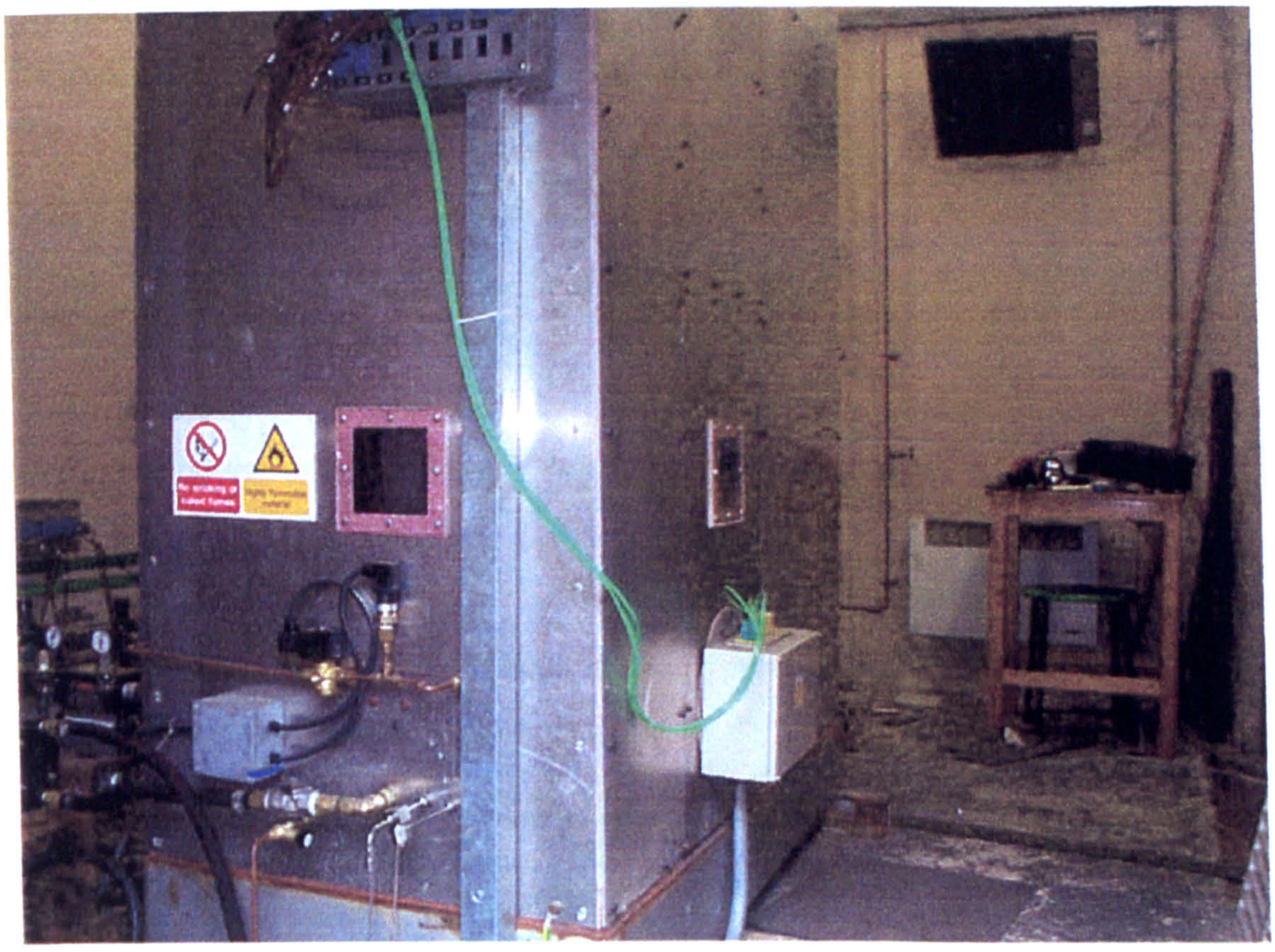

Figure 4.5. The vapour containment cabinet.

4.1.1 The Process Fluid Circuit

A photograph of the boiler is shown in Figure 4.6 [p.78], and a sketch showing its main features is given in Figure 4.7 [p.79]. The boiler has been fabricated in stainless steel, and has welded flanges at the top and the bottom of the cylinder to allow easy access for modifications, cleaning and maintenance. The bottom closure of the boiler had a tapped pad with a flange for the return of condensate from the dump condenser, and for the addition and removal of test fluid. The top closure had been tapped with a flange to mount a stub piece internally and a spool piece externally, leading to the test condenser. The stub piece was cut at an angle of 45° to the horizontal to assist the return of condensate to the boiler.

Two small windows have been provided to allow observation of the condensate returning to the boiler, one window in the front and the other on the side. A tray was positioned below the stub piece to catch the condensate returning from the test condenser and to transport it to the bottom of the tube bundle for re-vaporisation. The condensate was prevented from splashing onto the surface of the boiling liquid by placing layers of fine gauze wire onto the tray.

The six cartridge heaters have been mounted on a flange attached to a pad low down on the boiler shell to ensure they are well submerged. These six heaters were arranged as two tube bundles of three, with one bundle positioned above the other. All electrical connections lay outside the containment cabinet and were terminated at a junction box. A circuit breaker has been added to each heater and connected to the high integrity earth. The cartridge heaters had built-in thermocouples to monitor their surface temperature.

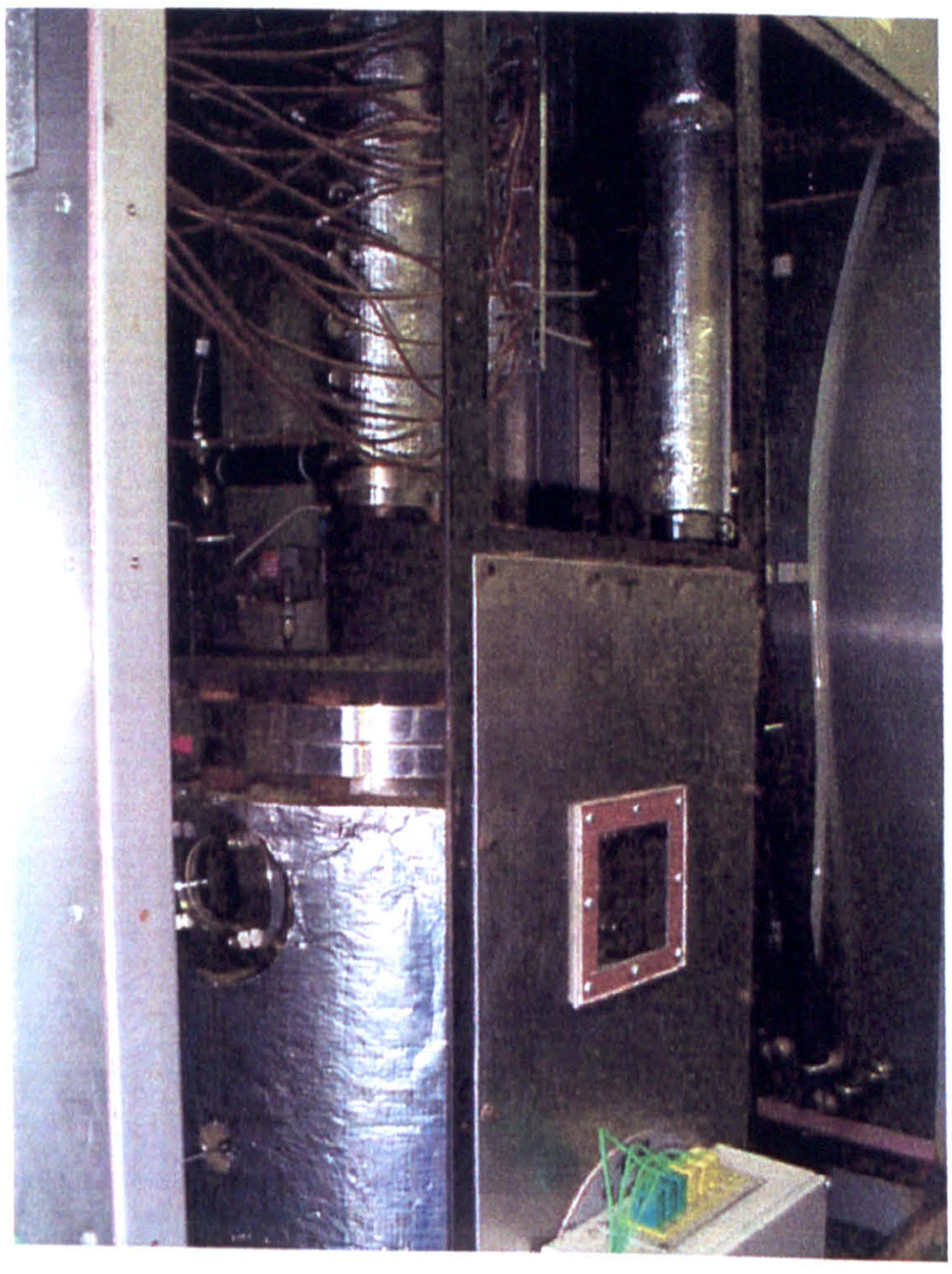

Figure 4.6. The boiler.

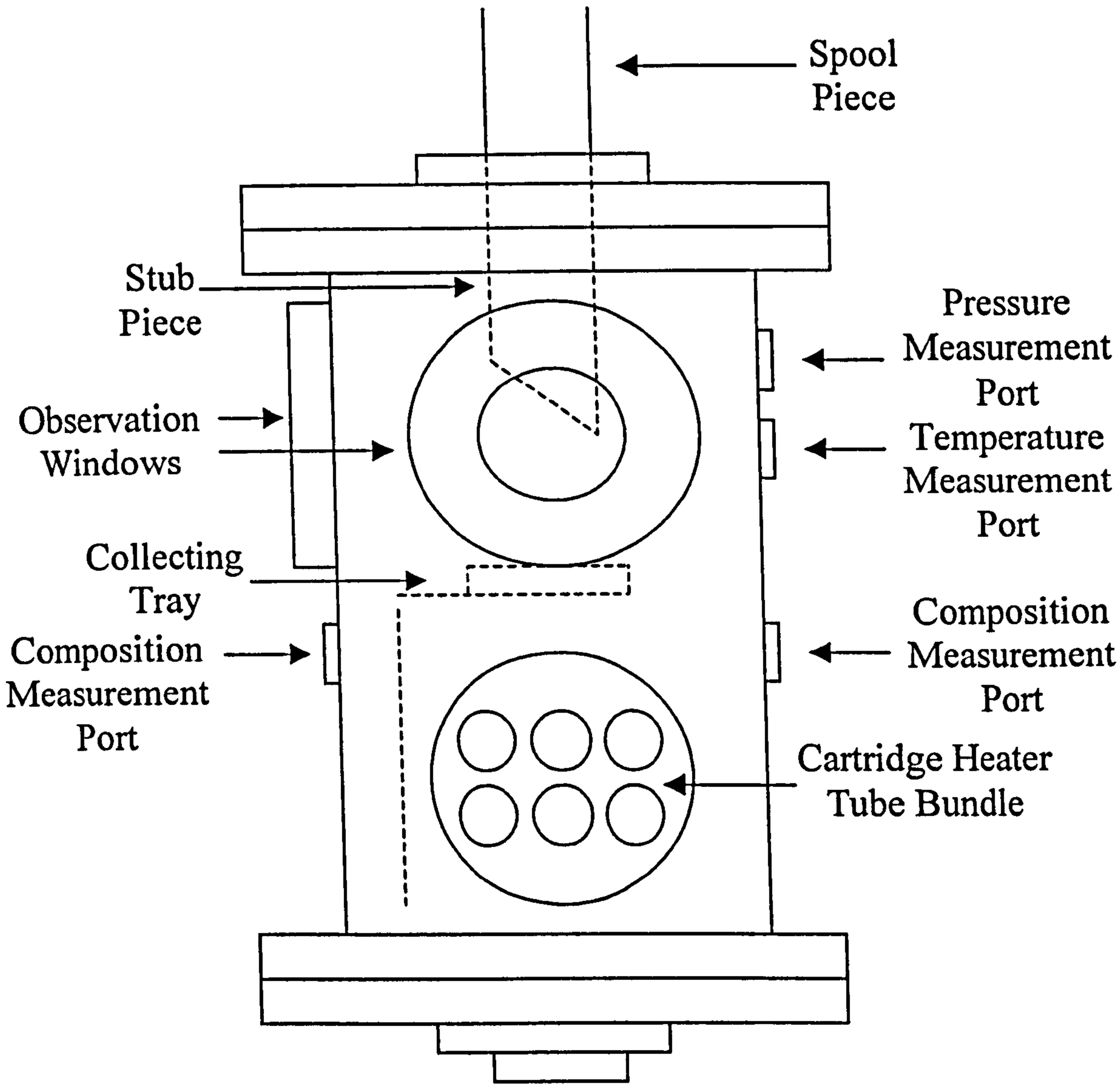

Figure 4.7. A sketch of the boiler features.

Two bosses have been provided in the boiler vapour space to allow connection of a pressure transducer/transmitter and a thermocouple for measuring the pressure and temperature respectively. A further two bosses have been provided below the liquid level, one in the main bath, the other in the reflux condensate return duct, to allow liquid samples to be removed from, and returned to, the boiler for composition measurement.

The sampling system was manufactured in narrow diameter stainless steel tubing. Withdrawal of samples was controlled by pneumatic and solenoid valves, and a variable speed gear pump pumped the sample through the system. The variable speed gear pump could be isolated and removed/inspected by manually closing small valves on the suction and discharge sides. Samples were cooled in a cooling water bath before entering the measuring device, and the water from this bath was passed over the measuring cell to control temperature. The composition measurement equipment could be isolated from the system by two manual valves on the inlet and outlet sides. The composition measurement equipment is shown in Figure 4.8 [p.81].

A line connected to the top leg of the test fluid circuit above the test condenser was connected to a small vacuum pump. Another line connected to the return leg of the test fluid circuit below the dump condenser was also connected to this small vacuum pump. On the discharge side of the pump was a line venting to atmosphere, and this pump was used to remove trapped air from the system.

4.1.2 The Test Condenser

The test condenser consisted of three identical test sections of copper base tube of 45mm internal diameter and 62mm external diameter which were flanged together to form an overall condenser length of approximately 1.5m. The base tube had a helical

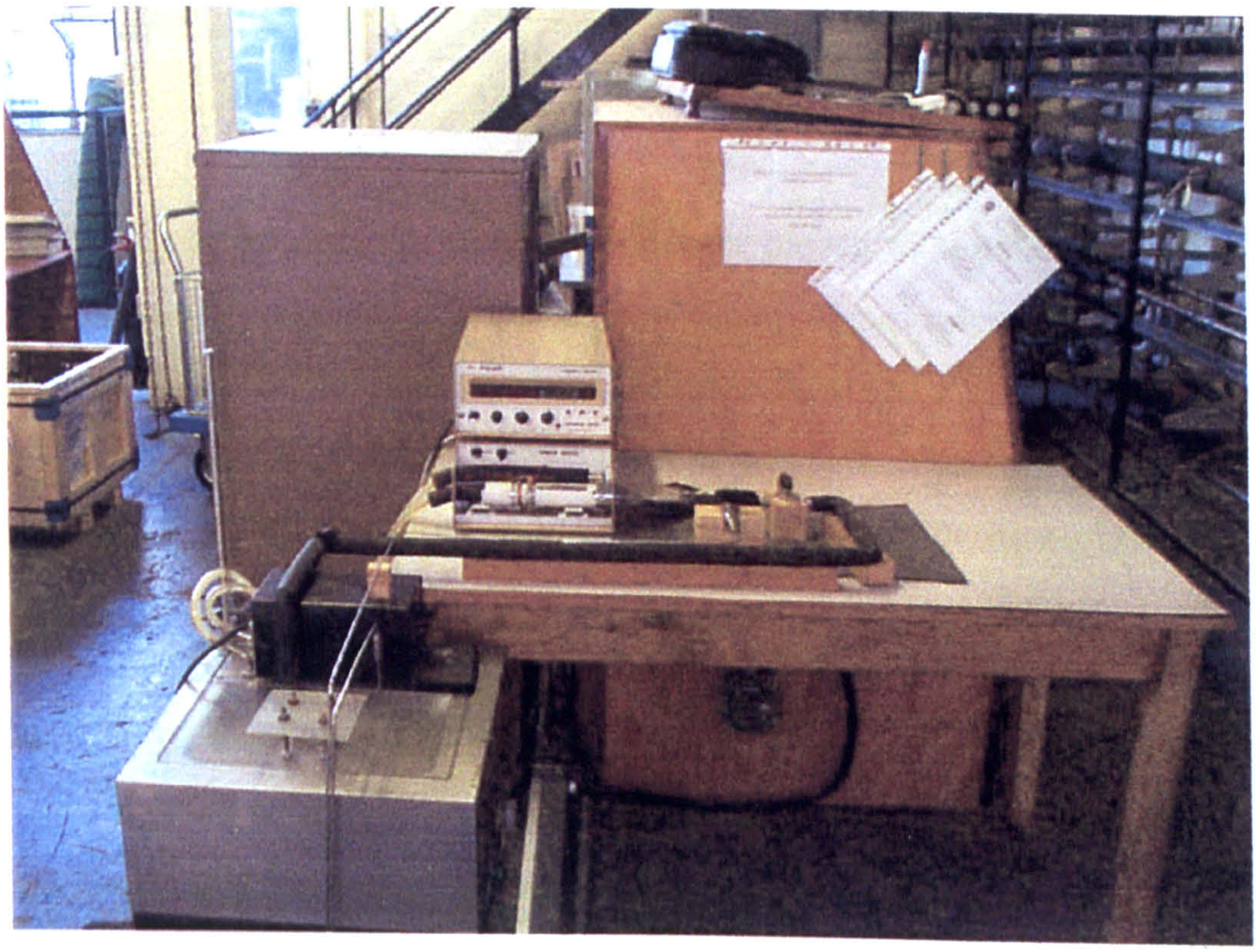

Figure 4.8. The on-line composition measurement equipment.

groove 4mm deep by 10mm wide with a 15mm pitch cut into its outer surface, over a distance of 33.5 pitches, which created a small rectangular flow channel once the stainless steel coolant sleeve has been fitted over the base tube. To ensure no cross-flow, the coolant sleeve has been vacuumed sealed to the base tube. The test condenser is shown in Figure 4.9 [p.83], and a sketch of one of the test sections is given in Figure 4.10 [p.84].

4.1.3 The Dump Condenser

Vapour that did not condense in the test condenser passed to the dump condenser. The dump condenser was made of stainless steel tubing 45mm internal diameter with a stainless steel jacket surrounding the base tube through which cooling water flowed. The overall length of the dump condenser was 2m. The condensate exiting from the dump condenser was returned to the bottom of the boiler via a return leg.

4.1.4 The Primary Coolant Circuit

Water was used as coolant for the condensers. It was stored in a head tank fed directly from the mains, with the tank level controlled by a floating valve and a control valve in the supply line. The inlet flow to the test condenser was pumped to each of the sections through a manifold, with the flow to each section controlled by independently operated solenoid valves. A three-way valve allowed adjustment of the inlet temperature to the sections by partial recycling of the outlet flow, and a control valve on the discharge side of the pump adjusted the flowrate. There was an air bleed and a pressure relief valve at the highest point.

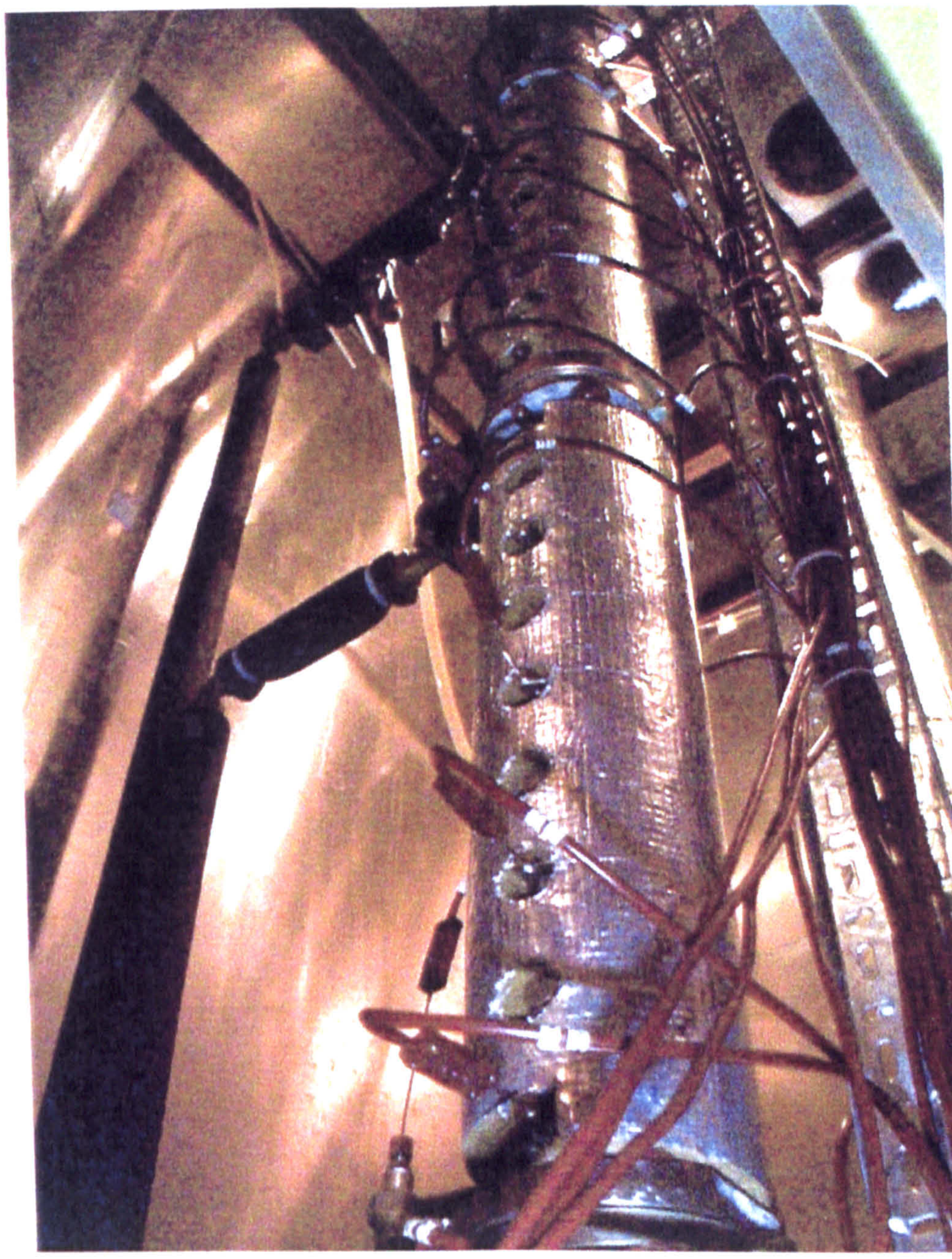

Figure 4.9. Test sections in the test condenser.

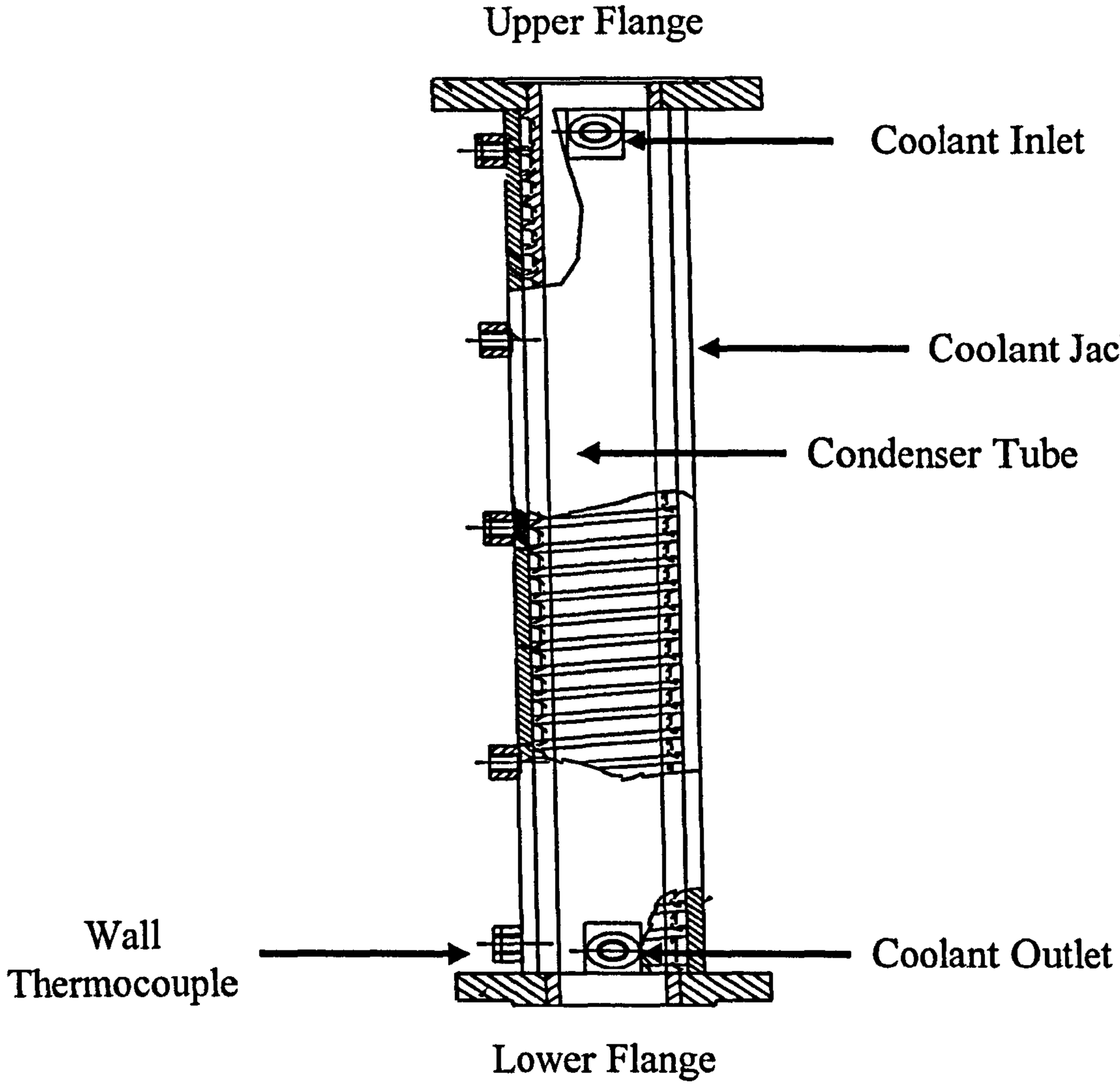

Figure 4.10. A sketch of a test section.

The flow to the dump condenser was pumped up through the annular jacket. A separate three-way valve allowed adjustment of the inlet temperature by partial recycling of the outlet flow. The flowrate was adjusted by a control valve on the discharge side of the pump. There was an air bleed and a pressure relief valve at the highest point.

The hot outlet flows from the reflux and dump condensers were mixed before passing back into the shell-side of a shell-and-tube heat exchanger (inter-cooler). Site water from the head tank entered the circuit on the cold side of this exchanger. The tubular exchanger was capable of removing approximately 8kW from the primary circuit using an area of approximately $1m^2$.

4.1.5 The Secondary Coolant Circuit

Water containing ethylene glycol flowed in a closed loop from a head tank connected directly to the mains supply, allowing operation of the secondary circuit below the normal freezing point of water. This mixture of ethylene glycol and water flowed on the tube side of the inter-cooler to remove heat from the primary coolant and rejected it to atmosphere in an air-cooled heat exchanger.

The air-cooled heat exchanger had an area of $1m^2$ and was capable of rejecting 8kW. The presence of flow in the secondary loop was monitored by a flow meter on the discharge side of the pump used to circulate the secondary coolant.

4.2 Description of the Instrumentation

All of the instruments in this test facility were scanned via a desktop PC using two multi-channel data acquisition units. The signals received by the acquisition units were processed to meaningful data, which was then displayed on the PC monitor.

The instrumentation was used to monitor the conditions of the vapour and condensate in the test and dump condensers, the coolant streams in the test and dump condensers, the secondary coolant stream, and the ambient air temperatures inside and outside the building housing the test facility. The location of the instrumentation in the test facility is shown in Figure 4.11 [p.87].

A total of twenty-nine thermocouples were installed in this test facility, and were calibrated over the temperature ranges 5 to 50°C or 5 to 100°C with the reference temperature measured by a platinum resistance thermometer. The accuracy of the thermocouples was calculated to be ± 0.4°C. Calibration details for the thermocouples are given in Appendix A2.1.

For each of the three test sections, five measurements of wall temperature were made. The vapour temperature was measured at the upper flange of each section and in the boiler vapour space. The condensate temperature at the outlet of the dump condenser was also measured. Built-in thermocouples allowed the temperatures of each of the cartridge heaters to be read from the control panel.

The coolant temperature at the inlet and outlet of each test section was measured, as was the coolant temperature at the inlet and outlet of the dump condenser. Measurements were made of the air temperature inside the metal containment

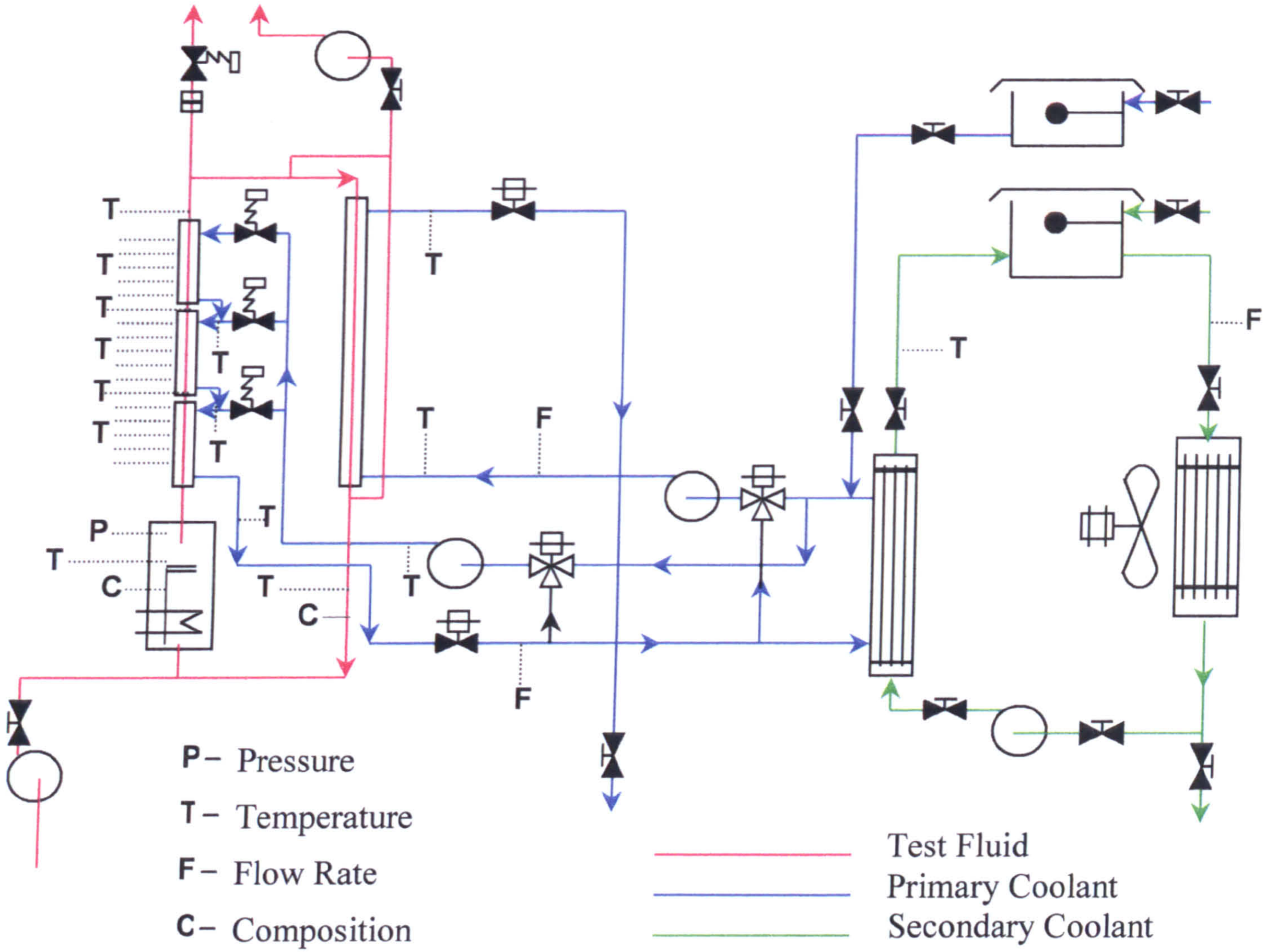

Figure 4.11. An instrumentation diagram of the reflux condensation facility.

cabinet, and of the air temperature outside the building housing the test facility. The temperature of the secondary coolant stream was also measured at the outlet of the inter-cooler.

A transducer/transmitter was placed in the boiler vapour space to measure the vapour pressure. The transducer/transmitter was calibrated by the manufacturer and had a reported accuracy of ± 1.2%. Details of the manufacturer's calibration are included in Appendix A2.2.

The flow rates through the test and dump condensers were measured by separate flow meters. These were calibrated by the manufacturer and had a reported accuracy of ± 1%. Details of the manufacturer's calibration are included in Appendix A2.3.

4.3 Description of the Data Acquisition Method

The data acquisition program used in this test facility was written using Microsoft Visual Basic version3.0. It was based on a similar program written for the HTFS Boiling and Condensing Facility also at NEL by Dr Chris Chu. The program allowed measurements to be taken from all of the instrumentation and then displayed on a series of screens.

A brief description of the program has been provided below. It is important to point out that the author was not involved in the production or any subsequent editing of the data acquisition program.

4.3.1 The Control Window

This window appeared when the program was run. From here, other windows were entered to perform specific actions. This window was the only one where the results of scanning the instrumentation were stored. The control window is shown in Figure 4.12 [p.92].

There was no built-in system for controlling which windows were entered from this main window. The author adopted a system that reflected the need to enter all of the information for identifying the scanned instrument readings.

4.3.2 The General Information Window

This was the first window entered from the Control Window. The date and time of the test run were entered to generate the filename where the results were stored. The test number and title were used as an alternative means of identifying the results. Strictly speaking, it was not necessary to enter the time as this was recorded when scanning the instruments. This window is shown in Figure 4.13 [p.92].

4.3.3 The Scanning Options Window

This window was used to take readings from the test facility instrumentation, and is shown in Figure 4.14 [p.93]. It was also used to enter atmospheric pressure readings, measured by a gauge in the main laboratory, and compositions of the test fluid in the boiler.

The interface between the software program and the instrumentation was the data acquisition unit. Two units were used in this facility, one to measure temperatures and the other to measure the test facility pressure, primary coolant flow rates and the level of power supplied to the cartridge heaters.

The options in this window allowed the instruments to be scanned by type or for all of the instruments to be scanned together. When the thermocouples were scanned, the program sent a signal to measure the output voltage from each of the thermocouples in turn. The output voltages were used to convert these signals to temperature measurements using the calibration equation of the relevant thermocouple.

If the pressure was measured, the program sent a signal to the pressure transducer/transmitter to measure its output voltage, which was then converted to a pressure reading using the calibration equation.

The coolant flow rate was measured by sending a signal to the relevant flow meter to measure the output frequency. The frequency was scanned over a short period of time, and the average was used in the calibration equation to produce a flow rate.

4.3.4 The Results Window

This was used to view the scanned instrument readings. These instrument readings were viewed firstly by clicking on the particular box, and then clicking the display button. This action brought up another window showing a table of the required measurements, and the results were viewed by clicking on this table. The windows

opened by selecting any of the boxes shown in Figure 4.15 [p.93] are shown in Figures 4.16 to 4.21. [pp.94-96].

4.3.5 The Print Options Window

This was used to obtain a hard copy of the scanned instrument readings. It was possible to generate a printed copy of Figures 4.16 to 4.21, or a full report of all instrument readings on a single page.

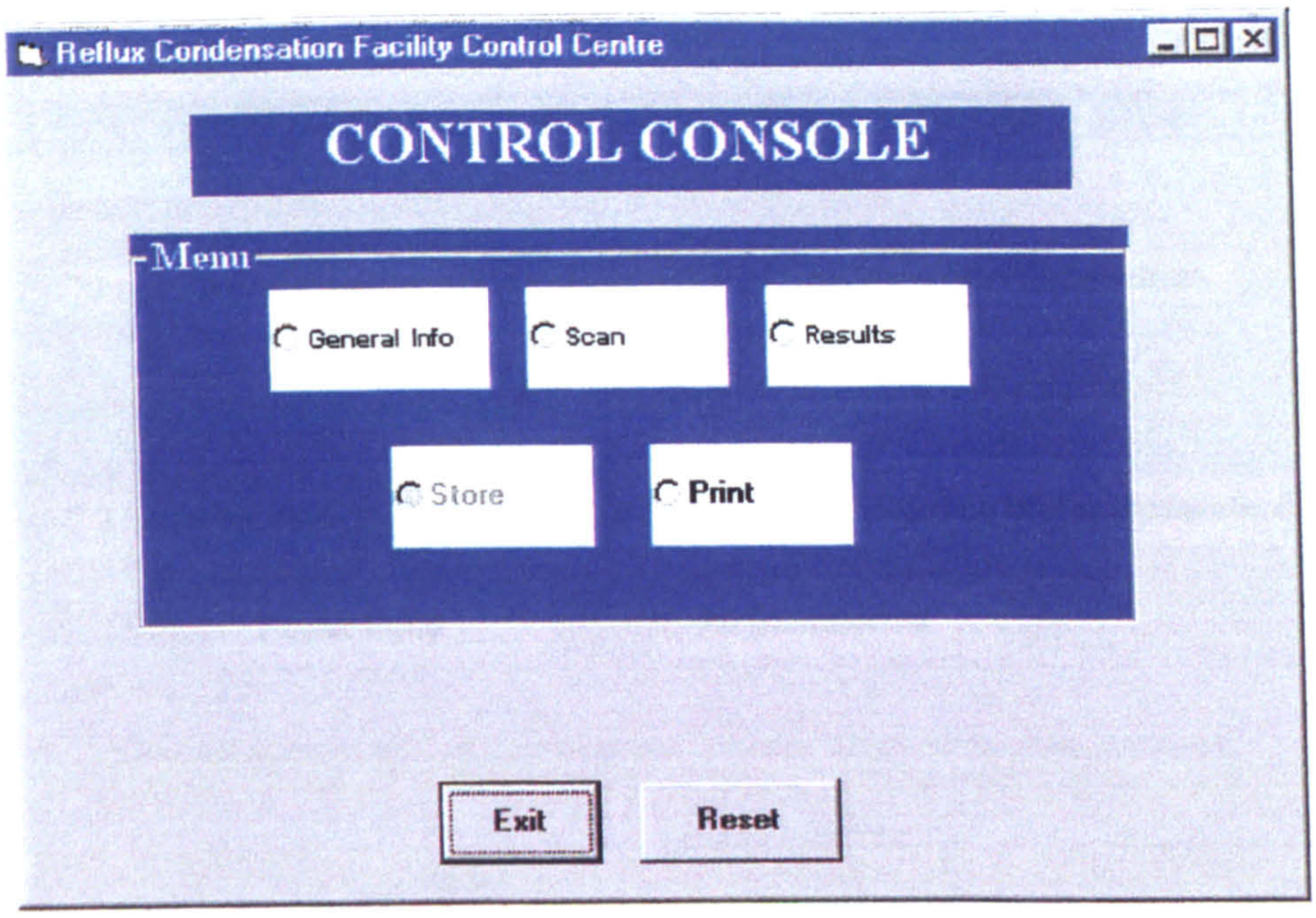

Figure 4.12. The control window in the data acquisition program.

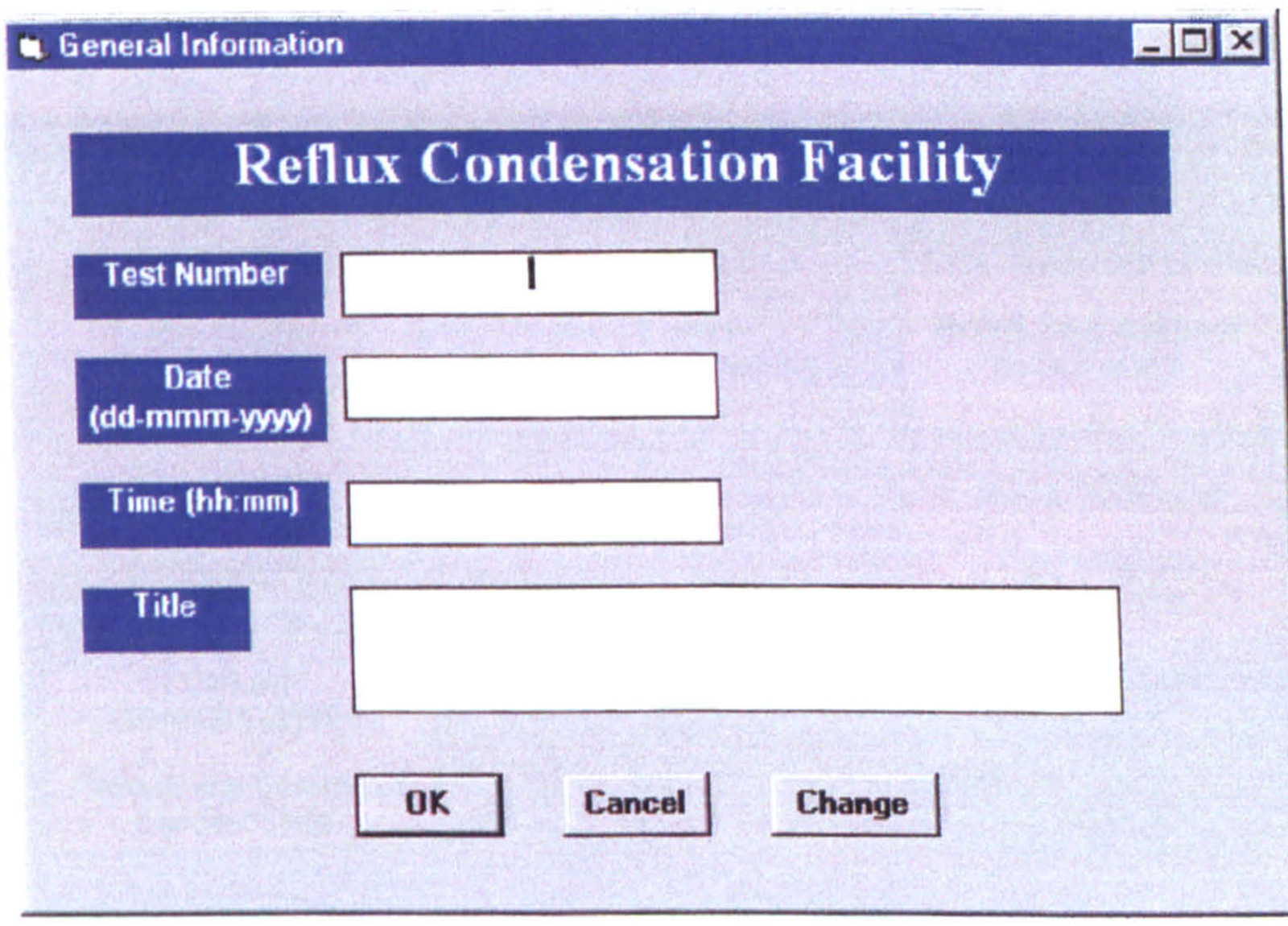

Figure 4.13. The general information window in the data acquisition program.

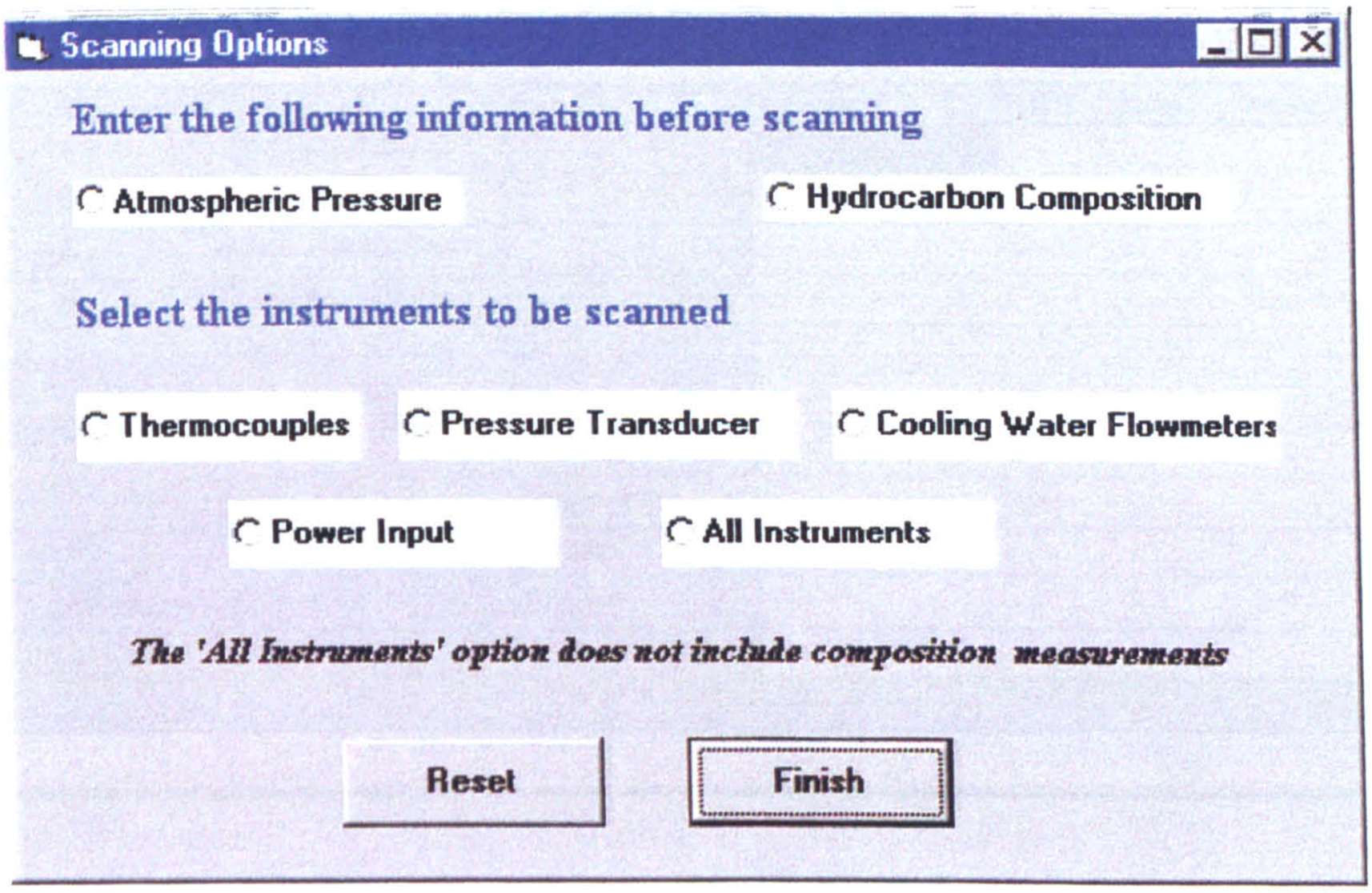

Figure 4.14. The scanning options window in the data acquisition program.

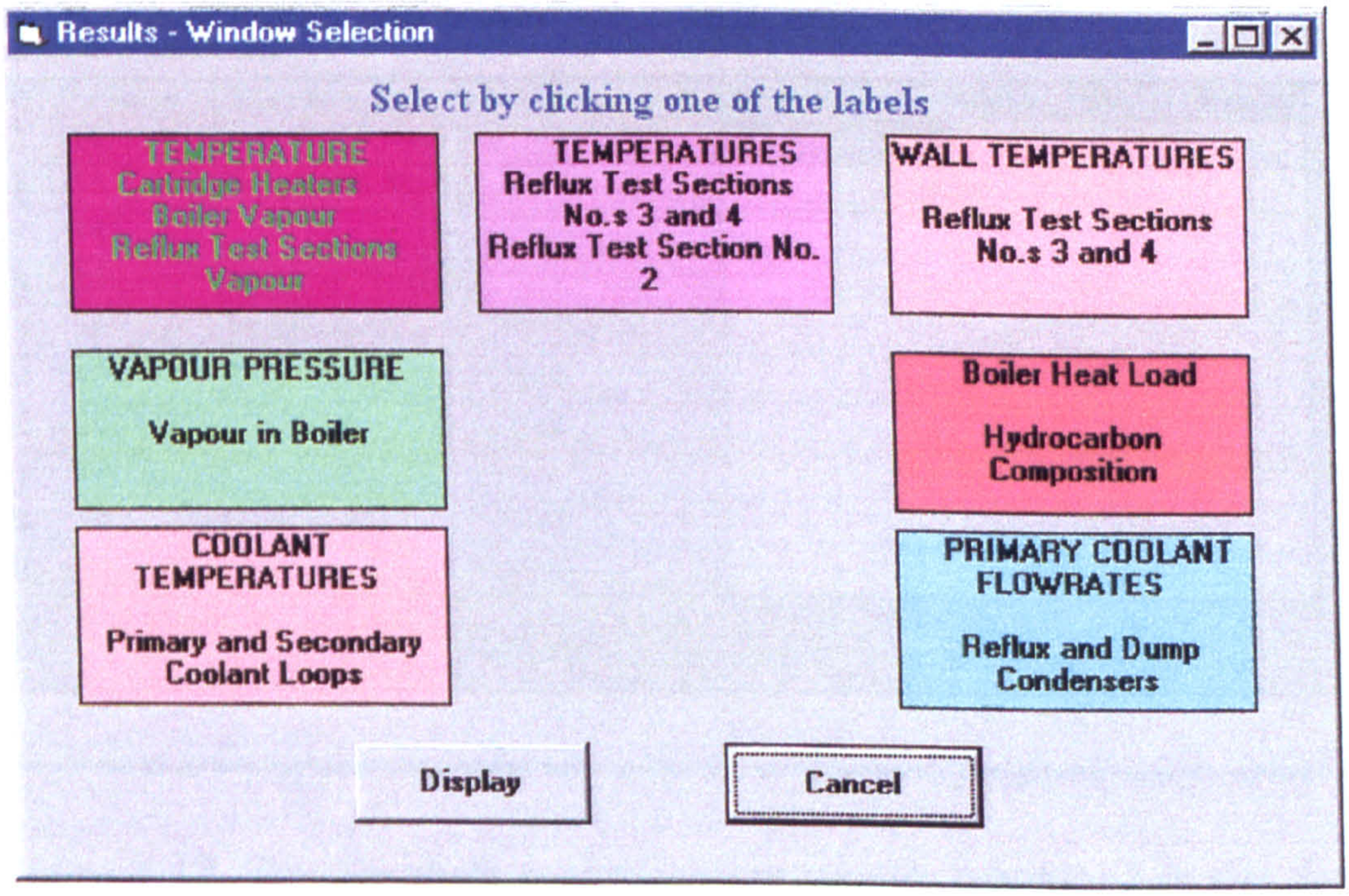

Figure 4.15. The results window in the data acquisition program.

Temperature Measurements - 1

ALT-F4 to close. Page-up
Page-down to flip through sheets

Unit: Celsius

T/C	Channel	Equipment	Stream	Average	RMS	Min.	Max.
1	1	Cartridge Heater					
2	2	Cartridge Heater					
3	3	Cartridge Heater					
4	4	Cartridge Heater					
5	5	Cartridge Heater					
6	6	Cartridge Heater					
7	7	Boiler	Vapour				
8	8	VCC	Ambient Air				
9	9	Reflux TS No. 2	Vapour				
10	10	Reflux TS No. 3	Vapour				
11	11	Reflux TS No. 4	Vapour				

Figure 4.16. Temperature measurement results window 1 in the data acquisition program.

Temperature Measurements - 2

ALT-F4 to close. Page-up, page-down to move to other results

Unit: Celsius

T/C	Channel	Equipment	Stream	Average	RMS	Min.	Max.
12	12	Entry to TS No.3	C.W.				
13	13	Entry to TS No.4	C.W.				
14	14						
15	15						
16	16	Intercooler	CW/Glycol				
17	17	Reflux TS No.2	Wall				
18	18		Wall				
19	19		Wall				
20	20		Wall				
21	21		Wall				

Figure 4.17. Temperature measurement results window 2 in the data acquisition program.

Temperature Measurements - 3

ALT-F4 to close. Page-up, page-down to move to other results

Unit: Celsius

T/C	Channel	Equipment	Stream	Average	RMS	Min.	Max.
22	22	Reflux TS No. 3	Wall				
23	23		Wall				
24	24		Wall				
25	25		Wall				
26	26		Wall				
27	27	Reflux TS No. 4	Wall				
28	28		Wall				
29	29		Wall				
30	30		Wall				
31	31		Wall				

Figure 4.18. Temperature measurement results window 3 in the data acquisition program.

Temperature Measurements - 4

ALT-F4 to close. Page-up, page-down to move other results.

Unit: Celsius

T/C	Channel	Equipment	Stream	Average	RMS	Min.	Max.
32	32	Dump Condenser	Condensate				
33	33	Reflux TS	C.W. inlet				
34	34		C.W. outlet				
35	35	Dump Condenser	C.W. inlet				
36	36		C.W. outlet				
16	16	Intercooler outlet	Secondary coolant				
37	37	Outhouse	Ambient Air				

Figure 4.19. Temperature measurement results window 4 in the data acquisition program.

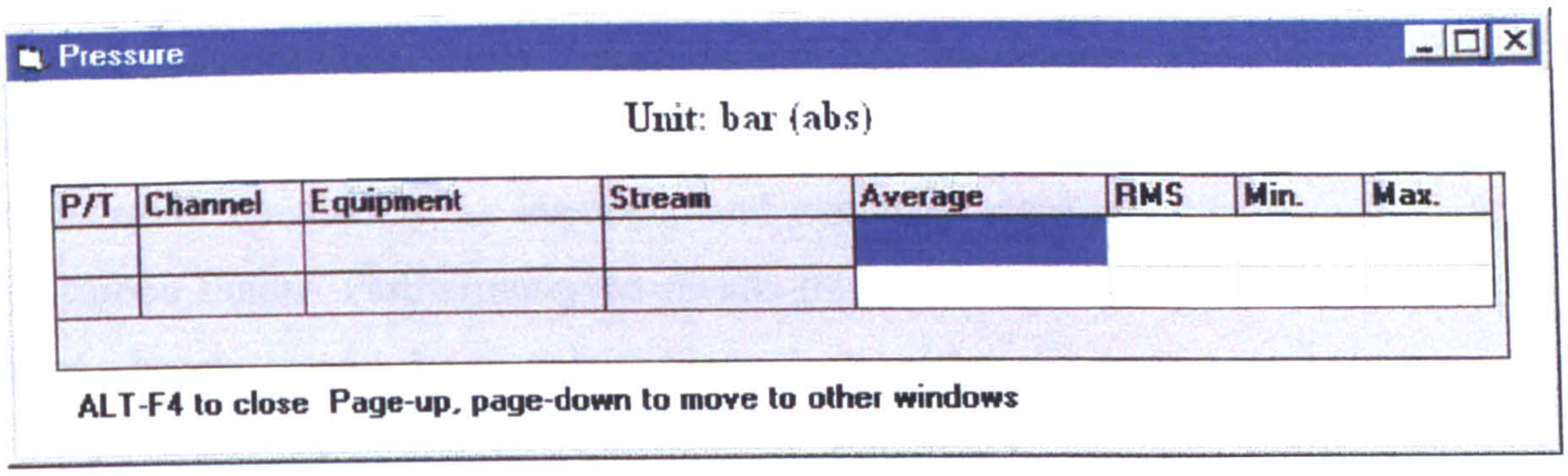

Figure 4.20. Pressure measurement results window in the data acquisition program.

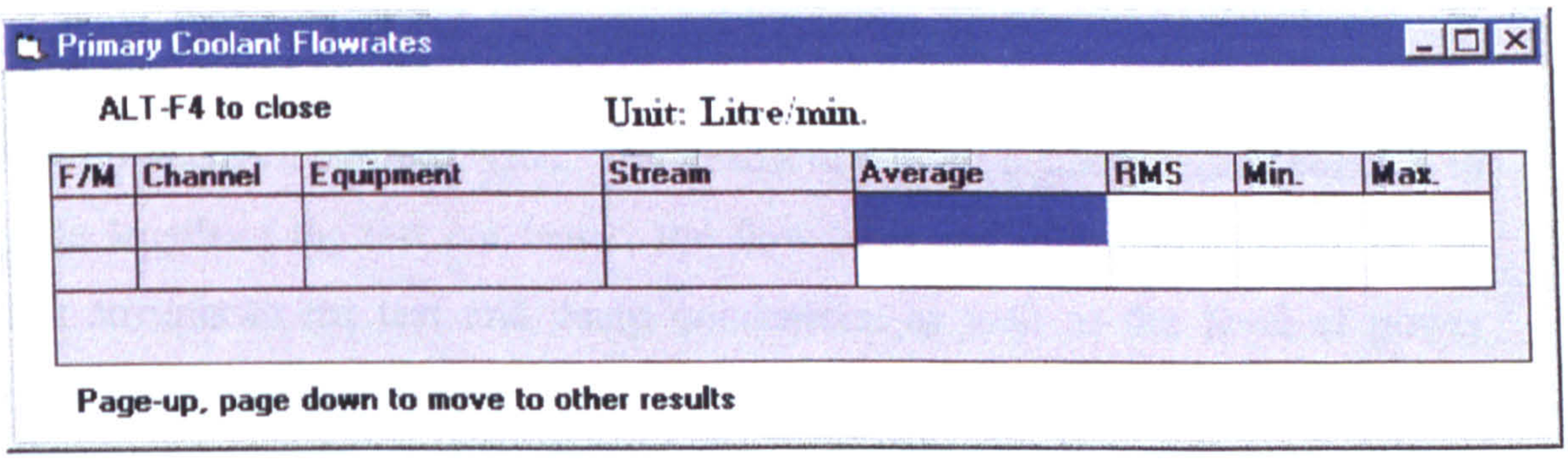

Figure 4.21. Primary coolant flow rate measurement results window in the data acquisition program.

4.4 Description of the Experimental Method

Following commissioning work with purified water, two single component hydrocarbons were used, firstly n-pentane and then iso-octane. These fluids were used prior to the binary hydrocarbon mixtures to ascertain whether the measurement systems were functioning as intended, and that they were suitable for use with hydrocarbon fluids. Furthermore, the results from the single component tests were used as a benchmark for the work with binary hydrocarbon mixtures.

The methods outlined below follow procedures developed and carried out by the author, based on experience gained during the commissioning stage of the project. The procedures for starting-up and shutting-down the test facility and the general method of getting the facility to a steady state formed the basic structure of the operating procedures drafted by the author.

The experimental programme for tests with the single component hydrocarbons and their binary mixtures was based on the results of tests carried out during commissioning with purified water. The design of the test facility made it possible to vary the length of the test condenser, the flow rates and inlet temperatures of the coolant streams to the test and dump condensers, as well as the level of power supplied to the cartridge heaters.

The operating pressure (and hence temperature) of the test facility was controlled by controlling the rates of heating and cooling. The rate of heating was changed by varying the level of power supplied to the cartridge heaters, and the rate of cooling by varying the flow rates of coolant to the test and dump condensers. Further control of the operating pressure could have been possible by varying the inlet temperatures of the coolant streams to both condensers. However, in practice this was found to be

less reliable than the other two methods mentioned, and so the inlet temperatures of both coolant streams were fixed. It was normal practice to set the inlet temperatures of both coolant streams at least 10°C above the measured atmospheric temperature. This condition could be controlled by the secondary cooling circuit to ensure steady operation of the test facility.

To ensure a measurable temperature rise on the coolant side of the test condenser, and thus reduce the likelihood of errors in the heat balance calculations, the coolant flow rate to the test condenser was set at a fixed value. The rate of coolant was chosen as approximately two-thirds of the maximum flow rate when operating with all three of the test sections in series. This had been found to give a measurable temperature rise on the coolant side across each of the test sections.

The length of the test condenser and the level of power supplied to the cartridge heaters were both varied. The length of the test condenser was varied by changing the number of test sections that were operated in series, from a minimum of one to a maximum of three. The power level supplied to the cartridge heaters was capable of being varied between 1 and 6kW.

4.4.1 General Procedure

Before adding any fluid, the test fluid circuit was purged several times with oxygen-free nitrogen, before a vacuum was drawn and maintained for twenty-four hours. This was carried out to ensure the test fluid circuit was kept as clean as possible, and that traces of any previous fluid were completely removed without having to add special cleaning chemicals.

For each test fluid, the volume of liquid used was approximately 20 litres. This ensured that the liquid level in the boiler was well above the level of the cartridge heaters, and also above the level of the composition measurement ports.

The test facility was charged with fluid through a line connected to the base of the boiler shell, with a pneumatically operated transfer pump and a manual valve positioned in this line to assist the filling process. A vacuum pump was used to remove any air from the test fluid circuit prior to start-up, thus ensuring that the temperature and pressure measured in the boiler vapour space corresponded as closely as possible to a saturation condition. With the volatile hydrocarbon test fluids, it was possible for small amounts of the fluid to be lost through natural evaporation, or when removing any air from the system prior to start-up.

Having established saturation conditions in the boiler with the heaters turned off, the primary and secondary coolant pumps were switched on. The flow rate of secondary coolant was set at a nominal value to ensure a steady flow through the air-cooled heat exchanger. The flow rate of primary coolant through the dump condenser was kept at a maximum to help completely condense the exit vapour from the test condenser.

The flow rate of primary coolant through the test condenser was reduced to the required flow rate by partly closing the control valve. In addition, the number of test sections to be operated was set by opening or closing the relevant solenoid valves. These valves would allow the flow of coolant to reach the inlet ports of the test sections when open. It was normal during start-up for all three of the test sections to be opened to coolant flow, and it was usual to set the flow in one of two ways, as illustrated in Figure 4.22 [p.100]:

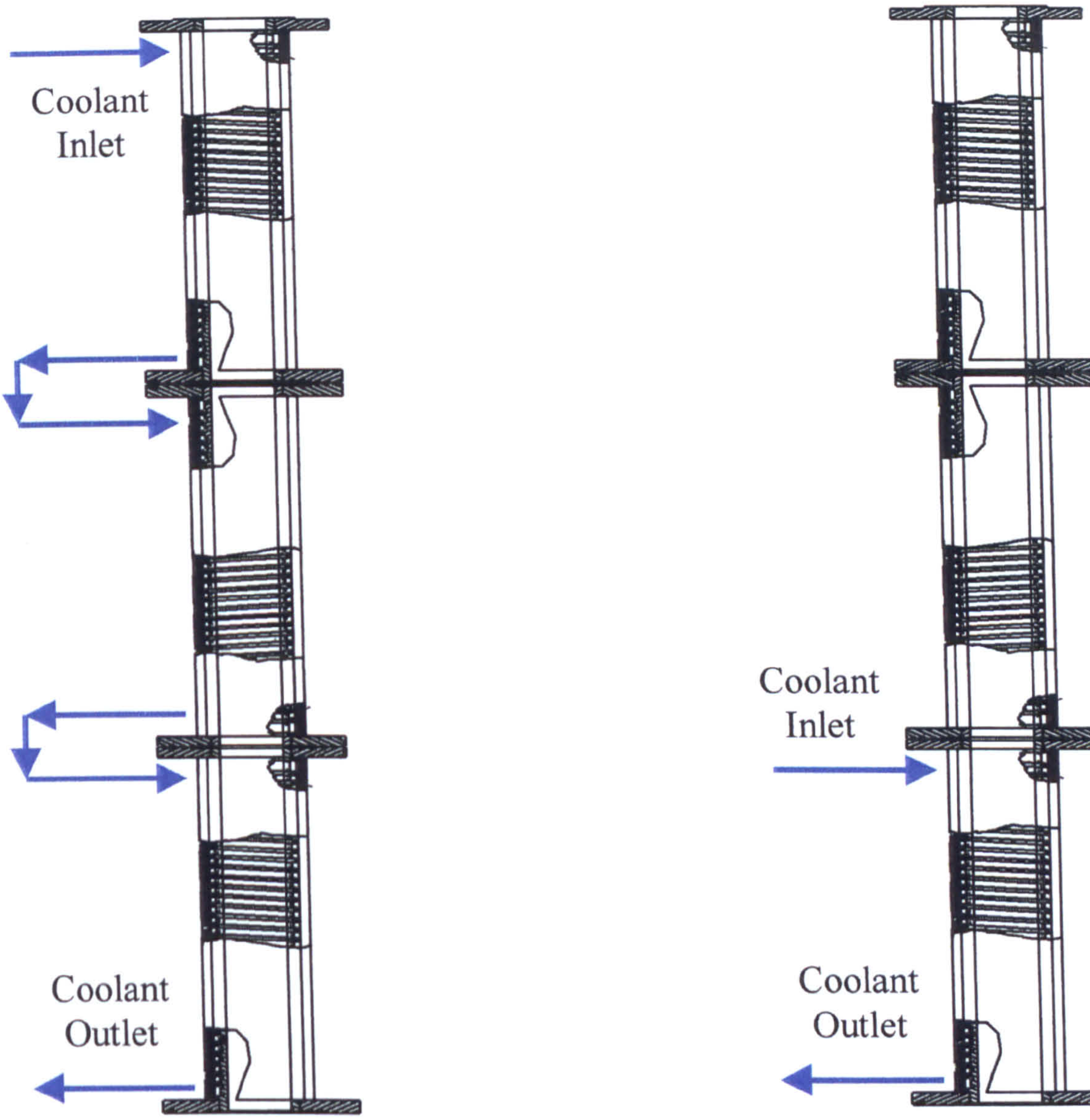

Figure 4.22. The arrangement of test condenser test sections during experimental work.

1. Coolant was set to flow into the top test section only, flow through the remaining two test sections and exit from the outlet of the lowest test section, or

2. Coolant was set to flow into the bottom test section, flow through this test section, and exit from the outlet of this test section.

Such a system ensured that the test sections were operated in series rather than in parallel, and that it was possible to investigate the effect of condenser length on the reflux condensation process. Unfortunately, it was later discovered that the manifold system installed to control the flow of coolant to each of the test sections had failed to shut-off coolant flow to the middle and top test sections when it was assumed only the bottom test section was operating. As a result, only the test data and subsequent analysis for those tests carried out across all three of the test sections has been included in this thesis.

The inlet temperatures of the coolant streams to the test and dump condensers were adjusted by changing the settings of the three way temperature-controlled valves. Finally, the power level supplied to the cartridge heaters was set by adjusting the voltmeter and ammeter readings to produce either half power, or full power levels. These conditions were maintained until the facility was deemed to be operating at steady state, which normally took between two-and-a-half to three hours. The test facility was deemed to be operating under steady state conditions when the measured operating temperatures on the test fluid side did not vary by more than 0.2°C.

At this point, the data acquisition software was used to record the operating conditions of the test facility. Readings from all the instrumentation were taken and stored as a file, with a full printout of the readings also made. The practice was

adopted of taking four snapshots of each steady state condition, which took around eight minutes to complete.

Having recorded the fourth snapshot, the operating conditions of the test facility were adjusted to reach the next steady-state condition. Around half-an-hour was required before the new steady state condition was reached, after which the data acquisition software was used again to record four snapshots of this condition. This was repeated until all the experimental conditions were covered and data had been recorded at each of the conditions achieved.

Having completed the experiment, the cartridge heaters were switched off by reducing the voltmeter and ammeter settings. The flow of primary coolant to the test condenser was maximised by fully opening the flow control valve, and all three of the test sections were opened. The primary and secondary coolant pumps were left running until the test facility had cooled by around twenty degrees before they were switched off. After this, all power to the facility was turned off.

4.4.2 Experimental Method when testing with n-Pentane

The primary coolant flow rate through the test condenser was set at approximately 6 litres/minute, and the inlet temperature of this stream was set at 25°C. Tests were run at 3 and 6kW across all three of the test sections, and were then repeated across the lowest of the test sections in the test condenser.

Tests run at 6kW achieved the highest operating temperatures and pressures. This also meant that the amount of condensate produced in the test condenser was greatest, thus the condensate film Reynolds numbers in the test condenser were

higher than those at any other condition. By reducing the level of power to 3kW and then by changing the number of test sections from three to one, it was the aim to cover a range of saturation conditions and condensate film Reynolds numbers.

4.4.3 Experimental Method when testing with Iso-octane

The primary coolant flow rate through the test condenser was set at approximately 6 litres/minute, and the inlet temperature of this stream was set at 25°C. Tests were run at 2kW across all three of the test sections, and were then repeated across the lowest of the test sections in the test condenser.

The difference between these tests and that carried out using n-pentane was the change in power level supplied to the cartridge heaters. Initial tests with iso-octane at 3kW were carried out but quickly terminated when it was observed that the condensate film produced in the test condenser did not drain freely from the bottom of the condenser.

Instead, it was seen that intermittent discharging of the condensate occurred rather than the smooth flow of liquid observed when testing with n-pentane. On reducing the power level to 2kW it was found that the condensate was able to drain unhindered from the test condenser.

Consequently, it was decided safer to carry out tests at 2kW and to vary the number of test sections in operation between one and three. This enabled a narrow range of saturation conditions and condensate film Reynolds numbers to be covered.

The results of these single component hydrocarbon tests were used to show how the condensate-film heat transfer coefficient varied with the condensate film Reynolds number.

4.4.4 Experimental Method when testing with Binary Hydrocarbon Mixtures

The binary hydrocarbon mixtures were each prepared in-house by mixing the two pure components in different quantities to obtain the desired mole fraction amount in the liquid. The mixtures were prepared on a mass basis, in a large plastic container, and were immediately transferred and added to the test facility.

The primary coolant flow rate through the test condenser was set at approximately 6 litres/minute, and the inlet temperature of this stream was set at 25°C. Tests were run at 3 and 6kW across all three of the test sections, and were then repeated across the lowest test sections in the test condenser.

It was the aim of these experiments to show how the heat transfer coefficients on the condensing side varied with the condensate film and vapour Reynolds numbers. Once more, this was achieved by adjusting the levels of heating and the test condenser surface area to cover a range of saturation conditions and condensate film and vapour Reynolds numbers.

In addition, composition measurements were also made of the reflux condensate from the test condenser and of the exit condensate from the dump condenser. Compositions were measured on-line using a vibrating cell densitometer only when the test facility was operating under steady state conditions.

A small flow rate of the condensate stream to be measured was sampled from the test fluid circuit by opening the relevant valves and switching on a small, variable speed gear pump. Before passing into the densitometer, the sample was cooled in a water bath, and the water in this bath was passed over the measuring cell to control the temperature. During the actual measurement, the sample was isolated in the cell by closing all valves and stopping the pump. The temperature of the cell was allowed to equalise before a reading was recorded.

4.5 Description of the Calculation Methods

This section describes the methods used to analyse the experimental data from the test facility. It begins by defining some of the surface and flow areas required for calculations on the condensing side and the coolant side for both the test and dump condensers. This is followed by a description of the method used for evaluating the physical properties of the coolant, the condensate film, and the condensing vapour. The data analysis procedure for the single component hydrocarbon tests is then given followed by that for the binary hydrocarbon mixture tests.

The author spent considerable time developing the data analysis systems for the single component hydrocarbon tests and those with binary hydrocarbon mixtures. The sequence of calculations was developed to enable the mean experimental heat transfer coefficients on the condensing side to be calculated using the instrumentation available in the test facility. The data analysis system took the form of a series of spreadsheets which, in addition to storing the experimental test data, carried out the following:

- Prediction of the physical properties of the coolant streams in each of the test sections and in the dump condenser, of the reflux condensate from the test

condenser, of the condensate in the dump condenser, and of the vapour in the test condenser,

- Heat transfer calculations across each of the test sections in operation and the dump condenser,

- Mass balance calculations across each of the test sections in operation and across the dump condenser, and estimation of the vapour velocity entering the bottom of the test condenser,

- Determination of the logarithmic-mean temperature differences, and evaluation of the mean overall heat transfer coefficients across each of the test sections in operation,

- Evaluation of the mean tube-wall heat transfer resistances for each of the test sections in operation,

- Determination of the coolant Reynolds and Prandtl numbers and evaluation of the mean coolant heat transfer coefficients for each of the test sections in operation, and

- Calculation of the condensate film and vapour Reynolds and Prandtl numbers, and evaluation of the mean experimental condensing-side heat transfer coefficients for each of the test sections in operation.

In developing the system, the author created user-defined functions, written in Visual Basic program code to perform the majority of the calculations. This became particularly useful when it was necessary for the calculations to perform simple linear interpolations, or when conditional statements were included.

Copies of these functions have been included in the appendices for reference. The functions written for analysis of the single component hydrocarbon tests are given in Appendix A3 and those for analysis of the binary hydrocarbon mixture tests are given in Appendix A4.

4.5.1 Geometry Calculations

The inner heat transfer surface area of the dump condenser was calculated using

$$A_{i,DC} = \pi \, d_{i,DC} L_{DC} \tag{4.5.1}$$

The inner heat transfer surface area of a single test section was calculated using a similar equation.

$$A_{i,TS} = \pi \, d_{i,TS} L_{TS} \tag{4.5.2}$$

As the number of test sections in operation varied, so the total inner heat transfer surface area of the test condenser also varied. However, as the test sections were geometrically identical, the total inner heat transfer surface area of the test condenser

was obtained simply by multiplying the area of one test section found in (4.5.2) by the number of test sections in operation.

As described in Chapter 4.1.2, the outer surfaces of the test sections were machined to produce a small rectangular channel through which the coolant flowed. A sketch of a typical test section was shown in Figure 4.10 [p.84], and a sketch showing the coolant flow channel in more detail is given in Figure 4.23 [p.109].

The flow area of this small rectangular coolant flow channel was calculated by

$$S_{flow,c} = w_c h_c \tag{4.5.3}$$

The coolant flow channel machined into the outer surface of each of the test sections followed a helical path around the outer surface of the test section. Making the assumption that the geometry of the coolant flow channel could be likened to a helical coil of rectangular cross-section, the length that the coolant flowed through in a single test section was found using ESDU (1978).

$$L_{flow,c,TS} = \pi\, d_o N_r \left[1 + \frac{s^2}{\pi^2 d_o^2}\right]^{1/2} \tag{4.5.4}$$

This was also the length through which heat was transferred to the coolant from the condensing vapour inside the test section. The outer heat transfer surface area relevant to the coolant heat transfer coefficient was found by multiplying the length

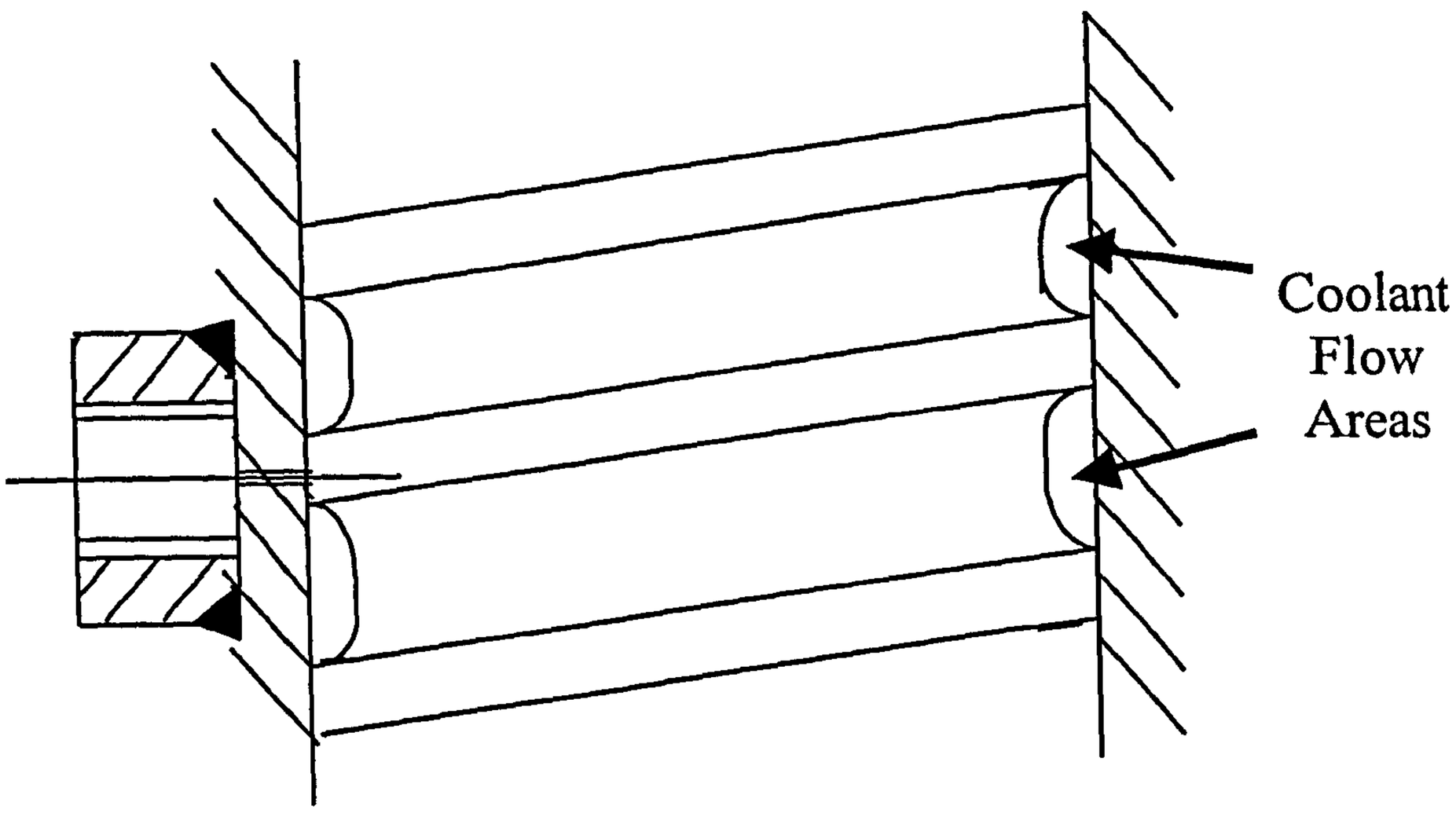

Figure 4.23. Details of the coolant flow channel around a test section.

of the channel, as calculated from (4.5.4) above, by the heated perimeter of the rectangular channel.

Figure 4.24 [p.111] shows a sketch of the rectangular channel and highlights the surfaces through which heat was transferred, thus the heated perimeter was defined by (4.5.5) below.

$$p_{heat,c} = w_c + 2h_c \tag{4.5.5}$$

Therefore, the equation for the outer heat transfer surface area of a test section relevant to the coolant heat transfer coefficient was defined as

$$A_{o,c,TS} = L_{flow,c,TS}\, p_{heat,c} \tag{4.5.6}$$

$$A_{o,c,TS} = \pi\, d_o N_r \left[1 + \frac{s^2}{\pi^2 d_o^2}\right]^{1/2} (w_c + 2h_c) \tag{4.5.7}$$

The total surface area for the test condenser was found simply by multiplying this area by the number of test sections operating.

The thickness of the test section wall through which heat was transferred was calculated using (4.5.8), where d_w was the base tube diameter and not the outer diameter of the test section.

Surfaces in RED have heat transferred through them.

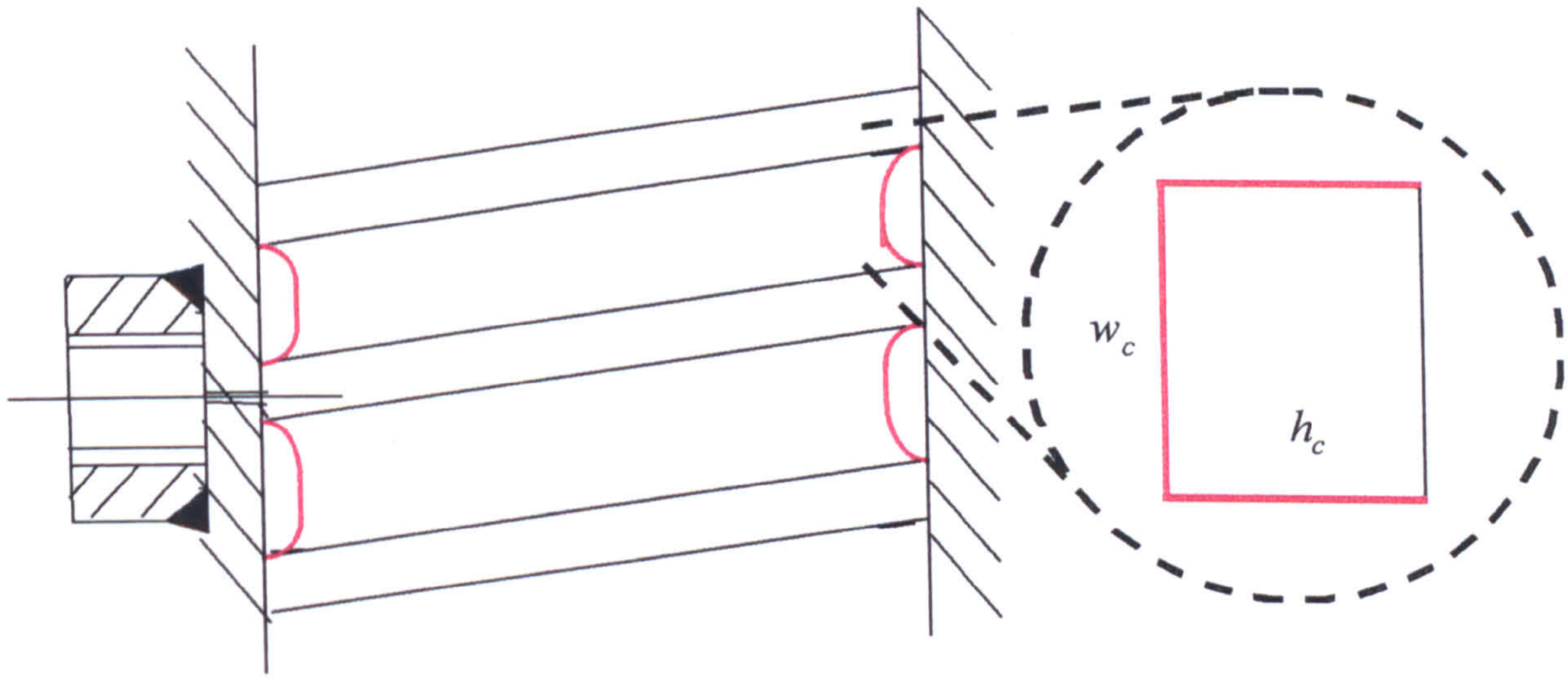

Figure 4.24. The heat transfer surfaces of the coolant flow channel.

$$x_w = \frac{d_w - d_i}{2} \tag{4.5.8}$$

As no coolant was in contact with the outer diameter of the test section, it was assumed that no heat was transferred through this surface to the coolant. The temperature difference between the base tube diameter and the outer diameter of the test section was therefore assumed to be small. Thus the thickness of the tube wall through which heat was assumed to pass was taken as the distance between the tube inner diameter and the outer diameter of the base tube.

The outer heat transfer surface area of a single test section relative to this base tube diameter, and used in the calculation of the tube-wall heat transfer resistance, was therefore determined from

$$A_{o,w,TS} = \pi \, d_{w,TS} L_{TS} \tag{4.5.9}$$

4.5.2 Physical Property Calculations

All physical property calculations were carried out using the Physical Property Data Service (PPDS) software package. To determine any of the physical properties, specific information had to be provided for the model to execute properly. This information concerned the thermodynamic state and composition of the phase, full details of which are provided below.

COMPONENT NAME	Name of the stream component as recognised by PPDS.

COMPONENT NUMBER	Reference value for the named stream component as recognised by PPDS. Each component has a unique value.
COMPOSITION	Molar concentration of the stream component.
PHASE	Numerical value to indicate if the phase is vapour or liquid.
IDEAL	Numerical value to indicate if the calculation is for an ideal or real mixture.
TEMPERATURE	Defines the stream temperature in Kelvin.
PRESSURE	Defines the stream pressure in Pascals.
PROPERTY	Numerical value which specifies the physical property to be evaluated. Each physical property is identified by a unique numerical value.

4.5.3 Data Analysis for Single Component Hydrocarbon Tests

Figure 4.25 [p.115] illustrates the flows of mass and energy across a typical test section in the test condenser for a single component hydrocarbon. Vapour enters the bottom of the test section at its saturation temperature and with some mass flow rate. A fraction of this vapour is condensed, and so the mass flow rate of vapour leaving the top of the test section is less than that entering. As the condensation is known to occur isothermally, and this was confirmed by measurement of the vapour temperature progressively up through the test condenser, the exit temperature of the vapour equals that at the inlet.

Some condensate may also enter the test section. The condensate temperature was not measured but it will be somewhere between the inner wall temperature and the vapour saturation temperature. Due to condensation of some fraction of the vapour, the mass flow rate of condensate is higher at the bottom of the test section than it was at the top. The temperature of the condensate leaving the test section may also have changed but once more no measurement was made.

The heat released by the condensation of a fraction of the vapour is passed to the coolant. The mass flow rate of coolant through the test section remains constant, but its temperature will be higher at the outlet than it was at the inlet.

Heat Transfer Calculations across the Test Condenser

The heat released by this condensation was determined from (4.5.10), where the coolant specific heat capacity was calculated as a function of its inlet temperature and stream pressure using PPDS.

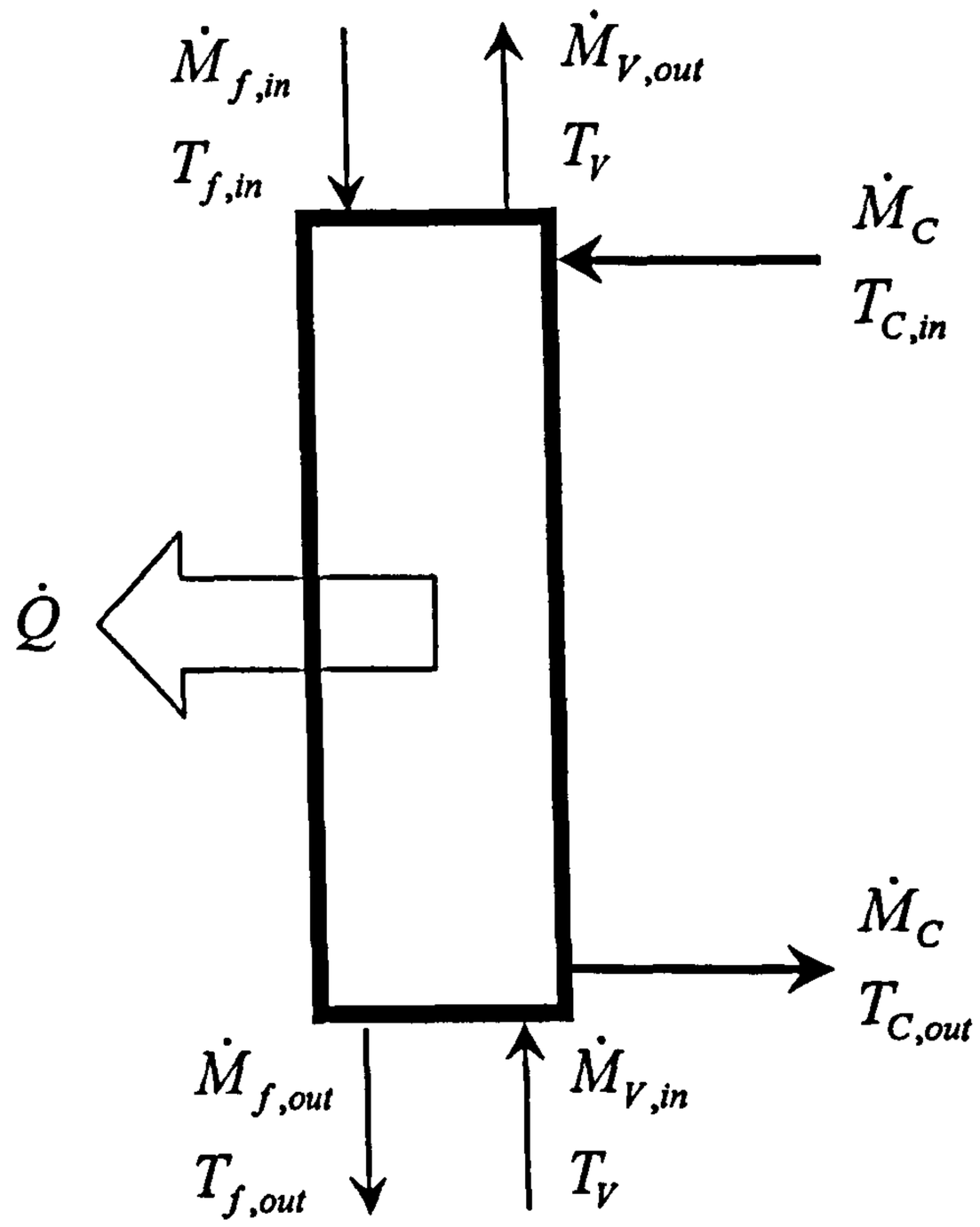

Figure 4.25. Mass and energy balances when condensing a single component hydrocarbon.

$$\dot{Q}_c = \dot{M}_c Cp_c \left(T_{c,out} - T_{c,in}\right) + \dot{Q}_{losses} \tag{4.5.10}$$

Despite the provision of insulation on the outer surfaces of the test and dump condensers, some heat may still be lost to the surroundings through these surfaces. This loss could have been estimated from measurements made of the surface and surrounding air temperatures. As no instrumentation was available for accurately measuring these temperatures, it was assumed that the rate of heat loss was negligible. This point is discussed later in Chapter 5.

Thus the second term on the right-hand side of (4.5.10) was assumed to be zero.

$$\dot{Q}_c = \dot{M}_c Cp_c \left(T_{c,out} - T_{c,in}\right) \tag{4.5.11}$$

The mean overall heat transfer coefficient was found from

$$\overline{U}_i = \frac{\dot{Q}_c}{A_i \Delta T_{\ln}} \tag{4.5.12}$$

The logarithmic-mean temperature difference, commonly used for the condensation of single components, was defined by

$$\Delta T_{\ln} = \frac{\left(T_{c,out} - T_{c,in}\right)}{\ln\left[\dfrac{T_v - T_{c,in}}{T_v - T_{c,out}}\right]} \tag{4.5.13}$$

The mean overall heat transfer coefficient was related to the other heat transfer resistances by the equation

$$\frac{1}{\overline{U}_i} = \frac{1}{\overline{\alpha}_{f,i}} + \left(\frac{A_i}{A_{o,c}}\right)\frac{1}{\overline{\alpha}_c} + \left(\frac{A_i}{A_{o,w}}\right)\frac{x_w}{\lambda_w} \qquad (4.5.14)$$

The heat transfer surface areas were calculated using the relevant equations defined in Chapter 4.5.1. The mean coolant heat transfer coefficient was determined using an experimentally derived correlation. This correlation was unique to this test facility, and is discussed in more detail in Chapter 5.2. The tube-wall material thermal conductivity was calculated as a function of the mean tube wall temperature, as measured by the five thermocouples across each test section.

Rearranging (4.5.14), the mean experimental condensate-film heat transfer coefficient was found from

$$\frac{1}{\overline{\alpha}_{f,i}} = \frac{1}{\overline{U}_i} - \left\{\left(\frac{A_i}{A_{o,c}}\right)\frac{1}{\overline{\alpha}_c} + \left(\frac{A_i}{A_{o,w}}\right)\frac{x_w}{\lambda_w}\right\} \qquad (4.5.15)$$

(4.5.11) to (4.5.13) were applied to determine the rates of heat transfer and the mean experimental heat transfer coefficients involved in each of the test sections, and were then applied across the entire length of the test condenser.

Mass Transfer Calculations across the Test Condenser

The mass of vapour condensed in a test section was found by dividing the amount of heat transferred, found from (4.5.11), by the latent and sensible heat effects, where both these terms were calculated as a function of the vapour temperature and pressure using PPDS.

$$\left(\dot{M}_{v,in} - \dot{M}_{v,out}\right) = \frac{\dot{Q}_c}{\Delta h_v + Cp_f\left(T_v - T_{f,out}\right)} \tag{4.5.16}$$

With no instrumentation available to measure the extent of liquid sub-cooling in a test section, an estimate was made of the condensate film mass flow rate at the bottom of each test section. This was done by ignoring the contribution due to sub-cooling, which is usually much smaller in comparison to the latent heat term, using

$$\left(\dot{M}_{v,in} - \dot{M}_{v,out}\right) = \frac{\dot{Q}_c}{\Delta h_v} \tag{4.5.17}$$

The mass flow rate of condensate leaving the test section was found by adding the result of (4.5.17) to the mass flow rate of condensate entering the test section.

$$\dot{M}_{f,out} = \dot{M}_{f,in} + \left(\dot{M}_{v,in} - \dot{M}_{v,out}\right) \tag{4.5.18}$$

For the analysis over the entire test condenser length, the reflux condensate temperature was estimated based on the work of Rohsenow (1956).

$$T_{f,out} = 0.68T_v + 0.32\overline{T}_w \tag{4.5.19}$$

Thus an estimate of the reflux condensate flow rate, with the allowance of condensate sub-cooling, was found from (4.5.16).

Heat and Mass Transfer Calculations across the Dump Condenser

With the same assumption of negligible heat losses across the dump condenser cooling jacket, the heat released by the complete condensation of the vapour leaving the test condenser was determined using the measured conditions from the dump condenser coolant stream. The coolant specific heat capacity was calculated as a function of its inlet temperature and stream pressure using PPDS.

$$\dot{Q}_{c,DC} = \dot{M}_c Cp_c \left(T_{c,out} - T_{c,in}\right)_{DC} \tag{4.5.20}$$

In addition to condensation in the dump condenser, the condensate produced was sub-cooled below the vapour saturation temperature. The mass of condensate that was returned to the boiler from the dump condenser was therefore found using (4.5.21), where the latent heat and condensate specific heat capacity were both evaluated as functions of temperature and pressure using PPDS.

$$\dot{M}_{f,out,DC} = \frac{\dot{Q}_{c,DC}}{\Delta h_v + Cp_f\left(T_v - T_{f,out}\right)_{DC}} \tag{4.5.21}$$

The mass flow rate of vapour entering the test condenser was taken as the sum of the mass flow rate of condensate from the test and dump condensers, which would vary depending upon whether condensate sub-cooling in the test condenser was taken into consideration in the analysis.

4.5.4 Data Analysis for Binary Hydrocarbon Mixture Tests

Figure 4.26 [p.121] illustrates the flows of mass and energy across the test condenser for a binary hydrocarbon mixture. A fraction of the vapour mixture that enters the test condenser is condensed, and so the flow rate of vapour leaving the test condenser is less than that entering. In addition, the temperature of the vapour decreases, and the concentration of the more volatile component in the exit vapour stream is assumed to be less than that in the inlet stream.

As the composition of the exit vapour phase and of the reflux condensate from the test condenser were both measured, a mass balance was carried out across the full length of the condenser. It was assumed that no condensate entered at the top of the test condenser. The condensate leaves the bottom of the condenser at a temperature somewhere between the inner wall temperature and the vapour inlet temperature.

All heat released by cooling and condensing the vapour, and any sensible heat transfer in the condensate film is passed to the coolant. The mass flow rate of coolant through the test section remains constant, but its temperature will be higher

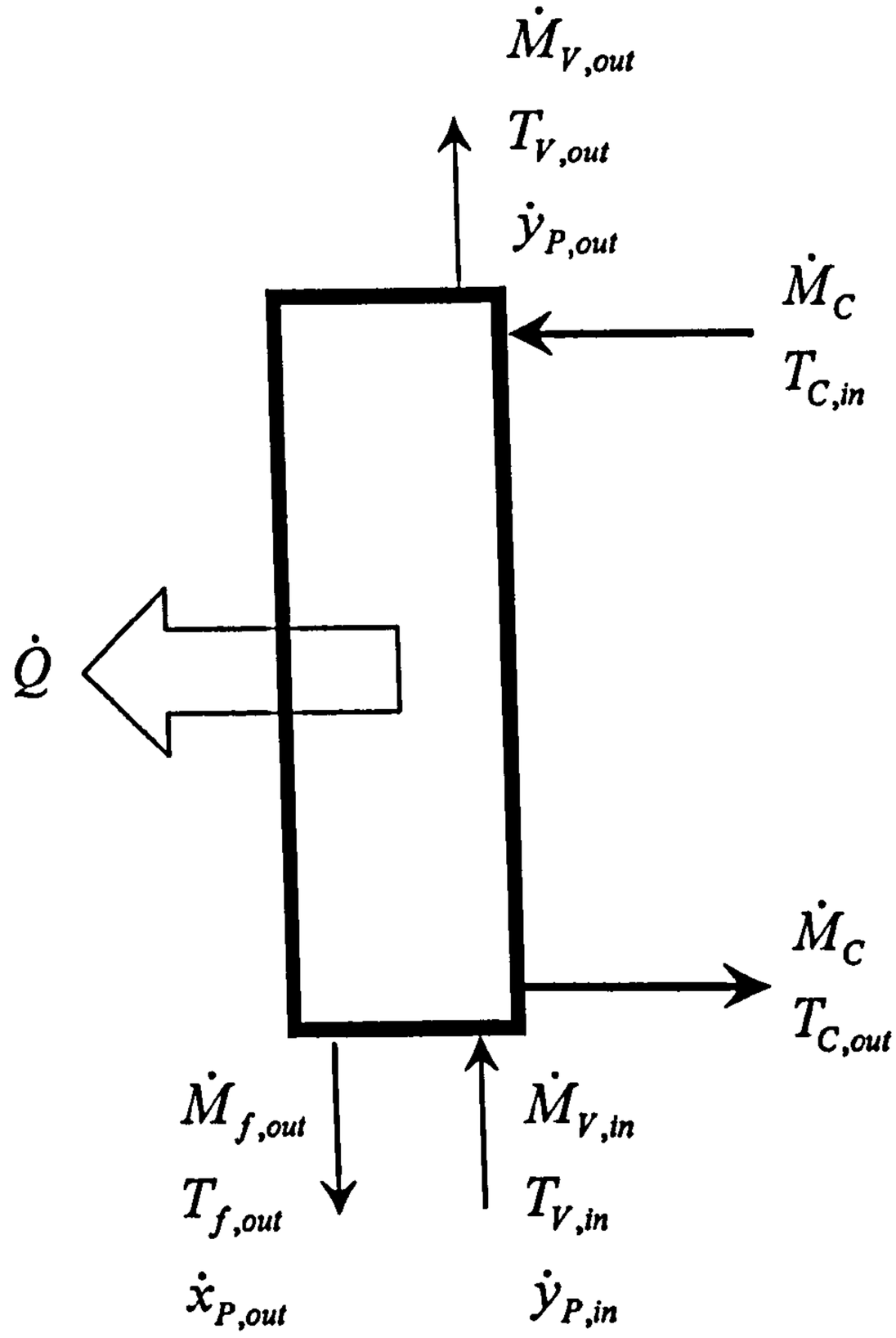

Figure 4.26. Mass and energy balances when condensing a binary hydrocarbon mixture.

at the outlet than it was at the inlet. Once more it is assumed that the amount of heat lost through the coolant jacket on the test condenser was negligible.

Heat Transfer Calculations across the Test Condenser

The heat released was determined from (4.5.11), where the coolant specific heat capacity was calculated as a function of its inlet temperature and stream pressure. As before, it was assumed that heat losses through the coolant jacket and insulating sleeve were negligible.

$$\dot{Q}_c = \dot{M}_c Cp_c \left(T_{c,out} - T_{c,in}\right) \tag{4.5.11}$$

The mean overall heat transfer coefficient was determined using (4.5.12), where the inner heat transfer surface area was calculated using the equation defined in Chapter 4.5.1.

$$\overline{U}_i = \frac{\dot{Q}_c}{A_i \Delta T_{\ln}} \tag{4.5.12}$$

The logarithmic-mean temperature difference could be defined in terms of the inlet and outlet vapour and coolant temperatures measured across the test section. However, it was found that in a few cases, the very small temperature differences measured at each end of a test section were identical. Thus calculation of the logarithmic-mean temperature difference by this method gave rise to an error in the calculation. To overcome this problem, the logarithmic-mean temperature difference

was defined by (4.5.13), where the vapour temperature used was that measured at the outlet of the test section, i.e. the lowest measured vapour temperature.

$$\Delta T_{\ln} = \frac{\left(T_{c,out} - T_{c,in}\right)}{\ln\left[\frac{T_v - T_{c,in}}{T_v - T_{c,out}}\right]} \tag{4.5.13}$$

The mean overall heat transfer coefficient was related to the other heat transfer coefficients by the equation below. The heat transfer surface areas were calculated using the relevant equations from Chapter 4.5.1, and the mean coolant and tube-wall heat transfer resistances were calculated as described in Chapter 4.5.3.

$$\frac{1}{\overline{U}_i} = \frac{1}{\overline{\alpha}_{cs,i}} + \left(\frac{A_i}{A_{o,c}}\right)\frac{1}{\overline{\alpha}_c} + \left(\frac{A_i}{A_{o,w}}\right)\frac{x_w}{\lambda_w} \tag{4.5.22}$$

The condensing-side resistance included the contribution from the condensate-film and the condensing vapour.

$$\frac{1}{\overline{\alpha}_{cs,i}} = \left(\frac{1}{\overline{\alpha}_{f,i}} + \frac{1}{\overline{\alpha}_{v,i}}\right) \tag{4.5.23}$$

This procedure was carried out across each of the test sections in operation to evaluate the rates of heat transfer and the mean experimental heat transfer coefficients, and was then repeated across the entire test condenser length. The

logarithmic-mean temperature difference calculated across the entire test condenser length was found from

$$\Delta T_{\ln,TC} = \frac{\left(T_{v,in} - T_{c,out}\right) - \left(T_{v,out} - T_{c,in}\right)}{\ln\left[\frac{T_{v,in} - T_{c,out}}{T_{v,out} - T_{c,in}}\right]} \tag{4.5.24}$$

Mass Transfer Calculation across the Test Condenser

The flow rate of reflux condensate produced by cooling and condensing a fraction of the vapour entering the test condenser was found by dividing the condenser coolant heat load by the mixture latent and sensible heat terms.

$$\dot{M}_{f,out,TC} = \frac{Q_{c,TC}}{\Delta h_{v,mix,TC} + Cp_{f,mix,TC}\left(T_v - T_{f,out}\right)_{TC}} \tag{4.5.25}$$

Once more, the method of Rohsenow was used to estimate the temperature of the reflux condensate film at the bottom of the test condenser.

$$T_{f,out} = 0.68T_v + 0.32\overline{T}_w \tag{4.5.19}$$

Strictly speaking, the vapour temperature in (4.5.19) should be replaced by the interface temperature, but no direct calculation of this temperature was made. However, to investigate the effect of using the interface temperature in place of the

vapour temperature, an estimate of the interface temperature was found by rearranging the (4.5.26)

$$\dot{q}_{c,TC} = \frac{1}{\overline{\alpha}_f} + \frac{x_w}{\lambda_w} + \frac{1}{\overline{\alpha}_c}\left(T_I - \overline{T}_c\right) \qquad (4.5.26)$$

For both mixtures it was found that the interface temperature was approximately 20°C less than the vapour temperature. Therefore, using the interface temperature meant that greater sub-cooling of the condensate occurred, and hence the condensate film mass flow rate and Reynolds number were reduced. The condensate-film heat transfer coefficients differed by less than 1%, and the heat transfer coefficients calculated on the vapour side displayed less than 10% difference. Thus it was felt reasonable to use the vapour temperature in estimating the temperature of the reflux condensate film.

The mixture latent heat of vaporisation and the mixture specific heat capacity of the condensate film were defined in terms of the single component values and the mass fractions of liquid condensate obtained by measurement.

$$\Delta h_{v,mix,TC} = \left\lfloor \Delta h_{v,P} \dot{x}_{P,out} + \Delta h_{v,O}\left(1 - \dot{x}_{P,out}\right) \right\rfloor_{TC} \qquad (4.5.27)$$

$$Cp_{f,mix,TC} = \left\lfloor Cp_{f,P} \dot{x}_{P,out} + Cp_{f,O}\left(1 - \dot{x}_{P,out}\right) \right\rfloor_{TC} \qquad (4.5.28)$$

Heat and Mass Transfer Calculations across the Dump Condenser

Using the assumption that heat losses from the dump condenser were negligible, the heat released by cooling and condensing the exit vapour from the test condenser was found from (4.5.20).

$$\dot{Q}_{c,DC} = \dot{M}_c Cp_c \left(T_{c,out} - T_{c,in}\right)_{DC} \tag{4.5.20}$$

As well as cooling and completely condensing the exit vapour from the test condenser, the dump condenser also sub-cooled the condensate below the vapour temperature. As both these temperatures were measured, it was possible to calculate the amount of sensible heat transfer due to condensate sub-cooling.

$$\dot{M}_{f,out,DC} = \frac{Q_{c,DC}}{\Delta h_{v,mix,DC} + Cp_{f,mix,DC}\left(T_v - T_{f,out}\right)_{DC}} \tag{4.5.29}$$

The mixture latent heat of the condensate film was defined by

$$\Delta h_{v,mix,DC} = \left[\Delta h_{v,P}\dot{x}_{P,out} + \Delta h_{v,O}\left(1 - \dot{x}_{P,out}\right)\right]_{DC} \tag{4.5.30}$$

The mixture specific heat capacity was defined by

$$Cp_{f,mix,DC} = \left[Cp_{f,P}\dot{x}_{P,out} + Cp_{f,O}\left(1 - \dot{x}_{P,out}\right)\right]_{DC} \tag{4.5.31}$$

The flow rate of vapour generated in the boiler was the sum of the flow rate of condensate leaving the dump condenser, and the flow rate of reflux condensate produced in the test condenser.

$$\dot{M}_{v,in,TC} = \dot{M}_{f,out,TC} + \dot{M}_{f,out,DC} \tag{4.5.32}$$

Re-writing the above equation in terms of the more volatile component enabled the composition of the vapour entering the test condenser to be determined.

$$\dot{y}_{P,in,TC} = \frac{\left(\dot{M}_{f,out}\dot{x}_{P.out}\right)_{TC} + \left(\dot{M}_{f,out}\dot{x}_{P.out}\right)_{DC}}{\dot{M}_{v,in,TC}} \tag{4.5.33}$$

Having found the compositions of the vapour entering and leaving the test condenser, the change in concentration of the vapour stream due to condensation was easily found.

5.0 Results and Discussions

This chapter contains the main results of all the experimental work carried out during this research and its discussion.

The chapter begins by looking at the work carried out to commission the instrumentation used to measure the density and its relation to composition. This technique was used to provide information on the composition of liquid samples, and hence examine the mass transfer process inside the test condenser.

Following this was the work carried out to determine the coolant-side heat transfer coefficient inside the test condenser. Owing to the surface geometry of the test condenser, there was no standard method available for determining the mean coolant-side heat transfer coefficient. An experimental procedure was adopted to determine a correlation that could be used to predict this value with the required degree of accuracy.

The remainder of the chapter is devoted to the experimental programme of work that was carried out using single component hydrocarbons, and then binary mixtures of these two components. The single components are discussed first, since these tests were carried out to test the sensitivity of the instruments with hydrocarbons, and to provide a basis for the tests with binary hydrocarbon mixtures.

5.1 Composition Measurement

5.1.1 Introduction

To examine the transfer of mass between the vapour and condensate during reflux condensation in a single vertical tube, it was necessary to measure the composition of some of the streams entering and leaving the test condenser. The method chosen to determine the composition of these streams was to measure their density, and the instrument used was a vibrating U-shaped cell densitometer.

The densitometer is a fairly common device used for making accurate measurements of density. It can be used as a stand-alone device, where a sample is injected into the measuring cell, or as an on-line measurement device, where the sample flows through the cell. Although other methods for determining the composition of liquid mixtures are available, such as the preferential absorption of components (as in chromatography), absorption of electromagnetic waves (infra-red or ultra-violet), refractive index, and pH, the densitometer had been previously used at NEL to successfully measure the densities of a range of liquids. An outline of the principles involved in using a densitometer has been provided in Appendix A5.1.

In choosing to use density to determine mixture composition, it was necessary to ensure that the densities of the two single components were reasonably different from each other to allow for distinction. As the values tabulated in Appendix A1.1 and A1.2 indicate, the densities of n-pentane and iso-octane display a marked difference, which made density a suitable variable to use.

A description of the on-line measurement system was given in Chapter 4.1.1, and was shown in Figure 4.8 [p.81]. A small sample of the stream, whose composition

was to be measured, was withdrawn from the test fluid circuit from a suitable location. The sample was then pumped through a cooling water bath and into the densitometer cell. The sample was isolated in this cell and its composition determined from the period of vibration reading indicated on the cell's processing unit. This period of vibration reading was related to the density of the sample contained within the cell. The composition and density were related by a pre-determined equation found by experiment.

The compositions of the reflux condensate and the condensate from the dump condenser were measured. As the composition of the condensate from the dump condenser was always the same as the exit vapour from the test condenser, measuring the liquid phase removed the need to sample a vapour stream. This meant that only liquid samples were withdrawn from the test fluid circuit, thus removing the difficulty of having to deal with two-phase samples.

Therefore, no direct measurement of the composition of the vapour stream entering the test condenser was made. The composition of this stream was determined by combined heat and mass balances from these measured compositions, and from the heat load determined through measurements on the coolant sides of the test and dump condensers.

5.1.2 Instrument Calibration

The two fluids used to determine the densitometer calibration constant were air and purified water, as supplied by the manufacturer. These fluids were recommended for use in the manufacturer's handbook supplied with the instrument.

The densitometer and its processing unit were electronically connected through sockets located at the rear of the equipment. A cooling water bath was connected to the ports on the outside of the measuring cell by flexible tubing. This allowed water to flow over the cell, and thus enabled control of the temperature at which measurements were taken. Temperature was measured by a K-type thermocouple inserted in a separate port alongside the measuring cell. The digital display connected to the thermocouple showed the measured temperature to within 0.1°C.

When the upper and lower ports in the measuring cell were open to atmosphere, air flowed through the cell. Measurements of the period of vibration were taken only after temperature equilibration in the cell had been achieved. The temperature of the cell was said to be at equilibrium when enough time had passed for the period of vibration value, displayed to six figures after the decimal point, to remain unchanged, or until only the last figure in the reading changed. Once this had occurred, the period of vibration was noted.

Having done this, the thermostat controls on the cooling water bath were adjusted to increase the temperature inside the measuring cell. After enough time had passed for equilibration at this higher temperature, the period of vibration reading at this new temperature was noted. This process was repeated until period of vibration values for air at atmospheric conditions were made over the temperature range 10.4 to 15.4 °C at1.0°C intervals.

To measure the period of vibration of purified water, a small sample was injected into the measuring cell through the bottom port using a syringe. The syringe was left connected to the bottom port of the measuring cell, and the upper port was sealed using a small plastic plug. Care was taken when injecting the purified water through the syringe that the volume of the cell was fully filled, and that no air bubbles were present inside the cell.

Once the temperature of the measuring cell was at equilibrium, the reading for the period of vibration for the purified water was noted. Having done this, the thermostat controls on the cooling water bath were adjusted to increase the temperature inside the measuring cell. After enough time had passed for equilibration at this new temperature, the period of vibration reading at this new temperature was noted. This process was repeated until period of vibration values for purified water were made over the temperature range 10.4 to 15.4 °C at1.0°C intervals.

This entire procedure was repeated on several different days to give a large set of results for the period of vibration of air and purified water over the temperature range 10.4 to 15.4 °C, and over a narrow range of atmospheric pressures. The manufacturer of the densitometer stated that the instrument calibration constant was dependent on temperature because of the elasticity module of the particular glass used in manufacturing the cell, as well as the thermal expansion coefficient of the oscillator itself. These results were used to show this was indeed the case, and to determine the significance of temperature over the measured range.

The densitometer calibration constant was found from

$$K_\rho = \frac{\rho_{H_2O} - \rho_a}{\left(t^2_{H_2O} - t^2_a\right)} \tag{5.1.1}$$

The densities of air and purified water were obtained using PPDS. The measured period of vibration readings for air and purified water are shown in Appendix A5, Tables A5.1 and A5.2, respectively, and the densities predicted by the computer package are shown in Appendix A5, Tables A5.3 and A5.4, for air and purified water respectively.

5.1.3 Measuring the Density of Hydrocarbons

The same procedure was used to measure the period of vibration for the two single component hydrocarbons, n-pentane and iso-octane.

To measure the period of vibration of n-pentane, a small sample was injected into the measuring cell through the bottom port using a syringe. The syringe was left connected to the bottom port of the measuring cell, and the upper port was sealed using a small plastic plug. Care was taken when injecting the sample through the syringe that the volume of the cell was fully filled, and that no air bubbles were present inside the cell.

Once the temperature of the measuring cell was at equilibrium, the reading for the period of vibration for the n-pentane was noted. Having done this, the thermostat controls on the cooling water bath were adjusted to increase the temperature inside the measuring cell. After enough time had passed for equilibration at this new temperature, the period of vibration reading at this new temperature was noted. This process was repeated until period of vibration values for n-pentane were made over the temperature range 10.4 to 15.4 °C at1.0°C intervals.

Having done this, the sample was withdrawn from the measuring cell using the syringe, the seal removed, and the air hose connected to the upper port in the measuring cell. The built-in pump was turned on to dry the cell and the temperature reduced to 10.4 °C. On returning to this temperature, the period value was monitored until it had reached the same value for air as was recorded previously. It could then be said with confidence that no trace of the sample existed in the measuring cell. The cell was cleaned out fully by flushing the cell with acetone between periods of drying.

This was repeated three times, to give a full set of results for the period of vibration value of n-pentane over the temperature range 10.4 to 15.4 °C. The entire procedure was carried out with the n-pentane replaced by iso-octane. The period of vibration readings for the single component hydrocarbons are given in Appendix A5, Tables A5.5 and A5.6, and their measured densities are given in Tables A5.7 and A5.8.

To produce an empirical correlation relating the composition of a binary hydrocarbon mixture to its density, it was necessary to prepare binary mixture samples containing n-pentane and iso-octane, covering a range of mole fractions, and determine their period of vibration values.

For such a binary mixture, the mole fraction of n-pentane in the mixture is defined as

$$\tilde{x}_P = \frac{\left(m_P/\tilde{M}_P\right)}{\left(m_P/\tilde{M}_P\right)+\left(m_O/\tilde{M}_O\right)} \qquad (5.1.2)$$

These binary mixtures were prepared by specifying the mass of n-pentane that each mixture would contain, which was kept constant for each of the mixtures. Using (5.1.2), the mass of iso-octane required was easily calculated from the above equation.

These samples were prepared in the laboratory by adding together the masses of n-pentane and iso-octane in a small conical flask placed on a balance. Iso-octane was slowly added to the flask until the balance displayed the required mass, or as close to it as was possible. The flask was sealed and the final mass noted. The reading on the display was set to zero, and then the n-pentane was added to the flask until the display showed the required mass, or as close as was possible. Having noted the

actual masses of n-pentane and iso-octane used to prepare each sample, the actual mole fraction of the mixture was determined using (5.1.2).

It was assumed that the loss of any hydrocarbon material through natural evaporation was minimal, and so the calculated mole fraction of the mixtures did not change. Each of the mixtures prepared was kept stored in the small conical flask until needed for measurement. Measurement of the mixture period of vibration was carried out in exactly the same way as for the single component hydrocarbons. The period of vibration readings for each of the mixtures are given in Appendix A5, Tables A5.9 to A5.12.

5.1.4 The Densitometer Calibration Constant

Using the values shown in Appendix A5, Tables A5.1 through to Table A5.4, the densitometer calibration constant was calculated using (5.1.1). The results of these calculations are shown in Table 5.1, where the constant was expressed in units of kg/m^3s^2.

As these values showed, the densitometer calibration constant was not influenced significantly by the effect of pressure. At the lowest measured temperature of 10.4℃, the difference between the calibration constants at the lowest and highest measured pressures was calculated as 0.0016 kg/m^3s^2, or 0.001%. At the highest measured temperature of 15.4℃, this difference was found to be 0.004 kg/m^3s^2, or 0.003%.

Table 5.1.

Calculated densitometer calibration constants.

	P (bar)					
T (°C)	*1.00178*	*1.00279*	*1.00686*	*1.00821*	*1.00991*	*1.01024*
10.4	158.9347	158.9390	158.9363	158.9305	158.9521	158.9331
11.4	158.9177	158.9226	158.9200	158.9128	158.9355	158.9156
12.4	158.9027	158.9050	158.9044	158.9006	158.9207	158.9012
13.4	158.8898	158.8921	158.8919	158.8880	158.9068	158.8881
14.4	158.8788	158.8806	158.8834	158.8764	158.8957	158.8764
15.4	158.8718	158.8732	158.8890	158.9001	158.8824	158.8674

Making the assumption that the calibration constant was independent of pressure, the above table was simplified to just show the calibration constant at five different measured temperatures. Theses new calibration constants were simply the numerical average of the values shown at each of the different measured pressures in Table 5.1. These average densitometer calibration constants are shown in Table 5.2.

Table 5.2 also showed the effect of temperature on the densitometer calibration constant. The difference between the average calibration constants across the measured temperature range was found to be 0.0569 kg/m^3s^2, or 0.04%. This was however, a factor of ten greater than that calculated for the effect of pressure, and suggested that temperature was more significant.

Table 5.2.

Calculated average densitometer calibration constants.

$T\,(°C)$	$K_\rho\,(kg/m^3s^2)$
10.4	158.9376
11.4	158.9207
12.4	158.9057
13.4	158.8928
14.4	158.8818
15.4	158.8807

A more thorough investigation of the effect of temperature was made by predicting the density of purified water using the calculated densitometer calibration constants, and comparing these values with the known density of purified water. For each of the temperatures in the range, the density of purified water was calculated using the average densitometer calibration constant shown in Table 5.2. The density of purified water was then re-calculated using the numerical average of all the densitometer calibration constants shown in Table 5.2, and the results compared with the known density.

The density of the purified water was calculated using a rearrangement of (5.1.1).

$$\rho_{H_2O} = \rho_a + K_\rho\left(t_{H_2O}^2 - t_a^2\right) \tag{5.1.3}$$

As calculation of the purified water density was dependent on both the period of vibration and density of air, these comparisons were made at each of the measured

pressures shown in Table 5.1 .The full results of these comparisons are given in Appendix A5, Tables A5.17 through to A5.22.

As these results show, the density of the purified water was slightly more accurately predicted when the calibration constant determined at the specific temperature was used as opposed to the average calibration constant over this temperature range. The overall average calibration constant was found to over-predict the density by 0.03%, and under-predict by 0.02%. In contrast, when using the temperature dependent calibration constant, the density was over-predicted by 0.01%, and under-predicted by as little as 0.008%.

It was felt that because these differences were so small, the use of an average calibration constant across this temperature was unlikely to introduce any significant error to the predicted density. The calibration constant that was used to determine the density of the hydrocarbons across this same range of temperature was, therefore, taken as 158.9032 kg/m^3s^2.

5.1.5. Relationship between Composition and Density

The density of the pure hydrocarbon samples, and the binary hydrocarbon mixture samples, was determined by applying equation (5.1.3), with the period of vibration values recorded for the hydrocarbon sample, and those recorded for air at the same measured temperature.

$$\rho_{hc} = \rho_a + \overline{K}_\rho \left(t_{hc}^2 - t_a^2 \right) \tag{5.1.4}$$

This method of calculating the density of the hydrocarbon sample was preferred to that using the density and period of vibration of purified water, because it involved taking the difference between two similar numbers, and this was known to be error prone.

$$\rho_{hc} = \rho_{H_2O} - \overline{K}_{\rho}\left(t_{H_2O} - t_{hc}\right)\left(t_{H_2O} + t_{hc}\right) \qquad (5.1.5)$$

In using (5.1.4) however, it was necessary to decide which period of vibration and density values for air were to be used in the calculation. As shown in Table A4.1 in Appendix A5, the period of vibration values changed very little across the measured pressure range. As it was previously decided that pressure was insignificant, the period of vibration readings were combined at each of the measured temperatures to give an average period of vibration. These values are shown in Table 5.3 below, along with the average air density values that were used to calculate the densities of the hydrocarbon samples.

Table 5.3.

Average period of vibrations and densities for air.

$T\,(°C)$	$\bar{t}_{AIR}\ (s)$	$\overline{\rho}_{AIR}\ (kg/m^3)$
10.4	2.641970	1.2372
11.4	2.641773	1.2328
12.4	2.641580	1.2285
13.4	2.641386	1.2242
14.4	2.641192	1.2199
15.4	2.640998	1.2157

The hydrocarbon densities calculated using these values are provided in Appendix A5, Tables A5.7 and A5.8 for the single components, and Tables A5.13 through to A5.16 for the binary mixtures.

Using PPDS it was possible to make a comparison between the measured densities and those predicted by the physical properties package. These comparisons were used to investigate how well the physical properties package compared to the measured values. The results of these comparisons are shown in the following tables below, Tables 5.4 and 5.5 for the single component hydrocarbons, and Tables 5.6 to 5.9 for the binary hydrocarbon mixtures.

As the values in these tables show, there is good agreement between the measured and predicted densities. It is also seen that both the predicted and measured densities show the mixture density to increase as the concentration of the more volatile n-pentane component decreases.

Table 5.4.

Comparison between measured and predicted densities of n-pentane.

T (℃)	Mean Measured Value (kg/m^3)	Predicted Value (kg/m^3)	Difference (kg/m^3)	Difference (%)
10.4	637.6391	635.979	1.6601	0.2610
11.4	636.5863	635.017	1.5693	0.2471
12.4	635.5192	634.054	1.4652	0.2311
13.4	634.4916	633.089	1.4026	0.2215
14.4	633.3672	632.121	1.2462	0.1971
15.4	632.2549	631.151	1.1039	0.1749

Table 5.5.

Comparison between measured and predicted densities of iso-octane.

T (°C)	Mean Measured Value (kg/m^3)	Predicted Value (kg/m^3)	Difference (kg/m^3)	Difference (%)
10.4	701.7136	700.874	0.8396	0.1198
11.4	700.7840	700.034	0.7500	0.1071
12.4	699.8596	699.193	0.6666	0.0953
13.4	698.9290	698.350	0.5790	0.0829
14.4	698.0092	697.507	0.5022	0.0720
15.4	697.0756	696.663	0.4126	0.0592

Table 5.6.

Comparison between measured and predicted densities of an n-pentane/iso-octane mixture containing 0.2244 moles of n-pentane/mole.

T (°C)	Mean Measured Value (kg/m^3)	Predicted Value (kg/m^3)	Difference (kg/m^3)	Difference (%)
10.4	691.4161	689.995	1.4211	0.2060
11.4	690.4642	689.132	1.3322	0.1933
12.4	689.5071	688.268	1.2391	0.1800
13.4	688.5473	687.402	1.1453	0.1666
14.4	687.5890	686.535	1.0540	0.1535
15.4	686.5953	685.666	0.9293	0.1355

Table 5.7.

Comparison between measured and predicted densities of an n-pentane/iso-octane mixture containing 0.4018 moles of n-pentane/mole.

T (℃)	Mean Measured Value (kg/m^3)	Predicted Value (kg/m^3)	Difference (kg/m^3)	Difference (%)
10.4	682.1153	680.199	1.9163	0.2817
11.4	681.1511	679.316	1.8351	0.2701
12.4	680.1868	678.432	1.7548	0.2587
13.4	679.2165	677.546	1.6705	0.2466
14.4	678.2614	676.658	1.6034	0.2370
15.4	677.2638	675.769	1.4948	0.2212

Table 5.8.

Comparison between measured and predicted densities of an n-pentane/iso-octane mixture containing 0.5889 moles of n-pentane/mole.

T (℃)	Mean Measured Value (kg/m^3)	Predicted Value (kg/m^3)	Difference (kg/m^3)	Difference (%)
10.4	671.1924	668.473	2.7194	0.4068
11.4	670.2053	667.567	2.6383	0.3952
12.4	669.1987	666.660	2.5387	0.3808
13.4	668.1937	665.751	2.4427	0.3669
14.4	667.1865	664.841	2.3455	0.3528
15.4	666.1524	663.928	2.2244	0.3350

Table 5.9.

Comparison between measured and predicted densities of an n-pentane/iso-octane mixture containing 0.7713 moles of n-pentane/mole.

T (℃)	Mean Measured Value (kg/m^3)	Predicted Value (kg/m^3)	Difference (kg/m^3)	Difference (%)
10.4	658.1962	655.365	2.8312	0.4320
11.4	657.1548	654.435	2.7198	0.4156
12.4	656.1358	653.504	2.6318	0.4027
13.4	655.0769	652.571	2.5059	0.3840
14.4	654.0441	651.636	2.4081	0.3695
15.4	652.9909	650.700	2.2909	0.3521

With this large data set, the following strategy was adopted for predicting the mixture composition from its measured density. The period of vibration reading measured using the densitometer was used to calculate the density of the hydrocarbon mixture using

$$\rho_{hc} = \rho_a + \overline{K}_\rho \left(t_{hc}^2 - t_a^2 \right) \tag{5.1.4}$$

Using the measured densities and mixture compositions, the data were plotted on a graph at a specified temperature within the measured range. The graph was used to generate an equation describing the best fit to the data. It was convenient to have the best-fit equation in the form of a second-order polynomial, or quadratic equation, of the general form

$$\rho_{hc} = K_0 + K_1\tilde{x}_P + K_2\tilde{x}_P^2 \tag{5.1.6}$$

Having already determined the density of the mixture from (5.1.4), the composition of the mixture was found by solving the quadratic equation described in (5.1.6) as follows.

$$K_2\tilde{x}_P^2 + K_1\tilde{x}_P + (K_0 - \rho_{hc}) = 0 \tag{5.1.7}$$

$$\tilde{x}_P = \frac{-K_1 \pm \sqrt{K_1^2 - 4K_2(K_0 - \rho_{hc})}}{2K_2} \tag{5.1.8}$$

In addition, the full data set was combined on one graph, and a further quadratic equation obtained. This latter equation was used to investigate the effect of temperature on the ability to predict the composition of the mixture. The values of the constants in (5.1.6) for each of these equations are shown in Table 5.10.

Using the measured densities for each of the mixtures, the temperature-dependent correlations were used to predict compositions. In addition, the temperature-independent correlation was also used to predict composition based on the measured densities. The results of these calculations were then used to conclude whether the composition should be determined using a temperature-dependent correlation or not. The results of these calculations are shown in Tables 5.11 to 5.14.

Table 5.10.

Constants in the expressions relating mixture density and composition.

T (°C)	K_0	K_1	K_2
10.4	701.5506	-37.39155	-26.66161
11.4	700.3729	-35.39565	-27.94799
12.4	699.4464	-35.49350	-27.98846
13.4	698.5224	-35.67810	-27.92203
14.4	697.5955	-35.70671	-28.08484
15.4	696.6533	-35.84989	-28.10518
10.4-15.4	699.0235	-35.91923	-27.78502

Table 5.11.

Effect of temperature on the ability to predict the composition of a mixture of n-pentane and iso-octane containing 0.2244 moles of n-pentane.

	T-dependent Difference		T-independent Difference	
T (°C)	(*moles*)	(%)	(*moles*)	(%)
10.4	-0.0081	-3.4815	0.0392	21.1361
11.4	-0.0116	-4.9049	0.0188	9.1460
12.4	-0.0117	-4.9479	-0.0012	-0.5215
13.4	-0.0116	-4.9149	-0.0208	-8.4702
14.4	-0.0119	-5.0429	-0.0399	-15.0976
15.4	-0.0123	-5.1777	-0.0593	-20.911

Table 5.12.

Effect of temperature on the ability to predict the composition of a mixture of n-pentane and iso-octane containing 0.4018 moles of n-pentane.

	T-dependent Difference		T-independent Difference	
T (°C)	(*moles*)	(%)	(*moles*)	(%)
10.4	-0.0018	-0.4503	0.0351	9.5700
11.4	-0.0084	-2.0473	0.0181	4.7194
12.4	-0.0082	-2.0098	0.0014	0.3491
13.4	-0.0079	-1.9353	-0.0152	-3.6339
14.4	-0.0077	-1.8912	-0.0312	-7.2045
15.4	-0.0076	-1.8641	-0.0477	10.6119

Table 5.13.

Effect of temperature on the ability to predict the composition of a mixture of n-pentane and iso-octane containing 0.5889 moles of n-pentane.

	T-dependent Difference		T-independent Difference	
T (°C)	(*moles*)	(%)	(*moles*)	(%)
10.4	0.0133	2.3048	0.0439	8.0482
11.4	0.0054	0.9286	0.0290	5.1885
12.4	0.0053	0.9054	0.0141	2.4573
13.4	0.0053	0.9156	-0.0006	-0.1014
14.4	0.0052	0.8951	-0.0152	-2.5125
15.4	0.0052	0.8916	-0.0300	-4.8429

Table 5.14.

Effect of temperature on the ability to predict the composition of a mixture of n-pentane and iso-octane containing 0.7713 moles of n-pentane.

	T-dependent Difference		T-independent Difference	
T (°C)	(*moles*)	(%)	(*moles*)	(%)
10.4	0.0173	2.2881	0.0439	6.0385
11.4	0.0091	1.1884	0.0303	4.0957
12.4	0.0091	1.1981	0.0172	2.2799
13.4	0.0087	1.1423	0.0037	0.4756
14.4	0.0088	1.1603	-0.0094	-1.2080
15.4	0.0090	1.1772	-0.0227	-2.8529

As the results of these comparisons show, the temperature-dependent correlations were more accurate in predicting the composition of the mixture from its measured density. The maximum absolute difference between the known and predicted mixture compositions using the temperature-dependent correlations was found to be 5%, whereas using the temperature-independent correlation this difference was found to be 21%.

It was also noticed that the temperature-independent correlation produced quite large differences between the known and predicted mixture compositions at either end of the temperature range. This was not observed with any of the temperature-dependent correlations.

Furthermore, it was seen that the highest discrepancies between the known and predicted mixture compositions occurred where the proportion of the more volatile n-pentane component in the mixture was smallest. This suggested that losses of n-pentane occurred during the laboratory work, which meant that the actual amount of n-pentane in the mixture was less than originally calculated.

If the amount of n-pentane in the mixture were less than that estimated, the prediction of the amount of n-pentane in the mixture would become less accurate where the actual amounts were small. The graph used to derive the correlation relating mixture composition to its density would have to be shifted along the mixture composition axis. This would allow for a change in composition of the mixture. This problem was overcome by working with mixtures whose composition contained significant amounts of both n-pentane and iso-octane.

The method outlined above produced a temperature-dependent correlation that was used to predict the composition of samples to within 5% of the measured density. These measured compositions were, used along with the results of heat balance calculations, to determine the flow rate and composition of the vapour entering the test condenser. Theses material balance calculations were based on the assumption that the differences in composition of the inlet and outlet vapour streams were greater than the accuracy of the composition measurement equipment. In addition, it was assumed that the differences in composition between the exit vapour and exit condensate from the test condenser were also greater than this accuracy.

A number of steps were taken to try and ensure that these assumptions were upheld during experimental work with the binary hydrocarbon mixtures. A greater separation of the components in the vapour mixture was more likely if the concentration of the more volatile component in the feed vapour stream was not unreasonably high. By preparing batch liquid mixtures that contained more of the

less volatile material, the composition of the feed vapour to the test condenser was unlikely to contain too high a concentration of the more volatile component. Thus it was to be expected that as a result of condensation, the exit vapour stream from the test condenser was likely to exhibit a significant increase in concentration of the more volatile concentration, greater than a 5% variation.

Consequently, the composition of the reflux condensate leaving the test condenser was expected to display a significant concentration of the less volatile component. Again, the difference in concentrations between the exit streams was therefore likely to be much greater than 5%.

To ensure that the results of the composition measurements were as accurate as possible, and that the accuracy of the composition measurement equipment was not adversely affected, it was normal to allow the sample stream to flow through the measuring cell prior to taking a reading. This ensured that any trace of a previous sample was removed, as contamination of the cell was likely to alter the period of vibration reading, and hence density, of the sample.

5.2 Expression for the mean Coolant Heat Transfer Coefficient in the Test Condenser

5.2.1 Introduction

As previously discussed, the outer surface of the test condenser tube was machined to produce a much greater surface area than was originally available. A narrow rectangular groove was cut into the outer surface of each of the three test sections at a slight pitch. This created a small rectangular channel for the coolant to flow through when the coolant sleeve was fitted over the base tube of the test section.

The same standards of manufacture were applied to each of the three test sections that combine to form the test condenser. This meant that after machining, the surface areas on the outside of each test section were identical. This was important because it meant all three of the test sections were identical in terms of the inner and outer heat transfer surface areas, as well as the length of the coolant flow paths.

This increase in the outer surface area of the test sections ensured that there was a measurable temperature rise in the coolant, and that the coolant-side heat transfer coefficient was at least an order of magnitude greater than the heat transfer coefficient on the condensing-side. This reduced the likelihood of error in calculating the rates of heat transfer across the test sections, and ensured that the controlling resistance to the transfer of heat was that on the condensing-side.

It meant, however, that because of the complex flow geometry, there was no apparent correlation for determining the coolant-side heat transfer coefficient. As the value of the experimental condensing-side heat transfer coefficient was to be

determined from the other resistances involved, it was necessary to find a means for accurately determining its value.

Wilson (1915) first proposed a method that could be used for determining an individual film heat transfer coefficient from simple experimental measurements. Different researchers have employed this method for a range of process conditions, and over different surfaces. This method was used here to derive a unique correlation for the mean coolant heat transfer coefficient in a test section.

The method was carried out during commissioning work on the test facility, using steam as the condensing fluid, and was carried out across the lowest of the three test sections. There were several reasons for this. Firstly, as all three of the test sections were geometrically identical this meant that any correlation derived from one test section could be applied with the same level of confidence to the others. Secondly, the lower pressure drop with one test section meant that a wider range of coolant flow rates were available. And finally, previous commissioning tests had shown that the surface area in one test section was almost capable of completely condensing the steam generated at full heat load.

5.2.2 Theory

For the condensation of a single component vapour inside a tube, where all heat transfer surface areas are free from dirt or fouling, the mean overall heat transfer coefficient was given by

$$\frac{1}{\overline{U}_i} = \frac{1}{\overline{\alpha}_{f,i}} + \frac{A_i}{A_{o,w}} \frac{x_w}{\lambda_w} + \frac{A_i}{A_{o,c}} \frac{1}{\overline{\alpha}_c} \qquad (5.2.1)$$

All heat transfer surface areas and the tube wall thickness were defined previously in Chapter 4.5.1. By rearrangement of (5.2.1), the mean experimental condensate-film heat transfer coefficient was determined from

$$\frac{1}{\overline{\alpha}_{f,i}} = \frac{1}{\overline{U}_i} - \left[\frac{A_i}{A_{o,w}} \frac{x_w}{\lambda_w} + \frac{A_i}{A_{o,c}} \frac{1}{\overline{\alpha}_c} \right] \tag{5.2.2}$$

The mean overall heat transfer coefficient was calculated from

$$\overline{U}_i = \frac{\dot{Q}_c}{A_i \Delta T_{\ln}} \tag{5.2.3}$$

The rate of heat transfer to the coolant, assuming no heat losses through the test section cooling jacket, was given by

$$\dot{Q}_c = \dot{M}_c C p_c \Delta T_c \tag{5.2.4}$$

The logarithmic-mean temperature difference for isothermal condensation was calculated using

$$\Delta T_{\ln} = \frac{\left(T_{c,out} - T_{c,in}\right)}{\ln\left(\frac{T_v - T_{c,in}}{T_v - T_{c,out}}\right)} \tag{5.2.5}$$

In order to simplify (5.2.2), two assumptions were made. The first assumption was that the resistance to the transfer of heat through the test condenser tube walls was constant. A constant resistance was to be expected if the mean tube wall temperature showed only a slight change across a range of saturation conditions. The tube wall heat transfer resistance is normally regarded as being negligible in comparison to the other resistances involved during condensation.

The second assumption was that the resistance to the transfer of heat through the condensate film was constant. If a suitable correlation for calculating the condensate-film heat transfer resistance was available, it would have been possible to incorporate this into the theoretical development to account for the changes on the condensing side with the variation in the rate of heat transfer. However, no such correlation was available, and thus it was impossible to account for changes on the condensing side in this manner.

The method used here involved varying the conditions on the coolant side whilst trying to maintain those on the condensing side. Despite the gradual reduction in the coolant flow rate, this was compensated for by an increase in coolant temperature difference, with the overall effect being a constant rate of heat transfer.

The condensate film heat transfer resistance was related to the thickness of the film, which was in turn related to the mass flow rate of condensate. For a constant heat load across the test section, the mass flow rate of condensate was approximately constant, so the condensate-film heat transfer coefficient was also constant. The reduction of the latent heat caused by the increase in saturation conditions was typically less than 1% across this small range of temperatures.

With these assumptions, (5.2.2) was modified to read

$$\frac{1}{\overline{U}_i} = Y + \frac{A_i}{A_{o,c}} \frac{1}{\overline{\alpha}_c} \tag{5.2.6}$$

The constant Y was used to represent

$$Y = \frac{1}{\overline{\alpha}_{f,i}} + \frac{A_i}{A_{o,w}} \frac{x_w}{\lambda_w} \tag{5.2.7}$$

As the aim of this work was to derive by experiment a correlation for the mean coolant heat transfer coefficient, it was necessary to substitute into (5.2.6) an alternative expression for this term. A suitable function for expressing the mean coolant heat transfer coefficient for forced convective flow was

$$Nu_c = \mathrm{f}(Re_c, Pr_c) \tag{5.2.8}$$

For the case of transferring heat to a coolant, (5.2.8) was more definitely written in the form presented by Dittus and Boelter (1930), where K has the value of 0.024.

$$Nu_c = K\, Re_c^{0.8}\, Pr_c^{0.4} \tag{5.2.9}$$

Sieder and Tate (1936), presented an alternative to this, where K has the value of 0.027

$$Nu_c = K\, Re_c^{0.8}\, Pr_c^{0.33} \left(\frac{\eta_c}{\eta_w}\right)^{0.14} \tag{5.2.10}$$

The bracketed term accounted for the change in viscosity of the fluid between the wall and the bulk of the fluid. It was only necessary to include this term where the fluid viscosity showed significant variation between these two locations as a result of the temperature difference. As the inner wall temperatures lay very close to the vapour temperatures during these tests, the variation in viscosity was negligible.

Thus the mean coolant heat transfer coefficient was expressed as

$$\overline{\alpha}_c = K\, Re_c^{0.8}\, Pr_c^{0.4} \left(\frac{\lambda_c}{d_{eh}}\right) \tag{5.2.11}$$

Substituting (5.2.11) into (5.2.6) gave

$$\frac{1}{\overline{\overline{U}}_i} = Y + \left(\frac{A_i}{A_{o,c}}\right) \frac{1}{K\, Re_c^{0.8}\, Pr_c^{0.4} \left(\frac{\lambda_c}{d_{eh}}\right)} \tag{5.2.12}$$

This equation was further simplified by assuming that the coolant thermal conductivity remained relatively unchanged over the temperature range. Referring to physical property data for water, it was seen that for a temperature difference of between 15 and 20 °C, the thermal conductivity changed by around 4%. Therefore it seemed reasonable to make the assumption of a constant coolant thermal conductivity.

$$K' = K\left(\frac{\lambda_c}{d_{eh}}\right) \tag{5.2.13}$$

With this assumption, (5.2.12) became

$$\frac{1}{\overline{U}_i} = Y + \left(\frac{A_i}{A_{o,c}}\right)\frac{1}{K'\,Re_c^{0.8}\,Pr_c^{0.4}} \tag{5.2.14}$$

By plotting a graph of $1/\overline{U}_i$ against $\left(A_i/A_{o,c}\right)1/Re_c^{0.8}\,Pr_c^{0.4}$ for a range of coolant Reynolds and Prandtl numbers, a straight line was obtained with a gradient of $1/K'$ and an intercept on the vertical axis equal to Y.

Having evaluated the gradient of this line, the value was used to work back to derive the desired expression for the mean coolant heat transfer coefficient.

$$g = \frac{1}{K'} \tag{5.2.15}$$

$$g = \frac{1}{K\left(\frac{\lambda_c}{d_{eh}}\right)} \tag{5.2.16}$$

$$K = \frac{1}{g}\left(\frac{d_{eh}}{\lambda_c}\right) \tag{5.2.17}$$

Therefore, the final expression for the mean coolant heat transfer coefficient was given by (5.2.18), where all coolant physical properties were evaluated using PPDS.

$$\overline{\alpha}_c = \frac{1}{g} Re_c^{0.8}\ Pr_c^{0.4} \tag{5.2.18}$$

5.2.3 Experimental Method

To use this technique, it was necessary to conduct an experiment covering a wide range of coolant Reynolds and Prandtl numbers whilst condensing steam in a single test section of the test condenser. Steady state was reached for a fixed level of heat input and coolant inlet temperature, with a steady coolant flow rate through the test section.

Several readings were taken at this steady state before the coolant flow rate was adjusted. No deliberate adjustment was made to the inlet temperature of the coolant. After enough time had elapsed for a new steady state condition to be achieved, the measurement process was repeated at this new condition.

By periodically reducing the flow rate of coolant through the test section, the operating pressure and temperature inside the test condenser were gradually increased. The reduction in coolant flow rate was compensated for by an increase in the coolant temperature rise across the test section. Thus, conditions on the condensing side were kept reasonably constant whilst covering a range of coolant Reynolds and Prandtl numbers.

Several measurements were taken of each steady state condition. After this the facility was shut down. The entire procedure was then repeated on several different occasions to give a large data set with which to develop a correlation.

5.2.4 Validation of the Expression

The data recorded during these experiments have been included in Appendix A6, Tables A6.1 to A6.5 for reference purposes. The results of the calculations to determine the coolant Reynolds and Prandtl numbers, and those to determine the mean overall heat transfer coefficient, to produce the plots have also been included in Appendix A6, Tables A6.6 to A6.10.

Comparison of the measured temperatures and pressures recorded in the boiler vapour space with values found from reference tables in Rogers and Mayhew (1988), show that there is poor agreement between the measured saturation temperatures and pressures. As discussed in Appendix A2.2, this was attributed to a poor calibration equation for the pressure transducer/transmitter located in the boiler vapour space.

The vapour temperatures measured up through the test condenser showed good agreement with that measured in the boiler vapour space, and can be taken to indicate

the saturation conditions. A saturation pressure was calculated using PPDS based on the measured vapour temperature, and this was found to give good agreement with values found in Rogers and Mayhew. Thus condensate film and vapour physical properties were evaluated as functions of the measured vapour temperature, and the saturation pressure calculated using this measured temperature.

The data gathered was used to investigate the validity of the assumptions made in developing the equation for the mean coolant heat transfer coefficient. The first of these assumptions was that the resistance to heat transfer through the tube wall was constant. As previously stated, if the mean tube wall temperature remained fairly constant across the range of saturation conditions, a constant tube-wall heat transfer resistance was expected.

The tube wall heat transfer coefficient was calculated as a function of the tube wall material thermal conductivity, using

$$\overline{\alpha}_w = \frac{\lambda_w}{x_w} \tag{5.2.19}$$

Typical values are shown in Table 5.15, and the full set of calculations is provided in Appendix A6, Tables A6.11 to A6.15. The analysis of this resistance over the range of experimental conditions showed that this assumption was valid, as the change in the mean tube-wall heat transfer coefficient during a typical test run was calculated to be much less than 1%.

Table 5.15.

Analysis of the mean tube-wall heat transfer resistance.

Test Number	$\overline{\alpha}_w$ $(W/m^2°C)$	$\Delta\overline{\alpha}_w$ (%)
1	84780-84922	-0.1675
2	84967-85084	-0.1377
3	84944-85064	-0.1413
4	84824-84907	-0.0978
5	84918-85071	-0.1802

The second assumption made was that the resistance to heat transfer through the condensate film was constant. From the graphs plotted, the value of the intercept on the vertical axis was used to calculate the resistance due to the condensate film by rearranging (5.2.7) to give

$$\frac{1}{\overline{\alpha}_{f,l}} = Y - \left(\frac{A_l}{A_{o,w}}\right)\frac{x_w}{\lambda_w} \qquad (5.2.20)$$

As previously shown, the second term on the right-hand side of (5.2.20) was approximately constant throughout each of the five test runs. Although the value of the vertical intercept found from each of the five different graphs was seen to vary slightly, the condensate-film heat transfer resistance calculated in this way displayed a very slight variation overall.

An independent check was made using Nusselt theory to calculate the mean condensate-film heat transfer coefficient at the bottom of a vertical surface. This analysis did not assume that Nusselt's equation was the most appropriate correlation to use for the particular condensing situation. It was used here merely as an analysis tool to investigate an assumption made. The equation used for determining this resistance was convenient for incorporating experimental measurements.

$$\overline{\alpha}_{f,t} = 0.943\left[\frac{\lambda_f^3 g_n \rho_f (\rho_f - \rho_v)\Delta h_v}{\eta_f L}\right]^{1/4} (T_v - T_w)^{-1/4} \qquad (5.2.21)$$

The wall temperature was taken as the arithmetic mean of the five individual wall temperatures measured in the test section. The results of this analysis are shown in Table 5.16. The full set of results is provided in Appendix A6, Tables A6.11 to A6.15.

Table 5.16.

Analysis of the mean condensate-film heat transfer coefficient using Nusselt theory.

Test Number	$\overline{\alpha}_{f,t}$ ($W/m^2°C$)	$\Delta\overline{\alpha}_{f,t}$ (%)
1	7634-8072	-5.7375
2	8435-8638	-2.4066
3	8217-8424	-2.5192
4	8000-8209	-2.6125
5	7875-8041	-2.1079

The values shown in Table 5.16 were those obtained at either end of the coolant flow range, and the results show that the change on the condensing side was indeed small, and thus safe to assume that this resistance was constant.

In developing the expression for the mean coolant heat transfer coefficient, it was further assumed that the coolant thermal conductivity did not vary significantly during any of the test runs, and could therefore be assumed constant.

The experimental data showed that the rise in the coolant temperature through the test section was around 6°C at the highest coolant flow rate, and 13-17°C at the lowest coolant flow rate. The coolant thermal conductivity was evaluated at the coolant inlet and outlet temperatures, and the variation was measured across the temperature range during each of the test runs. As the results in Table 5.17 show, the change in the coolant thermal conductivity across the range of measured coolant temperature rises was not much greater than 2%, therefore justifying the assumption made.

Table 5.17.

Analysis of the coolant thermal conductivity.

Test Number	$\Delta\lambda_c$ $(W/m°C)$	$\Delta\lambda_c$ (%)
1	0.00585-0.01352	0.9387-2.1758
2	0.00499-0.01117	0.7903-1.7755
3	0.00519-0.01132	0.8237-1.8008
4	0.00488-0.01105	0.7798-1.7728
5	0.00584-0.01388	0.9292-2.2172

The gradients of the best-fit lines obtained for each of the five test runs are given in Table 5.18. The equations of these lines were used to predict the inverse of the mean overall heat transfer coefficient, which was then compared to the actual measured value. The results of these calculations for each of the five tests were compared, and it was found that the scatter of predictions around the actual measured values produced a maximum over-prediction of the measured values by 12% and a maximum under-prediction of the measured values by 9%.

Table 5.18.

Gradients of lines fitted to experimental data.

Test Number	Gradient ($m^2°C/W$)
1	0.425535
2	0.425356
3	0.469811
4	0.387414
5	0.442786

In order to reconcile the differences found between these gradients, all data were combined to produce an overall graph, and the gradient of the best-fit line from this graph was used in the expression for the mean coolant heat transfer coefficient. This overall graph is shown in Figure 5.1 [p.164].

The equation of the overall best-fit line was used to calculate the inverse of the mean overall heat transfer coefficient, which was then compared to the actual measured value. The results of these calculations showed that using the overall best-fit equation produced a maximum over-prediction of 14%, and a maximum under-

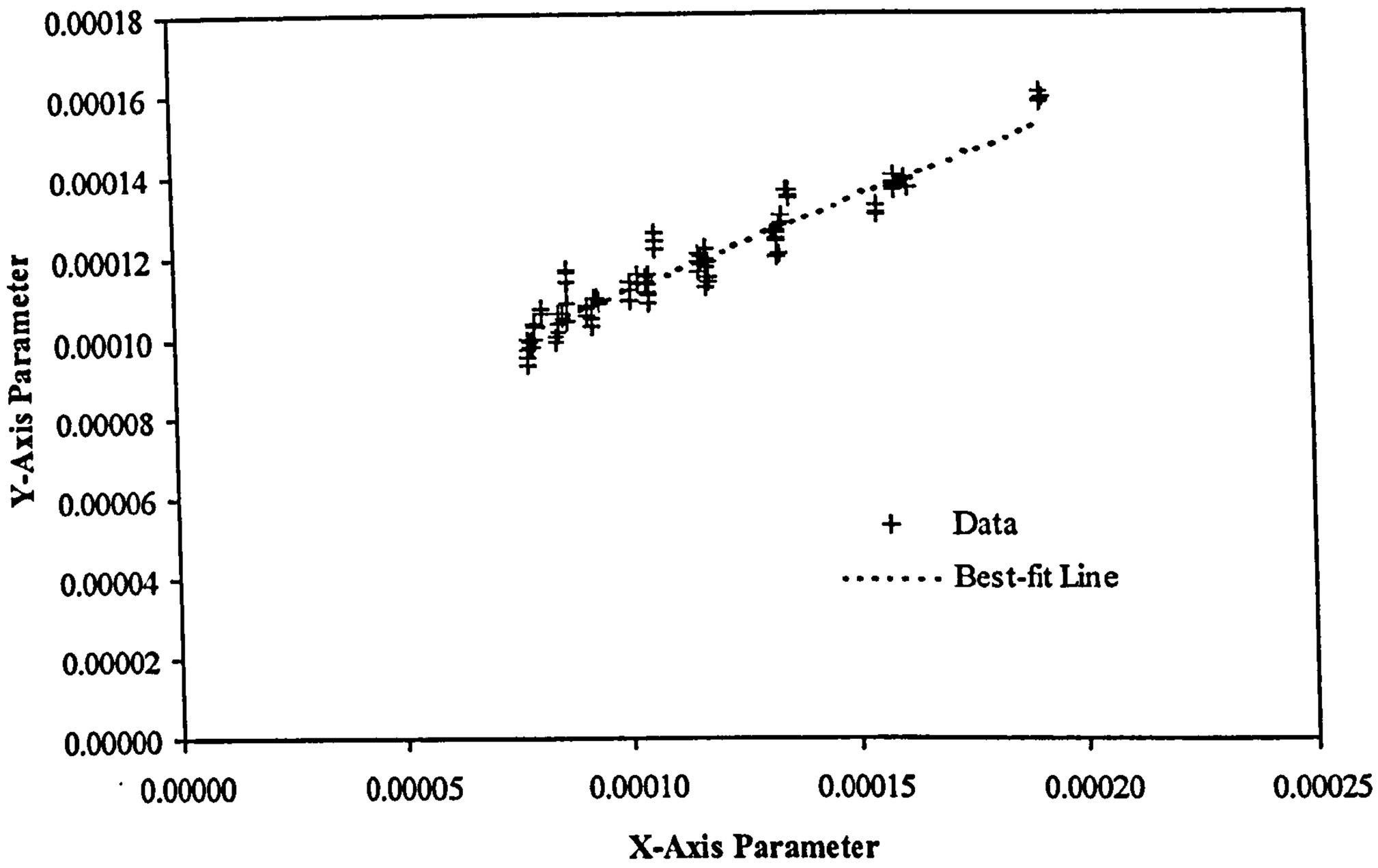

Figure 5.1. The overall Wilson plot for the condensation of steam in a single test section.

prediction of 16% in comparison to the measured values. This represented a slight loss in accuracy in comparison to using the individual equations, although the differences between the maximum over- and under-predictions are not too severe.

Using the gradient of this overall best-fit line, (5.2.18) was more accurately expressed as

$$\overline{\alpha}_c = \frac{1}{0.456785} Re_c^{0.8} \, Pr_c^{0.4} \tag{5.2.22}$$

Therefore, the unique correlation for the mean coolant heat transfer coefficient was

$$\overline{\alpha}_c = 2.1892 \, Re_c^{0.8} \, Pr_c^{0.4} \tag{5.2.23}$$

This expression was then used to determine the range of mean coolant heat transfer coefficients during the test runs. These values were compared to the mean coolant heat transfer coefficients calculated using the gradients of the individual graphs shown in Table 5.18, and the results are shown in Table 5.19.

The results show that using the gradients of the best-fit lines from the individual and overall graphs to calculate the mean coolant heat transfer coefficients produced similar values. In comparing the mean coolant heat transfer coefficients predicted by the gradient of the overall plot to those predicted from the individual plots the maximum difference was found to be 15% and the minimum difference 3%.

Table 5.19.

Comparison of mean coolant heat transfer coefficients.

	$\overline{\alpha}_c$ $(W/m^2°C)$	
Test Number	Overall Plot	Individual Plot
1	7104-15641	7626-16790
2	8757-17565	9404-18864
3	8536-17422	8299-16939
4	8394-16839	9897-19854
5	8528-17204	8797-17748

To demonstrate that using an overall gradient, and hence (5.2.23), in comparison to the individual gradients shown in Table 5.18, had no adverse effect on the accuracy of the mean condensate-film heat transfer coefficient, a sensitivity analysis on the mean condensate-film heat transfer coefficient was carried out. A simplified form of the equation relating the individual heat transfer resistances to the overall resistance was used.

$$\frac{1}{\overline{U}_i} = \frac{1}{\overline{\alpha}_{f,i}} + \frac{1}{\overline{\alpha}_c} \tag{5.2.24}$$

The mean condensate-film heat transfer coefficient was calculated by rearranging this equation to give

$$\frac{1}{\overline{\alpha}_{f,i}} = \frac{1}{\overline{U}_i} - \frac{1}{\overline{\alpha}_c} \qquad (5.2.25)$$

Based on the assumption that the condensing vapour was a single component hydrocarbon, an estimate was needed for the mean overall heat transfer coefficient. The value used in this sensitivity analysis was 1000W/m^2°C, which was taken from Coulson and Richardson (1990), where the approximate overall heat transfer coefficient for low boiling hydrocarbons (on the hot side, and water on the cold side) for a shell-and-tube exchanger, was given as 400-1200W/m^2°C. A typical value taken from Table 5.19 for the mean coolant heat transfer coefficient was 15000W/m^2°C.

Based on these values, a mean condensate-film heat transfer coefficient was calculated from (5.2.25), and is shown in Tables 5.20. Then, the mean coolant heat transfer coefficient was adjusted by 3% and then 15%, and the mean condensate-film heat transfer coefficient re-calculated for both of these changes. These results are also shown in Table 5.20.

As the results of this sensitivity analysis show, the effect on the mean condensate-film heat transfer coefficient was extremely small. The maximum difference found between the condensate-film heat transfer coefficients calculated was approximately 1%. Thus it was assumed that no significant error was introduced by using the expression for the mean coolant heat transfer coefficient derived from the overall Wilson plot as opposed to one derived using an individual plot.

Table 5.20.

Sensitivity analysis for the mean condensate-film heat transfer coefficient.

$\overline{U}_i$ (W/m^2°C)	$\overline{\alpha}_c$ (W/m^2°C)	$\overline{\alpha}_{f,i}$ (W/m^2°C)
1000	15000	1071
1000	14450-15450	1074-1069
1000	12750-17250	1085-1061

The mean coolant heat transfer coefficients calculated using the expression in (5.2.23) were compared with those predicted using the equations of Dittus and Boelter (5.2.26) and with Eagle and Ferguson (1930) (5.2.27), whose equation applies strictly to water.

$$\overline{\alpha}_c = 0.024\, Re_c^{0.8}\, Pr_c^{0.4} \left(\frac{\lambda_c}{d_{eh}}\right) \tag{5.2.26}$$

$$\overline{\alpha}_c = 4200\,(1.35 + 0.05T_c)\frac{u_c^{0.8}}{d_{eh}^{0.2}} \tag{5.2.27}$$

The results of these comparisons are shown in Table 5.21, and it shows that although neither correlation accurately predicts the actual mean coolant heat transfer coefficient found by the empirical equation, they do predict values of similar magnitude.

Table 5.21.

Comparison of mean coolant heat transfer coefficients by different correlations.

Test Number	Empirical ($W/m^2°C$)	Dittus-Boelter ($W/m^2°C$)	Eagle-Ferguson ($W/m^2°C$)
1	7104-15641	8489-18739	8532-18032
2	8757-17565	10599-21312	10624-20654
3	8536-17422	10321-21108	10339-20440
4	8394-16839	10064-20262	9995-19469
5	8528-17204	10271-20787	10418-20163

At lower coolant flow rates, the mean coolant heat transfer coefficient was predicted slightly better by the Dittus-Boelter equation, which over-predicted the coefficient calculated by the empirical correlation by around 20%. At higher coolant flow rates, the mean coolant heat transfer coefficient was predicted slightly better by the Eagle-Ferguson equation, which over predicted the coefficient calculated by the empirical equation by around 16%.

Thus, the empirical correlation in (5.2.23) has been shown to be more accurate than two standard correlations that are readily available for calculating the mean heat transfer coefficient during forced convective flow. The method used to derive the correlation from a large data set was shown to produce a slight reduction in the accuracy of the predicted mean coolant heat transfer coefficient. However, this was found to have a negligible effect on the value of the mean condensate-film coefficient.

5.3 Single Component Hydrocarbons and Binary Hydrocarbon Mixture Tests

This section contains the general findings based on the experimental work carried out using single component hydrocarbons and then binary hydrocarbon mixtures. It is then followed by a discussion of the results specific to the single components and to the binary mixtures.

5.3.1 Balance of Heat across the Test Facility

A full heat balance across the test facility was described by the equation below, which states that heat generated by the cartridge heaters can be accounted for in the heat loads across the test and dump condensers and the heat losses to the surroundings.

$$\dot{Q} = \dot{Q}_{c,TC} + \dot{Q}_{c,DC} + \dot{Q}_{losses} \tag{5.3.1}$$

As there are inaccuracies in the measurement of temperatures and flow rates used in determining the coolant heat loads and the heat losses, the overall heat balance described in (5.3.1) will never be exact.

As discussed in Chapter 4.5.3, the lack of suitable instrumentation in the test facility meant that no measurement of heat loss was made during the experimental work. These heat losses were identified as those lost by the transfer of heat through the hot surfaces of the test facility, including those surfaces covered by insulating material,

and by the removal of heat by the air stream ventilating the containment cabinet. These processes are illustrated in Figure 5.2 [p.172].

By only considering the heat loads measured across the test and dump condensers, 85-93% of the measured power input to the cartridge heaters during all single component hydrocarbon tests, and 83-87% during tests with the binary hydrocarbon mixtures was accounted for. The failure to account for more of the heat input supplied by the cartridge heaters caused some concern, and as a result some short experiments were conducted at the end of this research project to address this problem. The results have not been included in this thesis as they were merely used by the author to give an indication of the problem, and furthermore, were based on approximate measurements.

By measuring the surface temperature at various points of the test fluid circuit and the air temperature inside the containment cabinet, the heat loss to the surrounding air was calculated across some of the uninsulated surface areas. This showed some heat was lost through these surfaces, and further heat losses were possible from the insulated surfaces, which displayed a higher temperature than the surrounding air. Unfortunately, it was difficult to make accurate measurements of the surface temperatures, owing to the lack of suitable instrumentation, the need to keep the containment cabinet open during these tests, and to determine the number of locations from which to make measurements of the surface temperatures.

The rate of heat loss to the ventilating air stream was estimated by measuring the temperature of the ambient air and of the air inside the containment cabinet. The flow rate of ventilating air through the cabinet was estimated using information on the exhaust fan supplied by the manufacturer. These measurements also showed that heat was removed from the test facility by the ventilating air stream.

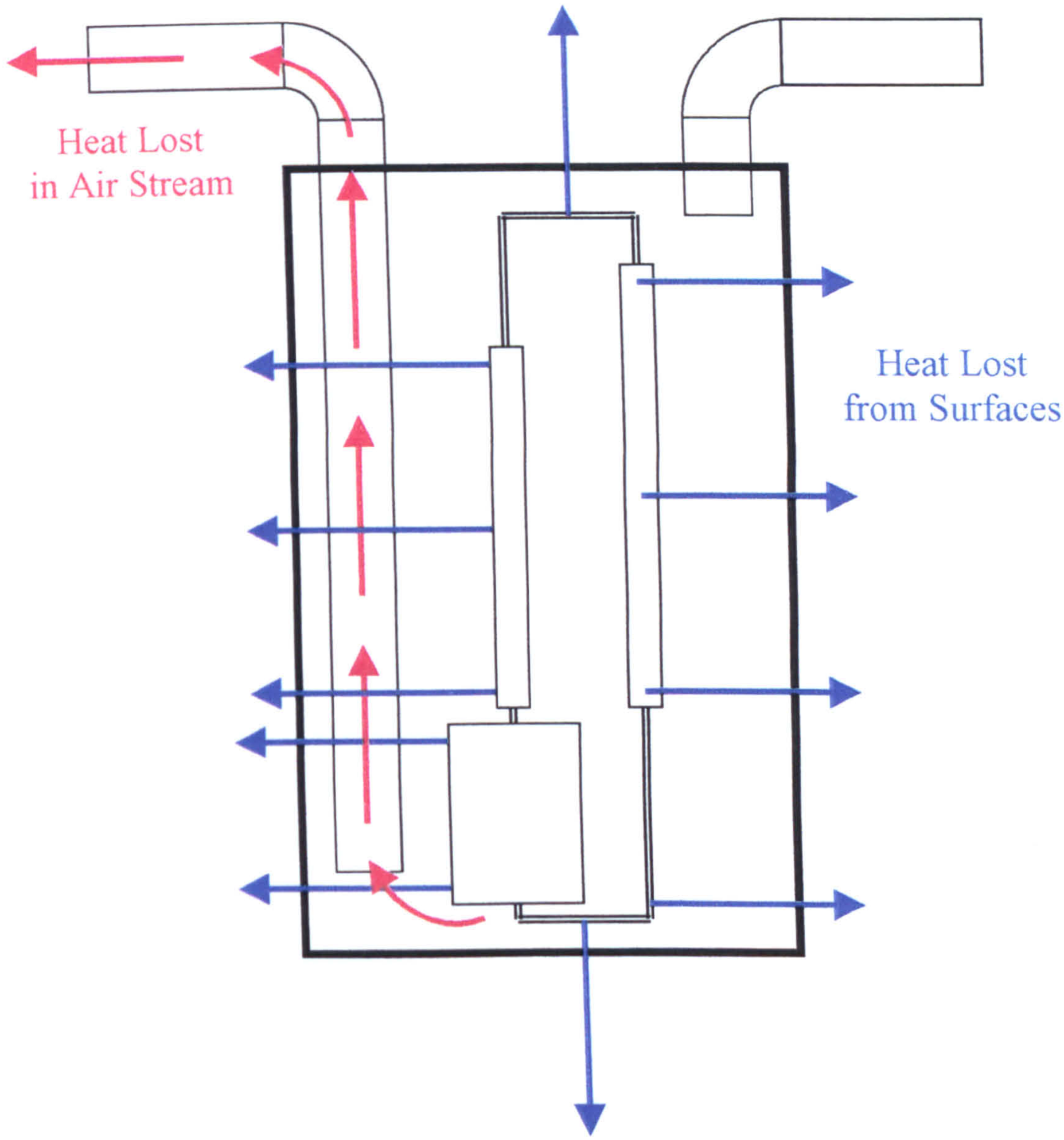

Figure 5.2. Identification of heat losses.

As the results of these experiments showed, an improvement to the heat balance was obtained by considering the loss of heat by both these processes. Thus, further work in this area is suggested to improve the analysis of the measurements taken during experimental work.

The estimation of heat lost to the ventilating air stream could perhaps be improved by making additional measurements of the air temperature inside the containment cabinet to provide a more overall representation of the cabinet air temperature. Furthermore, evaluation of the flow rate of the ventilating air stream could be improved either by installing a flow meter, or measuring the velocity of the air stream.

Additional heat losses might occur through the walls of the containment cabinet, and these could be estimated by measuring the surface temperature of the cabinet and that of the surroundings. This calculation might be improved if these measurements were made at several different locations to give an overall representation of the surface and surrounding temperatures.

5.3.2 Varying the Test Condenser Length

The experimental procedure described in Chapter 4.4.1 stated that it was the intention of the experimental programme of work to investigate the effect of condenser length on the reflux condensation process. It was felt that the length of the test condenser would be an important parameter in both the heat and mass transfer processes involved in reflux condensation, as it meant varying both the available heat transfer surface area and the inter-phase area between the vapour and condensate.

As also mentioned in Chapter4.4.1, it was discovered impossible to control the length of the test condenser by altering the number of test sections as the control system intended. This control system comprised three independently operated solenoid valves on the inlet lines to each of the test sections, and the flow of coolant between the test sections was controlled by opening and closing these valves. In the normal position these valves were closed, which meant that the operator was required to open a valve to direct coolant to the inlet port of the test section. As Figure 4.22 [p.100] illustrated, the test sections were operated in series rather than in parallel, with the coolant always assumed to flow downward through the test sections.

However, it was discovered that the positioning of the solenoid valves and the connections between the test sections allowed the coolant flow to split in two directions at the inlet port to the lower test section. Thus for experimental test work carried out where the lowest test section was supplied with coolant, this coolant stream was split at the inlet port. As assumed the coolant flowed through the lower test section and exited from the outlet port, where its flow rate was measured, but in addition, some part of the coolant flowed up through the middle test section, and also through the highest test section. Although this split flow rate was not measured by any flow meter, its presence was detected by a rise in the coolant temperature across these other test sections.

This split coolant flow meant that additional condensation occurred inside the test condenser, which was likely to increase the mass flow rate of condensate in the test sections, thus increasing the condensate film Reynolds number, and causing a decrease in the value of the mean condensate-film heat transfer coefficient. As a result, all experimental test work carried out across the lowest test was invalidated and has not been reported in this thesis.

To overcome this problem, it is suggested that an additional three solenoid valves are installed at the outlet sides of each of the three test sections. The original solenoid valve on the inlet side, and the new solenoid valve on the outlet side, would form a new control system for each test section. Both valves in each set would have to be operated simultaneously to ensure that the test section is opened or closed to the flow of coolant at both ends at the same time.

The installation of such a system might prove difficult owing to the limited space surrounding the test condenser within the containment cabinet, and the possible difficulty in siting the additional solenoid valves, and their components. However, if the effect of condenser length on the reflux condensation were to be properly investigated, it might be beneficial to install such a system as outlined above.

Although it might be felt that this problem could be overcome by installing manually operated valves on the outlet sides of each test section, this presents a potential operating hazard. As the containment cabinet houses the test fluid circuit, it has been classified an area of high risk, and special precautions were enforced by the Health & Safety Executive. Thus it would not be feasible to have manually operated equipment inside, as the cabinet should be sealed during normal operation. A more elaborate system such as the one suggested here is required.

5.3.3 Measuring the Flooding Velocity

As highlighted in Chapter 3, flooding in reflux condensers is a major design consideration. A reflux condenser must be operated below the flooding point for normal, steady operation to be maintained. If the condenser is at or above this point, steady operation will cease.

Although a study of the flooding phenomenon in reflux condensers was not of primary interest in this particular research project, it was felt necessary to carry out some analysis of the reflux operation in the test condenser during experimental work. Therefore, the velocity of the vapour inlet stream at the bottom of the test condenser was calculated, and was compared with the predictions of a known equation for determining the vapour flooding velocity.

The equation chosen to predict the flooding velocity was a modified from of that due to Alekseev, Poberezkin, and Gerasimov (1972). McQuillan and Whalley (1984) compared flooding correlations, and that due to Alekseev et al. was found to give the most accurate calculated values. This method has been recommended by HTFS for calculating flooding velocities, and is described by Whalley (1984).

$$\dot{v}_v = \frac{K_v \left[g_n \sigma \left(\rho_f - \rho_v \right) \right]^{1/4}}{\rho_v^{1/2}} \qquad (5.3.2)$$

As this correlation was found to have an accuracy of 50% for air-water systems and 60% with non air-water systems, it is recommended that the vapour velocity calculated by (5.3.2) be divided by a factor of 1.6 to give a more conservative estimate of that required to cause flooding.

The actual velocity of the vapour entering at the bottom of the test condenser was calculated from the vapour mass flow rate, obtained from the heat and mass balance calculations. The equation used to determine this velocity is shown below.

$$\dot{u}_v = \frac{\dot{M}_v / \rho_v}{S_{i,TC}} \tag{5.3.3}$$

The results of the flooding velocity calculations for the single component hydrocarbons are shown in Figure 5.3 [p.178]. The full set of calculations for n-pentane have been included in Appendix A7, Tables A7.25 to A7.28, and in Appendix A8, Tables A8.25 to A8.28 for iso-octane.

The measured velocities were compared to the conservative prediction of flooding velocity, where the safety factor was included in the calculation, and the non-conservative prediction, where the safety factor was not included. As Figure 5.3 [p.178] illustrates, the non-conservative prediction method appears to give results that were more consistent with experimental observations, as it predicts a vapour flooding velocity greater than the measured value. Therefore, as observed, the reflux condensate was able to drain unhindered from the bottom of the test condenser.

The differences observed in the measured velocities between the n-pentane and iso-octane tests can perhaps be attributed to the large differences in the vapour densities of the two components. At the conditions measured in the test condenser, the vapour density of iso-octane was much smaller than that of n-pentane and consequently the volumetric flow rate of iso-octane vapour at the bottom of the test condenser was greater. This resulted in much higher inlet vapour velocities being reached with iso-octane vapour in comparison to those with n-pentane vapour.

The same analysis was applied to the tests with the binary hydrocarbon mixtures, and the results are shown in Figure 5.4 [p.179]. The full set of calculations for the first mixture have been included in Appendix A9, Tables A9.19 to A9.21, and in Appendix A10, Tables A10.19 to A10.21 for the second mixture.

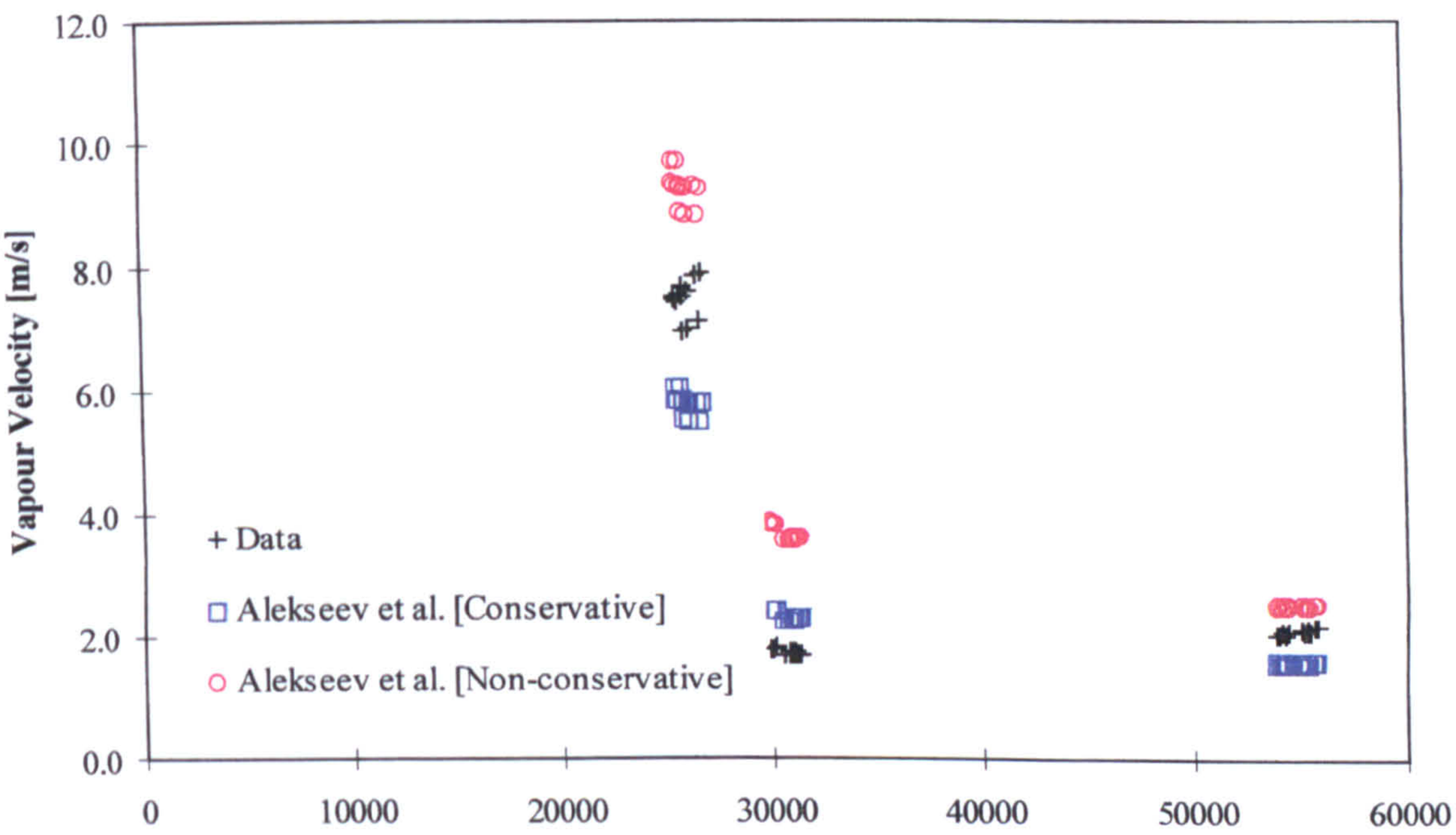

Figure 5.3. Flooding velocities in the test condenser during single component hydrocarbon tests.

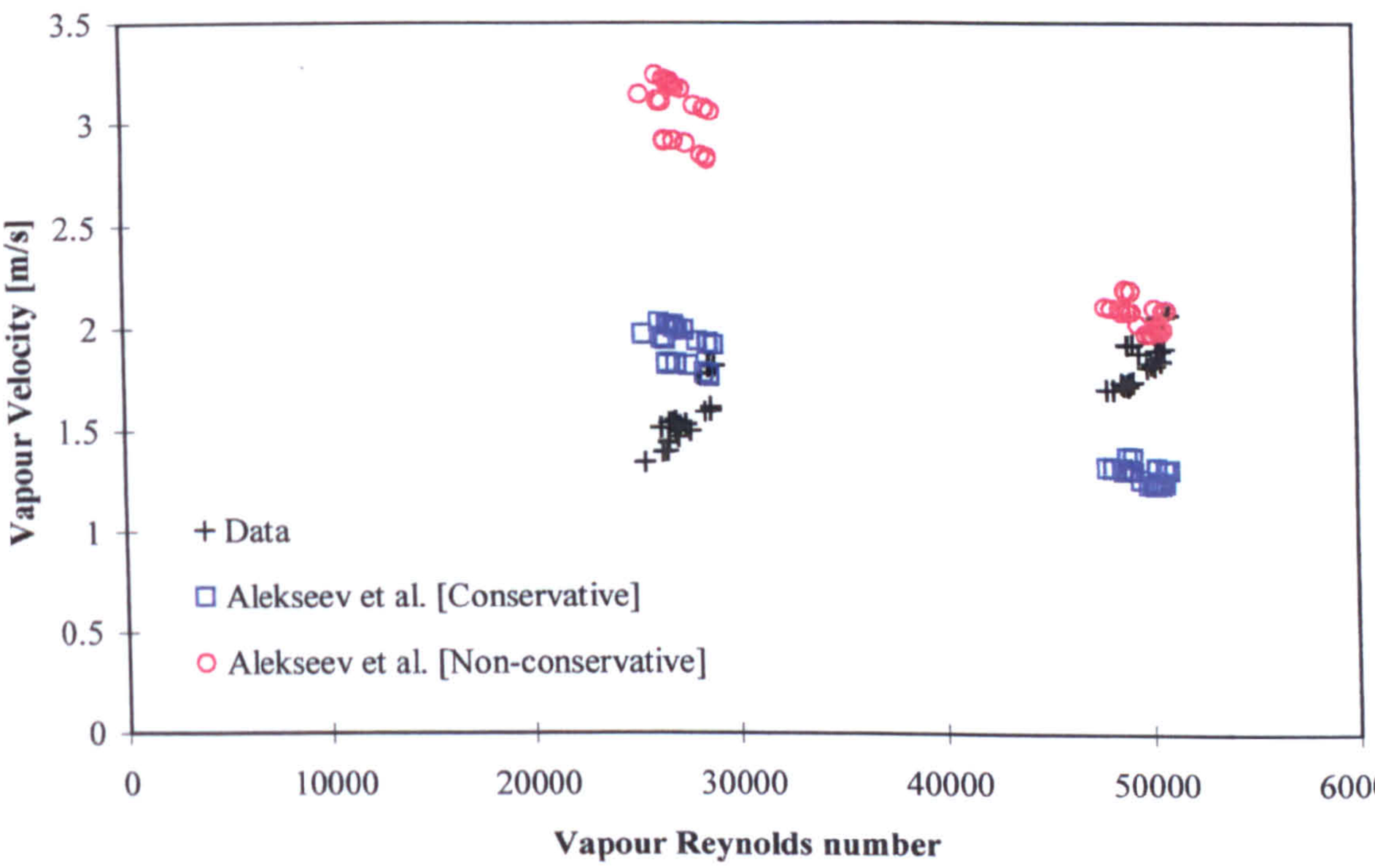

Figure 5.4. Flooding velocities in the test condenser during binary hydrocarbon mixture tests.

As these results show, the prediction of the flooding velocity is once again sensitive to the inclusion of a safety factor. The measured velocities were found to be both lower and higher than the predicted velocities when compared to the conservative estimate, but were found to be lower when compared to the non-conservative prediction. As the reflux condensate was seen to be steadily discharged from the bottom of the test condenser during the binary mixture tests, the non-conservative prediction of flooding velocity agrees better with experimental observation.

This analysis serves as a good illustration of the problem encountered in predicting flooding velocities in reflux condensers. At the present time, no single correlation has been developed that can accurately predict the flooding velocity under reflux conditions. As a result, a safety factor often has to be included in the prediction method to account for the inaccuracies, but does not guarantee accurate prediction of the flooding velocity.

5.4 Single Component Hydrocarbon Tests

The test data and data analysis calculations for the single component hydrocarbon tests are provided in Appendices A7 for the n-pentane and A8 for the iso-octane, respectively.

The focus in carrying out tests with single component hydrocarbons was to measure the experimental condensate-film heat transfer coefficient, and the method for evaluating this variable was explained in Chapter 4.5.3. These tests were carried out to provide a basis for further tests with binary hydrocarbon mixtures of the same two single components used here.

These mean experimental condensate-film heat transfer coefficients were compared with the predictions of classic Nusselt theory, and with the method recommended by HTFS, as described by McNaught (1990). The method recommended by HTFS utilises the Nusselt equation for the laminar region and the correction to the Nusselt equation by Kutateladze for the laminar-wavy region. The transition Reynolds number from the laminar-wavy region to the turbulent region is estimated using proprietary methods, and the correlation of Chun and Seban (1971) is used for the heat transfer coefficient in the turbulent regime. Both the classic Nusselt theory and the method recommended by HTFS assume that the only external force acting on the condensate film is gravity, and furthermore, in the method recommended by HTFS, the presence of waves on the condensate surface and turbulence in the condensate film are both considered.

The averaging process for determining the mean condensate-film heat transfer coefficient from the local value assumed that the condensate film Reynolds number was zero at the top of the surface. As the calculations were carried out across each of

the test sections progressively down the test condenser tube, this assumption was only valid for the highest test section.

$$\frac{1}{\overline{\alpha}_f} = \frac{1}{Re_f} \int_0^{Re_f} \frac{dRe}{\alpha_f} \qquad (5.4.1)$$

It was therefore necessary to manipulate the values calculated by the methods of Nusselt and HTFS to determine the correct mean values. This manipulation was based on the following equation

$$\frac{1}{\overline{\alpha}} = \frac{1}{\overline{U}\ A_T} \int_{\dot{Q}_T} \frac{d\dot{Q}}{\alpha\ \Delta T} \qquad (5.4.2)$$

Values of the mean experimental condensate-film heat transfer coefficient for the n-pentane and the iso-octane tests are shown in Appendices A7 and A8, Tables A7.13to A7.16 for the n-pentane results and Tables A8.13 to A8.16 for the iso-octane, respectively. The comparisons with Nusselt's equation and the method of HTFS are shown in Appendices A7 and A8, Tables A7.17to A7.20 for the n-pentane tests and Tables A8.17 to A8.20 for the iso-octane tests, respectively. These results are also presented graphically in Figure 5.5 [p.184].

As the measured values show, the resistance to heat transfer presented by the condensate film increased as the film flowed down the inside surface of the test condenser. When condensing n-pentane inside the test condenser, the mean experimental condensate-film heat transfer coefficient was found to vary from around 1600W/m^2°C in the top test section to around 700W/m^2°C in the bottom test

section. Similarly, when condensing iso-octane, this value varied from around 1000W/m^2°C at the top to around 500W/m^2°C at the bottom of the test condenser.

As the condensate flow rate was increased through additional condensation, the thickness of the film increased as it flowed down the surface of the tube wall. There might also be some thickening of the film by the upward flow of vapour through the condenser. This effect would become more pronounced nearer the bottom of the tube, where both the vapour and condensate flows are greatest. A thick film would present more resistance to heat transfer than a thin film.

As these values show, there is some disagreement between the experimental values and the predictions of both the Nusselt and HTFS methods at all points in the test condenser. However, it is evident that the method of HTFS more closely predicts the experimental values than Nusselt's method.

The n-pentane test results show that the maximum differences between the experimental values and those predicted by Nusselt were 66% for the highest test section, 87% for the middle test section, and 124% for the lowest test section. When compared with the predictions of the HTFS method, these differences were found to be 33, 26, and 45%, respectively.

For the iso-octane tests, the results showed that the maximum differences between the experimental values and those predicted by Nusselt were 49% for the highest test section, 39% for the middle test section, and 55% for the lowest test section. When compared with the predictions of the HTFS method, these differences were found to be 29, 14, and 22%, respectively.

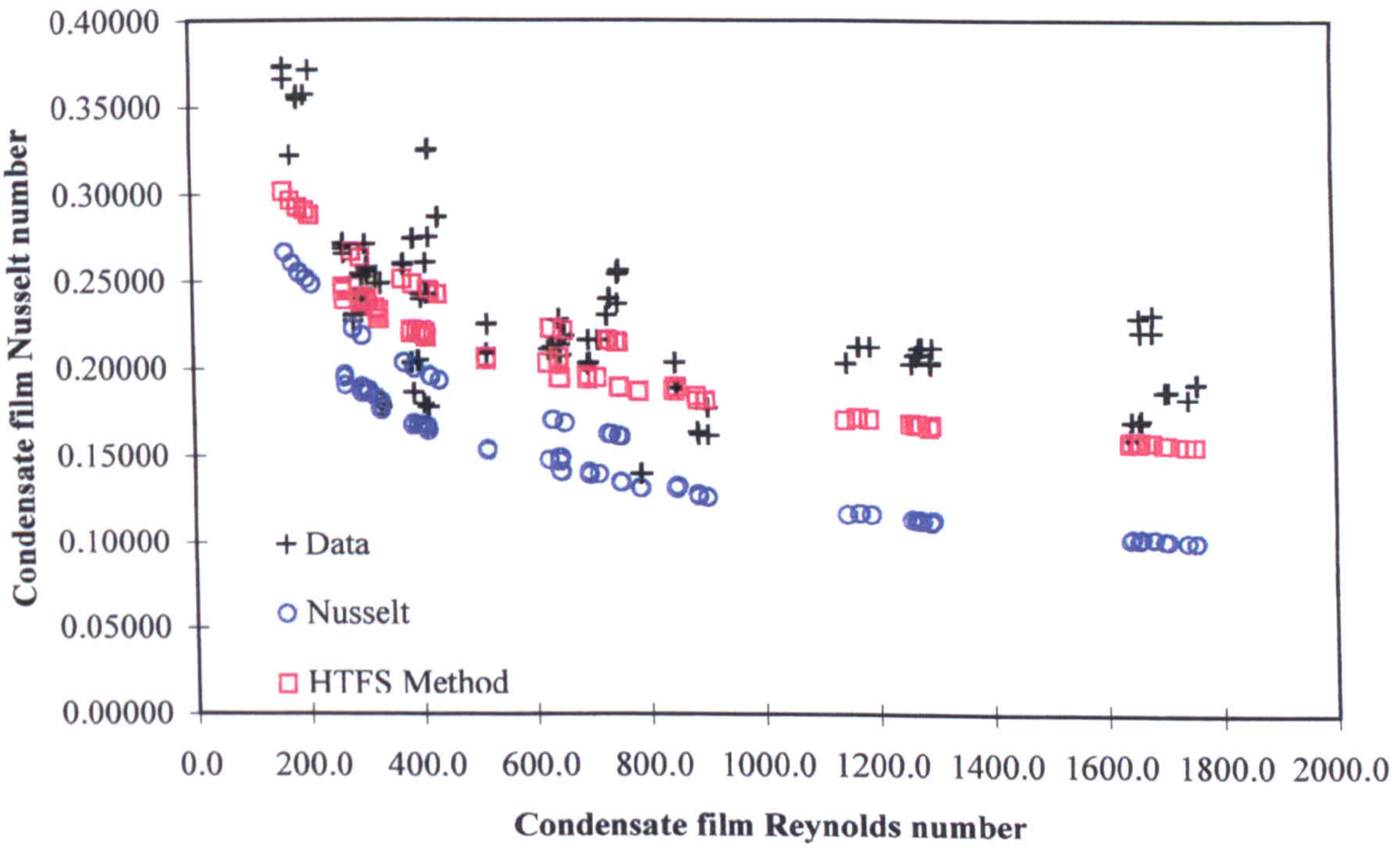

Figure 5.5. Plot of condensate film Reynolds numbers against condensate film Nusselt numbers measured across the test sections.

In comparing the measured values and the predictions of Nusselt and by the method of HTFS, it can be seen that there is considerable scatter amongst the data. This scatter can perhaps be explained by the small temperature differences measured on the coolant side across the test sections, which increases the possibility of error in the calculations.

In an attempt to improve upon these findings, a further analysis was carried out across the entire length of the test condenser. The mean overall, coolant and tube wall heat transfer resistances were evaluated across the entire test condenser, and were used to evaluate the mean experimental condensate-film heat transfer coefficient. As sub-cooling of the reflux condensate from the test condenser was considered in this overall analysis, the mass flow rates, and thus condensate film Reynolds numbers, differed from the previous analysis.

Once more comparisons were made between the mean experimental condensate-film heat transfer coefficients and those values predicted by the methods of Nusselt and of HTFS. The results of these calculations are shown in Appendices A7 and A8, Tables A7.21 to A7.24 for the n-pentane tests and Tables A8.21 to A8.24 for the iso-octane tests. Figure 5.6 [p.186] shows the measured experimental condensate film Reynolds numbers plotted against the Nusselt number. Also shown in this plot are the predictions of classic Nusselt theory and those by the method of HTFS.

These comparisons show that the data were better predicted by the method of HTFS than by that of Nusselt. For the n-pentane tests, the maximum difference between the experimental values and those predicted by the method of Nusselt was 78%, whereas when compared with the method of HTFS, this difference was found to be 23%. For the iso-octane tests, the same comparisons were made, and these differences were found to be 33% and 12%, respectively.

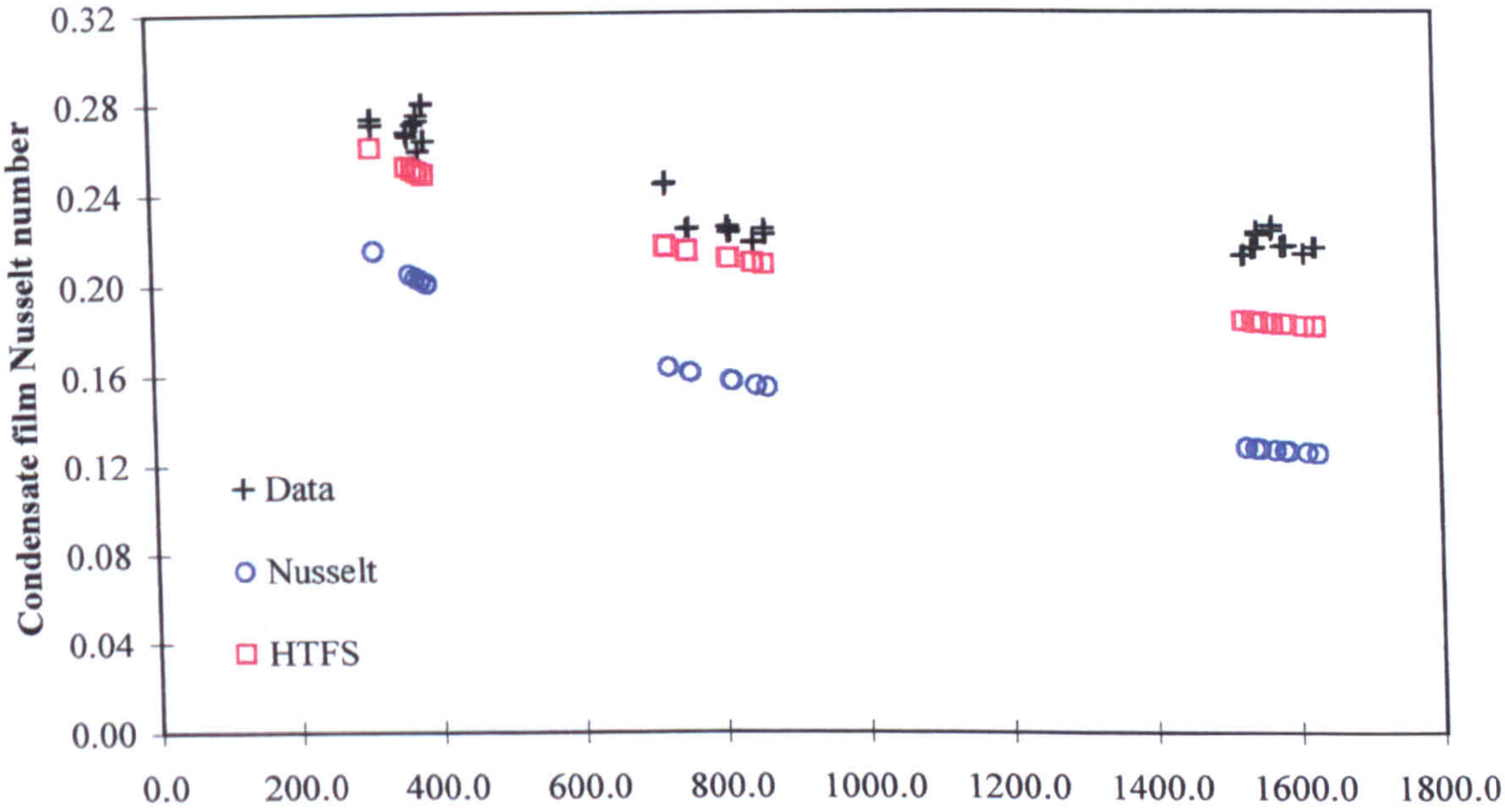

Figure 5.6. Plot of condensate film Reynolds numbers against condensate film Nusselt numbers measured across the test condenser.

The higher disagreement with the predictions based on Nusselt's method is perhaps evidence of the departure from the idealised conditions of a smooth, laminar falling-film, and the range of Reynolds numbers measured for these single component tests was seen to be well above those assumed for the laminar region.

The close approximation in predicting the measured values of the mean condensate-film heat transfer coefficient using the HTFS method might suggest that the most important external force acting on the condensate film is that of gravity. Any force exerted by the upward flowing vapour on the condensate film does not have a significant influence on the resistance to heat transfer.

For steady operation of a reflux condenser, the condensate must be capable of draining freely from the bottom of the unit. This situation will occur where the force acting on the condensate film at the bottom of the unit due to gravity exceeds any other forces acting on the film. As both the forces due to gravity and vapour shear will be greatest at the bottom of the tube, gravity will control the process. Thus, it might be expected that gravity should dominate the reflux condensation process at all points along the condenser.

Another graph was produced with the condensate film Reynolds numbers plotted against the ratio of the experimental Nusselt number to that predicted by the method of HTFS, as shown in Figure 5.7 [p.188]. A best-fit line was attached to this data from which a correlation was produced relating this ratio to the condensate film Reynolds number. The equation derived is shown below.

$$\frac{Nu_f}{Nu_{f,HTFS}} = 0.00010373\,Re_f + 1.0145 \qquad (5.4.3)$$

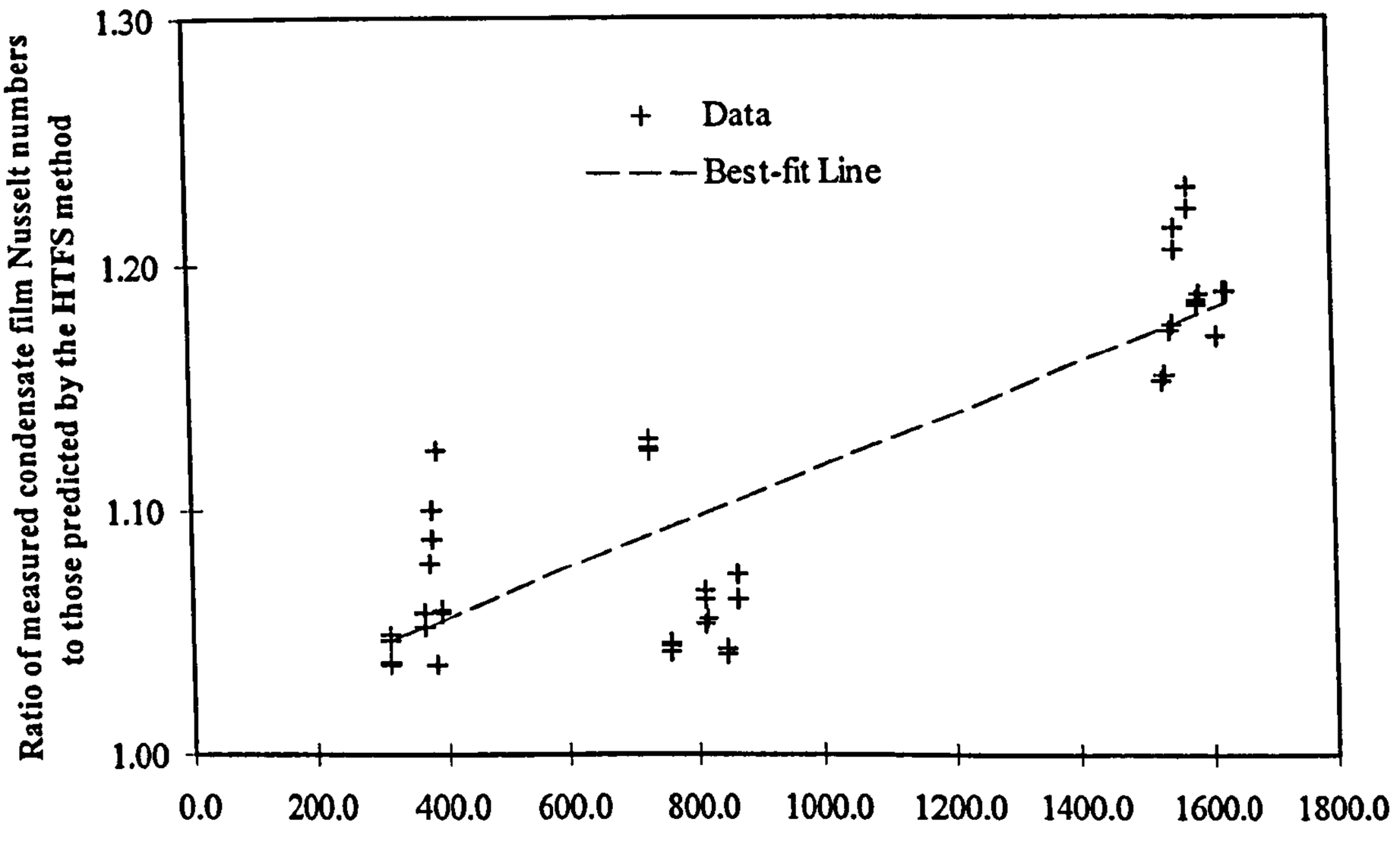

Figure 5.7. Comparison of experimental Nusselt number to that predicted by the method of HTFS measured across the test condenser.

This equation was used to predict the mean experimental condensate-film heat transfer coefficient for both the n-pentane and iso-octane tests. It was found that the greatest difference between the measured and predicted values was 7%.

Although this empirical correlation offered an improvement over the method recommended by HTFS for predicting the mean condensate-film heat transfer coefficient, it was unclear whether it represented a significant result. As it is based on a limited data set, it is perhaps wise to suggest that more data be gathered to verify these results before basing any conclusions on these findings.

However, it is possible that the empirical correlation improves the prediction by the method of HTFS because of a contribution from the upward flowing vapour. The method of HTFS is based on co-current vapour and condensate flows, where the condensing vapour is assumed to have no effect on the condensate film. With counter-current systems, such as that set-up in the test condenser, the upward flow of vapour may increase the waviness of the phase interface over that achieved in co-current systems. This increased disturbance at the interface may alter the heat transfer process by providing a greater heat transfer surface area between the phases, or causing the film to become more turbulent. This would perhaps explain why the measured heat transfer coefficients were greater than those predicted by the method of HTFS.

As it was the purpose of this section of the research to establish that the measurement systems employed in the test facility functioned well enough with hydrocarbons, and to provide some basis for work with binary hydrocarbon mixtures, no further analysis of the single component tests was carried out.

5.5 Binary Hydrocarbon Mixture Tests

The test data and the subsequent data analysis calculations for the binary hydrocarbon mixture tests are provided in Appendix A9 for the first mixture and Appendix A10 for the second mixture. The initial composition of the first mixture charged to the boiler had an n-pentane mole fraction of 0.25, and the second mixture had an n-pentane mole fraction of 0.35.

These compositions were chosen to produce a vapour feed that was not too rich with the more volatile n-pentane component. If the feed vapour stream had contained a very high concentration of n-pentane, any composition change produced in the test condenser might not have been detectable with the composition measurement equipment used here. Those liquids charged to the boiler gave rise to feed vapour streams which contained between 50% and 70% n-pentane.

For both mixtures, it was seen that as the vapour travelled upward through the test condenser, its temperature decreased. This was caused by the removal of sensible heat as the vapour was cooled before being condensed. As the composition measurements show, the concentration of the less volatile iso-octane component is lower at the outlet of the test condenser than at the inlet, which meant that iso-octane was condensed preferentially.

By carrying out heat and mass balances across the test and dump condensers, using the methods described in Chapter 4.5.4, it was possible to determine the composition of the feed vapour stream at the bottom of the test condenser. With these values, it was then possible to calculate the change in concentration of the n-pentane component in the vapour between the top and bottom of the test condenser. This change in concentration of the more volatile component between the outlet and inlet

vapour streams was defined as the enrichment that occurred through partial condensation.

These results are shown in Tables A9.10 to A9.12 in Appendix A9 for the first mixture and in Tables A10.10 to A10.12 in Appendix A10 for the second mixture, respectively. These results are also presented graphically in Figure 5.8 [p.192], which shows the enrichment in relation to the test condenser heat flux.

As Figure 5.8 [p.192] indicates for the first mixture, this enrichment was influenced by the heat flux across the test condenser. The results show that the composition of n-pentane in the vapour stream leaving the test condenser increased by between approximately 15 and 53% in comparison to the feed vapour inlet composition, and that the greater enrichment took place at lower levels of heat flux.

The stray group of points for the first mixture (the group of points located well below the other groups for the same mixture) could be attributed to an error in the composition measurement of the exit vapour stream from the test condenser. It was possible that the measuring cell was contaminated with remnants of the liquid used to measure the composition of the reflux condensate, as both measurements appear to be very similar, and do not follow the observed trend for the other measurements taken with this mixture. This error would have been carried through the subsequent mass balance calculations, and hence the calculated vapour inlet composition would be incorrect.

With the second mixture, the separation of components in the binary hydrocarbon vapour mixture showed much less variation with the level of heat flux in the test condenser. The composition of the exit vapour stream was found to be between approximately 16 and 26% richer in the more volatile component when compared to

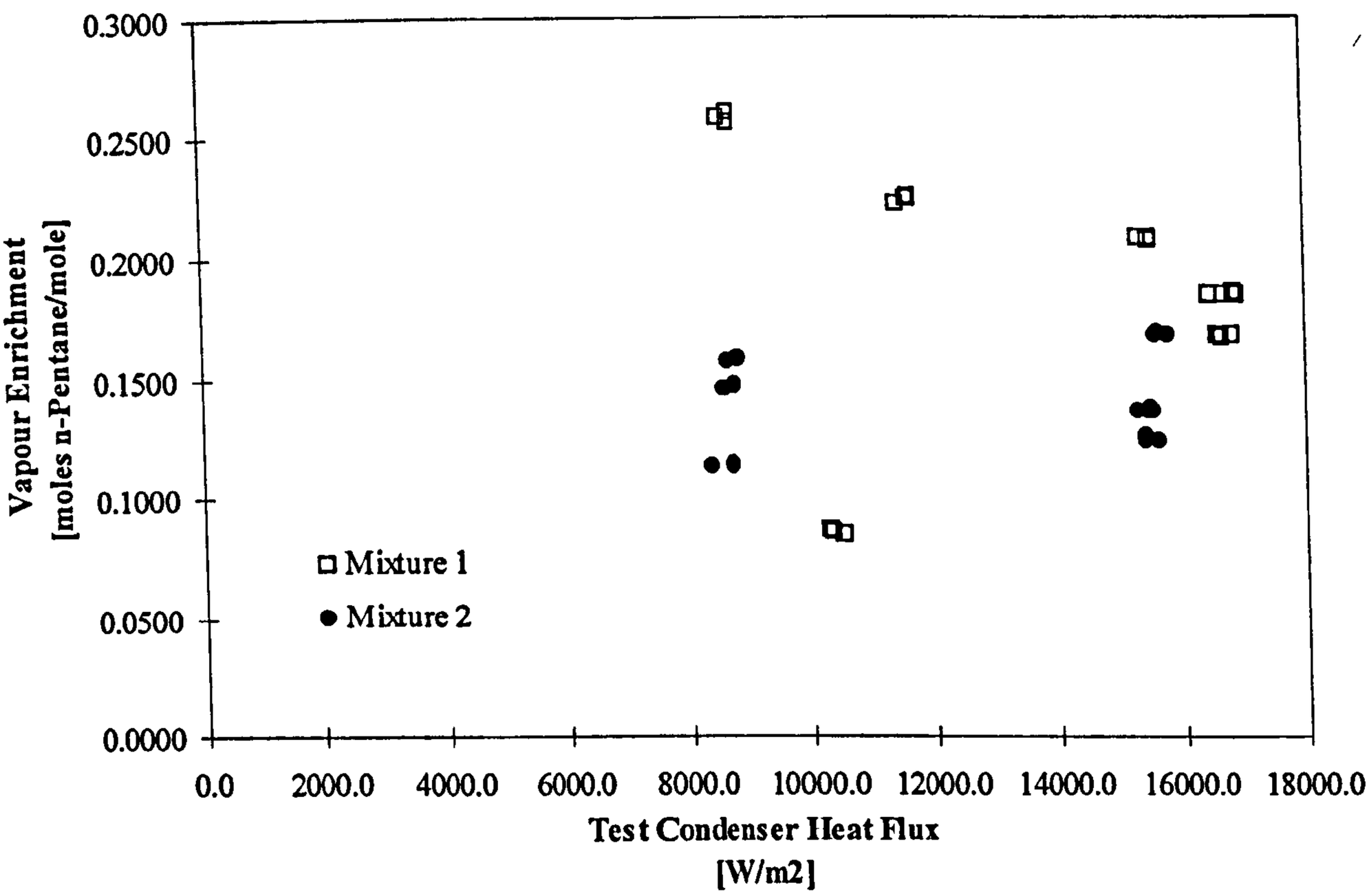

Figure 5.8. Effect of test condenser heat flux on the separation of a binary hydrocarbon mixture.

the composition of the feed vapour stream. The results indicate that the relationship between the heat flux and the degree of separation was less obvious than that obtained for the previous mixture.

During condensation of vapour mixtures, the separation of the components within the vapour phase is improved if the condensation takes place at low heat flux. This is because at low levels of heat flux, the convective motion of the vapour is lower, and hence the concentration gradient within the vapour dominates the mass transfer behaviour. Therefore, the mixture is capable of separating more effectively under these conditions. The results obtained with the first mixture display this trend, whereas those obtained with the second mixture do not show this so clearly.

In comparing the two mixtures, it was seen that a much greater enrichment of the vapour phase was obtained when the initial feed vapour stream contained a smaller concentration of the more volatile component. It is unclear what significance this result has, if any, although it may only reflect a limitation of the test facility and the operating conditions employed to produce these measured separations.

As information obtained from the literature review suggested that reflux condensers were often used because they operated as the equivalent of several thermodynamic stages, it was felt it would be useful to investigate how this test condenser performed. Based on the work of Lintern and Haseler (1995), the number of thermodynamic stages represented by the test condenser was found from

$$\varepsilon = \frac{\tilde{y}_{P,out} - \tilde{y}_{P,in}}{\tilde{y}^{*}_{P,out} - \tilde{y}_{P,in}} \qquad (5.5.1)$$

The results of these calculations are shown in Appendix A9, Tables A9.10 to A9.12 for the first mixture and in Appendix A10, Tables A10.10 to A10.12 for the second mixture, respectively. They are also shown graphically in Figure 5.9 [p.195].

As these results show, the number of thermodynamic stages was found to be less than one for both mixtures. For the first mixture, the number of thermodynamic stages was in the range of 0.26 to 0.78, whilst for the second mixture this range was 0.51 to 0.66.

For the first mixture, the wider spread of values can be attributed to the error in the composition measurement, and if these were neglected the range of thermodynamic stages for the first mixture became 0.53 to 0.78. Therefore, the number of thermodynamic stages was similar for the two mixtures, and the heat flux did not appear to have any significant effect on the number of stages.

As the test condenser has been found to represent less than one thermodynamic stage when operated under these conditions, it can be implied that does not offer much advantage in achieving further separation of the components in a vapour mixture if used in conjunction with distillation apparatus. Thus use of such a device under these conditions would have to be questioned.

Although Lintern and Haseler concluded that a reduction in heat flux should increase the number of thermodynamic stages, their analysis was more involved than the one reported here, and the heat fluxes were well below those actually obtained in the reported experimental work. Further experimental work could be carried out to determine whether reducing the test condenser heat flux could increase the number of thermodynamic stages. This would allow the effect of heat flux on the enrichment of the vapour stream to be more thoroughly investigated.

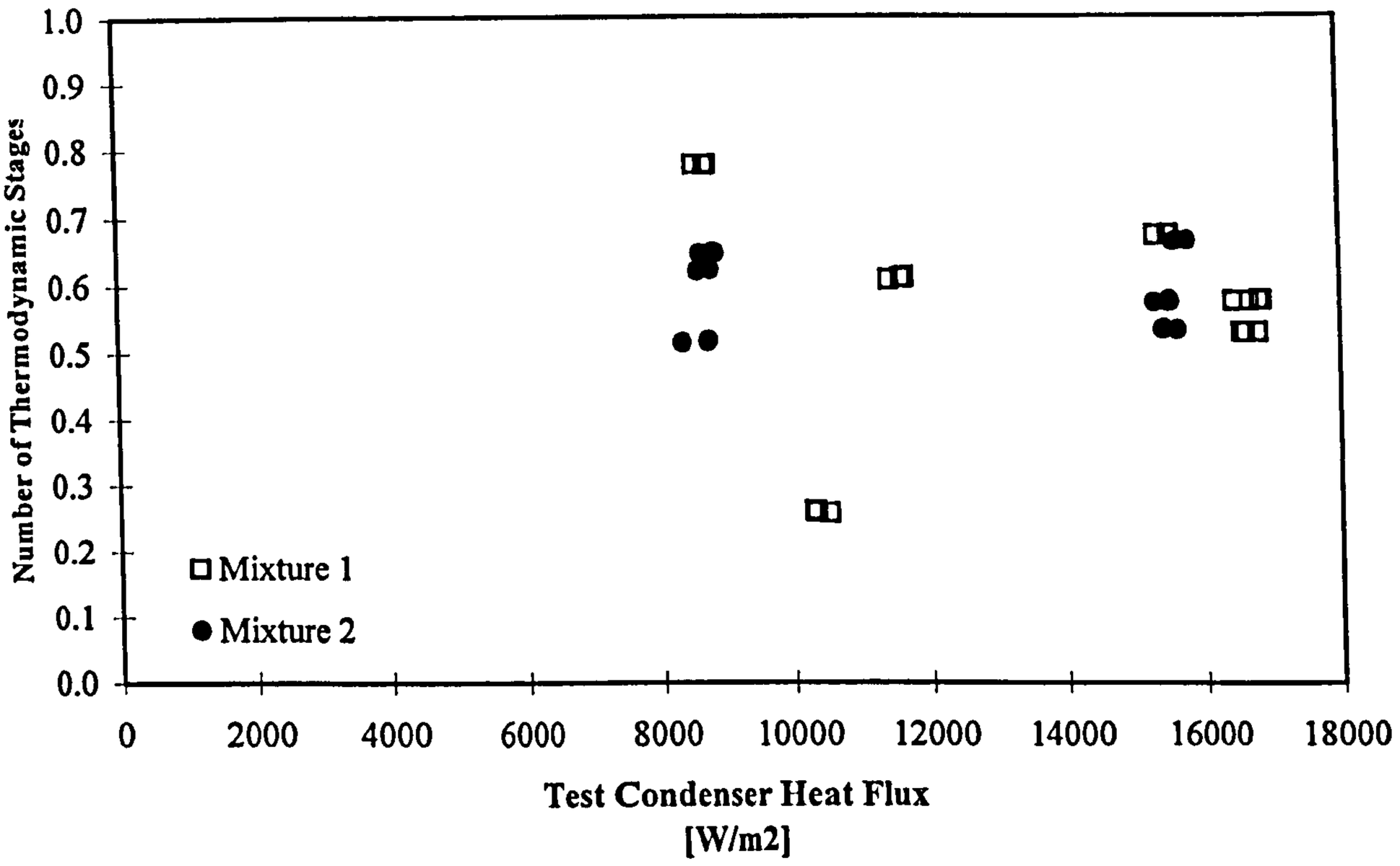

Figure 5.9. Number of thermodynamic stages represented by the test condenser.

5.5.1 Measuring the Condensing-side Heat Transfer Resistances

In the following analysis, the resistance to heat transfer on the condensing side was assumed to be made up of contributions from the condensate film and the vapour. The overall condensing-side heat transfer resistance was taken to be the sum of the resistances due to the condensate film and that due to the vapour. By measuring the mean overall coefficient, and calculating the mean coolant and the mean tube-wall heat transfer coefficients, the resistance on the condensing side was found by the method described in Chapter 4.5.4.

Having determined the overall resistance on the condensing-side, the individual resistances due to the condensate film and the vapour were determined. From heat and mass balances carried out across the test and dump condensers, the mass flow rate of reflux condensate was determined, from which the condensate film Reynolds number was found. The method of HTFS was used to make an initial estimate of the mean condensate-film heat transfer coefficient at the bottom of the test condenser, and this was then corrected using the empirical relationship given in Chapter 5.4.

The resistance due to the vapour was then found by subtracting the resistance due to the condensate film from the total condensing-side resistance. This vapour resistance was termed the effective vapour-side heat transfer resistance, and the results of these calculations are provided in Appendix A9, Tables A9.13 to A9.15 for the first mixture and in Appendix A10, Tables A10.13 to A10.15 for the second mixture, respectively.

For the first mixture, the mean effective vapour-side coefficients were found in the range 360-490W/m$^{2\circ}$ C at low heat flux and in the range 670-720W/m$^{2\circ}$C at high

heat flux. The mean condensate-film heat transfer coefficients showed less variation with heat flux, and were found in the range 800-890 W/m^2°C.

For the second mixture, the mean effective vapour-side coefficients were found in the range 400-450W/m^2°C at low heat flux, whilst at high heat flux the range was 750-820W/m^2°C. The mean condensate-film heat transfer coefficients showed less variation with heat flux, and were found in the range 850-960 W/m^2°C

Thus the resistance to heat transfer is lowered at high heat flux. This can be attributed to the effect of turbulence in the vapour at high heat fluxes, where the vapour Reynolds numbers are higher, and so heat transfer within the vapour phase is improved. Since the mean condensate-film coefficient values are greater than the effective vapour-side coefficients, this implies that the controlling resistance to heat transfer is that due to the vapour.

When condensing vapour mixtures where a large temperature difference exists between the inlet and outlet vapour, sensible heat transfer effects in the vapour phase become more significant due to the large condensing range. In addition, in reflux condensation it is necessary to operate at relatively low vapour velocities to ensure that the condenser is below the vapour flooding velocity. These low vapour velocities lead to low values of the heat transfer coefficient associated with sensible heat transfer from the gas phase. In the data presented here the heat transfer coefficient on the vapour side is much smaller than that on the condensate side, and so the process controlling the overall rate is the heat transfer from the vapour.

5.5.2 Analysis of the Vapour-side Heat Transfer Resistance

The following analysis uses equations presented by McNaught (1979), based on the method first published by Silver (1947) for condenser design.

The total heat flux due to condensation of a vapour mixture can be expressed as

$$\dot{q}_T = U(T_v - T_c) \tag{5.5.2}$$

The heat flux due to sensible cooling of the bulk vapour-phase from the bulk temperature to the interface temperature can be defined in terms of a gas (or vapour)-phase heat transfer coefficient.

$$\dot{q}_v = \alpha_v(T_v - T_I) \tag{5.5.3}$$

For convenience, an effective gas-phase heat transfer coefficient can be defined as

$$\dot{q}_T = \alpha_{v,eff}(T_v - T_I) \tag{5.5.4}$$

Also,

$$\dot{q}_T = \alpha'_f (T_I - T_c) \tag{5.5.5}$$

In (5.5.5) the heat transfer coefficient includes the contributions from the condensate film, the coolant and the tube wall.

Hence, combining (5.5.2) to (5.5.5) gives

$$\frac{1}{U} = \frac{1}{\alpha'_f} + \frac{1}{\alpha_{v,eff}} \tag{5.5.6}$$

or

$$\frac{1}{U} = \frac{1}{\alpha'_f} + \frac{\left(\frac{\dot{q}_v}{\dot{q}_T}\right)}{\alpha_v} \tag{5.5.7}$$

Thus,

$$\alpha_{v,eff} = \frac{\alpha_v}{\left(\frac{\dot{q}_v}{\dot{q}_T}\right)} \tag{5.5.8}$$

Replacing the heat fluxes by the rates of heat transferred across the condenser surface area, (5.5.8) can be re-written as

$$\alpha_{v,eff} = \frac{\alpha_v}{\left(\frac{d\dot{Q}_v}{d\dot{Q}_T}\right)} \tag{5.5.9}$$

The differential term in (5.5.9) can be represented as

$$\frac{d\dot{Q}_v}{d\dot{Q}_T} = \frac{\dot{M}_v Cp_v dT}{\dot{M} dh} = \dot{x}_v Cp_v \frac{dT}{dh} \tag{5.5.10}$$

To evaluate the differential term, a temperature-enthalpy diagram for the condensing system is needed, where the above equation is evaluated at several points along the condensation curve, and the results are integrated to find the required condenser surface area. The type of condensation curve used for the system is dependent on the assumption made about the condensation process, as discussed previously in Chapter 3.4. In the Silver and Bell and Ghaly (1972) methods for condenser design, this differential term is normally obtained from the integral or differential condensation curve.

Here, however, rather than a condensing curve, actual experimental data were used. The differential in (5.5.10) was replaced by the following equation, where the inlet and outlet vapour temperatures were measured directly, and the coolant heat load across the test condenser, and the inlet vapour flow rate were easily calculated from measurements.

$$\frac{dT}{dh} = \frac{T_{v,in} - T_{v,out}}{\left(\dot{Q}_{c,TC} / \dot{M}_{v,in,TC}\right)} \tag{5.5.11}$$

As this equation evaluated the differential term over the full range of condensing conditions as opposed to local values, the vapour quality term in (5.5.10) was replaced by the mean vapour quality through the test condenser. This mean vapour quality was taken to be the average vapour quality between the top and bottom of the test condenser, and was evaluated using the calculated vapour flow rates at these points. Its use was justified by the linear nature of the integral condensation curve generated by the HTFS heat exchanger design program, which used the same process conditions as inputs for the program.

Making these substitutions, (5.5.7) was re-written as

$$\frac{1}{U} = \frac{1}{\alpha'_f} + \frac{1}{\alpha_v}\left(\frac{\dot{x}_v Cp_v\left[T_{v,in} - T_{v,out}\right]}{\dot{Q}_{c,TC}/\dot{M}_{v,in,TC}}\right) \tag{5.5.12}$$

Hence, an experimental gas-side heat transfer coefficient was obtained from

$$\frac{1}{\alpha_v} = \frac{\frac{1}{U} - \frac{1}{\alpha'_f}}{\left(\frac{\dot{x}_v Cp_v\left[T_{v,in} - T_{v,out}\right]}{\dot{Q}_{c,TC}/\dot{M}_{v,in,TC}}\right)} \tag{5.5.13}$$

This was then compared to a dry-gas heat transfer coefficient, with or without the inclusion of a mass transfer correction factor based on the film-theory method. The dry-gas heat transfer coefficient was determined from measured flow rates and temperatures using

$$\bar{\alpha}_{v,i,TC} = 0.023 \frac{\lambda_v}{d_{i,TC}} Re_v^{0.8} \, Pr_v^{0.4} \tag{5.5.14}$$

All vapour physical properties were determined using the PPDS software program, evaluated using the single component values and the component mass fractions obtained through mass balances, and where the vapour Reynolds number was based on an average vapour mass flow rate through the test condenser.

The mass transfer correction factor was defined in terms of a heat transfer rate factor, calculated as a function of the condensing vapour mass flux and the dry-gas heat transfer coefficient.

$$\theta = \frac{\phi}{e^{\phi} - 1} \tag{5.5.15}$$

The condensing vapour mass flux in ϕ was estimated by making the assumption that this flux was equal to the mass flux of the reflux condensate film, with the same concentration of components as those in the film.

$$\phi = \frac{\dot{m}_{f,out,TC} Cp_v}{\bar{\alpha}_{v,i,TC}} \tag{5.5.16}$$

The mass flow rate of the reflux condensate was found from

$$\dot{M}_{f,out,TC} = \frac{\dot{Q}_{c,TC}}{\Delta h_{v,mix,TC} + Cp_{f,mix,TC}\left(T_v - T_f\right)} \tag{5.5.17}$$

The results of these calculations are shown in Appendix A9, Tables A9.16 to A9.18 for the first mixture and in Appendix A10, Tables A10.16 to A10.18 for the second mixture, respectively. They are also presented graphically in Figure 5.10 [p.204], which shows that the experimental values lie between the dry-gas value uncorrected for mass transfer and the dry-gas value corrected for mass transfer.

The effect of using the dry-gas heat transfer coefficient was investigated by using these values to predict an effective gas-side heat transfer coefficient following (5.5.9). The results of these calculations for the first mixture are also shown in Appendix A9, Tables A9.16 to A9.18 and in Appendix A10, Tables A10.16 to A10.18 for the second mixture, respectively. They are presented graphically in Figure 5.11 [p.205].

As the results show, the use of a dry-gas heat transfer coefficient to calculate an effective gas-side heat transfer coefficient over-predicts the measured values at both low and high heat fluxes. For the first mixture, the measured values were found to be in the range 360-700W/m^2°C, whereas the calculated values lay in the range 700-1000W/m^2°C. With the second mixture, the range of values for the measured coefficients was 400-825W/m^2°C, and for the calculated values the range was 710-1200W/m^2°C.

Furthermore, these results show that inclusion of a mass transfer correction factor based on the film theory method causes an under-prediction of the effective gas-side heat transfer coefficient at both low and high levels of heat flux. For the first

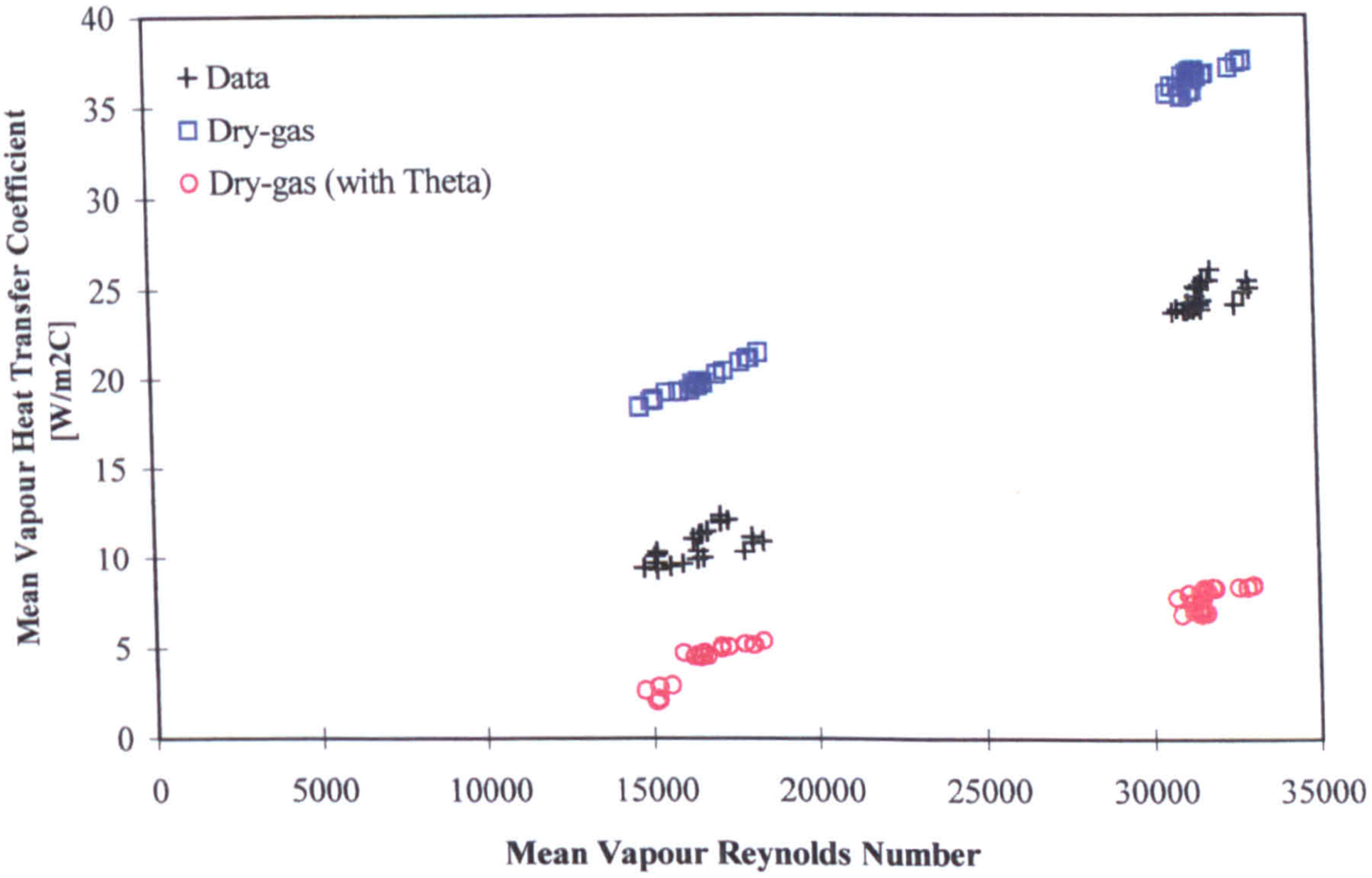

Figure 5.10. Comparison of mean gas heat transfer coefficients.

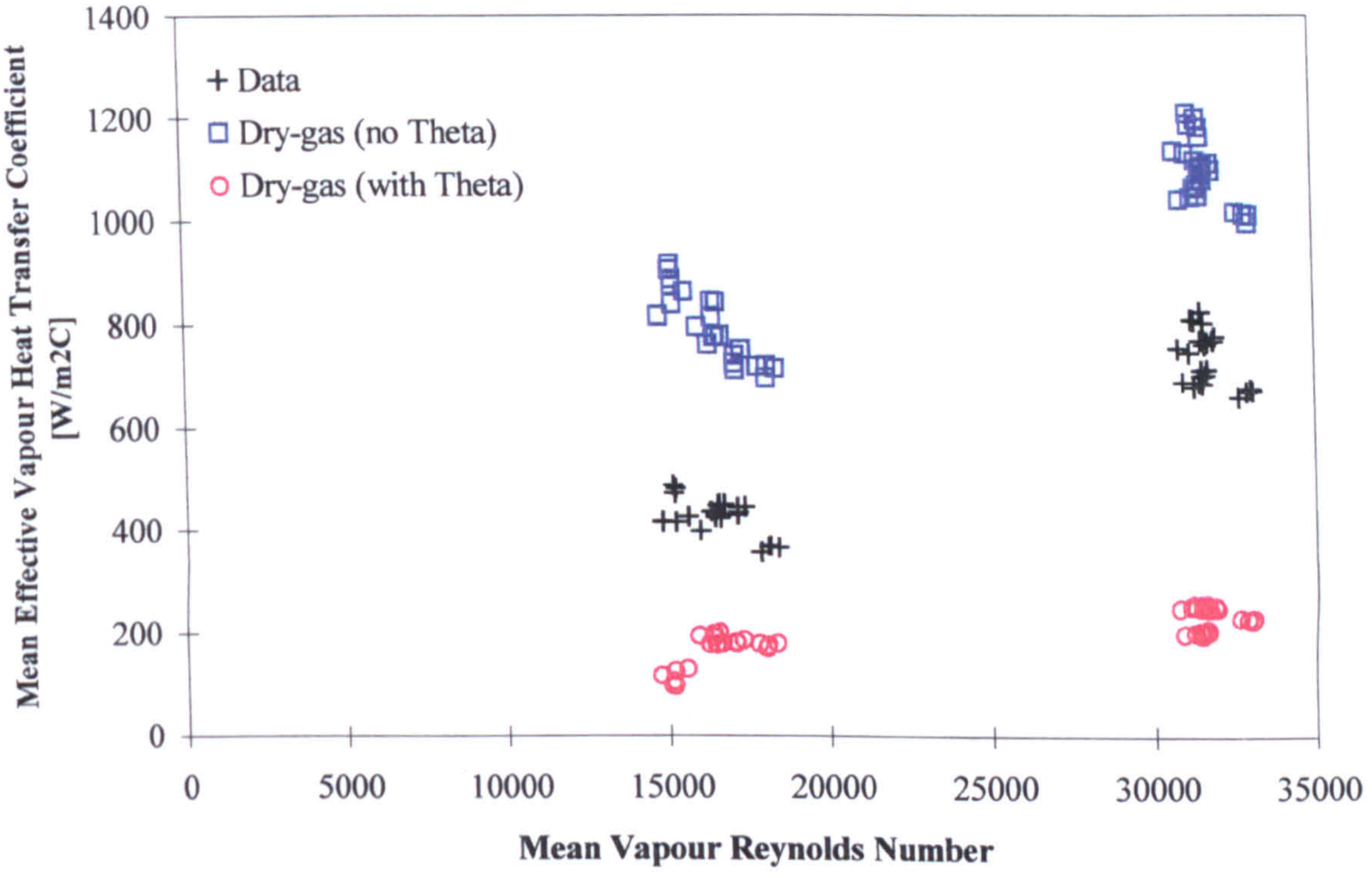

Figure 5.11. Comparison of mean effective gas heat transfer coefficients.

mixture, the calculated values were in the range 100-230 W/m^2°C, and for the second mixture the range of values obtained was 180-260 W/m^2°C.

Thus, the use of a dry-gas heat transfer coefficient was found to under-predict the resistance to heat transfer on the vapour side at both low and high levels of heat transfer. In addition, the inclusion of a mass transfer correction factor was seen to over-estimate this resistance.

In comparing the measured and dry-gas heat transfer coefficients, it was found that the results could be improved upon if an enhancement factor was included. In the absence of a mass transfer correction factor, this enhancement factor was defined as

$$F_e = \frac{\overline{\alpha}_v}{\overline{\alpha}_{v,i,TC}} \tag{5.5.18}$$

If a mass transfer correction factor was included with the dry-gas heat transfer coefficient, then this enhancement factor was defined by

$$F_e = \frac{\overline{\alpha}_v}{\overline{\alpha}_{v,i,TC}\,\theta} \tag{5.5.19}$$

This enhancement factor may be necessary to account for the effect of a wavy film, or the effect of vapour and liquid flowing counter-currently, on the transfer processes taking place.

For the first mixture, this enhancement factor was found to have approximate values in the range 0.5-0.68 with no mass transfer correction factor, and 2.0-5.0 with a mass transfer correction factor. With the second mixture, these ranges were 0.5-0.69 and 2.1-3.1, respectively.

The use of such an enhancement suggests that in the presence of counter-current vapour and liquid flows, a wavy interface may have a more pronounced effect on the heat and mass transfer processes than is normally expected with co-current flows.

It is possible that the counter-current flow produces a greater disturbance of the condensate film surface. This results in a large number of waves at the surface of the condensate film, and so the boundary that separates the liquid and vapour becomes highly distorted. Such a distortion could increase the available interfacial area for both heat and mass transfer, which might lead to increased rates of transfer across the film.

This finding may also have implications in the use of the film theory method, where the rates of heat and mass transfer are evaluated locally through the condenser using heat and mass transfer coefficients. In the method presented by Colburn and Drew (1937), the gas-side heat transfer coefficient is also evaluated using the dry-gas heat transfer coefficient calculated using an equation of the form of (5.5.14), and the mass transfer coefficient is then determined using an analogy between heat and mass transfer. Further work is necessary to examine and verify the extent of this effect on the calculated rates using the film theory method in comparison with the experimental data presented here.

5.5.3 Assessment of Condenser Thermal Design Methods

To further support the analysis described above, comparison was made between the data and the predictions of the standard design tool for industrial condensers. The most common method for the thermal design of condensers is the Silver method. This method uses either the integral or differential condensation curve to evaluate the differential term in (5.5.10) at various locations along the condenser, with the resistance on the vapour side defined in terms of a dry-gas heat transfer coefficient, corrected for the effect of mass transfer following the film-theory method.

The integral or differential condensation curve is generated by a physical properties package. Of the two types, the integral curve is simpler to use as there are no mass balance calculations as required with the differential curve. In comparing the two types of curve, it was decided to use the integral condensation curve in this analysis. Not only is this curve normally used in the design of co-current condensers, it also predicts a less dramatic drop in the condensing temperature because it assumes the two phases remain in intimate contact with each other. In the differential curve, the vapour is assumed to be in equilibrium with the condensate that has just formed on the surface. This leads to a reduction in the vapour temperature at the interface, and hence a decrease in the condensation driving force.

To carry out these comparisons the HTFS heat exchanger design software TASC version 4.01 was used. TASC was provided with information on the coolant temperatures and heat load across the test condenser, the vapour inlet and outlet qualities, and the vapour inlet compositions, as well as an estimate of the vapour pressure calculated using from the vapour temperature measured in the boiler vapour space.

The program was run in checking mode to produce output results of the exit vapour temperature and an estimate of the condenser surface area to meet the specified coolant heat load. These calculations were carried out assuming that the vapour and condensate flowed co-currently through a vertical condenser, and so followed the integral condensation curve. TASC also produced estimates of the amount of vapour condensed and the actual heat load exchanged during the condensation.

From these results it was then possible to determine an integral condensation value for the differential term in (5.5.11). As with the calculations performed using actual data, the new values for the differential term in (5.5.11) were based on average values through the test condenser. As before, this approach was justified owing to the linear nature of the integral condensation curves obtained for each of the test runs.

The mass transfer correction factor defined by the film theory, and shown in (5.5.15), was also included in this analysis. As TASC predicted similar condensate and heat loads but a larger surface area, it was assumed that the rates of heat and mass transfer in the test condenser and in the TASC condenser were proportional to the condenser surface areas. Thus the mass transfer correction factor for the TASC condenser was found by multiplying the mass flux parameter defined by (5.5.16) by the TASC surface area ratio. Had the surface area of the condenser predicted by TASC been equal to the actual test condenser surface area, this ratio would have been equal to one, and the rates of heat and mass transfer in both condensers would have been identical.

The results were used to predict values of the mean effective gas-side heat transfer coefficient, with and without a mass transfer correction factor. The values obtained for the first mixture are shown in Tables A9.16 to A9.18 of Appendix A9, and in Tables A10.16 to A10.19 of Appendix A10 for the second mixture, respectively.

They are also shown in Figure 5.12 [p.211], with the results of the previous analysis work shown on these same axes.

The use of Silver's method, in the absence of a mass transfer correction factor, caused an under-prediction of the measured effective gas-side heat transfer coefficient. For the first mixture, the values lay in the range 200-440W/m^2°C, whilst for the second mixture this range was 233-334W/m^2°C. With the inclusion of a mass transfer correction term, the data were still under-predicted, with the values for the first mixture in the range 130-270W/m^2°C, and for the second mixture the range was 169-221W/m^2°C.

A further analysis of Silver's method was carried out by substituting the experimentally derived gas heat transfer coefficient in the test condenser for the dry-gas heat transfer coefficient calculated in (5.5.13). The results of these calculations are shown in Tables A9.16 to A9.18 of Appendix A9 for the first mixture, and in Tables A10.16 to A10.19 of Appendix A10 for the second mixture, respectively. They are also shown in Figure 5.13 [p.212] along with the results obtained from the original comparison with Silver's method.

The use of this modified Silver's method, in the absence of a mass transfer correction factor, once more caused an under-prediction of the measured effective gas-side heat transfer coefficient. For the first mixture, the values lay in the range 105-298W/m^2°C, whilst for the second mixture this range was 122-235W/m^2°C. With the inclusion of a mass transfer correction term, the data were still under-predicted, with the values for the first mixture in the range 44-139W/m^2°C, and for the second mixture the range was 60-128W/m^2°C.

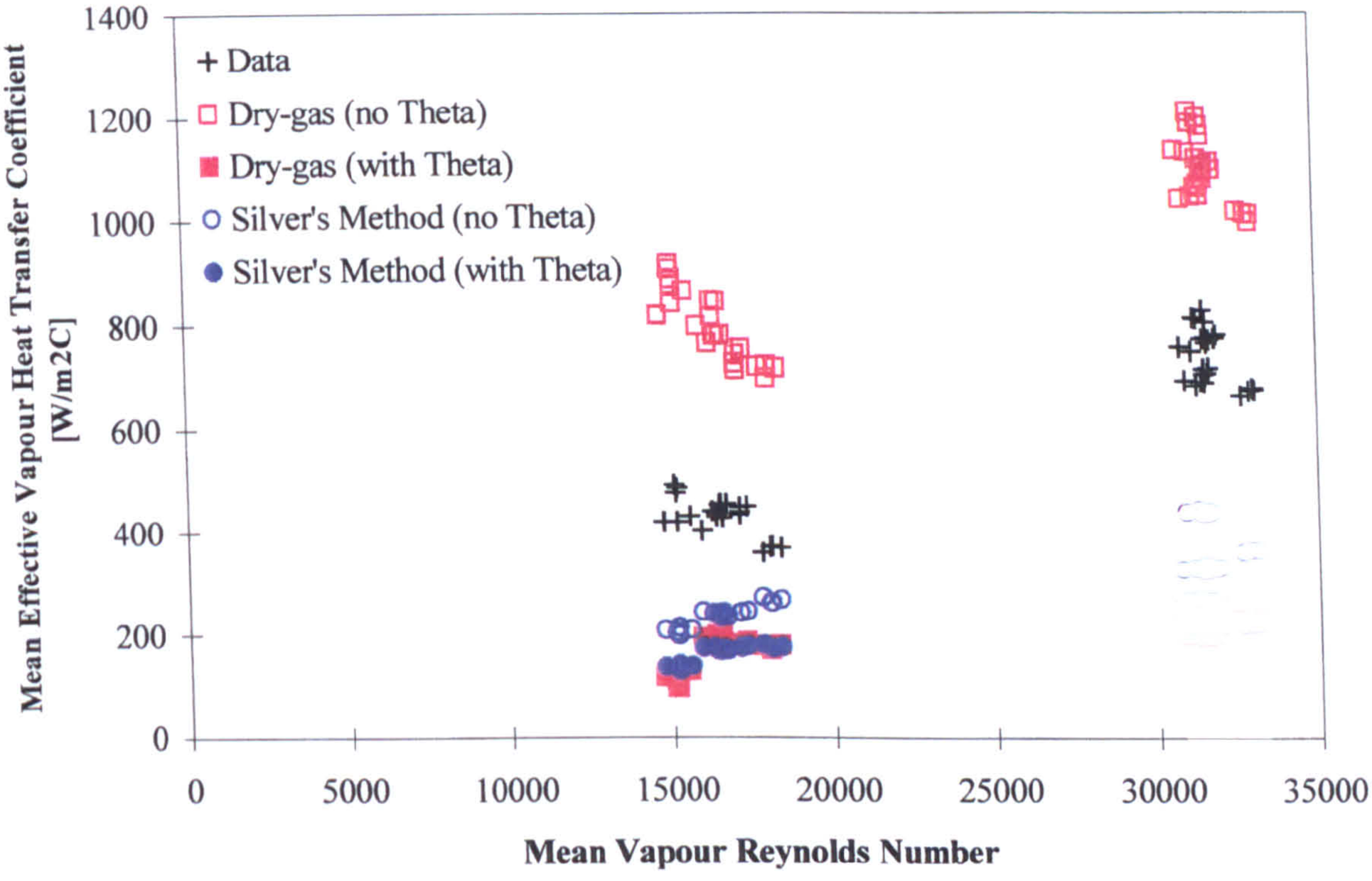

Figure 5.12. Comparison of results with predictions of Silver's method.

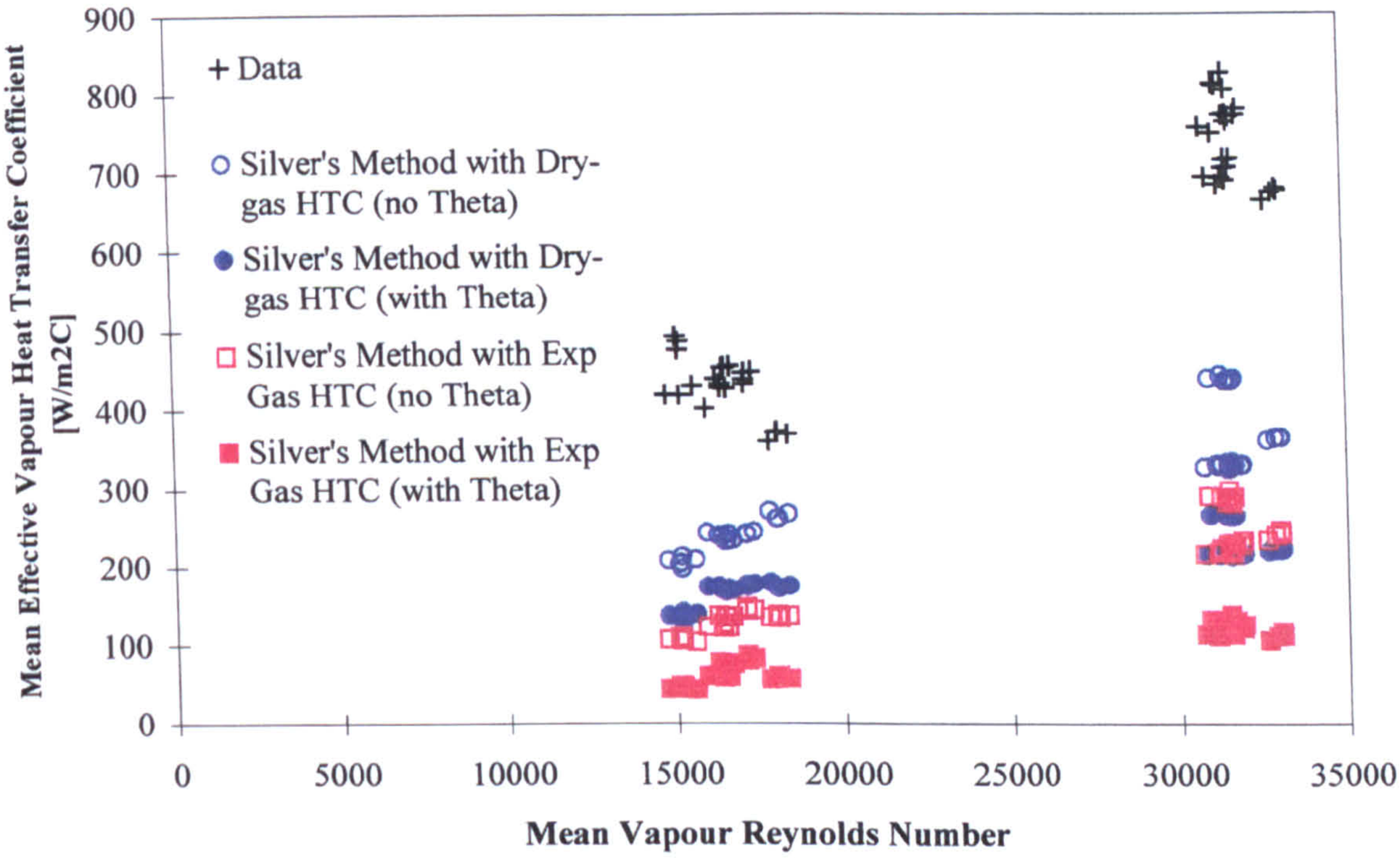

Figure 5.13. Effect of gas heat transfer coefficient using Silver's method.

With these, and the results of the previous analysis, it is worth noting that the greatest discrepancies between the measured and predicted values occur when the integral condensation curve is used in conjunction with the actual measured gas-phase heat transfer coefficient. This tends to suggest that the use of an integral condensation curve for the design of reflux condensers will lead to a severe over-estimation of the surface area required.

Although some improvement was obtained by using a dry-gas heat transfer coefficient instead of the actual measured value, i.e. the typical approach of the Silver method with no correction for mass transfer effects, it was seen that a distinct difference still existed between the measured and predicted values. As the dry-gas heat transfer coefficients were shown (see Figure 5.10 [p.204]) to be much larger than the measured values, it is felt that this is just a compensatory effect.

It is perhaps not surprising to find that use of the integral condensation curve produced such large discrepancies between the measured and predicted values. The main assumption of the integral condensation curve is that both vapour and condensate flow in the same direction through the condenser, and so remain in intimate contact with one another. Thus, the rates of heat and mass transfer are such that equilibrium conditions between the vapour and condensate are maintained at every point throughout the condenser.

In a reflux condenser, the vapour and condensate flow in opposite directions, and thus leave from opposite ends of the condenser. This means that the rates of heat and mass transfer will be different from those that are assumed in the derivation of the integral condensation curve. These departures from the assumed conditions were investigated by examining the output results from the TASC program runs.

With both mixtures, the outlet temperature of the vapour predicted by TASC was less than the actual measured value and the TASC prediction of the exit vapour composition contained a higher concentration of the more volatile component than the measured value. The temperature-composition profile of the vapour in the test condenser did not follow that of the integral condensation curve. Therefore the rates of heat and mass transfer in the test condenser were different from those required to maintain local equilibrium between the vapour and condensate phases. These departures from the assumed conditions are illustrated in Figure 5.14 [p.215].

Examining this diagram, it can be seen that the measured temperature-composition profile of the condensing vapour differs from that assumed by the integral condensation curve. The temperature drop in the condensing vapour is less than that implied by the integral curve, and based on this measured value, the outlet vapour contains a higher concentration of the more volatile component than equilibrium assumes.

Based on the measured test condenser heat load, the integral curve predicts a greater separation of the vapour mixture than the data show, but the surface area required by the condenser is much larger than that of the test condenser. The predicted outlet vapour temperatures and compositions based on the integral condensation curve are shown in Appendix A9, Tables A9.10 to A9.12 for the first mixture, and in Appendix A10, Tables A10.10 to A10.12 for the second mixture.

These temperature-composition diagrams are prepared assuming equilibrium exists between the liquid and vapour phases, and that the resistance to mass transfer under these conditions is small enough to enable separation of the mixture components. In condenser design, it is not necessary to know the local rates of heat and mass transfer in the condenser to produce such a diagram as they are based on thermodynamic models.

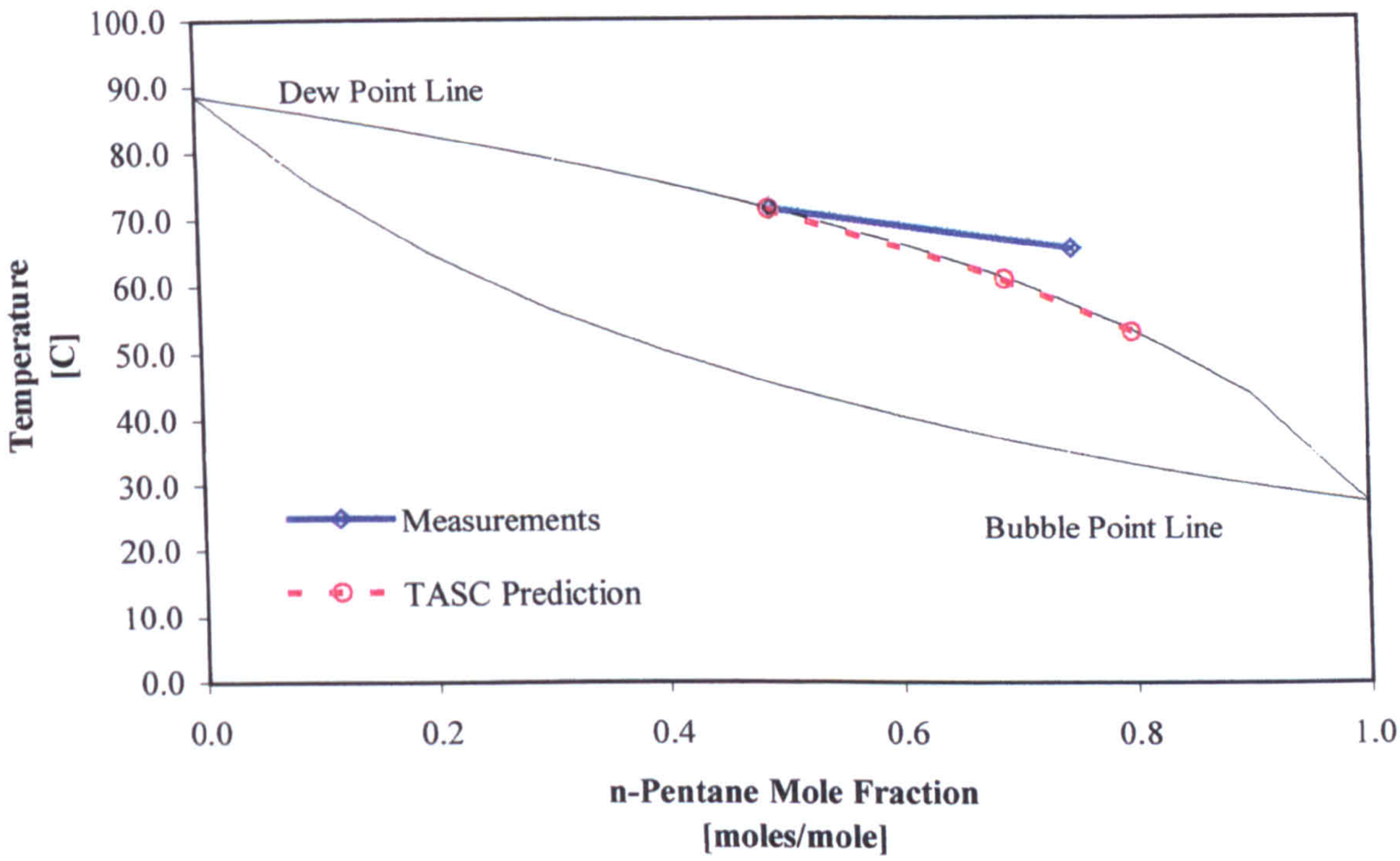

Figure 5.14. Typical temperature-composition profile.

If the vapour feed could be condensed at a very high rate, the dominant mass transfer process is convection towards the interface, diffusional resistances are negligible, and the composition of the condensate would match that of the vapour. This would be represented in Figure 5.14 [p.215] by a vertical line connecting the bubble and dew point lines. In practice however, diffusional resistances to mass transfer on the vapour side are present, and in co-current condensation this resistance is presumed to give a temperature-composition profile similar to that shown by the integral condensation curve.

As the evolving gas temperature shown by the integral condensation curve is independent of the actual rates of heat and mass transfer in the condenser, the gradient of the temperature-enthalpy diagram used in equilibrium condenser thermal design methods will also be independent of these rates. In the equilibrium method, mass transfer resistances are assumed to be low, and diffusional mass transfer is assumed to dominate. The change in temperature of the condensing vapour is used to determine the composition change, and the mixture components separate by diffusing through the vapour phase.

However, where the mass transfer process is dominated by convection rather than diffusion, the changes in temperature and composition of the vapour will differ from those assumed by the integral condensation curve. The composition of the condensate will be closer to that of the bulk vapour and the decrease in temperature of the vapour will be smaller, as illustrated in Figure 5.14 [p.215]. Therefore, the gradient of the temperature-enthalpy curve will be less than that predicted by the integral condensation curve.

As the gradient of the actual temperature-enthalpy curve is over-estimated by the integral condensation curve, using this gradient will under-estimate the effective vapour-side heat transfer coefficients, which can be explained by referring back to

(5.5.9) and (5.5.10). This was illustrated in the values of the predicted mean effective vapour heat transfer coefficients shown in Figure 5.13 [p.212].

Another feature of the reflux condensation process that would likely be missed by use of an integral condensation curve is the possibility of re-evaporating the more volatile component within the condensate film nearer the bottom of the tube. This increases the concentration of the more volatile component in the vapour, and thus enhances the separation.

Thus it appears that a trade-off is required to produce a reflux condenser unit that improves the separation of vapour mixtures in comparison to a co-current condenser. This trade-off involves operating at low heat flux to produce a condensate that is both warmer and contains a higher concentration of the less volatile component than could be obtained with a co-current condenser. This was identified in the work of Lintern and Haseler (1994), who compared the performance of a dephlegmator with a co-current condenser in separating mixtures of the same hydrocarbon mixtures used in this work. The results of their work showed that if the dephlegmator were operated at low heat flux, the concentration of the more volatile component in the condensate could be reduced.

Operating at low heat flux in the same geometry would mean an increase in the heat transfer resistance in the vapour due to a reduction in the vapour Reynolds number. However, this might still offer better heat transfer rates than those predicted by the integral condensation curve (see Figure 5.13 [p.212]). Further experimental work is required to determine whether the heat flux in the test condenser can be suitably varied to investigate its relationship with the separation of the components in the vapour mixture.

Webb et al. (1997) have investigated the applicability of condensation curves in predicting the actual condensation process using data from condensation experiments using a horizontal condenser of commercial scale. The results from this work show that both the integral and differential condensation curves poorly predicted the data, whereas the film model was very successful. Using the film theory gave a condensation curve that lay between the integral and differential curves and followed the same profile of the data. The authors attributed this success to the ability of the film theory in predicting the relative rates of condensation and therefore the evolving vapour composition and its saturation temperature.

As the reflux condensation process is one in which separation occurs, the successful design of a reflux condenser will be heavily dependent on the correct evaluation of the rates of mass transfer. It is strongly suggested by this work and the findings of Webb et al. that a film theory model may be much more appropriate for an accurate condenser design.

Based on these results, some comment can be made on the use of pre-determined equilibrium condensation curves for condenser thermal design. Despite the fact that this approach is less accurate than the film theory method, it is used as a design tool to produce a rough estimate of the condenser size. However, based on the results presented here, a number of objections can be raised to the use of these curves for the design of reflux condensers.

1. The mass transfer process on the vapour side was influenced by convective motion of the vapour more than diffusion, which meant that the temperature-composition profile of the condensing vapour differed from that predicted by the integral condensation curve (as seen in Figure 5.14 [p.215]). Therefore, the gradient of the temperature-enthalpy curve based on actual data, which would be

used in the thermal design, was less than that based on the integral condensation curve.

2. As a result of over-estimating the gradient of the temperature-enthalpy curve, the effective vapour-side heat transfer coefficients (with or without a mass transfer correction) were under-predicted, as shown in Figures 5.12 [p.211] and 5.13 [p.212].

3. The ratio of the actual to required condenser surface areas predicted by TASC and based on the integral condensation curve was found to be in the range 0.22-0.37 for the first mixture, and 0.25-0.32 for the second mixture. Thus, the condenser size was grossly over-predicted by as much as 300% if based on the integral condensation curve.

6.0 Conclusions and Recommendations

This chapter summarises the research and gives the conclusions and recommendations for additional work.

6.1 Conclusions

6.1.1 Commissioning of a New Research Facility

Composition Measurement

1. An on-line sampling system for the withdrawal of liquid samples from the test facility and measurement of density via a vibrating u-tube densitometer was designed and commissioned.

2. Calibration of the densitometer was carried out following the manufacturer's guidelines, from which it was shown that the instrument calibration constant was less sensitive to pressure than temperature. An average instrument calibration constant was found to be suitable across the measured range of temperatures.

3. Off-line analysis work was carried out using n-pentane and iso-octane, and mixtures of these two single components in different quantities. The densities of these liquids were measured at different temperatures across a narrow temperature range. These measurements were used to develop temperature-dependent and temperature-independent correlations relating the mixture composition to its density.

4. These correlations were used to investigate the sensitivity to temperature of the relationship between mixture composition and density. It was found that a temperature-dependent correlation was able to predict the mixture composition to within 5% of its measured value, whereas the temperature-independent correlation predicted the mixture composition to within 21%. Thus, the temperature-dependent correlations were found to the most accurate method for predicting mixture density.

5. A strategy was developed using these empirical correlations for determining the composition of a liquid sampled from the test facility based on a measurement of the sample's density. These measured compositions were then used in mass balance calculations across the test condenser to determine the composition of the feed vapour stream.

Coolant Heat Transfer Coefficient

6. Experiments were carried out to develop an empirical correlation for determining the coolant heat transfer coefficient in the test condenser.

6.1.2 Condensation of Single Component Hydrocarbons

The author commissioned the new test facility using two single component hydrocarbons to confirm the suitability of the measurement systems installed, and to provide some basis for later work with binary hydrocarbon mixtures of the same two components. Tests were carried out at different condenser heat loads and across different condenser surface areas, whilst maintaining constant conditions on the coolant side to reduce the likelihood of error.

7. The results showed that the experimental condensate-film heat transfer coefficient decreased as the condensate film approached the bottom of the test condenser. This increased resistance to heat transfer was most probably caused by the thickening of the condensate film as its mass flow rate increased, and possibly by some thickening of the condensate film by the upward flowing vapour.

8. The experimental condensate-film heat transfer coefficient was compared with the methods of Nusselt and with that of HTFS, where it was assumed that gravity was the only external force acting on the condensate film. The method recommended by HTFS, where the possibility of surface waves on the condensate film at the phase interface and turbulence within the film were allowed, best predicted the measured values.

9. An empirical modification to the method of HTFS was suggested to improve the estimation of the mean condensate-film heat transfer coefficient. Use of this modification enabled the experimental values to be predicted to within 7%, compared to a prediction within 23% using the original method of HTFS. This empirical correction may be necessary to account for some enhancement due to the counter-current flow of vapour and liquid.

6.1.3 Condensation of Binary Hydrocarbon Mixtures

The author carried out experimental work using two binary hydrocarbon mixtures comprising different quantities of n-pentane and iso-octane to investigate the heat and mass transfer processes taking place during reflux condensation in a single vertical tube. Tests were carried out at different condenser heat loads and across different condenser surface areas, whilst constant conditions on the coolant side were

maintained to reduce the likelihood of error. The test work was aimed at investigating how the resistances to heat transfer varied with the conditions on the condensing side. The effect of varying the conditions on the condensing side to the separation of components in the vapour mixture was also studied.

10. Analysis of the heat transfer resistances on the condensing side showed that the resistance due to the condensate film was approximately constant for both mixtures despite the variation in condenser heat load. The resistance due to the vapour was found to be smaller in comparison, and varied with condenser heat load. The tendency for the vapour heat transfer resistance to decrease with increasing heat load was attributed to improved heat transfer due to greater turbulence in the vapour at higher heat loads. As the vapour resistance was smaller than that due to the condensate film, it was taken to be the controlling resistance to heat transfer on the condensing side.

11. The separation of the components in the vapour mixture was investigated in relation to the test condenser heat load. It was found that the greatest separation occurred at lower heat loads, although the results were less obvious with the second mixture than with the first mixture. This was an expected result because at low condenser heat loads, the concentration gradient in the vapour is more pronounced, and the mass transfer process becomes dominated by diffusion.

12. The separation was also examined by determining the number of thermodynamic stages represented by the test condenser. It was found that under the conditions of the experimental work, the test condenser represented less than one thermodynamic stage, and that the condenser heat load had no affect on this number. Although this did not support the conclusions of previous work reported in the literature, it was felt that this was attributed to the differences in operating conditions. Thus it was suggested that further experimental work be carried out

to determine whether or not the test condenser could be operated more effectively.

13. Analysis of the heat transfer resistance on the vapour side revealed that the normal approach of using a dry-gas heat transfer coefficient was inappropriate, and led to an under-prediction of the effective vapour-side heat transfer resistance. If the dry-gas heat transfer coefficient was then corrected for the effect of mass transfer using the film theory method, the effective vapour-side heat transfer resistance was over-predicted.

14. These results were improved by the inclusion of an enhancement factor, whose magnitude varied depending on whether or not the mass transfer correction term was included. The use of this enhancement factor might be necessary to account for the effect of the counter-current flow on the phase interface. It was suggested that this type of flow increased the available surface area for heat and mass transfer above that normally expected with co-current flows, and hence altered the transfer rates.

15. The results were assessed against the predictions of Silver's method for condenser design using the HTFS heat exchanger design software TASC version 4.01. Silver's method used the integral condensation curve and the dry-gas heat transfer coefficient, which could be corrected for the effects of mass transfer using film theory. The Silver method over-predicted the effective vapour-side heat transfer resistance with and without the inclusion of a mass transfer correction term.

16. The measurements were then compared to a modified Silver's method, where the dry-gas heat transfer coefficient was replaced by the experimentally derived

vapour-side heat transfer coefficient. This was found to further over-predict the heat transfer resistance, and was attributed to the inappropriate use of the integral condensation curve.

17. An assessment was made of the measured vapour temperature-composition profile in comparison to the predictions of the integral condensation curve. The measurements did not follow the path of the integral curve, which was attributed to mass transfer effects in the vapour caused by convective motion of the vapour toward the condensing surface.

18. Use of the pre-determined integral condensation curve has been shown to be inappropriate for the thermal design of reflux condensers. The gradient of the temperature-enthalpy curve based on the integral curve over-estimates the actual gradient, and so the condenser size is greatly over-estimated. In addition, the separation achieved in the condenser is less than that predicted by equilibrium condensation. It is possible that the need to operate at relatively low vapour velocities in reflux condensers, in order to avoid the flooding point, exaggerates the mass transfer effects above that expected for co-current condensation under the same operating conditions.

6.2 Recommendations for Further Work

Further experimental work is required to validate the results reported in this thesis, and hence support the previous conclusions.

1. The measurement of heat losses is seen as an immediate improvement to the existing experimental procedure. The loss of heat to the surroundings through

the surfaces of the test facility, and to the air stream ventilating the containment cabinet were identified, and suggestions on how these might be estimated were discussed. It is felt that incorporating these into the data analysis would improve confidence in the measurements. An alternative to this approach would be to minimise the heat lost to the surroundings by further insulating the surfaces of the test facility, in particular the flanges of the boiler and the test sections.

2. Measurements of the temperature of the condensate leaving the test condenser, and of the composition of the feed vapour into the test condenser would have been beneficial in this study. It is suggested that instrumentation be installed in the facility to enable these measurements, to develop the heat and mass balances across the test and dump condensers. It is appreciated that measurement of either of these variables will be difficult due to problems in locating the necessary instrumentation at, or around, the bottom of the test condenser, and the need to avoid disturbing the vapour and liquid at this location. However, it is felt that with these additional measurements, a more detailed description of the heat and mass transfer processes would be possible, and would be based on experimental data.

3. A more detailed description of the heat and mass transfer processes taking place inside the test facility could be obtained if the condensate produced in the test condenser were collected and weighed. Again it is appreciated that such a measurement will be difficult due to problems in locating the necessary instrumentation and equipment at, or around, the bottom of the condenser. However, this procedure would enable a very reliable check on the heat and mass balances across the condensers and would improve the accuracy of the data analysis calculations.

4. It was observed during some of the experimental work carried out and reported in this thesis, that the temperature differences measured between the condensing vapour and the coolant streams were very small. Due to these very small differences and the limited accuracy of the thermocouple calibration, the potential for error was increased. It is suggested that a more accurate method of calibrating the thermocouples used in the facility is used prior to any future experimental work in order to reduce this potential error.

5. The method used to calibrate the vibrating u-tube densitometer, which was used to determine the composition of liquid samples withdrawn from two different locations of the test facility, was based on the procedure recommended by the instrument manufacturer. This method used air and purified water as the calibrating fluids, and it was observed that these two fluids had vibration periods that were significantly different from each other. It may be possible to improve the calibration of this instrument if the two fluids that are used have vibration periods that are more similar in magnitude. A detailed review of the calibration method for this particular vibrating u-tube densitometer is required.

6. The results presented here suggested that the test condenser heat flux had a significant effect on the ability to separate the components of a vapour mixture, and also on the number of thermodynamic stages. However, analytical results reported in the literature suggest that at lower heat flux the separation is improved and the number of thermodynamic stages increased. It would be useful, therefore, to investigate how the condenser compares at lower heat flux levels than those reported here.

7. The data were compared to the predictions of Silver's method using the HTFS heat exchanger design software TASC version 4.01, and this was found to be unsuitable for estimating both the heat transfer resistances, and the exit vapour

compositions. Comparison of the data with the method of Colburn and Drew, which is a more realistic model of the condensation process in which the rates of heat and mass transfer are determined locally through the condenser, might yield better results.

References

Abdelmessih A. N., Rabas T. J. and Panchal C. B., (1997), "*Reflux condensation of pure vapours with and without noncondensable gas inside plain and enhanced tubes*". AIChE Symp. Ser., vol.93, no.314, pp.227-232.

Ackermann G., (1937), *"Heat transfer and molecular mass transfer in the same field of high temperatures and large partial pressure differences"*, Ver. Deutsch Ing. Forschungsheft, vol. 8, no. 382, pp. 1-10.

Alekseev V. P., Poberezkin A. E., and Gerasimov P. V., (1972), *"Determination of flooding rates in regular packings"*, Heat Transfer-Soviet Research, vol. 4, no. 6, pp. 159-163.

Bell K. J., (1988), "*Design of reflux condensers*", Heat Transfer Equipment Design, Hemisphere Publishing Corporation, pp. 527-534.

Bell K. J. and Ghaly M. A., (1972), *"An approximate generalised design method for multicomponent/partial condensers"*, AIChE Symp. Ser., vol. 69, no. 131, pp. 72-79.

Bernhard D. P. and Rowles H. C., (1988), " *Recovery of valuable hydrocarbons using dephlegmator technology*", Advances in Cryogenic Engineering, vol. 33, pp.983-989.

Bernhard D. P. Goodwin T. P. and Rowles H. C., (1986), *"Recovery of hydrocarbon liquids using dephlegmator technology"*, Paper AM-86-7, National Petroleum Refiners Association (Technical Papers).

Boyko L. D. and Kruzhilin G. N., (1967), *"Heat transfer and hydraulic resistances during condensation of steam in a horizontal tube and in a bundle of tubes"*, Int. J. Heat Mass Transfer, vol. 10, pp. 361-373.

Carpenter E. F. and Colburn A. P., (1951), *"The effect of vapour velocity on condensation inside tubes"*, Proc. Of General Discussion on Heat Transfer, 20-26, Inst. Mech. Engrs./ASME.

Di Cave S., Mazzarotta B. and Sebastiani E., (1987), "*Mathematical model for process design and simulation of dephlegmators (partial condensers) for binary mixtures*", Can. J. Chem. Eng., vol. 65, no. 4, pp. 559-564.

Chen S. L., Gerner F. M. and Tien C. L., (1987), "*General Film Condensation Correlations*", Experimental Heat Transfer, vol. 1, pp. 93-107.

Chiu C. H., (1990), "*Advances in gas separation*", Hydrocarbon Processing, vol. 69, no. 1, pp. 69-72.

Chun K. R. and Seban R. A., (1971), "*Heat transfer to evaporating liquid films*", Trans. ASME, J Heat Transfer, vol. 93, no. 4, pp. 391-396.

Chunangad K. S., (1994), "*Sizing of vertical-in-tube reflux condensers*", MS Thesis, School of Chemical Engineering, Oklahoma State University, Stillwater.

Clements L. D. and Colver C. P., (1973), "*Filmwise condensation of light hydrocarbons and their mixtures in a vertical reflux condenser*", AIChE Symp. Ser., vol. 69, no. 131, pp. 18-22.

Colburn A. P., (1933), *"The calculation of condensation where a portion of the condensate layer is in turbulent motion"*, Trans. AIChE, vol. 30, pp. 187-193.

Colburn A. P. and Drew T. B., (1937), *"The condensation of mixed vapours"*, AIChE Trans., vol. 33, pp. 197-215.

Colburn A. P. and Hougen O. A., (1934), *"Design of cooler condensers for mixtures of vapours with non-condensing gases"*, Ind. Eng. Chem., vol. 26, pp. 1178-1182.

Coulson J. M. and Richardson J. F., (1990), "*Chemical Engineering*", vol. 1, 4th Ed., Pergamon Press.

Dittus F. W. and Boelter L. M. K., (1930), Uni. California (Berkeley) Pubs. Eng., vol. 2, no. 443.

Dukler A. E., (1960), *"Fluid mechanics and heat transfer in vertical falling film systems"*, Chem., Eng. Prog. Symp. Series, vol. 56, no.30, pp. 1-10.

Eagle A. and Ferguson R. M., (1930), "*The coefficients of heat transfer from tube to water*", Proc. Inst. Mech. Eng., vol. 2, no. 985.

ESDU, (1978), "*Internal forced convective heat transfer in coiled pipes*", Data Item no. 78031.

ESDU, (1986), "*Reflux condensation in vertical tubes*", Data Item no. 89038.

Grigull U., (1942), "*W·rme✦bergang beu der kondensation mit turbulenter wasserhaut*", Forsch. Ingenieurwes, vol. 13, pp. 49-57 and VDI Z, vol. 86, pp. 444-445.

Kent E. R. and Pigford R. L., (1956), "*Fractionation during condensation of vapour mixtures*", AIChE J., vol. 2, p. 63.

Kirkbride C. G., (1934), *"Heat transfer by condensing vapour on vertical tubes"*, Trans. AIChE, vol. 30, pp. 170-186.

Kirschbaum E., (1930), "*Dechema Monogr*", no. 12, bd. 2, Verlag Chemie.

Krishna R. and Standart G. L., (1979), *"Mass energy transfer in multicomponent mixtures"*, Chem. Eng. Commun., vol. 3, pp. 201-275.

Kunz H. R. and Yerazunis S., (1967), *"An analysis of film condensation, film evaporation and single phase heat transfer"*, Papers presented at 9th ASME-AIChE Heat Transfer Meeting, Seattle, 7-HT-1.

Kutateladze S. S., (1963), *"Fundamentals of Heat Transfer"*, Academic Press.

Labuntsov D. A., (1957), "*Heat transfer in film condensation of pure steam on vertical surfaces and horizontal tubes.*" Teploenergetika, vol. 4, no. 7, pp. 72-80.

Lee J, (1964), *"Turbulent film condensation"*. AIChE J. vol. 10, pp. 540-544.

Lintern A. and Haseler L. E., (1993), "*Numerical modelling of dephlegmators*", HTFS Research Report, RS936.

Lintern A. and Haseler L. E., (1994), "*Numerical calculations for dephlegmators (1) Methods*", HTFS Research Report, RS958.

Lintern A. and Haseler L. E., (1995), "*Dephlegmator performance calculations*", HTFS Research Report, RS987.

McNaught J. M., (1979), *"Mass transfer correction term in design methods for multicomponent/partial condensers"*, Condensation Heat Transfer, ASME, 18th Nat. Heat Transfer Conf., San Diego, California.

McNaught J. M., (1990), "*Average heat transfer coefficient for the condensate film on a vertical surface with no vapour shear*", HTFS Handbook Sheet CM8.

McNaught J. M. and Emerson W. H., (1977), "*A development of some approximate design methods for multicomponent condensation*", HTFS Research Report, RS211.

McQuillan K. W. and Whalley P. B., (1984), *"Comparison between flooding correlations and experimental flooding data"*, UKAEA Report AERE-R11267.

Mikheev M. A., (1956), *"Heat Transfer Fundamentals"*, Gosenergoizdat, Moscow.

Nusselt W., (1916), *"Die oberflachenkondensation des wasserdampfes"* Zeitschr. Ver. Deutsch., Ing., vol. 60, no. 27, pp. 541-546 and vol. 60, no. 28, pp. 569-575.

Rogers G. F. C. and Mayhew Y. R., (1988), *"Thermodynamic and Transport Properties of Fluids"*, 4th Ed., Blackwell Publishers.

Rohsenow W. M., (1956), "*Heat transfer and temperature distribution in laminar film condensation*", Trans. ASME, Ser. C. J. vol. 78, pp. 1645-1648.

Sardesai R. G., Palen J. W. and Taborek J., (1983*), "Modified resistance proration method for condensation of vapour mixtures"*. AIChE Symp. Ser, vol. 79, no. 225, pp. 41-46.

Sieder E. N. and Tate G. E.,(1936), *"Heat transfer and pressure drop of liquids in tubes"*, Ind. Eng. Chem., vol. 28, no. 1429.

Silver L., (1947), *"Gas cooling with aqueous condensation"*, Trans. Instn. Chem. Engrs., vol. 25, pp. 30-42.

Soliman M., Schuster J. R. and Berenson P. J., (1968), *"A general heat transfer correlation for annular flow condensation"*, J. Heat Transfer, vol. 90, pp. 267-276.

Stewart W. E. and Prober R., (1964), *"Matrix calculation of multicomponent mass transfer in isothermal systems"*, Ind. Eng. Chem. Fundam., vol. 3, pp. 224-235.

Subramanyam S., (1983), "*Sizing of reflux condensers*", MS Thesis, School of Chemical Engineering, Oklahoma State University, Stillwater.

Toor H. L., (1957), *"Diffusion in three component gas mixtures"*, AIChE J., vol. 3, p. 198.

Toor H. L., (1964), "*Solution of the linearised equations of multicomponent mass transfer*", AIChE J., vol. 10, no. 4, p. 448 and 460.

Tröster E., (1960), "*Berechnung der Trennwirkung von Teilkondensatoren*", Chem. Ing. Tech., vol.22, pp.525-531.

Ward D. E., (1960), *"How to design a multiple component partial condenser"*, Petrochem. Eng., vol. 32, no. 10, pp. C42-C48.

Webb D. R., Stevenson R. and Ax K., (1997), "*Assessment of condensation curves in the design of binary vapour condensers*", 5th UK Nat. Heat Transfer Conf., London.

Whalley P. B., (1984), *"Correlation for flooding in vertical tubes"*, HTFS Handbook Sheet TM11.

Wilson E. E., (1915), "*A basis for rational design of heat transfer apparatus*", Trans. ASME, vol. 37, no. 546, pp. 47-82.

Zivi S. M., (1964), *"Estimation of steady-state steam void fraction by means of the principle of minimum entropy production"*, J. Heat Transfer, vol. 86C, no. 2, pp. 247-252.

Appendix A1 Single Component Hydrocarbon Properties

A1 Single Component Hydrocarbon Properties

A1.1 n-Pentane

Chemical Formula	C_5H_{12}
Molecular Weight (amu)	72.151
Critical Temperature (°C)	196.65
Critical Pressure (bar)	33.75
Normal Boiling Point (°C)	36.07
Melting Point (°C)	-129.68

Liquid properties evaluated at 25.0°C and 1.01325 bar.

Density (kg/m3)	621.723
Dynamic Viscosity (N s/m2)	0.000215
Thermal Conductivity (W/m °C)	0.11371
Specific Heat Capacity (constant pressure) (J/kg °C)	2323.408
Specific Enthalpy (J/kg)	-368438.2
Specific Entropy (JJ/kg °C)	-1186.458
Specific Latent Heat (J/kg)	364432.3

A1.2 Iso-octane (2,2,4-trimethylpentane)

Chemical Formula	C_8H_{18}
Molecular Weight (amu)	114.232
Critical Temperature (°C)	270.70
Critical Pressure (bar)	25.63
Normal Boiling Point (°C)	99.23
Melting Point (°C)	-107.15

Liquid properties evaluated at 25.0°C and 1.01325 bar.

Density (kg/m3)	688.495
Dynamic Viscosity (N s/m2)	0.000476
Thermal Conductivity (W/m °C)	0.099777
Specific Heat Capacity (constant pressure) (J/kg °C)	2069.270
Specific Enthalpy (J/kg)	-302802.4
Specific Entropy (JJ/kg °C)	-816.081
Specific Latent Heat (J/kg)	302240.2

Appendix A2 Instrument Calibrations

A2 Instrument Calibrations

A2.1 Thermocouple Calibrations

All thermocouples in this test facility were T-type thermocouples (copper/nickel). When supplied from the manufacturer, the standard calibration gives them an accuracy of approximately ±1.0°C. It was normal practice to calibrate the thermocouples in-house to improve this accuracy. The author carried out the calibrations described below.

Thermocouple calibrations were carried out using either a HETOFRIG oil bath or an ISOTECH block. When using the oil bath, thermocouples were usually grouped together in bundles of five, where the five thermocouples were measuring the same temperature range. When using the block calibrator it was normal to be calibrating a single thermocouple. The reference temperature for all calibrations was a platinum resistance thermometer.

Calibration Procedure using the HETOFRIG Bath

The HETOFRIG bath was filled with a silicon-based oil, whose temperature was controlled using the built-in heating and cooling elements. The platinum resistance was lowered into the oil, making sure it was well below the surface of the oil before it was secured in place.

The thermocouple bundle was then lowered into the bath alongside the platinum resistance thermometer, and secured in place. Care was taken when inserting the

bundle to only submerge the thermocouple wires and not the plugs themselves. The thermostat controls were adjusted to provide the correct ratio of heating and cooling to achieve the first calibration temperature. The exact temperature of the oil in the bath was measured by the platinum resistance thermometer, and was shown on its processing unit.

The temperature was allowed to settle before any readings were taken. As the thermocouples were still connected to the data acquisition unit, this was used to manually scan the thermocouples inside the oil bath. The output voltage signal for each thermocouple in the bundle was noted at temperature equilibration.

Having noted the readings at the first temperature, the thermostat controls were adjusted to increase the temperature in the bath. Again, the real temperature was monitored using the platinum resistance thermometer, and time was allowed for this value to stabilise before the thermocouples were manually scanned and their output signals noted. This system was repeated for the full temperature calibration range.

Calibration Procedure using the ISOTECH Block Calibrator

A built-in thermostat in the ISOTECH block calibrator allowed the temperature of the block to be lowered or raised depending on the requirements. The platinum resistance was lowered into one of two wells in the block, making sure it was well inside and in contact with the core of the block.

The thermocouple was then lowered into the other well in the block, again making sure it was in good thermal contact with the core of the block. The thermostat

controls were adjusted to achieve the first calibration temperature. The exact temperature of the block was measured by the platinum resistance thermometer, and was shown on its processing unit.

The temperature was allowed to settle before any readings were taken. As the thermocouple was still connected to the data acquisition unit, this was used to manually scan the thermocouple inside the block. The output voltage signal for the thermocouple was noted at temperature equilibration.

Having noted the readings at the first temperature, the thermostat controls were adjusted to increase the temperature in the block. Again, the real temperature was monitored using the platinum resistance thermometer, and time was allowed for this value to stabilise before the thermocouple was manually scanned and the output signal noted. This system was repeated for the full temperature calibration range.

Calibration Results

The results were used to produce a plot of the thermocouple output voltage signal against the reference temperature, as measured by the platinum resistance thermometer. A best-fit line was fitted to the data in the form of a second-order polynomial expression, having the general form

$$T = K_0 + K_1 V_e + K_2 V_e^2 \qquad \text{(A2.1)}$$

These polynomials represented the calibration equations for the thermocouples. The data acquisition software was programmed to measure the output voltage signals from the thermocouples, and then read the calibration constants for the relevant thermocouple. The software was then programmed to carry out the above calculation to produce a corresponding temperature. Details of the calibration constants obtained for each of the thermocouples in the test facility is shown in Table A2.1.

The accuracy of the calibration equations was investigated by comparing their predictions with the measurements made by the platinum resistance thermometer. Temperatures were calculated using the output voltage signals from the calibrations, and these calculated temperatures were compared with the actual temperature measurements of the platinum resistance thermometer. The results of the comparisons are shown in Table A2.2.

As the Table A2.2 shows, the minimum difference was found to be no less than 0.35°C, and the maximum difference was no greater than 0.4°C. Therefore, the thermocouples calibrated in-house are accurate to within ±0.4°C, and this is an improvement on the standard calibration of approximately ±1.0°C as specified by the manufacturer.

Table A2.1. Thermocouple calibration coefficients.

Thermocouple	K_0	K_1	K_2
7	0.5195	25520	-513486
8	0.5193	25582	-580237
9	0.5610	25568	-508526
10	0.6117	25432	-469188
11	0.5563	25371	-447735
12	0.7248	25446	-557464
13	0.7245	25372	-549567
16	0.2496	25750	-540552
17	0.3865	25544	-522921
18	0.2525	25749	-561540
19	0.3125	25662	-533279
20	0.2028	25709	-552258
21	0.4983	25393	-442524
22	0.2799	25446	-491963
23	0.2387	25481	-497631
24	0.2879	25459	-509767
25	0.2799	25504	-481744
26	0.3216	25424	-454649
27	0.4480	25486	-514425
28	0.4480	25486	-514425
29	0.4480	25486	-514425
30	0.4480	25486	-514425
31	0.4480	25486	-514425
32	0.2094	25374	-478903
33	0.4948	25033	-490736
34	0.6354	25025	-499706
35	0.4818	25093	-526924
36	0.1859	25761	-569266
37	0.0975	25925	-656860

Table A2.2. Accuracy of thermocouple calibrations.

Thermocouple	Maximum Deviation (°C)	Minimum Deviation (°C)
7	-0.086	0.093
8	-0.015	0.013
9	-0.107	0.129
10	-0.413	0.180
11	-0.110	0.130
12	-0.070	0.065
13	-0.086	0.077
16	-0.078	0.068
17	-0.148	0.121
18	-0.093	0.086
19	-0.089	0.089
20	-0.073	0.048
21	-0.233	0.416
22	-0.068	0.099
23	-0.029	0.044
24	-0.053	0.062
25	-0.115	0.112
26	-0.352	0.193
27	-0.151	0.206
28	-0.151	0.206
29	-0.151	0.206
30	-0.151	0.206
31	-0.151	0.206
32	-0.080	0.098
33	-0.105	0.085
34	-0.047	0.055
35	-0.038	0.031
36	-0.052	0.082
37	-0.022	0.031

A2.2 Pressure Transducer/Transmitter Calibration

The pressure transducer/transmitter used in this facility was a Type 6200 BGA 60 GOGBUB, supplied by TransInstruments. The manufacturer supplied details of the calibration, and Dr Chris Chu used this information in the data acquisition program. When supplied from the manufacturer, the instrument was reported to have a maximum error of 1.2%. The calibration details of the transducer/transmitter are shown in the table below.

Table A2.3. Calibration details of pressure transducer/transmitter

Current Output (mA)	Pressure (barg)
4	0
20	6

These values were used to produce a linear plot of current output against pressure, and the equation of the line used to represent this plot was

$$P = 0.375 I_e - 1.5 \qquad \text{(A2.2)}$$

This equation was modified for use in the test facility's data acquisition system in two ways. Firstly, the signal received by the data acquisition unit was measured in volts, so the electrical current term in (A2.2) was replaced by the simple relation

$$I_e = \frac{V_e}{R_e} \tag{A2.3}$$

Thus (A2.2) was modified to read

$$P = \frac{375 \times V_e}{250} - 1.5 \tag{A2.4}$$

Secondly, the pressure range of the test facility was between –1barg and 5barg, and the instrument was calibrated over the pressure range 0barg to 6barg. Therefore, 1 was subtracted from (A2.4) to account for the difference in measured and calibrated pressure ranges. The modified equation was

$$P = \frac{375 \times V_e}{250} - 2.5 \tag{A2.5}$$

In reporting the pressure measurements during experimental test work, the absolute pressure was always given. The absolute pressure was obtained by making a separate measurement of the atmospheric pressure, and adding this value to the pressure read using the transducer/transmitter.

During the entire test work carried out, the atmospheric pressure reading was very close to 1barg. This meant that 1 has been subtracted from the calibration equation to compensate for the differences in the measured and calibrated pressures, and then 1 was added back onto the equation to obtain an estimate of the absolute pressure.

$$P = \frac{375 \times V_e}{250} - 1.5 - 1.0 + 1.0 \qquad \text{(A2.6)}$$

As (A2.6) illustrates, this appears to detract from the accuracy of the instrument calibration. It would have been more beneficial to have the pressure transducer/transmitter calibrated against absolute pressure readings as opposed to gauge pressure. This would have removed the need to make a separate measurement of the atmospheric pressure, following the procedure described above.

It was decided safer to regard the pressure measurement from this transducer/transmitter as an indication of the pressure, rather than one based on a satisfactory calibration method. The pressure inside the boiler vapour space was instead calculated from the measurement of vapour temperature also made in the boiler vapour space.

A2.3 Test Condenser Flow Meter Calibration

The flow meter used in this facility to measure the flow rate of cooling water through the test condenser was a Litre Meter Serial Number 220/53114, supplied by Litre Meter. The standard calibration supplied from the manufacturer, details of which were as shown in the table below, was used by Dr Chris Chu to produce a calibration equation in the test facility's data acquisition program.

Table A2.4. Calibration details of the test condenser coolant flow meter

Frequency (Hz)	Test Flow Rate (litres/minute)
717.2667	28.000
543.7800	21.200
387.5667	15.100
256.9850	9.980
180.7820	6.980
93.6693	3.640
43.9708	1.730
19.3657	0.755
2.4190	0.123

These values were used to produce a linear plot of the frequency against the test flow rate, and the equation of the line used to represent this plot was

$$\dot{V} = (0.039 \times f) - 0.011 \qquad \text{(A2.7)}$$

The equation of the best-fit line was improved by carrying out a statistical analysis. By this route, the new equation was found to be

$$\dot{V} = (0.038976 \times f) \tag{A2.8}$$

The differences between the flow rates calculated from these two equations were found to be negligible.

A2.4 Dump Condenser Flow Meter Calibration

The flow meter used in this facility to measure the flow rate of cooling water through the dump condenser was a Litre Meter Serial Number 45/57149, supplied by Litre Meter. As before, the standard calibration supplied from the manufacturer, details of which were as shown in the table below, was used by Dr Chris Chu to produce a calibration equation in the test facility's data acquisition program.

These values were used to produce a linear plot of the frequency against the test flow rate, and the equation of the line used to represent this plot was

$$\dot{V} = (0.013 \times f) - 0.0052 \tag{A2.9}$$

The equation of the best-fit line was improved by carrying out a statistical analysis. By this route, the new equation was found to be

$$\dot{V} = (0.012978 \times f) \qquad \text{(A2.10)}$$

The differences between the flow rates calculated from these two equations were found to be negligible.

Table A2.5. Calibration details of the test condenser coolant flow meter

Frequency (Hz)	Test Flow Rate (litres/minute)
488.3595	6.3300
372.6800	4.8400
272.1080	3.5400
219.8387	2.8600
163.0987	2.1200
119.0677	1.5400
63.3919	0.8060
25.5413	0.3200
3.2794	0.0427

Appendix A3 Single Component Hydrocarbon Data Analysis Functions

```
'DETERMINE THE COOLANT HEAT LOADS ACROSS EACH OF THE SECTIONS IN THE
TEST CONDENSER
'
'
'COOLANT HEAT LOAD ACROSS TEST SECTION 2
Function Qcool_2(Vdot_cool, rho_cool, Cp_cool, tci2, tco2)
   'COOLANT MASS FLOW RATE
   Mdot_cool = (Vdot_cool * rho_cool) / 60000
   'COOLANT HEAT LOAD
   Qcool_2 = Mdot_cool * Cp_cool * (tco2 - tci2)
End Function
'
'
'COOLANT HEAT LOAD ACROSS TEST SECTION 3
Function Qcool_3(Vdot_cool, rho_cool, Cp_cool, tci3, tco3)
   'COOLANT MASS FLOW RATE
   Mdot_cool = (Vdot_cool * rho_cool) / 60000
   'COOLANT HEAT LOAD
   Qcool_3 = Mdot_cool * Cp_cool * (tco3 - tci3)
End Function
'
'
'COOLANT HEAT LOAD ACROSS TEST SECTION 4
Function Qcool_4(Vdot_cool, rho_cool, Cp_cool, tci4, tco4)
   'COOLANT MASS FLOW RATE
   Mdot_cool = (Vdot_cool * rho_cool) / 60000
   'COOLANT HEAT LOAD
   Qcool_4 = Mdot_cool * Cp_cool * (tco4 - tci4)
End Function
'
'
'COOLANT HEAT LOAD ACROSS DUMP CONDENSER
Function Qcool_d(Vdot_cool, rho_cool, Cp_cool, tci, tco)
   'COOLANT MASS FLOW RATE
   Mdot_cool = (Vdot_cool * rho_cool) / 60000
   'COOLANT HEAT LOAD
```

```
    Qcool_d = Mdot_cool * Cp_cool * (tco - tci)
End Function
'LOG-MEAN TEMPERATURE DIFFERENCE ACROSS TEST SECTION 2
Function lmtd2(Tv, tci2, tco2)
    'COOLANT TEMPERATURE DIFFERENCE
    dt_cool = tco2 - tci2
    'FIRST TERMINAL TEMPERATURE DIFFERENCE
    dt1 = Tv - tci2
    'SECOND TERMINAL TEMPERATURE DIFFERENCE
    dt2 = Tv - tco2
    'LOG-MEAN TEMPERATURE DIFFERENCE
    lmtd2 = dt_cool / (Log(dt1 / dt2))
End Function
'
'
'LOG-MEAN TEMPERATURE DIFFERENCE ACROSS TEST SECTION 3
Function lmtd3(Tv, tci3, tco3)
    'COOLANT TEMPERATURE DIFFERENCE
    dt_cool = tco3 - tci3
    'FIRST TERMINAL TEMPERATURE DIFFERENCE
    dt1 = Tv - tci3
    'SECOND TERMINAL TEMPERATURE DIFFERENCE
    dt2 = Tv - tco3
    'LOG-MEAN TEMPERATURE DIFFERENCE
    lmtd3 = dt_cool / (Log(dt1 / dt2))
End Function
'
'
'LOG-MEAN TEMPERATURE DIFFERENCE ACROSS TEST SECTIONS 2 AND 3
Function lmtd23(Tv, tci2, tco3)
    'COOLANT TEMPERATURE DIFFERENCE
    dt_cool = tco3 - tci2
'FIRST TERMINAL TEMPERATURE DIFFERENCE
dt1 = Tv - tci2
'SECOND TERMINAL TEMPERATURE DIFFERENCE
dt2 = Tv - tco3
'LOG-MEAN TEMPERATURE DIFFERENCE
```

```
    lmtd23 = dt_cool / (Log(dt1 / dt2))
End Function
'
'LOG-MEAN TEMPERATURE DIFFERENCE ACROSS TEST SECTION 4
Function lmtd4(Tv, tci4, tco4)
    'COOLANT TEMPERATURE DIFFERENCE
    dt_cool = tco4 - tci4
    'FIRST TERMINAL TEMPERATURE DIFFERENCE
    dt1 = Tv - tci4
    'SECOND TERMINAL TEMPERATURE DIFFERENCE
    dt2 = Tv - tco4
    'LOG-MEAN TEMPERATURE DIFFERENCE
    lmtd4 = dt_cool / (Log(dt1 / dt2))
End Function
'
'
'LOG-MEAN TEMPERATURE DIFFERENCE ACROSS TEST SECTIONS 2,3 AND 4
Function lmtd234(Tv, tci2, tco4)
    'COOLANT TEMPERATURE DIFFERENCE
    dt_cool = tco4 - tci2
    'FIRST TERMINAL TEMPERATURE DIFFERENCE
    dt1 = Tv - tci2
    'SECOND TERMINAL TEMPERATURE DIFFERENCE
    dt2 = Tv - tco4
    'LOG-MEAN TEMPERATURE DIFFERENCE
    lmtd234 = dt_cool / (Log(dt1 / dt2))
End Function
'
'
'MEAN HEAT TRANSFER COEFFICIENTS
'
'
'MEAN OVERALL HEAT TRANSFER COEFFICIENT ACROSS TEST SECTION 2
Function Um2(Qcool_2, Di, lmtd2)
    'INTERNAL HEAT TRANSFER SURFACE AREA OF TEST SECTION 2
    ai = 3.14159 * Di * 0.5025
    'MEAN OVERALL HEAT TRANSFER COEFFICIENT
```

```
    Um2 = Qcool_2 / (ai * lmtd2)
End Function
'
'
'MEAN OVERALL HEAT TRANSFER COEFFICIENT ACROSS TEST SECTION 3
Function Um3(Qcool_3, Di, lmtd3)
    'INTERNAL HEAT TRANSFER SURFACE AREA OF TEST SECTION 3
    ai = 3.14159 * Di * 0.5025
    'MEAN OVERALL HEAT TRANSFER COEFFICIENT
    Um3 = Qcool_3 / (ai * lmtd3)
End Function
'
'
'MEAN OVERALL HEAT TRANSFER COEFFICIENT ACROSS TEST SECTION 4
Function Um4(Qcool_4, Di, lmtd4)
    'INTERNAL HEAT TRANSFER SURFACE AREA OF TEST SECTION 4
    ai = 3.14159 * Di * 0.5025
    'MEAN OVERALL HEAT TRANSFER COEFFICIENT
    Um4 = Qcool_4 / (ai * lmtd4)
End Function
'
'
'MEAN COOLANT HEAT TRANSFER COEFFICIENT ACROSS TEST SECTION 2
Function coolhtc2(Vdot_cool, rho_cool2, mu_cool2, Cp_cool2, k_cool2)
    'COOLANT VELOCITY
    u_cool2 = (Vdot_cool / 60000) / 0.00004
    'COOLANT REYNOLDS NUMBER
    Re_cool2 = (rho_cool2 * u_cool2 * 0.0057) / mu_cool2
    'COOLANT PRANDTL NUMBER
    Pr_cool2 = (Cp_cool2 * mu_cool2) / k_cool2
    'MEAN COOLANT HEAT TRANSFER COEFFICIENT
    coolhtc2 = ((Re_cool2 ^ 0.8) * (Pr_cool2 ^ 0.4)) / 0.456785
End Function
'MEAN COOLANT HEAT TRANSFER COEFFICIENT ACROSS TEST SECTION 3
Function coolhtc3(Vdot_cool, rho_cool3, mu_cool3, Cp_cool3, k_cool3)
    'COOLANT VELOCITY
    u_cool3 = (Vdot_cool / 60000) / 0.00004
```

```
    'COOLANT REYNOLDS NUMBER
    Re_cool3 = (rho_cool3 * u_cool3 * 0.0057) / mu_cool3
    'COOLANT PRANDTL NUMBER
    Pr_cool3 = (Cp_cool3 * mu_cool3) / k_cool3
    'MEAN COOLANT HEAT TRANSFER COEFFICIENT
    coolhtc3 = ((Re_cool3 ^ 0.8) * (Pr_cool3 ^ 0.4)) / 0.456785
End Function
'
'
'MEAN COOLANT HEAT TRANSFER COEFFICIENT ACROSS TEST SECTION 4
Function coolhtc4(Vdot_cool, rho_cool4, mu_cool4, Cp_cool4, k_cool4)
    'COOLANT VELOCITY
    u_cool4 = (Vdot_cool / 60000) / 0.00004
    'COOLANT REYNOLDS NUMBER
    Re_cool4 = (rho_cool4 * u_cool4 * 0.0057) / mu_cool4
    'COOLANT PRANDTL NUMBER
    Pr_cool4 = (Cp_cool4 * mu_cool4) / k_cool4
    'MEAN COOLANT HEAT TRANSFER COEFFICIENT
    coolhtc4 = ((Re_cool4 ^ 0.8) * (Pr_cool4 ^ 0.4)) / 0.456785
End Function
'
'
'MEAN TUBEWALL HEAT TRANSFER COEFFICIENT ACROSS TEST SECTION 2
Function wallhtc2(tw2)
    'INTERPOLATE TO FIND TUBEWALL THERMAL CONDUCTIVITY
    If tw2 = 0 Then
        kwall2 = 378
    ElseIf tw2 = 100 Then
        kwall2 = 388
    ElseIf 0 < tw2 < 100 Then
        kwall2 = 378 + (tw2 / 10)
    End If
    'TUBEWALL HEAT TRANSFER RESISTANCE
    rwall2 = (0.054 - 0.045) / (2 * kwall2)
    'MEAN TUBEWALL HEAT TRANSFER COEFFICIENT
    wallhtc2 = 1 / rwall2
End Function
```

```
'
'
'MEAN TUBEWALL HEAT TRANSFER COEFFICIENT ACROSS TEST SECTION 3
Function wallhtc3(tw3)
   'INTERPOLATE TO FIND TUBEWALL THERMAL CONDUCTIVITY
   If tw3 = 0 Then
      kwall3 = 378
   Elself tw3 = 100 Then
      kwall3 = 388
   Elself 0 < tw3 < 100 Then
      kwall3 = 378 + (tw3 / 10)
   End If
   'TUBEWALL HEAT TRANSFER RESISTANCE
   rwall3 = (0.054 - 0.045) / (2 * kwall3)
   'MEAN TUBEWALL HEAT TRANSFER COEFFICIENT
   wallhtc3 = 1 / rwall3
End Function
'
'
'MEAN TUBEWALL HEAT TRANSFER COEFFICIENT ACROSS TEST SECTION 4
Function wallhtc4(tw4)
   'INTERPOLATE TO FIND TUBEWALL THERMAL CONDUCTIVITY
   If tw4 = 0 Then
      kwall4 = 378
   Elself tw4 = 100 Then
      kwall4 = 388
   Elself 0 < tw4 < 100 Then
      kwall4 = 378 + (tw4 / 10)
   End If
   'TUBEWALL HEAT TRANSFER RESISTANCE
   rwall4 = (0.054 - 0.045) / (2 * kwall4)
   'MEAN TUBEWALL HEAT TRANSFER COEFFICIENT
   wallhtc4 = 1 / rwall4
End Function
'
'
'VAPOUR AND CONDENSATE FILM MASS BALANCES
```

```
'
'
'CONDENSATE FILM MASS FLOW RATE FROM TEST SECTION 2
Function mcf2(Qcool_2, dhv)
   mcf2 = Qcool_2 / dhv
End Function
'
'CONDENSATE FILM MASS FLOW RATE FROM TEST SECTION 3
Function mcf3(Qcool_3, dhv, mcf2)
   mcf3 = (Qcool_3 / dhv) + mcf2
End Function
'
'
'CONDENSATE FILM MASS FLOW RATE FROM TEST SECTION 4
Function mcf4(Qcool_4, dhv, mcf3)
   mcf4 = (Qcool_4 / dhv) + mcf3
End Function
'
'
'CONDENSATE FILM MASS FLOW RATE FROM DUMP CONDENSER
Function mcfdc(Qcool_dc, dhv, Cp_film, Tv, T_film)
   mcfdc = Qcool_dc / (dhv + (Cp_film * (Tv - T_film)))
End Function
'
'
'VAPOUR MASS FLOW RATE ENTERING TEST SECTION 4
Function mvi4(mcf4, mcfdc)
   mvi4 = mcf4 + mcfdc
End Function
'
'
'VAPOUR MASS FLOW RATE FROM TEST SECTION 4
Function mv4(mvi4, Qcool_4, dhv)
   mv4 = mvi4 - (Qcool_4 / dhv)
End Function
'
'
```

```
'VAPOUR MASS FLOW RATE FROM TEST SECTION 3
Function mv3(mv4, Qcool_3, dhv)
    mv3 = mv4 - (Qcool_3 / dhv)
End Function
'
'
'VAPOUR MASS FLOW RATE FROM TEST SECTION 2
Function mv2(mv3, Qcool_2, dhv)
    mv2 = mv3 - (Qcool_2 / dhv)
End Function
'
'
'CONDENSATE FILM DIMENSIONLESS NUMBERS
'
'
'CONDENSATE FILM REYNOLDS NUMBER AT THE BOTTOM OF TEST SECTION 2
Function Re_cf2(cfmf2, mu_film)
    gamma2 = cfmf2 / (3.14159 * 0.045)
    Re_cf2 = (4 * gamma2) / mu_film
End Function
'
'
'CONDENSATE FILM REYNOLDS NUMBER AT THE BOTTOM OF TEST SECTION 3
Function Re_cf3(cfmf3, mu_film)
    gamma3 = cfmf3 / (3.14159 * 0.045)
    Re_cf3 = (4 * gamma3) / mu_film
End Function
'
'
'CONDENSATE FILM REYNOLDS NUMBER AT THE BOTTOM OF TEST SECTION 4
Function Re_cf4(cfmf4, mu_film)
    gamma4 = cfmf4 / (3.14159 * 0.045)
    Re_cf4 = (4 * gamma4) / mu_film
End Function
'
'
'CONDENSATE FILM PRANDTL NUMBER AT TEST SECTION 2
```

```
Function Pr_cf2(Cp_film, mu_film, k_film)
   Pr_cf2 = (Cp_film * mu_film) / k_film
End Function
'
'
'CONDENSATE FILM PRANDTL NUMBER AT TEST SECTION 3
Function Pr_cf3(Cp_film, mu_film, k_film)
   Pr_cf3 = (Cp_film * mu_film) / k_film
End Function
'CONDENSATE FILM PRANDLT NUMBER AT TEST SECTION 4
Function Pr_cf4(Cp_film, mu_film, k_film)
   Pr_cf4 = (Cp_film * mu_film) / k_film
End Function
'
'
'MEAN CONDENSATE-FILM HEAT TRANSFER COEFFICIENTS
'
'
'MEAN EXPERIMENTAL CONDENSATE-FILM HEAT TRANSFER COEFFICIENT AT THE
BOTTOM OF TEST SECTION 2
Function cfilmhtc2(Um2, coolhtc2, wallhtc2)
    'MEAN OVERALL HEAT TRANSFER RESISTANCE
    ur2 = 1 / Um2
    'MEAN COOLANT HEAT TRANSFER RESISTANCE
    cr2 = (0.07104 / 0.11402) * (1 / coolhtc2)
    'MEAN TUBEWALL HEAT  TRANSFER RESISTANCE
    wr2 = (0.07104 / 0.08525) * (1 / wallhtc2)
    'MEAN CONDENSATE-FILM HEAT TRANSFER COEFFICIENT
    cfilmhtc2 = 1 / (ur2 - (cr2 + wr2))
End Function
'
'
'MEAN EXPERIMENTAL CONDENSATE-FILM HEAT TRANSFER COEFFICIENT AT THE
BOTTOM OF TEST SECTION 3
Function cfilmhtc3(Um3, coolhtc3, wallhtc3)
    'MEAN OVERALL HEAT TRANSFER RESISTANCE
    ur3 = 1 / Um3
```

```
    'MEAN COOLANT HEAT TRANSFER RESISTANCE
     cr3 = (0.07104 / 0.11402) * (1 / coolhtc3)
    'MEAN TUBEWALL HEAT  TRANSFER RESISTANCE
     wr3 = (0.07104 / 0.08525) * (1 / wallhtc3)
    'MEAN CONDENSATE-FILM HEAT TRANSFER COEFFICIENT
     cfilmhtc3 = 1 / (ur3 - (cr3 + wr3))
End Function
'
'
'MEAN EXPERIMENTAL CONDENSATE-FILM HEAT TRANSFER COEFFICIENT AT THE
BOTTOM OF TEST SECTION 4
Function cfilmhtc4(Um4, coolhtc4, wallhtc4)
    'MEAN OVERALL HEAT TRANSFER RESISTANCE
     ur4 = 1 / Um4
    'MEAN COOLANT HEAT TRANSFER RESISTANCE
     cr4 = (0.07104 / 0.11402) * (1 / coolhtc4)
    'MEAN TUBEWALL HEAT  TRANSFER RESISTANCE
     wr4 = (0.07104 / 0.08525) * (1 / wallhtc4)
    'MEAN CONDENSATE-FILM HEAT TRANSFER COEFFICIENT
     cfilmhtc4 = 1 / (ur4 - (cr + wr4))
End Function
'
'
'MEAN CONDENSATE-FILM HEAT TRANSFER COEFFICIENT AT THE BOTTOM OF TEST
SECTION 2 USING NUSSELT
Function hfNu2(cfmf2, rho_film, rho_vap, k_film, mu_film)
   'MASS FLOW RATE OF CONDENSATE PER UNIT TUBE PERIPHERY
    gamma2 = cfmf2 / (3.14159 * 0.045)
   'DENSITY DIFFERENCE BETWEEN CONDENSATE FILM AND VAPOUR
    drho = rho_film - rho_vap
   'MEAN CONDENSATE-FILM HEAT TRANSFER COEFFICIENT
    hfNu2 = 0.925 * (((rho_film * drho * 9.81 * (k_film ^ 3)) / (mu_film * gamma2)) ^ 0.3333)
End Function
'
'
'MEAN CONDENSATE-FILM HEAT TRANSFER COEFFICIENT AT THE BOTTOM OF TEST
SECTION 3 USING NUSSELT
```

```
Function hfNu3(cfmf3, rho_film, rho_vap, k_film, mu_film, Qcool_2, lmtd2, Qcool_3, lmtd3,
lmtd23, hfNu2)
   'MASS FLOW RATE OF CONDENSATE PER UNIT TUBE PERIPHERY
    gamma3 = cfmf3 / (3.14159 * 0.045)
    'DENSITY DIFFERENCE BETWEEN CONDENSATE FILM AND VAPOUR
    drho = rho_film - rho_vap
    'MEAN CONDENSATE-FILM HEAT TRANSFER COEFFICIENT
    dhfNu3 = 0.925 * (((rho_film * drho * 9.81 * (k_film ^ 3)) / (mu_film * gamma3)) ^ 0.3333)
    'CORRECTED MEAN CONDENSATE-FILM HEAT TRANSFER COEFFICIENT
    hfNu3 = (Qcool_3 / lmtd3) * (1 / (((Qcool_2 + Qcool_3) / (dhfNu3 * lmtd23)) - (Qcool_2 /
(hfNu2 * lmtd2))))
End Function
'
'
'MEAN CONDENSATE-FILM HEAT TRANSFER COEFFICIENT AT THE BOTTOM OF TEST
SECTION 4 USING NUSSELT
Function hfNu4(cfmf4, rho_film, rho_vap, k_film, mu_film, Qcool_2, lmtd2, Qcool_3, lmtd3,
Qcool_4, lmtd4, lmtd234, hfNu2, hfNu3)
   'MASS FLOW RATE OF CONDENSATE PER UNIT TUBE PERIPHERY
    gamma4 = cfmf4 / (3.14159 * 0.045)
    'DENSITY DIFFERENCE BETWEEN CONDENSATE FILM AND VAPOUR
    drho = rho_film - rho_vap
    'MEAN CONDENSATE-FILM HEAT TRANSFER COEFFICIENT
    dhfNu4 = 0.925 * (((rho_film * drho * 9.81 * (k_film ^ 3)) / (mu_film * gamma4)) ^ 0.3333)
    'CORRECTED MEAN CONDENSATE-FILM HEAT TRANSFER COEFFICIENT
    hfNu4 = (Qcool_4 / lmtd4) * (1 / (((Qcool_2 + Qcool_3 + Qcool_4) / (dhfNu4 * lmtd234)) -
(Qcool_2 / (hfNu2 * lmtd2)) - (Qcool_3 / (hfNu3 * lmtd3))))
End Function
'
'
'MEAN CONDENSATE-FILM HEAT TRANSFER COEFFICIENT AT THE BOTTOM OF TEST
SECTION 2 USING CM8
Function hfcm82(cfmf2, rho_film, rho_vap, Cp_film, k_film, mu_film)
   'MASS FLOW RATE OF CONDENSATE PER UNTI TUBE PERIPHERY
    gamma2 = cfmf2 / (3.14159 * 0.045)
    'CONDENSATE FILM REYNOLDS NUMBER
    Re_fT2 = (4 * gamma2) / mu_film
```

```
'CONDENSATE FILM PRANDLT NUMBER
Pr_f2 = (Cp_film * mu_film) / k_film
'FIRST TRANSITION REGION REYNOLDS NUMBER
Re_tA2 = 2460 * (Pr_f2 ^ -0.65)
'SECOND TRANSITION REGION REYNOLDS NUMBER
Re_tB2 = 5100 * (Pr_f2 ^ -1.05)
'THIRD TRANSITION REGION REYNOLDS NUMBER
Re_tC2 = 7663 * (Pr_f2 ^ -1.267)
'SIGNIFICANCE OF TRANSITION REGION
If Re_tB2 > Re_tA2 Then
  Re_tX2 = Re_tA2
Elseif Re_tB2 <= Re_tA2 Then
  Re_tX2 = Re_tB2
End If
'DIMENSIONLESS MEAN CONDENSATE-FILM HEAT TRANSFER COEFFICIENT
If Re_fT2 <= 30 Then
  Dh_f2 = (1.467 * (Re_fT2 ^ -0.333))
Elseif 30 < Re_fT2 <= Re_tX2 Then
  Dh_f2 = Re_fT2 / (63.48 + (1.084 * ((Re_fT2 ^ 1.22) - 63.4)))
Elseif Re_tX2 < Re_fT2 <= Re_tC2 And Re_tX2 = Re_tB2 Then
  Dh_f2 = Re_fT2 / (63.48 + (1.084 * ((Re_fT2 ^ 1.22) - 63.4)) + (1.323 * (Re_tX2 ^ 0.22) *
(Re_fT2 - Re_tX2)))
  Elseif Re_fT2 > Re_tC2 And Re_tA2 < Re_tB2 Then
    Dh_f2 = Re_fT2 / (63.38 + (1.084 * (Re_tX2 ^ 1.22 - 63.4)) + (1.323 * (Re_tX2 ^ 0.22) *
(Re_tC2 - Re_tX2)) + (438.6 * (Pr_f2 ^ -0.65) * (Re_fT2 ^ 0.6 - Re_tC2 ^ 0.6)))
  Elseif Re_fT2 > Re_tX2 And Re_tX2 = Re_tB2 Then
    Dh_f2 = Re_fT2 / (63.48 + (1.084 * (Re_tX2 ^ 1.22 - 63.4)) + (438.6 * (Pr_f2 ^ -0.65) *
(Re_fT2 ^ 0.6 - Re_tX2 ^ 0.6)))
  End If
  'ACTUAL MEAN CONDENSATE-FILM HEAT TRANSFER COEFFICIENT
  hfcm82 = (k_film * Dh_f2) * (((rho_film * (rho_film - rho_vap) * 9.81) / mu_film ^ 2) ^
0.3333)
End Function
'
'
'MEAN CONDENSATE-FILM HEAT TRANSFER COEFFICIENT AT THE BOTTOM OF TEST
SECTION 3 USING CM8
```

```
Function hfcm83(cfmf3, rho_film, rho_vap, Cp_film, k_film, mu_film, Qcool_2, lmtd2,
Qcool_3, lmtd3, lmtd23, hfcm82)
   'MASS FLOW RATE OF CONDENSATE PER UNTI TUBE PERIPHERY
   gamma3 = cfmf3 / (3.14159 * 0.045)
   'CONDENSATE FILM REYNOLDS NUMBER
   Re_fT3 = (4 * gamma3) / mu_film
   'CONDENSATE FILM PRANDLT NUMBER
   Pr_f3 = (Cp_film * mu_film) / k_film
   'FIRST TRANSITION REGION REYNOLDS NUMBER
  Re_tA3 = 2460 * (Pr_f3 ^ -0.65)
  'SECOND TRANSITION REGION REYNOLDS NUMBER
  Re_tB3 = 5100 * (Pr_f3 ^ -1.05)
  'THIRD TRANSITION REGION REYNOLDS NUMBER
  Re_tC3 = 7663 * (Pr_f3 ^ -1.267)
  'SIGNIFICANCE OF TRANSITION REGION
  If Re_tB3 > Re_tA3 Then
     Re_tX3 = Re_tA3
  ElseIf Re_tB3 <= Re_tA3 Then
     Re_tX3 = Re_tB3
  End If
  'DIMENSIONLESS MEAN CONDENSATE-FILM HEAT TRANSFER COEFFICIENT
    If Re_fT3 <= 30 Then
       Dh_f3 = (1.467 * (Re_fT3 ^ -0.333))
    ElseIf 30 < Re_fT3 <= Re_tX3 Then
       Dh_f3 = Re_fT3 / (63.48 + (1.084 * ((Re_fT3 ^ 1.22) - 63.4)))
    ElseIf Re_tX3 < Re_fT3 <= Re_tC3 And Re_tX3 = Re_tB3 Then
       Dh_f3 = Re_fT3 / (63.48 + (1.084 * ((Re_fT3 ^ 1.22) - 63.4)) + (1.323 * (Re_tX3 ^ 0.22) *
(Re_fT3 - Re_tX3)))
    ElseIf Re_fT3 > Re_tC3 And Re_tA3 < Re_tB3 Then
       Dh_f3 = Re_fT3 / (63.38 + (1.084 * (Re_tX3 ^ 1.22 - 63.4)) + (1.323 * (Re_tX3 ^ 0.22) *
(Re_tC3 - Re_tX3)) + (438.6 * (Pr_f3 ^ -0.65) * (Re_fT3 ^ 0.6 - Re_tC3 ^ 0.6)))
    ElseIf Re_fT3 > Re_tX3 And Re_tX3 = Re_tB3 Then
       Dh_f3 = Re_fT3 / (63.48 + (1.084 * (Re_tX3 ^ 1.22 - 63.4)) + (438.6 * (Pr_f3 ^ -0.65) *
(Re_fT3 ^ 0.6 - Re_tX3 ^ 0.6)))
    End If
    'ACTUAL MEAN CONDENSATE-FILM HEAT TRANSFER COEFFICIENT
```

```
  ahfcm83 = (k_film * Dh_f3) * (((rho_film * (rho_film - rho_vap) * 9.81) / mu_film ^ 2) ^
0.3333)
  'CORRECTED MEAN CONDENSATE-FILM HEAT TRANSFER COEFFICIENT
  hfcm83 = (Qcool_3 / lmtd3) * (1 / (((Qcool_2 + Qcool_3) / (ahfcm83 * lmtd23)) - (Qcool_2 /
(hfcm82 * lmtd2))))
End Function
'
'
'MEAN CONDENSATE-FILM HEAT TRANSFER COEFFICIENT AT THE BOTTOM OF TEST
SECTION 4 USING CM8
Function hfcm84(cfmf4, rho_film, rho_vap, Cp_film, k_film, mu_film, Qcool_2, lmtd2,
Qcool_3, lmtd3, Qcool_4, lmtd4, lmtd234, hfcm82, hfcm83)
  'MASS FLOW RATE OF CONDENSATE PER UNTI TUBE PERIPHERY
  gamma4 = cfmf4 / (3.14159 * 0.045)
  'CONDENSATE FILM REYNOLDS NUMBER
  Re_fT4 = (4 * gamma4) / mu_film
  'CONDENSATE FILM PRANDLT NUMBER
  Pr_f4 = (Cp_film * mu_film) / k_film
  'FIRST TRANSITION REGION REYNOLDS NUMBER
  Re_tA4 = 2460 * (Pr_f4 ^ -0.65)
  'SECOND TRANSITION REGION REYNOLDS NUMBER
Re_tB4 = 5100 * (Pr_f4 ^ -1.05)
'THIRD TRANSITION REGION REYNOLDS NUMBER
Re_tC4 = 7663 * (Pr_f4 ^ -1.267)
'SIGNIFICANCE OF TRANSITION REGION
If Re_tB4 > Re_tA4 Then
   Re_tX4 = Re_tA4
ElseIf Re_tB4 <= Re_tA4 Then
   Re_tX4 = Re_tB4
End If
'DIMENSIONLESS MEAN CONDENSATE-FILM HEAT TRANSFER COEFFICIENT
If Re_fT4 <= 30 Then
   Dh_f4 = (1.467 * (Re_fT4 ^ -0.333))
ElseIf 30 < Re_fT4 <= Re_tX4 Then
   Dh_f4 = Re_fT4 / (63.48 + (1.084 * ((Re_fT4 ^ 1.22) - 63.4)))
ElseIf Re_tX4 < Re_fT4 <= Re_tC4 And Re_tX4 = Re_tB4 Then
```

```
      Dh_f4 = Re_fT4 / (63.48 + (1.084 * ((Re_fT4 ^ 1.22) - 63.4)) + (1.323 * (Re_tX4 ^ 0.22) *
(Re_fT4 - Re_tX4)))
   Elseif Re_fT4 > Re_tC4 And Re_tA4 < Re_tB4 Then
      Dh_f4 = Re_fT4 / (63.38 + (1.084 * (Re_tX4 ^ 1.22 - 63.4)) + (1.323 * (Re_tX4 ^ 0.22) *
(Re_tC4 - Re_tX4)) + (438.6 * (Pr_f4 ^ -0.65) * (Re_fT4 ^ 0.6 - Re_tC4 ^ 0.6)))
   Elseif Re_fT4 > Re_tX4 And Re_tX4 = Re_tB4 Then
      Dh_f4 = Re_fT4 / (63.48 + (1.084 * (Re_tX4 ^ 1.22 - 63.4)) + (438.6 * (Pr_f4 ^ -0.65) *
(Re_fT4 ^ 0.6 - Re_tX4 ^ 0.6)))
   End If
   'ACTUAL MEAN CONDENSATE-FILM HEAT TRANSFER COEFFICIENT
   ahfcm84 = (k_film * Dh_f4) * (((rho_film * (rho_film - rho_vap) * 9.81) / mu_film ^ 2) ^
0.3333)
   'CORRECTED MEAN CONDENSATE-FILM HEAT TRANSFER COEFFICIENT
   hfcm84 = (Qcool_4 / lmtd4) * (1 / (((Qcool_2 + Qcool_3 + Qcool_4) / (ahfcm84 * lmtd234))
- (Qcool_2 / (hfcm82 * lmtd2)) - (Qcool_3 / (hfcm83 * lmtd3))))
End Function
'
'
'CALCULATIONS FOR THE OVERALL TEST CONDENSER
'
'
'LOGARITHMIC-MEAN TEMPERATURE DIFFERENCE ACROSS TEST CONDENSER
Function lmtd_ov(Tv, tci2, tco4)
   'COOLANT TEMPERATURE DIFFERENCE
   dt_cool = tco4 - tci2
   'FIRST TERMINAL TEMPERATURE DIFFERENCE
   dt1 = Tv - tci2
   'SECOND TERMINAL TEMPERATURE DIFFERENCE
   dt2 = Tv - tco4
   'LOG-MEAN TEMPERATURE DIFFERENCE
   lmtd_ov = dt_cool / (Log(dt1 / dt2))
End Function
'
'
'MEAN OVERALL HEAT TRANSFER COEFFICIENT ACROSS TEST CONDENSER
Function Um_ov(Qcool_test, lmtd_ov)
   'INTERNAL HEAT TRANSFER SURFACE AREA OF TEST CONDENSER
```

```
  ai = 3.14159 * 0.045 * 1.5075
  'MEAN OVERALL HEAT TRANSFER COEFFICIENT
  Um_ov = Qcool_test / (ai * lmtd_ov)
End Function
'
'
'MEAN COOLANT HEAT TRANSFER COEFFICIENT ACROSS TEST CONDENSER
Function coolhtc_ov(Vdot_cool, rho_coolm, mu_coolm, Cp_coolm, k_coolm)
  'COOLANT VELOCITY
  u_coolm = (Vdot_cool / 60000) / 0.00004
  'COOLANT REYNOLDS NUMBER
  Re_coolm = (rho_coolm * u_coolm * 0.0057) / mu_coolm
  'COOLANT PRANDTL NUMBER
  Pr_coolm = (Cp_coolm * mu_coolm) / k_coolm
  'MEAN COOLANT HEAT TRANSFER COEFFICIENT
  coolhtc_ov = ((Re_coolm ^ 0.8) * (Pr_coolm ^ 0.4)) / 0.456785
End Function
'
'
'MEAN TUBEWALL HEAT TRANSFER COEFFICIENT ACROSS TEST CONDENSER
Function wallhtc_ov(tw2, tw3, tw4)
'CALCULATE MEAN WALL TEMPERATURE
twm = (tw2 + tw3 + tw4) / 3
'INTERPOLATE TO FIND TUBEWALL THERMAL CONDUCTIVITY
If twm = 0 Then
   kwallm = 378
ElseIf twm = 100 Then
   kwallm = 388
ElseIf 0 < twm < 100 Then
   kwallm = 378 + (twm / 10)
End If
'TUBEWALL HEAT TRANSFER RESISTANCE
  rwallm = (0.054 - 0.045) / (2 * kwallm)
  'MEAN TUBEWALL HEAT TRANSFER COEFFICIENT
  wallhtc_ov = 1 / rwallm
End Function
'
```

```
'
'REFLUX CONDENSATE FILM TEMPERATURE
Function Trc(Tv, tw4)
   Trc = (0.68 * Tv) + (0.32 * tw4)
End Function
'
'
'REFLUX CONDENSATE FILM FLOW RATE
Function mfrc(Qcool_test, dhv, Cp_film, Tv, Trc)
   mfrc = Qcool_test / (dhv + (Cp_film * (Tv - Trc)))
End Function
'
'
'CONDENSATE FILM REYNOLDS NUMBER AT THE BOTTOM OF TEST CONDENSER
Function Re_rcf(mfrc, mu_film)
   gammam = mfrc / (3.14159 * 0.045)
   Re_rcf = (4 * gammam) / mu_film
End Function
'
'
'CONDENSATE FILM PRANDTL NUMBER AT THE BOTTOM OF THE TEST CONDENSER
Function Pr_rcf(Cp_film, mu_film, k_film)
   Pr_rcf = (Cp_film * mu_film) / k_film
End Function
'
'
'MEAN EXPERIMENTAL CONDENSATE-FILM HEAT TRANSFER COEFFICIENT ACROSS
TEST CONDENSER
Function cfilmhtc_ov(Um_ov, coolhtc_ov, wallhtc_ov)
      'MEAN OVERALL HEAT TRANSFER RESISTANCE
       urov = 1 / Um_ov
      'MEAN COOLANT HEAT TRANSFER RESISTANCE
       crov = (0.07104 / 0.11402) * (1 / coolhtc_ov)
      'MEAN TUBEWALL HEAT  TRANSFER RESISTANCE
       wrov = (0.07104 / 0.08525) * (1 / wallhtc_ov)
      'MEAN CONDENSATE-FILM HEAT TRANSFER COEFFICIENT
       cfilmhtc_ov = 1 / (urov - (crov + wrov))
```

```
End Function
'
'
'MEAN CONDENSATE-FILM HEAT TRANSFER COEFFICIENT AT THE BOTTOM OF TEST
CONDENSER USING NUSSELT
Function hfNumean(cfilmflow, rho_film, rho_vap, k_film, mu_film)
   'MASS FLOW RATE OF CONDENSATE PER UNIT TUBE PERIPHERY
   gammamean = cfilmflow / (3.14159 * 0.045)
   'DENSITY DIFFERENCE BETWEEN CONDENSATE FILM AND VAPOUR
   drho = rho_film - rho_vap
   'MEAN CONDENSATE-FILM HEAT TRANSFER COEFFICIENT
   hfNumean = 0.925 * (((rho_film * drho * 9.81 * (k_film ^ 3)) / (mu_film * gammamean)) ^
0.3333)
End Function
'
'
'MEAN CONDENSATE-FILM HEAT TRANSFER COEFFICIENT AT THE BOTTOM OF TEST
CONDENSER USING CM8
Function hfcm8mean(cfilmflow, rho_film, rho_vap, Cp_film, k_film, mu_film)
   'MASS FLOW RATE OF CONDENSATE PER UNTI TUBE PERIPHERY
   gammamean = cfilmflow / (3.14159 * 0.045)
'CONDENSATE FILM REYNOLDS NUMBER
Re_fTmean = (4 * gammamean) / mu_film
'CONDENSATE FILM PRANDLT NUMBER
Pr_fmean = (Cp_film * mu_film) / k_film
'FIRST TRANSITION REGION REYNOLDS NUMBER
Re_tAmean = 2460 * (Pr_fmean ^ -0.65)
'SECOND TRANSITION REGION REYNOLDS NUMBER
Re_tBmean = 5100 * (Pr_fmean ^ -1.05)
'THIRD TRANSITION REGION REYNOLDS NUMBER
Re_tCmean = 7663 * (Pr_fmean ^ -1.267)
'SIGNIFICANCE OF TRANSITION REGION
If Re_tBmean > Re_tAmean Then
   Re_tXmean = Re_tAmean
ElseIf Re_tBmean <= Re_tAmean Then
   Re_tXmean = Re_tBmean
End If
```

```
'DIMENSIONLESS MEAN CONDENSATE-FILM HEAT TRANSFER COEFFICIENT
If Re_fTmean <= 30 Then
   Dh_fmean = (1.467 * (Re_fTmean ^ -0.333))
ElseIf 30 < Re_fTmean <= Re_tXmean Then
   Dh_fmean = Re_fTmean / (63.48 + (1.084 * ((Re_fTmean ^ 1.22) - 63.4)))
ElseIf Re_tXmean < Re_fTmean <= Re_tCmean And Re_tXmean = Re_tBmean Then
   Dh_fmean = Re_fTmean / (63.48 + (1.084 * ((Re_fTmean ^ 1.22) - 63.4)) + (1.323 *
(Re_tXmean ^ 0.22) * (Re_fTmean - Re_tXmean)))
ElseIf Re_fTmean > Re_tCmean And Re_tAmean < Re_tBmean Then
   Dh_fmean = Re_fTmean / (63.38 + (1.084 * (Re_tXmean ^ 1.22 - 63.4)) + (1.323 *
(Re_tXmean ^ 0.22) * (Re_tCmean - Re_tXmean)) + (438.6 * (Pr_fmean ^ -0.65) *
(Re_fTmean ^ 0.6 - Re_tCmean ^ 0.6)))
ElseIf Re_fTmean > Re_tXmean And Re_tXmean = Re_tBmean Then
   Dh_fmean = Re_fTmean / (63.48 + (1.084 * (Re_tXmean ^ 1.22 - 63.4)) + (438.6 *
(Pr_fmean ^ -0.65) * (Re_fTmean ^ 0.6 - Re_tXmean ^ 0.6)))
End If
'ACTUAL MEAN CONDENSATE-FILM HEAT TRANSFER COEFFICIENT
hfcm8mean = (k_film * Dh_fmean) * (((rho_film * (rho_film - rho_vap) * 9.81) / mu_film ^ 2)
^ 0.3333)
End Function
'
'
'PHYSICAL PROPERTY FACTOR FOR DETERMINING NUSSELT NUMBERS
Function Nufactor(mu_film, rho_film, rho_v, k_film)
   Nufactor = (((mu_film ^ 2) / (rho_film * (rho_film - rho_v) * 9.81)) ^ (1 / 3)) / k_film
End Function
'
'
'CONDENSATE FILM NUSSELT NUMBERS
Function Nufilm(Nufactor, cfilmhtc)
   Nufilm = Nufactor * cfilmhtc
End Function
'
'
'PREDICTED CONDENSATE-FILM HEAT TRANSFER COEFFICIENT
Function phcfilm(Nufactor, Nucfilmcm8, Recfilm)
   'CALCULATE NUSSELT NUMBER BASED ON BEST-FIT LINE CORRELATION
```

```
    Nucfilm = Nucfilmcm8 * ((0.00010373 * Recfilm) + 1.0145)
    'CALCULATE CONDENSATE-FILM HEAT TRANSFER COEFFICIENT
    phcfilm = Nucfilm / Nufactor
End Function
'
'
'FLOODING
'
'
'VAPOUR REYNOLDS NUMBER AT BOTTOM OF TUBE
Function Rev(mvin, mu_v)
'VAPOUR MASS FLUX
    vmassflux = (4 * mvin) / (3.14159 * (0.045 ^ 2))
'VAPOUR REYNOLDS NUMBER
    Rev = (vmassflux * 0.045) / mu_v
End Function
'
'
'VAPOUR VELOCITY ENTERING TEST CONDENSER
Function u_vap(mvi4, rho_vap)
    'VOLUME FLOW RATE OF VAPOUR ENTERING CONDENSER
    V_vap = mvi4 / rho_vap
    'CROSS-SECTIONAL FLOW AREA OF TEST CONDENSER
    si = (3.14159 / 4) * (0.045 ^ 2)
    'VAPOUR VELOCITY
    u_vap = V_vap / si
End Function
'
'
'PREDICTED VAPOUR FLOODING VELOCITY
Function vap_flood(mcf4, rho_film, rho_vap, sigma_film, mu_film)
    'CONDENSATE FILM VOLUME FLOW RATE PER UNIT TUBE PERIPHERY
'
'TEST CONDENSER TUBE FLOW AREA
si = (3.14159 / 4) * (0.045 ^ 2)
'CONDENSATE FILM VELOCITY
ucf = (mcf4 / rho_film) / si
```

```
'
vcf = (ucf * 0.045) / 4
'FROUDE NUMBER
Fr = vcf * ((9.81 * ((rho_film - rho_vap) ^ 3)) / (sigma_film ^ 3)) ^ 0.25
'BOND NUMBER
Bo = ((0.045 ^ 2) * 9.81 * (rho_film - rho_vap)) / sigma_film
'VISCOSITY CORRECTION
f = (1 + (mu_film / 0.001)) ^ -0.18
'GAS KUTATELADZE NUMBER
Kg = 0.286 * (Bo ^ 0.26) * (Fr ^ -0.22) * f
   'SUPERFICIAL FLOODING VELOCITY
   sfv = (Kg * (((rho_film - rho_vap) * sigma_film * 9.81) ^ 0.25)) / (rho_vap ^ 0.5)
   'CONSERVATIVE FLOODING VELOCITY
   vap_flood = sfv / 1.6
End Function
'
'
```

Appendix A4 Binary Hydrocarbon Mixture Data Analysis Functions

```
'DETERMINE THE COMPOSITIONS OF THE REFLUX LIQUID AND EXIT VAPOUR FROM
THE TEST CONDENSER
Function compphase(tphase)
  'DETERMINE THE DENSITY OF THE PHASE FROM ITS MEASURED PERIOD OF
VIBRATION READING
   rhophase = 1.2372 + (158.9032 * ((tphase ^ 2) - (2.64197 ^ 2)))
   'DETERMINE THE COMPOSITION OF THE PHASE FROM THIS DENSITY
   drhophase = 701.5506 - rhophase
   compphase = (-37.39155 + ((37.39155 ^ 2) + (4 * 26.66161 * drhophase)) ^ 0.5) / (2 *
26.66161)
End Function
'
'
'DETERMINE THE REFLUX CONDENSATE FILM TEMPERATURE
Function Trfilm(Tv4, Tw4)
   Trfilm = (0.68 * Tv4) + (0.32 * Tw4)
End Function
'
'
'DETERMINE THE COOLANT HEAT LOADS ACROSS EACH OF THE SECTIONS IN THE
TEST CONDENSER
'
'
'COOLANT HEAT LOAD ACROSS TEST SECTION 2
Function Qcool_2(Vdot_cool, rho_cool, Cp_cool, tci2, tco2)
   'COOLANT MASS FLOW RATE
   Mdot_cool = (Vdot_cool * rho_cool) / 60000
   'COOLANT HEAT LOAD
   Qcool_2 = Mdot_cool * Cp_cool * (tco2 - tci2)
End Function
'
'
'COOLANT HEAT LOAD ACROSS TEST SECTION 3
Function Qcool_3(Vdot_cool, rho_cool, Cp_cool, tci3, tco3)
   'COOLANT MASS FLOW RATE
   Mdot_cool = (Vdot_cool * rho_cool) / 60000
   'COOLANT HEAT LOAD
   Qcool_3 = Mdot_cool * Cp_cool * (tco3 - tci3)
End Function
```

```
'COOLANT HEAT LOAD ACROSS TEST SECTION 4
Function Qcool_4(Vdot_cool, rho_cool, Cp_cool, tci4, tco4)
   'COOLANT MASS FLOW RATE
   Mdot_cool = (Vdot_cool * rho_cool) / 60000
   'COOLANT HEAT LOAD
   Qcool_4 = Mdot_cool * Cp_cool * (tco4 - tci4)
End Function
'
'
'COOLANT HEAT LOD ACROSS DUMP CONDENSER
Function Qcool_d(Vdot_cool, rho_cool, Cp_cool, tci, tco)
   'COOLANT MASS FLOW RATE
   Mdot_cool = (Vdot_cool * rho_cool) / 60000
   'COOLANT HEAT LOAD
   Qcool_d = Mdot_cool * Cp_cool * (tco - tci)
End Function
'
'
'LOG-MEAN TEMPERATURE DIFFERENCE ACROSS TEST SECTION 2
Function lmtd2(Tvo2, tci2, tco2)
   'COOLANT TEMPERATURE DIFFERENCE
   dtc = tco2 - tci2
   'FIRST TERMINAL TEMPERATURE DIFFERENCE
   dt1 = Tvo2 - tci2
   'SECOND TERMINAL TEMPERATURE DIFFERENCE
   dt2 = Tvo2 - tco2
   'LOG-MEAN TEMPERATURE DIFFERENCE
   lmtd2 = dtc / (Log(dt1 / dt2))
End Function
'
'
'LOG-MEAN TEMPERATURE DIFFERENCE ACROSS TEST SECTION 3
Function lmtd3(Tvo3, tci3, tco3)
'COOLANT TEMPERATURE DIFFERENCE
dtc = tco3 - tci3
'FIRST TERMINAL TEMPERATURE DIFFERENCE
dt1 = Tvo3 - tci3
'SECOND TERMINAL TEMPERATURE DIFFERENCE
dt2 = Tvo3 - tco3
```

```
    'LOG-MEAN TEMPERATURE DIFFERENCE
    lmtd3 = dtc / (Log(dt1 / dt2))
End Function
'
'
'LOG-MEAN TEMPERATURE DIFFERENCE ACROSS TEST SECTION 4
Function lmtd4(Tvo4, tci4, tco4)
    'COOLANT TEMPERATURE DIFFERENCE
    dtc = tco4 - tci4
    'FIRST TERMINAL TEMPERATURE DIFFERENCE
    dt1 = Tvo4 - tci4
    'SECOND TERMINAL TEMPERATURE DIFFERENCE
    dt2 = Tvo4 - tco4
    'LOG-MEAN TEMPERATURE DIFFERENCE
    lmtd4 = dtc / (Log(dt1 / dt2))
End Function
'
'
'MEAN HEAT TRANSFER COEFFICIENTS
'
'
'MEAN OVERALL HEAT TRANSFER COEFFICIENT ACROSS TEST SECTION 2
Function Um2(Qcool_2, Di, lmtd2)
    'INTERNAL HEAT TRANSFER SURFACE AREA OF TEST SECTION 2
    ai = 3.14159 * Di * 0.5025
    'MEAN OVERALL HEAT TRANSFER COEFFICIENT
    Um2 = Qcool_2 / (ai * lmtd2)
End Function
'
'
'MEAN OVERALL HEAT TRANSFER COEFFICIENT ACROSS TEST SECTION 3
Function Um3(Qcool_3, Di, lmtd3)
    'INTERNAL HEAT TRANSFER SURFACE AREA OF TEST SECTION 3
    ai = 3.14159 * Di * 0.5025
    'MEAN OVERALL HEAT TRANSFER COEFFICIENT
    Um3 = Qcool_3 / (ai * lmtd3)
End Function
'
'
```

```
'MEAN OVERALL HEAT TRANSFER COEFFICIENT ACROSS TEST SECTION 4
Function Um4(Qcool_4, Di, lmtd4)
  'INTERNAL HEAT TRANSFER SURFACE AREA OF TEST SECTION 4
  ai = 3.14159 * Di * 0.5025
  'MEAN OVERALL HEAT TRANSFER COEFFICIENT
  Um4 = Qcool_4 / (ai * lmtd4)
End Function
'
'
'MEAN COOLANT HEAT TRANSFER COEFFICIENT ACROSS TEST SECTION 2
Function coolhtc2(Vdot_cool, rho_cool2, mu_cool2, Cp_cool2, k_cool2)
  'COOLANT VELOCITY
  u_cool2 = (Vdot_cool / 60000) / 0.00004
  'COOLANT REYNOLDS NUMBER
  Re_cool2 = (rho_cool2 * u_cool2 * 0.0057) / mu_cool2
  'COOLANT PRANDTL NUMBER
  Pr_cool2 = (Cp_cool2 * mu_cool2) / k_cool2
  'MEAN COOLANT HEAT TRANSFER COEFFICIENT
  coolhtc2 = ((Re_cool2 ^ 0.8) * (Pr_cool2 ^ 0.4)) / 0.456785
End Function
'
'
'MEAN COOLANT HEAT TRANSFER COEFFICIENT ACROSS TEST SECTION 3
Function coolhtc3(Vdot_cool, rho_cool3, mu_cool3, Cp_cool3, k_cool3)
  'COOLANT VELOCITY
  u_cool3 = (Vdot_cool / 60000) / 0.00004
  'COOLANT REYNOLDS NUMBER
  Re_cool3 = (rho_cool3 * u_cool3 * 0.0057) / mu_cool3
  'COOLANT PRANDTL NUMBER
  Pr_cool3 = (Cp_cool3 * mu_cool3) / k_cool3
  'MEAN COOLANT HEAT TRANSFER COEFFICIENT
  coolhtc3 = ((Re_cool3 ^ 0.8) * (Pr_cool3 ^ 0.4)) / 0.456785
End Function
'
'
'MEAN COOLANT HEAT TRANSFER COEFFICIENT ACROSS TEST SECTION 4
Function coolhtc4(Vdot_cool, rho_cool4, mu_cool4, Cp_cool4, k_cool4)
  'COOLANT VELOCITY
  u_cool4 = (Vdot_cool / 60000) / 0.00004
```

```
  'COOLANT REYNOLDS NUMBER
  Re_cool4 = (rho_cool4 * u_cool4 * 0.0057) / mu_cool4
  'COOLANT PRANDTL NUMBER
  Pr_cool4 = (Cp_cool4 * mu_cool4) / k_cool4
  'MEAN COOLANT HEAT TRANSFER COEFFICIENT
  coolhtc4 = ((Re_cool4 ^ 0.8) * (Pr_cool4 ^ 0.4)) / 0.456785
End Function
'
'
'MEAN TUBEWALL HEAT TRANSFER COEFFICIENT ACROSS TEST SECTION 2
Function wallhtc2(tw2)
  'INTERPOLATE TO FIND TUBEWALL THERMAL CONDUCTIVITY
  If tw2 = 0 Then
    kwall2 = 378
  Elseif tw2 = 100 Then
    kwall2 = 388
  Elseif 0 < tw2 < 100 Then
    kwall2 = 378 + (tw2 / 10)
  End If
  'TUBEWALL HEAT TRANSFER RESISTANCE
  rwall2 = (0.054 - 0.045) / (2 * kwall2)
  'MEAN TUBEWALL HEAT TRANSFER COEFFICIENT
  wallhtc2 = 1 / rwall2
End Function
'
'
'MEAN TUBEWALL HEAT TRANSFER COEFFICIENT ACROSS TEST SECTION 3
Function wallhtc3(tw3)
  'INTERPOLATE TO FIND TUBEWALL THERMAL CONDUCTIVITY
  If tw3 = 0 Then
    kwall3 = 378
  Elseif tw3 = 100 Then
    kwall3 = 388
  Elseif 0 < tw3 < 100 Then
    kwall3 = 378 + (tw3 / 10)
  End If
  'TUBEWALL HEAT TRANSFER RESISTANCE
  rwall3 = (0.054 - 0.045) / (2 * kwall3)
  'MEAN TUBEWALL HEAT TRANSFER COEFFICIENT
```

```
    wallhtc3 = 1 / rwall3
End Function
'
'
'MEAN TUBEWALL HEAT TRANSFER COEFFICIENT ACROSS TEST SECTION 4
Function wallhtc4(Tw4)
    'INTERPOLATE TO FIND TUBEWALL THERMAL CONDUCTIVITY
    If Tw4 = 0 Then
        kwall4 = 378
    ElseIf Tw4 = 100 Then
        kwall4 = 388
    ElseIf 0 < Tw4 < 100 Then
        kwall4 = 378 + (Tw4 / 10)
    End If
    'TUBEWALL HEAT TRANSFER RESISTANCE
    rwall4 = (0.054 - 0.045) / (2 * kwall4)
    'MEAN TUBEWALL HEAT TRANSFER COEFFICIENT
    wallhtc4 = 1 / rwall4
End Function
'
'
'MEAN EXPERIMENTAL CONDENSING-SIDE HEAT TRANSFER COEFFICIENT AT THE
BOTTOM OF TEST SECTION 2
Function csidehtc2(Um2, coolhtc2, wallhtc2)
    'MEAN OVERALL HEAT TRANSFER RESISTANCE
    ur2 = 1 / Um2
    'MEAN COOLANT HEAT TRANSFER RESISTANCE
    cr2 = (0.07104 / 0.11402) * (1 / coolhtc2)
    'MEAN TUBEWALL HEAT  TRANSFER RESISTANCE
    wr2 = (0.07104 / 0.08525) * (1 / wallhtc2)
    'MEAN CONDENSATE-FILM HEAT TRANSFER COEFFICIENT
    csidehtc2 = 1 / (ur2 - (cr2 + wr2))
End Function
'
'
'MEAN EXPERIMENTAL CONDENSING-SIDE HEAT TRANSFER COEFFICIENT AT THE
BOTTOM OF TEST SECTION 3
Function csidehtc3(Um3, coolhtc3, wallhtc3)
    'MEAN OVERALL HEAT TRANSFER RESISTANCE
```

```
    ur3 = 1 / Um3
    'MEAN COOLANT HEAT TRANSFER RESISTANCE
    cr3 = (0.07104 / 0.11402) * (1 / coolhtc3)
    'MEAN TUBEWALL HEAT  TRANSFER RESISTANCE
    wr3 = (0.07104 / 0.08525) * (1 / wallhtc3)
    'MEAN CONDENSATE-FILM HEAT TRANSFER COEFFICIENT
    csidehtc3 = 1 / (ur3 - (cr3 + wr3))
End Function
'
'
'MEAN EXPERIMENTAL CONDENSING-SIDE HEAT TRANSFER COEFFICIENT AT THE
BOTTOM OF TEST SECTION 4
Function csidehtc4(Um4, coolhtc4, wallhtc4)
    'MEAN OVERALL HEAT TRANSFER RESISTANCE
    ur4 = 1 / Um4
    'MEAN COOLANT HEAT TRANSFER RESISTANCE
    cr4 = (0.07104 / 0.11402) * (1 / coolhtc4)
    'MEAN TUBEWALL HEAT  TRANSFER RESISTANCE
    wr4 = (0.07104 / 0.08525) * (1 / wallhtc4)
    'MEAN CONDENSATE-FILM HEAT TRANSFER COEFFICIENT
    csidehtc4 = 1 / (ur4 - (cr + wr4))
End Function
'
'
'CALCULATIONS FOR THE OVERALL TEST CONDENSER
'
'
'LOGARITHMIC-MEAN TEMPERATURE DIFFERENCE ACROSS TEST CONDENSER
Function lmtd_ov(Tvi, Tvo, tci2, tco4)
   'FIRST TERMINAL TEMPERATURE DIFFERENCE
   dt1 = Tvi - tco4
   'SECOND TERMINAL TEMPERATURE DIFFERENCE
   dt2 = Tvo - tci2
   'LOG-MEAN TEMPERATURE DIFFERENCE
   lmtd_ov = (dt1 - dt2) / (Log(dt1 / dt2))
End Function
'
'
'MEAN OVERALL HEAT TRANSFER COEFFICIENT ACROSS TEST CONDENSER
```

```
Function Um_ov(Qcool_test, lmtd_ov)
   'INTERNAL HEAT TRANSFER SURFACE AREA OF TEST CONDENSER
   ai = 3.14159 * 0.045 * 1.5075
   'MEAN OVERALL HEAT TRANSFER COEFFICIENT
   Um_ov = Qcool_test / (ai * lmtd_ov)
End Function
'
'
'MEAN COOLANT HEAT TRANSFER COEFFICIENT ACROSS TEST CONDENSER
Function coolhtc_ov(Vdot_cool, rho_coolm, mu_coolm, Cp_coolm, k_coolm)
  'COOLANT VELOCITY
  u_coolm = (Vdot_cool / 60000) / 0.00004
  'COOLANT REYNOLDS NUMBER
  Re_coolm = (rho_coolm * u_coolm * 0.0057) / mu_coolm
  'COOLANT PRANDTL NUMBER
  Pr_coolm = (Cp_coolm * mu_coolm) / k_coolm
  'MEAN COOLANT HEAT TRANSFER COEFFICIENT
  coolhtc_ov = ((Re_coolm ^ 0.8) * (Pr_coolm ^ 0.4)) / 0.456785
End Function
'
'
'MEAN TUBEWALL HEAT TRANSFER COEFFICIENT ACROSS TEST CONDENSER
Function wallhtc_ov(twm)
   'INTERPOLATE TO FIND TUBEWALL THERMAL CONDUCTIVITY
   If twm = 0 Then
      kwallm = 378
   Elself twm = 100 Then
      kwallm = 388
   Elself 0 < twm < 100 Then
      kwallm = 378 + (twm / 10)
   End If
   'TUBEWALL HEAT TRANSFER RESISTANCE
   rwallm = (0.054 - 0.045) / (2 * kwallm)
   'MEAN TUBEWALL HEAT TRANSFER COEFFICIENT
   wallhtc_ov = 1 / rwallm
End Function
'
'
```

```
'MEAN EXPERIMENTAL CONDENSING SIDE HEAT TRANSFER COEFFICIENT ACROSS
TEST CONDENSER
Function csidehtc_ov(Um_ov, coolhtc_ov, wallhtc_ov)
    'MEAN OVERALL HEAT TRANSFER RESISTANCE
     urov = 1 / Um_ov
    'MEAN COOLANT HEAT TRANSFER RESISTANCE
     crov = (0.07104 / 0.11402) * (1 / coolhtc_ov)
    'MEAN TUBEWALL HEAT  TRANSFER RESISTANCE
     wrov = (0.07104 / 0.08525) * (1 / wallhtc_ov)
    'MEAN CONDENSATE-FILM HEAT TRANSFER COEFFICIENT
      csidehtc_ov = 1 / (urov - (crov + wrov))
End Function
'
'
'VAPOUR AND CONDENSATE FILM MASS BALANCES
'
'
'DETERMINE N-PENTANE MASS FRACTIONS FROM MOLE FRACTIONS
Function mfp(molfp)
   mfp = (molfp * 72.151) / ((molfp * 72.151) + ((1 - molfp) * 114.232))
End Function
'
'
'CONDENSATE FILM MASS FLOW RATE FROM TEST CONDENSER
Function mrfilm(Qcool_tc, mfp, dhvp, dhvo, Cp_filmp, Cp_filmo, Tv, Trfilm)
   'CALCULATE REFLUX FILM LATENT HEAT
      dhvrfilm = (mfp * dhvp) + ((1 - mfp) * dhvo)
   'CALCULATE REFLUX FILM SPECIFIC HEAT CAPACITY
    Cp_rfilm = (mfp * Cp_filmp) + ((1 - mfp) * Cp_filmo)
   'CALCULATE REFLUX FILM MASS FLOW RATE
    mrfilm = Qcool_tc / (dhvrfilm + (Cp_rfilm * (Tv - Trfilm)))
End Function
'
'
'CONDENSATE FILM MASS FLOW RATE FROM DUMP CONDENSER
Function mdfilm(Qcool_dc, mfp, dhvp, dhvo, Cp_filmp, Cpfilmo, Tv, T_dfilm)
   'CALCULATE DUMP FILM LATENT HEAT
    dhvdfilm = (mfp * dhvp) + ((1 - mfp) * dhvo)
   'CALCULATE DUMP FILM SPECIFIC HEAT CAPACITY
```

```
   Cp_dfilm = (mfp * Cp_filmp) + ((1 - mfp) * Cp_filmo)
   'CALCULATE DUMP FILM MASS FLOW RATE
   mdfilm = Qcool_dc / (dhvdfilm + (Cp_dfilm * (Tv - T_dfilm)))
End Function
'
'
'FEED VAPOUR MASS FRACTION
Function mfvi(mrfilm, mfprfilm, mdfilm, mfpdfilm, mvfeed)
   mfvi = ((mrfilm * mfprfilm) + (mdfilm * mfpdfilm)) / mvfeed
End Function
'
'
'CONVERT FEED VAPOUR MASS FRACTION TO MOLE FRACTION
Function xpvi(mfvi)
xpvi = (mfvi / 72.151) / ((mfvi / 72.151) + ((1 - mfvi) / 114.232))
End Function
'
'
'MIXTURE MOLAR FLOW RATE
Function molflow(molfp, massflow)
'DETERMINE MIXTURE MOLECULAR WEIGHT
   molm = (72.151 * molfp) + ((1 - molfp) * 114.232)
'DETERMINE MIXTURE MOLAR FLOW RATE
   molflow = 1000 * (massflow / molm)
End Function
'
'
'FLOODING PREDICTIONS
'
'
'VAPOUR VELOCITY ENTERING TEST CONDENSER
Function u_vap(mvi4, mvp, rho_vp, rho_vo)
   'VAPOUR VISCOSITY
   rho_v = (mvp * rho_vp) + ((1 - mvp) * rho_vo)
'VOLUME FLOW RATE OF VAPOUR ENTERING CONDENSER
V_vap = mvi4 / rho_v
'CROSS-SECTIONAL FLOW AREA OF TEST CONDENSER
si = (3.14159 / 4) * (0.045 ^ 2)
'VAPOUR VELOCITY
```

```
   u_vap = V_vap / si
End Function
'
'
'PREDICTED VAPOUR FLOODING VELOCITY
Function vap_flood(mcf4, mfp, mvp, rho_fp, rho_fo, rho_vp, rho_vo, sigma_fp, sigma_fo,
mu_fp, mu_fo)
   'CONDENSATE FILM DENSITY
   rho_f = (mfp * rho_fp) + ((1 - mfp) * rho_fo)
   'VAPOUR DENSITY
rho_v = (mvp * rho_vp) + ((1 - mvp) * rho_vo)
'CONDENSATE FILM SURFACE TENSION
sigma_f = (mfp * sigma_fp) + ((1 - mfp) * simgma_fo)
'CONDENSATE FILM VISCOSITY
mu_f = (mfp * mu_fp) + ((1 - mfp) * mu_fo)
'CONDENSATE FILM VOLUME FLOW RATE PER UNIT TUBE PERIPHERY
'
'TEST CONDENSER TUBE FLOW AREA
si = (3.14159 / 4) * (0.045 ^ 2)
'CONDENSATE FILM VELOCITY
ucf = (mcf4 / rho_f) / si
'
vcf = (ucf * 0.045) / 4
'FROUDE NUMBER
Fr = vcf * ((9.81 * ((rho_f - rho_v) ^ 3)) / (sigma_f ^ 3)) ^ 0.25
'BOND NUMBER
Bo = ((0.045 ^ 2) * 9.81 * (rho_f - rho_v)) / sigma_f
'VISCOSITY CORRECTION
f = (1 + (mu_f / 0.001)) ^ -0.18
'GAS KUTATELADZE NUMBER
Kg = 0.286 * (Bo ^ 0.26) * (Fr ^ -0.22) * f
'SUPERFICIAL FLOODING VELOCITY
sfv = (Kg * (((rho_f - rho_v) * sigma_f * 9.81) ^ 0.25)) / (rho_v ^ 0.5)
   'CONSERVATIVE FLOODING VELOCITY
   vap_flood = sfv / 1.6
End Function
'
'
```

```
'ANALYSIS OF THE GAS-PHASE HEAT TRANSFER RESISTANCE
'
'
'CONDENSATE FILM REYNOLDS NUMBER AT THE BOTTOM OF TEST CONDENSER
Function Re_rfilm(mrfilm, mfp, mu_filmp, mu_filmo)
    gammarfilm = mrfilm / (3.14159 * 0.045)
    'CALCULATE REFLUX FILM VISCOSITY
    mu_rfilm = (mfp * mu_filmp) + ((1 - mfp) * mu_filmo)
    'REFLUX FILM REYNOLDS NUMBER
    Re_rfilm = (4 * gammarfilm) / mu_rfilm
End Function
'
'
'CONDENSATE FILM PRANDTL NUMBER AT THE BOTTOM OF THE TEST CONDENSER
Function Pr_rfilm(mfp, Cp_filmp, Cp_filmo, mu_filmp, mu_filmo, k_filmp, k_filmo)
   'CALCULATE REFLUX FILM SPECIFIC HEAT CAPACITY
    Cp_rfilm = (mfp * Cp_filmp) + ((1 - mfp) * Cp_filmo)
    'CALCULATE REFLUX FILM VISCOSITY
    mu_rfilm = (mfp * mu_filmp) + ((1 - mfp) * mu_filmo)
    'CALCULATE REFLUX FILM THERMAL CONDUCTIVITY
    k_rfilm = (mfp * k_filmp) + ((1 - mfp) * k_filmo)
    'DETERMINE REFLUX FILM PRANDTL NUMBER
   Pr_rfilm = (Cp_rfilm * mu_rfilm) / k_rfilm
End Function
'
'
'MEAN CONDENSATE-FILM HEAT TRANSFER COEFFICIENT AT THE BOTTOM OF TEST
CONDENSER USING CM8
Function filmhtc_cm8(mfp, rho_filmp, rho_filmo, mvp, rho_vp, rho_vo, Cp_filmp, Cp_filmo,
k_filmp, k_filmo, mu_filmp, mu_filmo, Re_rfilm, Pr_rfilm)
   'DETERMINE REFLUX FILM DENSITY
    rho_rfilm = (mfp * rho_filmp) + ((1 - mfp) * rho_filmo)
    'DETERMINE REFLUX FILM SPECIFIC HEAT CAPACITY
    Cp_rfilm = (mfp * Cp_filmp) + ((1 - mfp) * Cp_filmo)
'DETERMINE REFLUX FILM THERMAL CONDUCTIVITY
    k_rfilm = (mfp * k_filmp) + ((1 - mfp) * k_filmo)
'DETERMINE REFLUX FILM VISCOSITY
    mu_rfilm = (mfp * mu_filmp) + ((1 - mfp) * mu_filmo)
'DETERMINE VAPOUR DENSITY
```

```
rho_v = (mvp * rho_vp) + ((1 - mvp) * rho_vo)
'FIRST TRANSITION REGION REYNOLDS NUMBER
Re_tAmean = 2460 * (Pr_rfilm ^ -0.65)
'SECOND TRANSITION REGION REYNOLDS NUMBER
Re_tBmean = 5100 * (Pr_rfilm ^ -1.05)
'THIRD TRANSITION REGION REYNOLDS NUMBER
Re_tCmean = 7663 * (Pr_rfilm ^ -1.267)
'SIGNIFICANCE OF TRANSITION REGION
If Re_tBmean > Re_tAmean Then
   Re_tXmean = Re_tAmean
ElseIf Re_tBmean <= Re_tAmean Then
   Re_tXmean = Re_tBmean
End If
'DIMENSIONLESS MEAN CONDENSATE-FILM HEAT TRANSFER COEFFICIENT
If Re_rfilm <= 30 Then
   Dh_fmean = (1.467 * (Re_rfilm ^ -0.333))
ElseIf 30 < Re_rfilm <= Re_tXmean Then
   Dh_fmean = Re_rfilm / (63.48 + (1.084 * ((Re_rfilm ^ 1.22) - 63.4)))
ElseIf Re_tXmean < Re_rfilm <= Re_tCmean And Re_tXmean = Re_tBmean Then
   Dh_fmean = Re_rfilm / (63.48 + (1.084 * ((Re_rfilm ^ 1.22) - 63.4)) + (1.323 *
(Re_tXmean ^ 0.22) * (Re_rfilm - Re_tXmean)))
ElseIf Re_rfilm > Re_tCmean And Re_tAmean < Re_tBmean Then
   Dh_fmean = Re_rfilm / (63.38 + (1.084 * (Re_tXmean ^ 1.22 - 63.4)) + (1.323 *
(Re_tXmean ^ 0.22) * (Re_tCmean - Re_tXmean)) + (438.6 * (Pr_rfilm ^ -0.65) * (Re_rfilm ^
0.6 - Re_tCmean ^ 0.6)))
ElseIf Re_rfilm > Re_tXmean And Re_tXmean = Re_tBmean Then
   Dh_fmean = Re_rfilm / (63.48 + (1.084 * (Re_tXmean ^ 1.22 - 63.4)) + (438.6 * (Pr_rfilm
^ -0.65) * (Re_rfilm ^ 0.6 - Re_tXmean ^ 0.6)))
End If
'ACTUAL MEAN CONDENSATE-FILM HEAT TRANSFER COEFFICIENT
filmhtc_cm8 = (k_rfilm * Dh_fmean) * (((rho_rfilm * (rho_rfilm - rho_vap) * 9.81) / mu_rfilm
^ 2) ^ 0.3333)
End Function
'
'
'CORRECTED MEAN CONDENSATE-FILM HEAT TRANSFER COEFFICIENT AT BOTTOM
OF TEST CONDENSER
Function filmhtc(Re_rfilm, filmhtc_cm8)
   filmhtc = (1.0145 + (0.00010373 * Re_rfilm)) * filmhtc_cm8
```

```
End Function
'
'
'CALCULATE EFFECTIVE EXPERIMENTAL GAS-PHASE HEAT TRANSFER COEFFICIENT
Function gashtc(csidehtc, filmhtc)
   gashtc = 1 / ((1 / csidehtc) - (1 / filmhtc))
End Function
'
'
'MEAN VAPOUR MASS FLOW RATE THROUGH TEST CONDENSER
Function meanmv(mvfeed, mdfilm)
   meanmv = 0.5 * (mvfeed + mdfilm)
End Function
'
'
'VAPOUR REYNOLDS NUMBER AT BOTTOM OF TUBE
Function Rev(meanmv, mvp, mu_vp, mu_vo)
'CALCULATE MASS FLUX AT BOTTOM OF TUBE
   mflux = meanmv / ((3.14159 / 4) * (0.045 ^ 2))
'CALCULATE VAPOUR VISCOSITY
   mu_v = (mvp * mu_vp) + ((1 - mvp) * mu_vo)
'CALCULATE VAPOUR REYNOLDS NUMBER
   Rev = (mflux * 0.045) / mu_v
End Function
'
'
'VAPOUR PRANDLT NUMBER AT BOTTOM OF TUBE
Function Prv(mvp, Cp_vp, Cp_vo, mu_vp, mu_vo, k_vp, k_vo)
'CALCULATE VAPOUR SPECIFIC HEAT CAPACITY
   Cp_v = (mvp * Cp_vp) + ((1 - mvp) * Cp_vo)
'CALCULATE VAPOUR VISCOSITY
   mu_v = (mvp * mu_vp) + ((1 - mvp) * mu_vo)
'CALCULATE VAPOUR THERMAL CONDUCTIVITY
   k_v = (mvp * k_vp) + ((1 - mvp) * k_vo)
'CALCULATE PRANDTL NUMBER
   Prv = (Cp_v * mu_v) / k_v
End Function
'
'
```

```
'DRY GAS-PHASE HEAT TRANSFER COEFFICIENT
Function drygashtc(mvp, k_vp, k_vo, Rev, Prv)
'CALCULATE VAPOUR THERMAL CONDUCTIVITY
   k_v = (mvp * k_vp) + ((1 - mvp) * k_vo)
'CALCULATE DRY-GAS HEAT TRANSFER COEFFICIENT
   drygashtc = 0.023 * (k_v / 0.045) * (Rev ^ 0.8) * (Prv ^ 0.4)
End Function
'
'
'MEAN VAPOUR MASS FRACTION THROUGH TEST CONDENSER
Function v_massfrac(mvfeed, mrfilm)
'DETERMINE VAPOUR QUALITY AT TOP OF TEST CONDENSER
   v_qualb = (mvfeed - mrfilm) / mvfeed
'MEAN VAPOUR QUALITY
   v_massfrac = 0.5 * (1 + v_qualb)
End Function
'
'
'GRADIENT OF TEMPERATURE-ENTHAPLY CURVE
Function dtdh(Tvin, Tvout, Qcool_tc, mvfeed)
   dt = Tvin - Tvout
   dh = Qcool_tc / mvfeed
   dtdh = dt / dh
End Function
'
'
'PARAMETER Z DEFINED BY SILVER'S METHOD
Function Z(v_qual, mvp, Cp_vp, Cp_vo, dtdh)
'DETERMINE THE VAPOUR SPECIFIC HEAT CAPACITY
   Cp_v = (mvp * Cp_vp) + ((1 - mvp) * Cp_vo)
'DETERMINE Z
   Z = v_qual * Cp_v * dtdh
End Function
'
'
'MEAN CONDENSING VAPOUR MASS FLUX THROUGH TEST CONDENSER
Function mconflux(mrfilm)
'DETERMINE INNER SURFACE AREA
   sa = 3.14159 * 0.045 * (0.5025 * 3)
```

```
'DETERMINE MASS FLUX
   mconflux = mrfilm / sa
End Function
'
'
'HEAT TRANSFER RATE FACTOR
Function phi(mconflux, mfp, Cp_vp, Cp_vo, drygashtc)
'DETERMINE THE CONDENSING FLUX SPECIFIC HEAT CAPACITY
   Cp_conflux = (mfp * Cp_vp) + ((1 - mfp) * Cp_vo)
'DETERMINE THE HEAT TRANSFER RATE FACTOR
   phi = (mconflux * Cp_conflux) / drygashtc
End Function
'
'
'MASS TRANSFER CORRECTION TERM FOR HEAT TRANSFER
Function theta(phi)
   theta = phi / (Exp(phi) - 1)
End Function
'
'
'INTEGRAL CONDENSATION OUTLET VAPOUR QUALITY
Function int_vqualb(mrfilm, mdfilm)
'DETERMINE VAPOUR QUALITY AT BOTTOM OF TUBE
   int_vqualb = mdfilm / (mrfilm + mdfilm)
End Function
'
'
```

Appendix A5 Composition Measurement using a Densitometer

A5 Composition Measurement using a Densitometer

A5.1 The Principle of Density Measurement

The measuring principle of the densitometer was based on the change in the natural frequency of vibration of the hollow U-shaped cell when it was filled with different samples of liquids or gases. The mass and thus the density of the liquid or gas sample changed the natural frequency due to the change in the mass of the cell.

To measure this natural frequency, the cell was electronically excited in a harmonic fashion perpendicular to its plane. The frequency of the cell was only influenced by that fraction of its volume filled by liquid or gas. Since this vibrating volume was easily controlled, it was unnecessary to make individual volume measurements.

For calculating density, the densitometer manufacturer recommended an approach as described below. Consider a hollow body of mass M suspended on a spring with an elasticity constant c, its volume V filled with a sample of density ρ. The natural frequency of this system was given by

$$f = \frac{1}{2\pi}\sqrt{\frac{c}{M + \rho V}} \qquad \text{(A5.1.1)}$$

Therefore, the period of vibration was the inverse of the natural frequency

$$t = \frac{1}{f} = 2\pi\sqrt{\frac{M + \rho V}{c}} \qquad \text{(A5.1.2)}$$

Squaring (A5.1.2) gave

$$t^2 = 4\pi^2\left[\frac{M + \rho V}{c}\right] \qquad \text{(A5.1.3)}$$

This equation was simplified by introducing two constant terms

$$a = \frac{4\pi^2 V}{c} \qquad \text{(A5.1.4a)}$$

$$b = \frac{4\pi^2 M}{c} \qquad \text{(A5.1.4b)}$$

Therefore, (A5.1.3) was reduced to

$$t^2 = b + \rho\, a \qquad \text{(A5.1.5)}$$

This meant that the density was now expressed as

$$\rho = \frac{\left(t^2 - b\right)}{a} \qquad \text{(A5.1.6)}$$

As a and b are instrument constants, they are independent of the fluids whose densities are measured. So, for two fluids of different density, and therefore natural frequency

$$\rho_1 = \frac{\left(t_1^2 - b\right)}{a} \qquad \text{(A5.1.7a)}$$

$$\rho_2 = \frac{\left(t_2^2 - b\right)}{a} \qquad \text{(A5.1.7b)}$$

The density difference between these two fluids was expressed as

$$\rho_1 - \rho_2 = \left(\frac{t_1^2 - b}{a}\right) - \left(\frac{t_2^2 - b}{a}\right) \qquad \text{(A5.1.8a)}$$

$$\rho_1 - \rho_2 = \frac{1}{a}\left(t_1^2 - t_2^2\right) - b + b \qquad \text{(A5.1.8b)}$$

Finally,

$$\rho_1 - \rho_2 = K_\rho \left(t_1^2 - t_2^2 \right) \qquad \text{(A5.1.9)}$$

The instrument calibration constant, K_ρ, was determined by measuring the period of vibration for two different fluids whose densities were known at the system temperature and pressure.

A5.2. Results for Air and Purified Water.

Table A5.1. Period of vibration readings for air (seconds).

	P (barg)					
T (°C)	*1.00686*	*1.00821*	*1.00991*	*1.01024*	*1.00279*	*1.00178*
10.4	2.641943	2.641958	2.642079	2.641967	2.641933	2.641939
11.4	2.641750	2.641763	2.641882	2.641768	2.641736	2.641741
12.4	2.641557	2.641575	2.641685	2.641574	2.641543	2.641545
13.4	2.641365	2.641379	2.641488	2.641380	2.641351	2.641353
14.4	2.641177	2.641183	2.641293	2.641186	2.641156	2.641159
15.4	2.640990	2.640987	2.641088	2.640990	2.640966	2.640965

Tables A5.2. Period of vibration readings for purified water (seconds).

T (°C)	*P (barg)*					
	1.00686	*1.00821*	*1.00991*	*1.01024*	*1.00279*	*1.00178*
10.4	3.644466	3.644507	3.644475	3.644497	3.644448	3.644477
11.4	3.644123	3.644170	3.644131	3.644156	3.644103	3.644134
12.4	3.643773	3.643805	3.643774	3.643799	3.643764	3.643779
13.4	3.643404	3.643434	3.643409	3.643432	3.643397	3.643412
14.4	3.643013	3.643054	3.643027	3.643054	3.643017	3.643032
15.4	3.642543	3.642479	3.642647	3.642657	3.642616	3.642624

Tables A5.3. Measured densities for air (kg/m^3).

T (℃)	*P (barg)*					
	1.00686	*1.00821*	*1.00991*	*1.01024*	*1.00279*	*1.00178*
10.4	1.2374	1.2391	1.2412	1.2416	1.2324	1.2312
11.4	1.2331	1.2347	1.2368	1.2372	1.2281	1.2269
12.4	1.2287	1.2304	1.2325	1.2329	1.2238	1.2225
13.4	1.2244	1.2261	1.2282	1.2286	1.2195	1.2183
14.4	1.2202	1.2218	1.2239	1.2243	1.2152	1.2140
15.4	1.2159	1.2176	1.2196	1.2200	1.2110	1.2098

Tables A5.4. Measured densities for purified water (kg/m^3).

T *(℃)*	*P (barg)*					
	1.00686	*1.00821*	*1.00991*	*1.01024*	*1.00279*	*1.00178*
10.4	1002.8966	1002.8966	1002.8966	1002.8966	1002.8966	1002.8966
11.4	1002.5542	1002.5542	1002.5542	1002.5542	1002.5542	1002.5542
12.4	1002.2084	1002.2084	1002.2084	1002.2084	1002.2084	1002.2084
13.4	1001.8593	1001.8593	1001.8593	1001.8593	1001.8593	1001.8593
14.4	1001.5068	1001.5068	1001.5068	1001.5068	1001.5068	1001.5068
15.4	1001.1511	1001.1511	1001.1511	1001.1511	1001.1511	1001.1511

A5.3. Results for Single Component Hydrocarbons

Table A5.5. Period of vibration readings for n-pentane (seconds).

T (°C)				
10.4	3.314249	3.314310	3.314193	3.314681
11.4	3.313093	3.313159	3.313041	3.313531
12.4	3.311929	3.311985	3.311914	3.312341
13.4	3.310764	3.310975	3.310744	3.311178
14.4	3.309581	3.309607	3.309597	3.309999
15.4	3.308364	3.308384	3.308422	3.308778

Tables A5.6. Period of vibration readings for iso-octane (seconds).

T (°C)				
10.4	3.374625	3.374638	3.374620	3.374680
11.4	3.373630	3.373547	3.373635	3.373684
12.4	3.372619	3.372547	3.372626	3.372665
13.4	3.371591	3.371544	3.371630	3.371627
14.4	3.370576	3.370534	3.370620	3.370637
15.4	3.369576	3.369513	3.369566	3.369631

Table A5.7. Measured densities of n-pentane (kg/m^3).

T (°C)				
10.4	637.5241	637.5883	637.4651	637.9791
11.4	636.4673	636.5368	636.4125	636.9285
12.4	635.4000	635.4590	635.3842	635.8337
13.4	634.3324	634.5545	634.3114	634.7681
14.4	633.2462	633.2736	633.2631	633.6859
15.4	632.1256	632.1466	632.1866	632.5609

Tables A5.8. Measured densities of iso-octane (kg/m^3).

T (°C)				
10.4	701.6967	701.7107	701.6914	701.7557
11.4	700.7904	700.7014	700.7958	700.8483
12.4	699.8647	699.7875	699.8722	699.9140
13.4	698.9215	698.8711	698.9632	698.9600
14.4	697.9923	697.9473	698.0395	698.0577
15.4	697.0805	697.0130	697.0697	697.1394

A5.4. Results for Binary Hydrocarbon Mixtures

Table A5.9. Period of vibration readings (seconds) for a mixture of n-pentane and iso-octane having an n-pentane mole fraction of 0.2244.

T (°C)				
10.4	3.364915	3.365008	3.365140	3.365039
11.4	3.363900	3.363968	3.364094	3.363978
12.4	3.362886	3.362922	3.363040	3.362919
13.4	3.361861	3.361861	3.361988	3.361871
14.4	3.360829	3.360818	3.360952	3.360801
15.4	3.359745	3.359734	3.359886	3.359717

Table A5.10. Period of vibration readings (seconds) for a mixture of n-pentane and iso-octane having an n-pentane mole fraction of 0.4018.

T (°C)				
10.4	3.356240	3.356534	3.356203	3.356292
11.4	3.355205	3.355467	3.355160	3.355218
12.4	3.354140	3.354394	3.354149	3.354156
13.4	3.353091	3.353309	3.353099	3.353104
14.4	3.352029	3.352245	3.352107	3.352042
15.4	3.350925	3.351135	3.351022	3.350997

Table A5.11. Period of vibration readings (seconds) for a mixture of n-pentane and iso-octane having an n-pentane mole fraction of 0.5889.

T (°C)				
10.4	3.345911	3.345936	3.346070	3.346328
11.4	3.344830	3.344839	3.344991	3.345267
12.4	3.343684	3.343762	3.343910	3.344188
13.4	3.342586	3.342654	3.342835	3.343089
14.4	3.341494	3.341565	3.341736	3.341980
15.4	3.340351	3.340427	3.340640	3.340862

Table A5.12. Period of vibration readings (seconds) for a mixture of n-pentane and iso-octane having an n-pentane mole fraction of 0.7713.

T (°C)				
10.4	3.333665	3.333741	3.333793	3.334071
11.4	3.332487	3.332586	3.332684	3.332974
12.4	3.331379	3.331473	3.331564	3.331869
13.4	3.330203	3.330319	3.330453	3.330710
14.4	3.329074	3.329195	3.329317	3.329597
15.4	3.327922	3.328019	3.328220	3.328438

Table A5.13. Measured densities for a mixture (kg/m^3) of n-pentane and iso-octane with an n-pentane mole fraction of 0.2244.

T (°C)				
10.4	691.2980	691.3974	691.5386	691.4306
11.4	690.3733	690.4460	690.5807	690.4567
12.4	689.4476	689.4860	689.6121	689.4828
13.4	688.5107	688.5107	688.6464	688.5214
14.4	687.5665	687.5548	687.6979	687.5366
15.4	686.5681	686.5563	686.7186	686.5382

Table A5.14. Measured densities for a mixture (kg/m^3) of n-pentane and iso-octane with an n-pentane mole fraction of 0.4018.

T (°C)				
10.4	682.0329	682.3465	681.9935	682.0884
11.4	681.0898	681.3691	681.0418	681.1036
12.4	680.1125	680.3832	680.1220	680.1295
13.4	679.1528	679.3852	679.1614	679.1667
14.4	678.1796	678.4097	678.2627	678.1935
15.4	677.1629	677.3865	677.2662	677.2396

Table A5.15. Measured densities for a mixture (kg/m^3) of n-pentane and iso-octane with an n-pentane mole fraction of 0.5889.

T (°C)				
10.4	671.0326	671.0592	671.2017	671.4761
11.4	670.0439	670.0535	670.2151	670.5085
12.4	668.9841	669.0670	669.2242	669.5197
13.4	667.9759	668.0481	668.2404	668.5103
14.4	666.9744	667.0498	667.2314	667.4905
15.4	665.9199	666.0006	666.2267	666.4624

Table A5.16. Measured densities for a mixture (kg/m^3) of n-pentane and iso-octane with an n-pentane mole fraction of 0.7713.

T (°C)				
10.4	658.0346	658.1152	658.1703	658.4648
11.4	656.9474	657.0523	657.1561	657.4633
12.4	655.9323	656.0318	656.1282	656.4511
13.4	654.8459	654.9686	655.1105	655.3825
14.4	653.8095	653.9375	654.0666	654.3629
15.4	652.7500	652.8526	653.0652	653.2958

A5.5 Comparison of the Densitometer Calibration Constants

Table A5.17. Density differences calculated at 1.00686barg.

	Temperature-dependent K_ρ		Temperature-independent K_ρ	
T (°C)	*(kg/m³)*	*(%)*	*(kg/m³)*	*(%)*
10.4	-0.0085	-0.0009	0.2083	0.0208
11.4	-0.0046	-0.0005	0.1054	0.0105
12.4	-0.0086	-0.0009	0.0073	0.0007
13.4	-0.0056	-0.0006	-0.0714	-0.0071
14.4	0.0098	0.0010	-0.1248	-0.0125
15.4	0.0527	0.0053	-0.0893	-0.0089

Table A5.18. Density differences calculated at 1.00821barg.

	Temperature-dependent K_ρ		Temperature-independent K_ρ	
T (°C)	*(kg/m³)*	*(%)*	*(kg/m³)*	*(%)*
10.4	0.0616	0.0061	0.1717	0.0171
11.4	-0.0498	-0.0050	0.0603	0.0060
12.4	-0.0322	-0.0032	-0.0163	-0.0016
13.4	-0.0302	-0.0030	-0.0961	-0.0096
14.4	-0.0343	-0.0034	-0.1688	-0.0169
15.4	0.1226	0.0123	-0.0193	-0.0019

Table A5.19. Density differences calculated at 1.00991barg.

	Temperature-dependent K_ρ		Temperature-independent K_ρ	
T (°C)	*(kg/m³)*	*(%)*	*(kg/m³)*	*(%)*
10.4	0.0915	0.0091	0.3083	0.0307
11.4	0.0932	0.0093	0.2033	0.0203
12.4	0.0939	0.0094	0.1099	0.0110
13.4	0.0882	0.0088	0.0223	0.0022
14.4	0.0873	0.0087	-0.0473	-0.0047
15.4	0.0109	0.0011	-0.1311	-0.0131

Table A5.20. Density differences calculated at 1.01024barg.

	Temperature-dependent K_ρ		Temperature-independent K_ρ	
T (°C)	*(kg/m³)*	*(%)*	*(kg/m³)*	*(%)*
10.4	-0.0284	-0.0028	0.1884	0.0188
11.4	-0.0319	-0.0032	0.0782	0.0078
12.4	-0.0286	-0.0029	-0.0127	-0.0013
13.4	-0.0295	-0.0029	-0.0954	-0.0095
14.4	-0.0342	-0.0034	-0.1688	-0.0169
15.4	-0.0833	-0.0083	-0.2253	-0.0225

Table A5.21. Density differences calculated at 1.00279barg.

	Temperature-dependent K_ρ		Temperature-independent K_ρ	
T (°C)	*(kg/m³)*	*(%)*	*(kg/m³)*	*(%)*
10.4	0.0089	0.0009	0.2257	0.0225
11.4	0.0118	0.0012	0.1218	0.0122
12.4	-0.0050	-0.0005	0.0109	0.0011
13.4	-0.0043	-0.0004	-0.0701	-0.0070
14.4	-0.0075	-0.0008	-0.1421	-0.0142
15.4	-0.0470	-0.0047	-0.1890	-0.0189

Table A5.22. Density differences calculated at 1.00178barg.

	Temperature-dependent K_ρ		Temperature-independent K_ρ	
T (°C)	*(kg/m³)*	*(%)*	*(kg/m³)*	*(%)*
10.4	-0.0184	-0.0018	0.1984	0.0198
11.4	-0.0187	-0.0019	0.0914	0.0091
12.4	-0.0195	-0.0019	-0.0035	-0.0004
13.4	-0.0187	-0.0019	-0.0846	-0.0084
14.4	-0.0211	-0.0021	-0.1557	-0.0155
15.4	-0.0559	-0.0056	-0.1979	-0.0198

Appendix A6 Expression for the Mean Coolant Heat Transfer Coefficient

A6.1 Test Data for Condensing Pure Steam

Table A6.1. Data for test run number 1.

Boiler Measurements			Test Section Measurements				
$\dot{Q}$	T_v	P_v	$\dot{V}_c$	$T_{c,in}$	$T_{c,out}$	T_v	$\overline{T}_w$
(W)	*(°C)*	*(bara)*	*(l/min)*	*(°C)*	*(°C)*	*(°C)*	*(°C)*
6045.1	39.1	0.076	9.787	27.8	34.6	38.9	35.1
6032.8	39.1	0.076	9.795	27.8	34.6	39.0	35.1
6028.9	39.2	0.076	9.787	27.9	34.6	38.9	35.1
6017.6	39.2	0.076	9.779	27.9	34.6	39.0	35.1
6018.2	40.2	0.081	7.659	27.3	35.9	40.2	36.3
6033.9	40.3	0.081	7.635	27.3	35.9	40.3	36.3
6021.1	40.2	0.081	7.655	27.3	35.9	40.2	36.3
6023.5	40.4	0.081	7.651	27.3	35.9	40.3	36.3
6040.1	42.3	0.090	5.667	26.9	38.2	42.2	38.3
6048.6	42.2	0.089	5.659	26.9	38.2	42.3	38.4
6036.7	42.3	0.090	5.679	26.9	38.2	42.2	38.4
6036.8	42.3	0.090	5.663	26.9	38.3	42.3	38.5
6027.1	45.2	0.103	3.714	26.1	41.8	45.1	41.5
6039.0	45.2	0.103	3.734	26.1	41.8	45.2	41.5
6044.4	45.3	0.104	3.734	26.1	41.9	45.3	41.5
6063.4	45.4	0.104	3.726	26.1	41.9	45.3	41.5

Table A6.2. Data for test run number 2.

Boiler Measurements			Test Section Measurements				
$\dot{Q}$	T_v	P_v	$\dot{V}_c$	$T_{c,in}$	$T_{c,out}$	T_v	$\bar{T}_w$
(W)	*(°C)*	*(bara)*	*(l/min)*	*(°C)*	*(°C)*	*(°C)*	*(°C)*
6042.2	46.6	0.113	10.407	37.1	43.3	46.6	43.5
6041.6	46.8	0.112	10.391	37.1	43.3	46.6	43.6
6045.8	46.7	0.113	10.407	37.1	43.3	46.8	43.7
6055.5	46.8	0.113	10.403	37.1	43.2	46.7	43.6
6047.7	47.3	0.116	9.378	37.0	43.9	47.3	44.2
6049.9	47.4	0.117	9.382	37.1	44.0	47.4	44.2
6056.1	47.5	0.117	9.413	37.1	44.0	47.4	44.3
6059.1	47.5	0.117	9.397	37.1	44.0	47.4	44.2
6039.4	48.0	0.120	8.372	36.8	44.6	48.1	44.9
6035.0	48.1	0.121	8.360	36.8	44.6	48.0	44.9
6021.9	48.1	0.120	8.360	36.8	44.6	48.0	44.8
6009.7	48.0	0.120	8.376	36.8	44.6	48.1	44.8
6023.0	48.7	0.124	7.183	36.4	45.3	48.7	45.5
6023.7	48.7	0.125	7.187	36.4	45.4	48.7	45.5
6038.1	48.8	0.125	7.183	36.4	45.4	48.7	45.5
6034.4	48.8	0.125	7.211	36.4	45.4	48.8	45.6
6018.1	49.5	0.130	6.221	36.0	46.3	49.5	46.3
6017.4	49.5	0.129	6.217	36.0	46.3	49.5	46.3
6017.3	49.5	0.130	6.232	36.0	46.4	49.5	46.3
6013.2	49.6	0.129	6.217	35.9	46.4	49.5	46.3

Table A6.2. Data for test run number 2 (continued).

Boiler Measurements			Test Section Measurements				
$\dot{Q}$	T_v	P_v	$\dot{V}_c$	$T_{c,in}$	$T_{c,out}$	T_v	$\overline{T}_w$
(W)	*(°C)*	*(bara)*	*(l/min)*	*(°C)*	*(°C)*	*(°C)*	*(°C)*
6036.6	50.4	0.135	5.328	35.5	47.4	50.3	47.2
6027.9	50.4	0.135	5.332	35.5	47.4	50.4	47.2
6040.2	50.4	0.135	5.359	35.5	47.4	50.4	47.2
6030.0	50.5	0.136	5.355	35.6	47.5	50.4	47.3
6067.2	51.9	0.144	4.432	35.3	49.1	51.9	48.7
6065.5	52.0	0.145	4.435	35.3	49.1	52.0	48.7
6056.0	52.0	0.144	4.435	35.3	49.2	52.0	48.7
6051.9	52.0	0.145	4.428	35.3	49.2	52.0	48.8

Table A6.3. Data for test run number 3.

Boiler Measurements			Test Section Measurements				
$\dot{Q}$	T_v	P_v	$\dot{V}_c$	$T_{c,in}$	$T_{c,out}$	T_v	$\overline{T}_w$
(W)	*(°C)*	*(bara)*	*(l/min)*	*(°C)*	*(°C)*	*(°C)*	*(°C)*
6028.7	45.9	0.108	10.360	36.0	42.3	45.9	42.5
6026.1	46.0	0.109	10.368	36.0	42.3	45.9	42.5
6032.1	45.9	0.109	10.395	36.0	42.3	45.9	42.5
6028.7	46.0	0.109	10.399	36.0	42.3	46.0	42.6
6021.4	46.5	0.111	9.440	35.9	42.7	46.3	43.0
6024.7	46.4	0.112	9.420	35.9	42.8	46.4	43.0
6007.1	46.4	0.111	9.424	35.9	42.8	46.4	43.0
6012.8	46.5	0.112	9.413	35.9	42.8	46.4	43.0
6032.6	47.3	0.115	8.544	36.0	43.6	47.2	43.7
6039.9	47.3	0.115	8.555	36.0	43.6	47.2	43.7
6041.7	47.2	0.116	8.567	36.0	43.6	47.2	43.7
6039.4	47.3	0.116	8.547	36.0	43.7	47.3	43.7
6028.5	47.9	0.120	7.569	35.8	44.4	47.9	44.4
6023.1	47.9	0.120	7.577	35.8	44.3	47.8	44.4
6014.2	47.9	0.121	7.569	35.8	44.4	47.9	44.4
6016.4	48.0	0.120	7.581	35.8	44.3	47.9	44.4
6024.8	48.8	0.125	6.404	35.3	45.4	48.8	45.2
6029.5	48.8	0.125	6.412	35.3	45.4	48.7	45.2
6029.0	48.8	0.126	6.412	35.3	45.3	48.7	45.3
6030.2	48.8	0.125	6.404	35.3	45.4	48.8	45.3

Table A6.3. Data for test run number 3 (continued).

Boiler Measurements			Test Section Measurements				
$\dot{Q}$	T_v	P_v	$\dot{V}_c$	$T_{c,in}$	$T_{c,out}$	T_v	$\overline{T}_w$
(W)	*(°C)*	*(bara)*	*(l/min)*	*(°C)*	*(°C)*	*(°C)*	*(°C)*
6046.5	49.9	0.132	5.437	35.0	46.6	49.8	46.3
6046.3	49.9	0.132	5.441	35.0	46.6	49.8	46.3
6058.3	49.8	0.132	5.429	35.0	46.5	49.8	46.3
6058.8	49.9	0.132	5.422	35.0	46.6	49.8	46.3
6101.4	51.4	0.141	4.330	34.5	48.4	51.5	47.9
6108.6	51.4	0.142	4.322	34.5	48.4	51.5	47.9
6119.8	51.5	0.142	4.319	34.5	48.4	51.5	47.9
6119.3	51.5	0.142	4.319	34.5	48.5	51.5	47.9

Table A6.4. Data for test run number 4.

Boiler Measurements			Test Section Measurements				
$\dot{Q}$	T_v	P_v	$\dot{V}_c$	$T_{c,in}$	$T_{c,out}$	T_v	$\overline{T}_w$
(W)	*(°C)*	*(bara)*	*(l/min)*	*(°C)*	*(°C)*	*(°C)*	*(°C)*
5918.2	40.6	0.083	10.407	31.1	36.8	40.5	37.1
5918.5	40.6	0.083	10.407	31.1	36.8	40.5	37.2
5914.2	40.6	0.084	10.422	31.0	36.8	40.5	37.2
5914.5	40.6	0.085	10.403	31.0	36.8	40.4	37.2
5911.6	40.9	0.086	9.549	30.7	37.1	40.8	37.3
5915.3	40.9	0.086	9.545	30.7	37.1	40.8	37.3
5934.6	40.9	0.086	9.549	30.7	37.1	40.8	37.4
5930.5	40.8	0.086	9.549	30.7	37.2	40.7	37.4
5960.6	41.6	0.089	8.735	30.8	37.9	41.4	38.2
5958.3	41.6	0.089	8.715	30.8	37.9	41.3	38.1
5960.7	41.6	0.089	8.719	30.8	37.9	41.5	38.1
5952.2	41.6	0.089	8.707	30.8	37.9	41.5	38.1
5934.5	41.4	0.087	7.838	29.6	37.7	41.3	37.8
5933.2	41.4	0.087	7.842	29.6	37.6	41.2	37.8
5923.5	41.3	0.087	7.846	29.6	37.6	41.2	37.7
5925.7	41.1	0.086	7.826	29.6	37.5	41.1	37.7
5957.5	41.8	0.090	6.638	29.1	38.4	41.8	38.4
5950.7	41.9	0.090	6.634	29.1	38.4	41.9	38.4
5957.8	41.9	0.090	6.634	29.1	38.3	41.8	38.4
5957.6	41.9	0.089	6.626	29.0	38.4	41.8	38.4

Table A6.4. Data for test run number 4 (continued).

Boiler Measurements			Test Section Measurements				
$\dot{Q}$	T_v	P_v	$\dot{V}_c$	$T_{c,in}$	$T_{c,out}$	T_v	$\overline{T}_w$
(W)	*(°C)*	*(bara)*	*(l/min)*	*(°C)*	*(°C)*	*(°C)*	*(°C)*
5973.1	42.6	0.093	5.710	28.6	39.3	42.6	39.2
5976.2	42.7	0.093	5.718	28.6	39.3	42.7	39.2
5983.5	42.7	0.093	5.729	28.6	39.3	42.5	39.2
5974.2	42.7	0.094	5.702	28.6	39.4	42.7	39.2
6021.6	44.3	0.100	4.502	28.4	41.2	44.3	40.8
6010.5	44.3	0.100	4.482	28.4	41.3	44.3	40.9
6019.6	44.4	0.100	4.506	28.4	41.3	44.4	40.9
6020.4	44.4	0.101	4.474	28.4	41.4	44.3	40.9

Table A6.5. Data for test run number 5.

Boiler Measurements			Test Section Measurements				
$\dot{Q}$	T_v	P_v	$\dot{V}_c$	$T_{c,in}$	$T_{c,out}$	T_v	$\overline{T}_w$
(W)	*(°C)*	*(bara)*	*(l/min)*	*(°C)*	*(°C)*	*(°C)*	*(°C)*
5951.9	45.4	0.106	10.407	34.0	41.0	45.3	41.3
5943.5	45.4	0.106	10.410	34.0	41.0	45.3	41.3
5941.6	45.5	0.106	10.407	34.0	41.1	45.4	41.4
5940.7	45.3	0.106	10.418	34.0	41.1	45.4	41.4
5922.9	45.9	0.108	9.456	33.8	41.6	45.9	41.9
5933.5	45.9	0.109	9.459	33.8	41.6	45.8	41.8
5948.5	45.9	0.108	9.463	33.8	41.6	45.9	41.8
5943.6	46.0	0.109	9.467	33.8	41.6	45.9	41.8
5934.6	46.6	0.112	8.431	33.4	42.3	46.5	42.5
5937.7	46.6	0.112	8.442	33.5	42.3	46.5	42.5
5933.1	46.6	0.113	8.434	33.5	42.3	46.4	42.5
5929.7	46.6	0.112	8.427	33.5	42.3	46.5	42.5
5928.7	47.5	0.118	7.413	33.2	43.2	47.3	43.3
5924.1	47.5	0.117	7.441	33.2	43.2	47.4	43.4
5931.7	47.5	0.118	7.402	33.2	43.3	47.5	43.4
5920.1	47.5	0.118	7.425	33.2	43.3	47.5	43.4
5906.9	48.5	0.121	6.486	32.9	44.4	48.5	44.4
5906.5	48.5	0.121	6.505	32.9	44.4	48.5	44.4
5920.3	48.6	0.121	6.497	32.9	44.4	48.5	44.5
5925.1	48.6	0.121	6.509	33.0	44.4	48.6	44.5

Table A6.5. Data for test run number 5 (continued).

Boiler Measurements			Test Section Measurements				
$\dot{Q}$	T_v	P_v	$\dot{V}_c$	$T_{c,in}$	$T_{c,out}$	T_v	$\overline{T}_w$
(W)	*(°C)*	*(bara)*	*(l/min)*	*(°C)*	*(°C)*	*(°C)*	*(°C)*
5915.6	50.3	0.132	5.449	32.4	46.1	50.2	46.0
5932.3	50.2	0.133	5.484	32.4	46.1	50.3	46.0
5944.6	50.3	0.134	5.468	32.5	46.2	50.3	46.0
5951.6	50.3	0.133	5.453	32.5	46.2	50.3	46.0
5942.3	52.5	0.148	4.439	31.8	48.7	52.5	48.0
5943.4	52.5	0.148	4.435	31.8	48.7	52.5	48.2
5942.9	52.6	0.149	4.435	31.8	48.7	52.6	48.1
5958.9	52.6	0.149	4.424	31.7	48.7	52.7	48.2

A6.2 Experimental Conditions when Condensing Pure Steam

Table A6.6. Results of test run number 1.

$\dot{Q}_{c,TS}$	$\Delta T_{\ln,TS}$	$\overline{U}_{t,TS}$	$\overline{\alpha}_{w,TS}$	Re_c	Pr_c
(W)	*(°C)*	*(W/m²°C)*	*(W/m²°C)*	*(-)*	*(-)*
4620.446	7.385	8806.57	84780.0	27701	5.6123
4624.223	7.385	8813.77	84780.0	27724	5.6123
4552.269	7.455	8595.92	84780.0	27760	5.5993
4548.548	7.455	8588.89	84780.0	27738	5.5993
4574.097	7.828	8225.33	84806.7	21448	5.6781
4559.764	7.938	8085.60	84806.7	21381	5.6781
4571.708	7.828	8221.03	84806.7	21437	5.6781
4569.319	8.048	7991.78	84806.7	21426	5.6781
4447.893	8.539	7332.68	84851.1	15734	5.7315
4441.614	8.423	7422.90	84853.3	15712	5.7315
4457.311	8.539	7348.20	84853.3	15767	5.7315
4484.088	8.457	7464.22	84855.6	15723	5.7315
4051.731	9.097	6269.92	84922.2	10134	5.8408
4073.549	9.097	6303.68	84922.2	10189	5.8408
4099.495	9.127	6322.75	84922.2	10189	5.8408
4090.712	9.254	6222.49	84922.2	10167	5.8408

Table A6.7. Results of test run number 2.

$\dot{Q}_{c,TS}$	$\Delta T_{\ln,TS}$	$\overline{U}_{t,TS}$	$\overline{\alpha}_{w,TS}$	Re_c	Pr_c
(W)	*(°C)*	*(W/m² °C)*	*(W/m² °C)*	*(-)*	*(-)*
4459.323	5.864	10705.47	84966.7	35494	4.5773
4452.467	6.082	10304.80	84968.9	35440	4.5773
4459.323	5.973	10509.24	84971.1	35494	4.5773
4385.712	6.154	10031.60	84968.9	35481	4.5773
4472.307	6.225	10112.73	84982.2	31924	4.5868
4474.002	6.225	10116.57	84982.2	31998	4.5773
4488.785	6.336	9973.02	84984.4	32104	4.5773
4481.155	6.336	9956.07	84982.2	32049	4.5773
4513.749	6.543	9711.17	84997.8	28392	4.6059
4507.280	6.655	9533.76	84997.8	28351	4.6059
4507.280	6.655	9533.76	84995.6	28351	4.6059
4515.906	6.543	9715.81	84995.6	28406	4.6059
4419.695	6.922	8988.47	85011.1	24175	4.6444
4471.843	6.841	9202.27	85011.1	24189	4.6444
4469.354	6.956	9045.07	85011.1	24175	4.6444
4486.776	6.956	9080.33	85013.3	24270	4.6444

Table A6.7. Results of test run number 2 (continued).

$\dot{Q}_{c,TS}$	$\Delta T_{ln,TS}$	$\overline{U}_{i,TS}$	$\overline{\alpha}_{w,TS}$	Re_c	Pr_c
(W)	*(°C)*	*(W/m²°C)*	*(W/m²°C)*	*(-)*	*(-)*
4430.745	7.155	8716.96	85028.9	20778	4.6834
4427.896	7.155	8711.35	85028.9	20765	4.6834
4481.673	7.069	8924.96	85028.9	20815	4.6834
4514.091	7.220	8800.77	85028.9	20725	4.6932
4385.251	7.425	8314.09	85048.9	17626	4.7329
4388.544	7.425	8320.34	85048.9	17639	4.7329
4410.766	7.425	8362.47	85048.9	17728	4.7329
4407.263	7.425	8355.83	85051.1	17749	4.7229
4230.618	7.754	7680.58	85082.2	14605	4.7529
4233.482	7.883	7560.17	85082.2	14615	4.7529
4264.159	7.784	7711.71	85082.2	14615	4.7529
4257.429	7.784	7699.54	85084.4	14592	4.7529

Table A6.8. Results of test run number 3.

$\dot{Q}_{c,TS}$	$\Delta T_{\ln,TS}$	$\overline{U}_{i,TS}$	$\overline{\alpha}_{w,TS}$	Re_c	Pr_c
(W)	*(°C)*	*(W/m² °C)*	*(W/m² °C)*	*(-)*	*(-)*
4513.149	6.228	10201.18	84944.4	34603	4.6834
4516.634	6.336	10033.97	84944.4	34629	4.6834
4528.396	6.228	10235.64	84944.4	34719	4.6834
4530.138	6.336	10063.97	84946.7	34733	4.6834
4438.958	6.629	9426.69	84955.6	31469	4.6932
4494.694	6.446	9815.58	84955.6	31403	4.6932
4496.602	6.446	9819.75	84955.6	31416	4.6932
4491.354	6.556	9644.08	84955.6	31379	4.6932
4490.081	6.807	9285.16	84971.1	28537	4.6834
4495.862	6.807	9297.12	84971.1	28574	4.6834
4502.168	6.696	9464.51	84971.1	28614	4.6834
4550.758	6.732	9516.37	84971.1	28547	4.6834
4501.506	6.933	9139.83	84986.7	25184	4.7031
4453.866	7.012	8941.70	84986.7	25210	4.7031
4501.506	6.933	9139.83	84986.7	25184	4.7031
4456.217	7.124	8804.96	84986.7	25224	4.7031

Table A6.8. Results of test run number 3 (continued).

$\dot{Q}_{c,TS}$	$\Delta T_{ln,TS}$	$\overline{U}_{i,TS}$	$\overline{\alpha}_{w,TS}$	Re_c	Pr_c
(W)	*(°C)*	*(W/m²°C)*	*(W/m²°C)*	*(-)*	*(-)*
4474.018	7.325	8598.36	85004.4	21103	4.7529
4479.607	7.325	8609.10	85004.4	21130	4.7529
4435.254	7.408	8428.12	85006.7	21130	4.7529
4474.018	7.325	8598.36	85006.7	21103	4.7529
4363.198	7.695	7981.57	85028.9	17813	4.7832
4366.408	7.695	7987.45	85028.9	17826	4.7832
4319.220	7.663	7934.23	85028.9	17787	4.7832
4351.161	7.695	7959.55	85028.9	17764	4.7832
4164.807	8.041	7291.25	85064.4	14049	4.8344
4157.112	8.041	7277.78	85064.4	14023	4.8344
4154.227	8.168	7159.60	85064.4	14013	4.8344
4184.113	8.071	7297.55	85064.4	14013	4.8344

Table A6.9. Results of test run number 4.

$\dot{Q}_{c,TS}$	$\Delta T_{ln,TS}$	$\overline{U}_{t,TS}$	$\overline{\alpha}_{w,TS}$	Re_c	Pr_c
(W)	*(°C)*	*(W/m²°C)*	*(W/m²°C)*	*(-)*	*(-)*
4111.614	6.221	9304.06	84824.4	31552	5.2065
4111.614	6.221	9304.06	84826.7	31552	5.2065
4189.984	6.258	9424.42	84826.7	31533	5.2181
4182.346	6.258	9407.24	84826.7	31476	5.2181
4236.776	6.482	9201.20	84828.9	28715	5.2532
4235.001	6.482	9197.35	84828.9	28703	5.2532
4236.776	6.482	9201.20	84831.1	28715	5.2532
4302.975	6.301	9613.23	84831.1	28715	5.2532
4299.297	6.628	9130.97	84848.9	26321	5.2415
4289.453	6.628	9110.06	84846.7	26261	5.2415
4291.422	6.628	9114.25	84846.7	26273	5.2415
4285.515	6.628	9101.70	84846.7	26237	5.2415
4403.770	6.984	8875.90	84840.0	23041	5.3851
4351.622	7.060	8676.22	84840.0	23053	5.3851
4353.842	6.949	8819.75	84837.8	23065	5.3851
4288.459	6.802	8874.89	84837.8	23006	5.3851

Table A6.9. Results of test run number 4 (continued).

$\dot{Q}_{c,TS}$	$\Delta T_{ln,TS}$	$\overline{U}_{t,TS}$	$\overline{\alpha}_{w,TS}$	Re_c	Pr_c
(W)	*(°C)*	*(W/m²°C)*	*(W/m²°C)*	*(-)*	*(-)*
4283.144	7.057	8543.58	84853.3	19311	5.4467
4280.563	7.172	8401.43	84853.3	19299	5.4467
4234.536	7.253	8218.91	84853.3	19299	5.4467
4321.589	7.206	8442.09	84853.3	19236	5.4592
4240.049	7.404	8061.16	84871.1	16438	5.5095
4245.990	7.523	7945.45	84871.1	16461	5.5095
4254.158	7.523	7960.74	84871.1	16493	5.5095
4273.680	7.437	8089.51	84871.1	16415	5.5095
3999.540	7.829	7191.14	84906.7	12906	5.5349
4012.879	7.735	7302.78	84908.9	12848	5.5349
4034.367	7.860	7225.13	84908.9	12917	5.5349
4036.769	7.766	7317.15	84908.9	12825	5.5349

Table A6.10. Results of test run number 5.

$\dot{Q}_{c,TS}$	$\Delta T_{ln,TS}$	$\overline{U}_{t,TS}$	$\overline{\alpha}_{w,TS}$	Re_c	Pr_c
(W)	*(°C)*	*(W/m² °C)*	*(W/m² °C)*	*(-)*	*(-)*
5042.207	7.353	9653.07	84917.8	33437	4.8865
5043.661	7.353	9655.85	84917.8	33447	4.8865
5114.239	7.390	9741.63	84920.0	33437	4.8865
5119.644	7.174	10046.04	84920.0	33473	4.8865
5105.535	7.539	9532.72	84931.1	30263	4.9075
5107.154	7.539	9535.75	84928.9	30272	4.9075
5109.314	7.539	9539.78	84928.9	30285	4.9075
5111.474	7.648	9407.66	84928.9	30298	4.9075
5195.083	7.935	9216.01	84944.4	26770	4.9501
5143.164	7.899	9165.03	84944.4	26858	4.9394
5138.290	7.899	9156.34	84944.4	26832	4.9394
5134.025	7.899	9148.74	84944.4	26810	4.9394
5132.862	8.322	8682.35	84962.2	23445	4.9716
5152.250	8.322	8715.15	84964.4	23533	4.9716
5176.498	8.244	8839.24	84964.4	23410	4.9716
5192.583	8.244	8866.70	84964.4	23482	4.9716

Table A6.10. Results of test run number 5 (continued).

$\dot{Q}_{c,TS}$	$\Delta T_{ln,TS}$	$\overline{U}_{i,TS}$	$\overline{\alpha}_{w,TS}$	Re_c	Pr_c
(W)	*(°C)*	*(W/m²°C)*	*(W/m²°C)*	*(-)*	*(-)*
5165.398	8.606	8449.03	84986.7	20391	5.0041
5180.530	8.606	8473.78	84986.7	20451	5.0041
5174.158	8.722	8351.20	84988.9	20425	5.0041
5138.389	8.688	8325.68	84988.9	20504	4.9932
5170.974	9.450	7702.59	85022.2	16960	5.0591
5204.188	9.331	7850.96	85022.2	17069	5.0591
5188.751	9.331	7827.67	85022.2	17054	5.0480
5174.517	9.331	7806.20	85022.2	17007	5.0480
5197.977	9.970	7339.28	85066.7	13651	5.1263
5193.293	9.970	7332.66	85071.1	13639	5.1263
5193.293	10.096	7241.15	85068.9	13639	5.1263
5211.321	10.126	7244.24	85071.1	13577	5.1376

A6.3 Investigation of Assumptions made in deriving Expression for Mean Coolant Heat Transfer Coefficient

Table A6.11. Analysis of conditions for test run number 1.

$\overline{\alpha}_w$ (W/m² °C)	$\lambda_{c,in}$ (W/m °C)	$\lambda_{c,out}$ (W/m °C)	$\overline{\alpha}_{f,1}$ From Graph (W/m² °C)	$\overline{\alpha}_{f,1}$ Nusselt (W/m² °C)
84780.0	0.62280	0.62873	14745.4	7677.5
84780.0	0.62280	0.62873	14745.4	7677.5
84780.0	0.62289	0.62873	14745.4	7634.3
84780.0	0.62289	0.62873	14745.4	7634.3
84806.7	0.62235	0.62984	14744.7	7770.5
84806.7	0.62235	0.62984	14744.7	7725.4
84806.7	0.62235	0.62984	14744.7	7770.5
84806.7	0.62235	0.62984	14744.7	7681.8
84851.1	0.62199	0.63176	14743.6	7804.3
84853.3	0.62199	0.63176	14743.5	7901.0
84853.3	0.62199	0.63176	14743.5	7853.8
84855.6	0.62199	0.63184	14743.5	7905.0
84922.2	0.62127	0.63471	14741.8	8072.2
84922.2	0.62127	0.63471	14741.8	8072.2
84922.2	0.62127	0.63479	14741.8	8022.5
84922.2	0.62127	0.63479	14741.8	7974.4

Table A6.12. Analysis of conditions for test run number 2.

$\overline{\alpha}_w$	$\lambda_{c,in}$	$\lambda_{c,out}$	$\overline{\alpha}_{f,i}$ From Graph	$\overline{\alpha}_{f,i}$ Nusselt
(W/m² ℃)	*(W/m ℃)*	*(W/m ℃)*	*(W/m² ℃)*	*(W/m² ℃)*
84966.7	0.63084	0.63591	18454.4	8494.1
84968.9	0.63084	0.63591	18454.3	8434.9
84971.1	0.63084	0.63591	18454.2	8568.1
84968.9	0.63084	0.63583	18454.3	8434.9
84982.2	0.63076	0.63639	18453.8	8522.2
84982.2	0.63084	0.63647	18453.8	8458.8
84984.4	0.63084	0.63647	18453.7	8462.8
84982.2	0.63084	0.63647	18453.8	8397.9
84997.8	0.63059	0.63694	18453.2	8550.2
84997.8	0.63059	0.63694	18453.2	8486.6
84995.6	0.63059	0.63694	18453.3	8421.5
84995.6	0.63059	0.63694	18453.3	8482.6
85011.1	0.63026	0.63749	18452.7	8510.2
85011.1	0.63026	0.63757	18452.7	8510.2
85011.1	0.63026	0.63757	18452.7	8448.9
85013.3	0.63026	0.63757	18452.6	8514.2
85028.9	0.62992	0.63827	18452.0	8541.6
85028.9	0.62992	0.63827	18452.0	8541.6
85028.9	0.62992	0.63835	18452.0	8541.6
85028.9	0.62984	0.63835	18452.0	8480.0

Table A6.12. Analysis of conditions for test run number 2 (continued).

$\overline{\alpha}_w$	$\lambda_{c,in}$	$\lambda_{c,out}$	$\overline{\alpha}_{f,i}$ From Graph	$\overline{\alpha}_{f,i}$ Nusselt
(W/m² ℃)	*(W/m ℃)*	*(W/m ℃)*	*(W/m² ℃)*	*(W/m² ℃)*
85048.9	0.62950	0.63912	18451.2	8576.6
85048.9	0.62950	0.63912	18451.2	8576.6
85048.9	0.62950	0.63912	18451.2	8576.6
85051.1	0.62958	0.63920	18451.1	8580.5
85082.2	0.62933	0.64043	18449.9	8634.5
85082.2	0.62933	0.64043	18449.9	8572.1
85082.2	0.62933	0.64050	18449.9	8572.1
85084.4	0.62933	0.64050	18449.8	8638.3

Table A6.13. Analysis of conditions for test run number 3.

$\overline{\alpha}_w$	$\lambda_{c,in}$	$\lambda_{c,out}$	$\overline{\alpha}_{f,i}$ From Graph	$\overline{\alpha}_{f,i}$ Nusselt
(W/m² °C)	*(W/m °C)*	*(W/m °C)*	*(W/m² °C)*	*(W/m² °C)*
84944.4	0.62992	0.63511	18802.5	8272.5
84944.4	0.62992	0.63511	18802.5	8216.7
84944.4	0.62992	0.63511	18802.5	8272.5
84946.7	0.62992	0.63511	18802.4	8276.5
84955.6	0.62984	0.63543	18802.1	8236.3
84955.6	0.62984	0.63551	18802.1	8292.3
84955.6	0.62984	0.63551	18802.1	8292.3
84955.6	0.62984	0.63551	18802.1	8236.3
84971.1	0.62992	0.63615	18801.4	8209.5
84971.1	0.62992	0.63615	18801.4	8209.5
84971.1	0.62992	0.63615	18801.4	8263.6
84971.1	0.62992	0.63623	18801.4	8209.5
84986.7	0.62975	0.63678	18800.8	8290.8
84986.7	0.62975	0.63670	18800.8	8290.8
84986.7	0.62975	0.63678	18800.8	8290.8
84986.7	0.62975	0.63670	18800.8	8236.5
85004.4	0.62933	0.63757	18800.1	8267.1
85004.4	0.62933	0.63757	18800.1	8267.1
85006.7	0.62933	0.63749	18800.0	8325.5
85006.7	0.62933	0.63757	18800.0	8325.5

Table A6.13. Analysis of conditions for test run number 3 (continued).

$\overline{\alpha}_w$	$\lambda_{c,in}$	$\lambda_{c,out}$	$\overline{\alpha}_{f,i}$ From Graph	$\overline{\alpha}_{f,i}$ Nusselt
(W/m² °C)	*(W/m °C)*	*(W/m °C)*	*(W/m² °C)*	*(W/m² °C)*
85028.9	0.62907	0.63851	18799.1	8308.9
85028.9	0.62907	0.63851	18799.1	8308.9
85028.9	0.62907	0.63843	18799.1	8363.8
85028.9	0.62907	0.63851	18799.1	8308.9
85064.4	0.62865	0.63989	18797.6	8424.4
85064.4	0.62865	0.63989	18797.6	8424.4
85064.4	0.62865	0.63989	18797.6	8369.0
85064.4	0.62865	0.63997	18797.6	8369.0

Table A6.14. Analysis of conditions for test run number 4.

$\overline{\alpha}_w$	$\lambda_{c,in}$	$\lambda_{c,out}$	$\overline{\alpha}_{f,i}$ From Graph	$\overline{\alpha}_{f,i}$ Nusselt
(W/m² °C)	*(W/m °C)*	*(W/m °C)*	*(W/m² °C)*	*(W/m² °C)*
84824.4	0.62571	0.63059	15587.9	8000.0
84826.7	0.62571	0.63059	15587.9	8058.2
84826.7	0.62563	0.63059	15587.9	8058.2
84826.7	0.62563	0.63059	15587.9	8058.2
84828.9	0.62536	0.63084	15587.8	7956.0
84828.9	0.62536	0.63084	15587.8	7956.0
84831.1	0.62536	0.63084	15587.7	8012.3
84831.1	0.62536	0.63093	15587.7	8066.4
84848.9	0.62545	0.63151	15587.2	8099.3
84846.7	0.62545	0.63151	15587.3	8040.8
84846.7	0.62545	0.63151	15587.3	8040.8
84846.7	0.62545	0.63151	15587.3	8040.8
84840.0	0.62440	0.63135	15587.5	7976.3
84840.0	0.62440	0.63126	15587.5	7976.3
84837.8	0.62440	0.63126	15587.6	7972.2
84837.8	0.62440	0.63118	15587.6	8078.8
84853.3	0.62395	0.63193	15587.1	8107.5
84853.3	0.62395	0.63193	15587.1	8053.0
84853.3	0.62395	0.63184	15587.1	8053.0
84853.3	0.62387	0.63193	15587.1	8053.0

Table A6.14. Analysis of conditions for test run number 4 (continued).

$\overline{\alpha}_w$	$\lambda_{c,in}$	$\lambda_{c,out}$	$\overline{\alpha}_{f,i}$ From Graph	$\overline{\alpha}_{f,i}$ Nusselt
(W/m² °C)	*(W/m °C)*	*(W/m °C)*	*(W/m² °C)*	*(W/m² °C)*
84871.1	0.62351	0.63267	15586.6	8140.1
84871.1	0.62351	0.63267	15586.6	8085.3
84871.1	0.62351	0.63267	15586.6	8085.3
84871.1	0.62351	0.63275	15586.6	8085.3
84906.7	0.62333	0.63422	15585.6	8149.5
84908.9	0.62333	0.63430	15585.6	8208.7
84908.9	0.62333	0.63430	15585.6	8153.4
84908.9	0.62333	0.63438	15585.6	8153.4

Table A6.15. Analysis of conditions for test run number 5.

$\bar{\alpha}_w$	$\lambda_{c,in}$	$\lambda_{c,out}$	$\bar{\alpha}_{f,i}$ From Graph	$\bar{\alpha}_{f,i}$ Nusselt
(W/m² °C)	*(W/m °C)*	*(W/m °C)*	*(W/m² °C)*	*(W/m² °C)*
84917.8	0.62822	0.63406	17349.3	7875.3
84917.8	0.62822	0.63406	17349.3	7875.3
84920.0	0.62822	0.63414	17349.2	7879.1
84920.0	0.62822	0.63414	17349.2	7970.6
84931.1	0.62805	0.63454	17348.8	7943.1
84928.9	0.62805	0.63454	17348.9	7894.3
84928.9	0.62805	0.63454	17348.9	7894.3
84928.9	0.62805	0.63454	17348.9	7850.6
84944.4	0.62771	0.63511	17348.3	7920.6
84944.4	0.62779	0.63511	17348.3	7920.6
84944.4	0.62779	0.63511	17348.3	7920.6
84944.4	0.62779	0.63511	17348.3	7920.6
84962.2	0.62753	0.63583	17347.7	7906.6
84964.4	0.62753	0.63583	17347.6	7954.4
84964.4	0.62753	0.63591	17347.6	7954.4
84964.4	0.62753	0.63591	17347.6	7954.4
84986.7	0.62728	0.63678	17346.9	7991.5
84986.7	0.62728	0.63678	17346.9	7991.5
84988.9	0.62728	0.63678	17346.8	7995.2
84988.9	0.62736	0.63678	17346.8	7995.2

Table A6.15. Analysis of conditions for test run number 5 (continued).

$\overline{\alpha}_w$	$\lambda_{c,in}$	$\lambda_{c,out}$	$\overline{\alpha}_{f,i}$ From Graph	$\overline{\alpha}_{f,i}$ Nusselt
(W/m² °C)	*(W/m °C)*	*(W/m °C)*	*(W/m² °C)*	*(W/m² °C)*
85022.2	0.62684	0.63812	17345.6	7962.3
85022.2	0.62684	0.63812	17345.6	8005.7
85022.2	0.62693	0.63819	17345.6	7962.3
85022.2	0.62693	0.63819	17345.6	7962.3
85066.7	0.62632	0.64012	17344.1	7950.1
85071.1	0.62632	0.64012	17343.9	8041.0
85068.9	0.62632	0.64012	17344.0	7953.6
85071.1	0.62624	0.64012	17343.9	7998.4

A6.4 Comparison of Methods to Calculate the Mean Coolant Heat Transfer Coefficient

Table A6.16. Coolant heat transfer coefficients for test run number 1.

Individual Graph ($W/m^2\,°C$)	Overall Graph ($W/m^2\,°C$)	Dittus-Boelter ($W/m^2\,°C$)	Eagle-Ferguson ($W/m^2\,°C$)
16777.4	15629.4	18721.5	18020.7
16788.4	15639.7	18733.8	18032.5
16790.4	15641.5	18738.7	18029.8
16779.4	15631.3	18726.4	18018.1
13735.9	12796.0	15316.5	14871.2
13701.5	12763.9	15278.1	14833.9
13730.2	12790.7	15310.1	14865.0
13724.4	12785.3	15303.7	14858.8
10760.8	10024.5	11992.2	11798.7
10748.7	10013.2	11978.6	11785.4
10779.0	10041.5	12012.5	11818.7
10754.7	10018.8	11985.4	11798.0
7626.0	7104.2	8488.8	8532.2
7658.9	7134.8	8525.4	8573.2
7645.7	7122.6	8510.7	8558.5

Table A6.17. Coolant heat transfer coefficients for test run number 2.

Individual Graph ($W/m^2\,°C$)	Overall Graph ($W/m^2\,°C$)	Dittus-Boelter ($W/m^2\,°C$)	Eagle-Ferguson ($W/m^2\,°C$)
18863.6	17565.3	21312.3	20654.3
18840.4	17543.7	21286.0	20628.9
18863.6	17565.3	21312.3	20654.3
18857.8	17559.9	21305.7	20638.4
17344.2	16150.5	19593.1	19047.9
17362.0	16167.1	19615.8	19072.0
17407.9	16209.8	19667.6	19122.4
17384.2	16187.8	19640.9	19096.4
15817.4	14728.8	17863.5	17435.2
15799.2	14711.9	17843.1	17415.2
15799.2	14711.9	17843.1	17415.2
15823.4	14734.4	17870.4	17441.8
13954.7	12994.3	15751.5	15445.7
13960.9	13000.1	15758.5	15459.8
13954.7	12994.3	15751.5	15452.9
13998.2	13034.8	15800.6	15501.0
12404.0	11550.4	13993.7	13805.5
12397.7	11544.4	13986.5	13798.4
12421.6	11566.7	14013.5	13831.4
12389.1	11536.4	13974.9	13798.4

Table A6.17. Coolant heat transfer coefficients for test run number 2 (continued).

Individual Graph ($W/m^2\,°C$)	Overall Graph ($W/m^2\,°C$)	Dittus-Boelter ($W/m^2\,°C$)	Eagle-Ferguson ($W/m^2\,°C$)
10919.8	10168.3	12311.0	12229.6
10926.4	10174.4	12318.4	12237.0
10970.6	10215.6	12368.3	12286.5
10971.7	10216.6	12371.2	12290.5
9411.0	8763.4	10607.2	10627.3
9416.1	8768.1	10612.9	10633.0
9416.1	8768.1	10612.9	10637.9
9404.3	8757.0	10599.5	10624.4

Table A6.18. Coolant heat transfer coefficients for test run number 3.

Individual Graph ($W/m^2\,°C$)	Overall Graph ($W/m^2\,°C$)	Dittus-Boelter ($W/m^2\,°C$)	Eagle-Ferguson ($W/m^2\,°C$)
16888.2	17369.8	21044.2	20379.1
16898.7	17380.6	21057.2	20391.6
16933.9	17416.8	21101.1	20434.1
16939.1	17422.1	21107.6	20440.4
15666.5	16113.3	19519.2	18944.5
15640.0	16086.0	19486.2	18921.3
15645.3	16091.4	19492.8	18927.7
15630.7	16076.4	19474.6	18910.0
14475.2	14888.0	18037.4	17573.7
14490.1	14903.4	18056.0	17591.8
14506.4	14920.1	18076.2	17611.6
14479.3	14892.2	18042.5	17586.9
13119.7	13493.9	16343.9	15994.8
13130.8	13505.3	16357.7	16000.9
13119.7	13493.9	16343.9	15994.8
13136.3	13511.0	16364.6	16007.6
11437.7	11763.9	14239.0	14025.4
11449.2	11775.7	14253.3	14039.5
11449.2	11775.7	14253.3	14032.9
11437.7	11763.9	14239.0	14025.4

Table A6.18. Coolant heat transfer coefficients for test run number 3 (continued).

Individual Graph ($W/m^2\,°C$)	Overall Graph ($W/m^2\,°C$)	Dittus-Boelter ($W/m^2\,°C$)	Eagle-Ferguson ($W/m^2\,°C$)
10012.8	10298.3	12460.0	12355.2
10018.6	10304.4	12467.3	12362.5
10001.0	10286.2	12445.3	12335.0
9990.6	10275.6	12432.5	12328.0
8316.2	8553.4	10341.8	10359.8
8303.9	8540.7	10326.5	10344.5
8299.3	8536.0	10320.8	10338.8
8299.3	8536.0	10320.8	10343.5

Table A6.19. Coolant heat transfer coefficients for test run number 4.

Individual Graph ($W/m^2\,°C$)	Overall Graph ($W/m^2\,°C$)	Dittus-Boelter ($W/m^2\,°C$)	Eagle-Ferguson ($W/m^2\,°C$)
19845.6	16831.7	20256.1	19455.7
19853.8	16838.7	20261.6	19468.6
19824.8	16814.1	20232.0	19440.2
18470.6	15665.6	18842.1	18152.6
18464.5	15660.3	18835.8	18146.5
18470.6	15665.6	18842.1	18152.6
18470.6	15665.6	18842.1	18161.6
17212.7	14598.6	17561.3	16978.8
17181.2	14571.9	17529.1	16947.7
17187.5	14577.3	17535.6	16953.9
17168.5	14561.2	17516.3	16935.2
15642.3	13266.7	15932.2	15462.0
15648.7	13272.1	15938.7	15460.7
15655.0	13277.6	15945.2	15467.0
15623.1	13250.5	15912.7	15427.8
13643.3	11571.3	13886.3	13550.7
13636.7	11565.8	13879.6	13544.1
13636.7	11565.8	13879.6	13537.4
13613.2	11545.8	13853.7	13524.4

Table A6.19. Coolant heat transfer coefficients for test run number 4 (continued).

Individual Graph ($W/m^2\,°C$)	Overall Graph ($W/m^2\,°C$)	Dittus-Boelter ($W/m^2\,°C$)	Eagle-Ferguson ($W/m^2\,°C$)
12048.8	10219.0	12254.7	12036.4
12062.3	10230.4	12268.4	12049.9
12080.8	10246.2	12287.3	12068.4
12035.3	10207.5	12240.9	12028.8
9947.0	8436.4	10114.1	10035.4
9911.6	8406.4	10078.1	10004.6
9954.1	8442.4	10121.3	10047.5
9897.5	8394.4	10063.7	9995.2

Table A6.20. Coolant heat transfer coefficients for test run number 5.

Individual Graph ($W/m^2\,°C$)	Overall Graph ($W/m^2\,°C$)	Dittus-Boelter ($W/m^2\,°C$)	Eagle-Ferguson ($W/m^2\,°C$)
17733.0	17189.7	20769.8	20136.5
17737.1	17193.6	20774.5	20141.2
17733.0	17189.7	20769.8	20146.1
17748.0	17204.2	20787.3	20163.2
16401.0	15898.4	19204.3	18686.0
16405.1	15902.5	19209.2	18690.8
16410.7	15907.8	19215.7	18697.1
16416.2	15913.2	19222.2	18703.4
14919.8	14462.7	17460.5	17071.6
14946.1	14488.2	17493.6	17097.5
14934.8	14477.2	17480.4	17084.5
14924.9	14467.6	17468.8	17073.2
13441.0	13029.2	15725.5	15452.7
13481.6	13068.5	15773.0	15499.4
13425.1	13013.7	15706.9	15441.7
13458.4	13046.0	15745.9	15480.1
12052.6	11683.3	14095.3	13945.6
12080.8	11710.6	14128.3	13978.3
12068.9	11699.1	14114.4	13964.5
12095.5	11724.8	14147.4	13991.7

Table A6.20. Coolant heat transfer coefficients for test run number 5 (continued).

Individual Graph ($W/m^2\,°C$)	Overall Graph ($W/m^2\,°C$)	Dittus-Boelter ($W/m^2\,°C$)	Eagle-Ferguson ($W/m^2\,°C$)
10446.7	10126.6	12208.8	12199.9
10500.3	10178.6	12271.5	12262.6
10483.4	10162.2	12253.4	12245.4
10460.4	10139.9	12226.5	12218.5
8827.8	8557.3	10308.2	10451.6
8821.4	8551.1	10300.8	10444.0
8821.4	8551.1	10300.8	10444.0
8797.4	8527.9	10271.4	10418.5

Appendix A7 n-Pentane Experimental Data and Data Analysis Calculations

A7.1. Test Data

Table A7.1. Data for test run number 1.

Boiler Measurements				Test Condenser Measurements										Dump Condenser Measurements			
$\dot{Q}$	T_v	P_v	$\dot{V}_c$	$T_{c,in}$ TS2	$T_{c,in}$ TS3	$T_{c,in}$ TS4	$T_{c,out}$	T_v TS2	T_v TS3	T_v TS4	$\overline{T}_w$ TS2	$\overline{T}_w$ TS3	$\overline{T}_w$ TS4	$\dot{V}_c$	$T_{c,in}$	$T_{c,out}$	T_f
(W)	*(°C)*	*(bara)*	*(l/min)*	*(°C)*	*(°C)*	*(°C)*	*(°C)*	*(°C)*	*(°C)*	*(°C)*	*(°C)*	*(°C)*	*(°C)*	*(l/min)*	*(°C)*	*(°C)*	*(°C)*
5820.5	47.9	1.500	6.263	25.8	29.4	32.2	34.4	48.0	47.9	47.9	28.8	31.4	34.5	2.998	22.6	29.6	24.9
5815.4	47.9	1.501	6.244	25.8	29.5	32.2	34.5	48.0	47.9	47.9	28.8	31.5	34.5	2.999	22.6	29.6	25.0
5817.5	47.9	1.502	6.248	25.8	29.5	32.2	34.5	48.0	47.9	47.9	28.8	31.4	34.5	2.998	22.6	29.7	25.0
5815.7	47.9	1.503	6.248	25.8	29.5	32.2	34.5	48.0	48.0	47.9	28.9	31.5	34.6	2.993	22.6	29.7	25.1
3119.2	34.3	0.960	6.232	21.3	23.8	25.3	26.4	34.3	34.2	34.2	23.4	24.7	26.5	3.023	18.2	21.2	17.4
3113.6	34.3	0.960	6.217	21.3	23.8	25.3	26.5	34.3	34.2	34.2	23.4	24.7	26.5	3.024	18.2	21.2	17.4
3110.2	34.3	0.959	6.224	21.2	23.7	25.3	26.4	34.2	34.2	34.2	23.4	24.7	26.5	3.019	18.2	21.1	17.4
3112.4	34.3	0.959	6.224	21.3	23.7	25.3	26.4	34.2	34.2	34.1	23.4	24.7	26.5	3.020	18.2	21.2	17.4

(TS2=top test section, TS3 =middle test section, TS4=bottom test section)

Table A7.2. Data for test run number 2.

Boiler Measurements				Test Condenser Measurements										Dump Condenser Measurements			
$\dot{Q}$	T_v	P_v	$\dot{V}_c$	$T_{c,in}$ TS2	$T_{c,in}$ TS3	$T_{c,in}$ TS4	$T_{c,out}$	T_v TS2	T_v TS3	T_v TS4	$\overline{T}_w$ TS2	$\overline{T}_w$ TS3	$\overline{T}_w$ TS4	$\dot{V}_c$	$T_{c,in}$	$T_{c,out}$	T_f
(W)	*(°C)*	*(bara)*	*(l/min)*	*(°C)*	*(°C)*	*(°C)*	*(°C)*	*(°C)*	*(°C)*	*(°C)*	*(°C)*	*(°C)*	*(°C)*	*(l/min)*	*(°C)*	*(°C)*	*(°C)*
5681.8	48.2	1.511	6.248	27.4	31.1	33.7	35.6	48.3	48.2	48.1	30.5	32.8	35.6	2.991	24.2	31.7	41.2
5706.2	48.2	1.513	6.236	27.4	31.1	33.7	35.6	48.3	48.2	48.2	30.5	32.8	35.6	2.981	24.3	31.8	41.3
5700.3	48.3	1.515	6.260	27.5	31.2	33.7	35.6	48.3	48.3	48.2	30.5	32.8	35.6	2.989	24.3	31.8	41.4
5708.0	48.3	1.517	6.248	27.5	31.2	33.8	35.6	48.4	48.3	48.3	30.6	32.9	35.7	2.985	24.3	31.8	41.5
3109.3	35.1	0.987	6.205	23.9	26.3	27.6	28.4	35.1	35.1	35.0	25.9	27.0	28.5	2.999	20.6	25.1	27.7
3109.0	35.1	0.986	6.205	23.9	26.3	27.6	28.4	35.1	35.1	35.0	25.9	27.0	28.5	3.003	20.6	25.0	27.7
3104.0	35.1	0.986	6.217	23.9	26.3	27.6	28.4	35.1	35.1	35.0	25.9	27.0	28.5	3.002	20.7	25.0	27.7
3110.0	35.1	0.986	6.221	23.9	26.3	27.6	28.4	35.1	35.1	35.0	25.9	26.9	28.5	3.012	20.6	25.0	27.7

(TS2=top test section, TS3 =middle test section, TS4=bottom test section)

Table A7.3. Data for test run number 3.

Boiler Measurements				Test Condenser Measurements										Dump Condenser Measurements			
$\dot{Q}$	T_v	P_v	$\dot{V}_c$	$T_{c,in}$ TS2	$T_{c,in}$ TS3	$T_{c,in}$ TS4	$T_{c,out}$	T_v TS2	T_v TS3	T_v TS4	$\overline{T}_w$ TS2	$\overline{T}_w$ TS3	$\overline{T}_w$ TS4	$\dot{V}_c$	$T_{c,in}$	$T_{c,out}$	T_f
(W)	*(°C)*	*(bara)*	*(l/min)*	*(°C)*	*(°C)*	*(°C)*	*(°C)*	*(°C)*	*(°C)*	*(°C)*	*(°C)*	*(°C)*	*(°C)*	*(l/min)*	*(°C)*	*(°C)*	*(°C)*
3063.9	32.0	0.903	6.123	21.5	23.3	24.6	26.0	32.0	32.0	32.0	23.1	24.6	26.1	3.006	18.4	22.4	20.5
3064.6	32.0	0.903	6.127	21.5	23.2	24.6	26.0	32.1	32.0	32.0	23.0	24.5	26.1	3.010	18.4	22.4	20.5
3071.6	32.0	0.903	6.131	21.5	23.2	24.6	26.0	32.0	32.0	32.0	23.0	24.5	26.1	3.015	18.3	22.4	20.5
3074.7	32.0	0.902	6.143	21.5	23.2	24.6	26.0	32.0	32.0	32.0	23.0	24.5	26.1	3.011	18.3	22.3	20.5
5823.6	47.5	1.499	6.150	26.7	30.0	32.7	35.2	47.6	47.5	47.5	29.5	32.3	35.3	2.984	23.2	30.9	41.1
5810.5	47.4	1.499	6.147	26.8	30.0	32.6	35.2	47.6	47.5	47.5	29.5	32.3	35.3	2.991	23.3	30.9	41.1
5826.4	47.5	1.501	6.147	26.8	30.0	32.7	35.2	47.6	47.5	47.5	29.5	32.3	35.3	2.991	23.3	31.0	41.1
5694.4	47.5	1.503	6.154	26.8	30.0	32.7	35.3	47.6	47.5	47.5	29.6	32.3	35.3	2.989	23.3	31.0	41.2

(TS2=top test section, TS3 =middle test section, TS4=bottom test section)

Table A7.4. Data for test run number 4.

Boiler Measurements				Test Condenser Measurements										Dump Condenser Measurements			
$\dot{Q}$	T_v	P_v	$\dot{V}_c$	$T_{c,in}$ TS2	$T_{c,in}$ TS3	$T_{c,in}$ TS4	$T_{c,out}$	T_v TS2	T_v TS3	T_v TS4	$\overline{T}_w$ TS2	$\overline{T}_w$ TS3	$\overline{T}_w$ TS4	$\dot{V}_c$	$T_{c,in}$	$T_{c,out}$	T_f
(W)	*(°C)*	*(bara)*	*(l/min)*	*(°C)*	*(°C)*	*(°C)*	*(°C)*	*(°C)*	*(°C)*	*(°C)*	*(°C)*	*(°C)*	*(°C)*	*(l/min)*	*(°C)*	*(°C)*	*(°C)*
5819.2	48.4	1.527	6.096	27.0	30.7	33.4	35.6	48.5	48.4	48.4	30.2	32.7	35.7	2.986	23.8	31.5	38.7
5822.8	48.4	1.527	6.111	27.0	30.7	33.4	35.6	48.5	48.4	48.4	30.2	32.7	35.7	2.985	23.9	31.5	38.7
5825.7	48.4	1.529	6.092	27.0	30.7	33.4	35.6	48.5	48.4	48.4	30.2	32.7	35.7	2.988	23.8	31.5	38.7
5827.7	48.4	1.529	6.100	27.0	30.7	33.4	35.6	48.5	48.4	48.4	30.2	32.7	35.7	2.989	23.9	31.5	38.8
3113.2	34.7	0.975	6.069	22.4	24.7	26.2	27.4	34.5	34.4	34.4	24.5	25.8	27.5	3.006	19.3	22.9	18.7
3114.6	34.7	0.975	6.057	22.4	24.7	26.2	27.4	34.5	34.4	34.4	24.5	25.8	27.5	2.997	19.2	22.9	18.7
3111.8	34.6	0.975	6.061	22.4	24.6	26.2	27.4	34.5	34.4	34.4	24.4	25.8	27.5	3.002	19.2	22.9	18.7
3118.6	34.6	0.975	6.049	22.4	24.6	26.1	27.4	34.5	34.4	34.4	24.4	25.8	27.5	3.004	19.2	22.9	18.7

(TS2=top test section, TS3 =middle test section, TS4=bottom test section)

A7.2 Heat Transfer Calculations

Table A7.5. Heat transfer results for test run number 1.

$\dot{Q}_{c,TS}$ TS2 (W)	$\dot{Q}_{c,TS}$ TS3 (W)	$\dot{Q}_{c,TS}$ TS4 (W)	$\dot{Q}_{c,TC}$ (W)	$\dot{Q}_{c,DC}$ (W)	$\dot{Q}_{c,T}$ (W)	$\dot{Q}_{c,T}/\dot{Q}$ (-)	$\Delta T_{ln,TS}$ TS2 (°C)	$\Delta T_{ln,TS}$ TS3 (°C)	$\Delta T_{ln,TS}$ TS4 (°C)
1566.933	1216.517	954.514	3737.964	1460.870	5198.834	0.8932	20.347	17.062	14.572
1605.573	1169.453	994.874	3769.900	1461.357	5231.257	0.8996	20.294	17.014	14.520
1606.601	1170.202	995.511	3772.315	1481.740	5254.054	0.9031	20.294	17.014	14.520
1606.601	1170.202	995.511	3772.315	1479.268	5251.583	0.9030	20.294	17.115	14.520
1085.288	650.324	476.537	2212.149	632.781	2844.930	0.9121	11.706	9.631	8.338
1082.676	648.759	518.607	2250.042	632.990	2883.032	0.9259	11.706	9.631	8.286
1083.952	692.825	475.925	2252.702	610.879	2863.581	0.9207	11.706	9.678	8.338
1040.539	692.825	475.925	2209.289	632.153	2841.442	0.9129	11.659	9.678	8.238

(TS2=top test section, TS3 =middle test section, TS4=bottom test section)

Table A7.6. Heat transfer results for test run number 2.

$\dot{Q}_{c,TS}$ TS2 (W)	$\dot{Q}_{c,TS}$ TS3 (W)	$\dot{Q}_{c,TS}$ TS4 (W)	$\dot{Q}_{c,TC}$ (W)	$\dot{Q}_{c,DC}$ (W)	$\dot{Q}_{c,T}$ (W)	$\dot{Q}_{c,T}/\dot{Q}$ (-)	$\Delta T_{ln,TS}$ TS2 (°C)	$\Delta T_{ln,TS}$ TS3 (°C)	$\Delta T_{ln,TS}$ TS4 (°C)
1605.298	1125.969	821.779	3553.045	1560.269	5113.314	0.8999	18.990	15.764	13.428
1602.215	1123.806	820.200	3546.221	1554.972	5101.193	0.8940	18.990	15.764	13.528
1608.300	1084.688	823.357	3516.345	1559.145	5075.490	0.8904	18.890	15.817	13.528
1605.217	1125.913	778.489	3509.620	1557.058	5066.678	0.8876	18.990	15.764	13.580
1035.957	560.454	344.668	1941.079	940.431	2881.510	0.9267	9.952	8.133	6.992
1035.957	560.454	344.668	1941.079	920.759	2861.838	0.9205	9.952	8.133	6.992
1037.961	561.538	345.335	1944.833	899.485	2844.319	0.9163	9.952	8.133	6.992
1038.629	561.899	345.557	1946.085	923.518	2869.603	0.9227	9.952	8.133	6.992

(TS2=top test section, TS3 =middle test section, TS4=bottom test section)

Table A7.7. Heat transfer results for test run number 3.

$\dot{Q}_{c,TS}$ TS2 (W)	$\dot{Q}_{c,TS}$ TS3 (W)	$\dot{Q}_{c,TS}$ TS4 (W)	$\dot{Q}_{c,TC}$ (W)	$\dot{Q}_{c,DC}$ (W)	$\dot{Q}_{c,T}$ (W)	$\dot{Q}_{c,T}/\dot{Q}$ (-)	$\Delta T_{ln,TS}$ TS2 (°C)	$\Delta T_{ln,TS}$ TS3 (°C)	$\Delta T_{ln,TS}$ TS4 (°C)
767.660	553.900	596.107	1917.667	838.873	2756.540	0.8997	9.572	8.032	6.676
725.485	596.928	596.497	1918.911	839.989	2758.900	0.9002	9.725	8.080	6.676
725.959	597.318	596.886	1920.164	862.465	2782.629	0.9059	9.625	8.080	6.676
727.380	598.487	598.055	1923.922	840.313	2764.235	0.8990	9.625	8.080	6.676
1409.794	1151.561	1064.845	3626.200	1598.954	5225.154	0.8972	19.203	16.112	13.511
1366.337	1108.370	1106.953	3581.660	1581.808	5163.468	0.8886	19.155	16.165	13.558
1366.337	1150.999	1064.326	3581.662	1602.621	5184.284	0.8898	19.155	16.112	13.511
1367.893	1152.310	1108.159	3628.362	1601.550	5229.912	0.9184	19.155	16.112	13.458

(TS2=top test section, TS3 =middle test section, TS4=bottom test section)

Table A7.8. Heat transfer results for test run number 4.

$\dot{Q}_{c,TS}$ TS2 (W)	$\dot{Q}_{c,TS}$ TS3 (W)	$\dot{Q}_{c,TS}$ TS4 (W)	$\dot{Q}_{c,TC}$ (W)	$\dot{Q}_{c,DC}$ (W)	$\dot{Q}_{c,T}$ (W)	$\dot{Q}_{c,T}/\dot{Q}$ (-)	$\Delta T_{ln,TS}$ TS2 (°C)	$\Delta T_{ln,TS}$ TS3 (°C)	$\Delta T_{ln,TS}$ TS4 (°C)
1566.561	1141.054	928.520	3636.135	1599.528	5235.663	0.8997	19.592	16.313	13.871
1570.416	1143.862	930.804	3645.082	1578.145	5223.227	0.8970	19.592	16.313	13.871
1565.533	1140.306	927.910	3633.749	1600.599	5234.349	0.8985	19.592	16.313	13.871
1567.589	1141.803	929.129	3638.521	1580.260	5218.781	0.8955	19.592	16.313	13.871
971.789	633.021	506.029	2110.840	754.622	2865.461	0.9204	10.910	8.929	7.584
969.868	631.770	505.028	2106.666	773.303	2879.969	0.9247	10.910	8.929	7.584
928.312	674.367	505.362	2108.042	774.593	2882.634	0.9264	10.963	8.976	7.584
926.475	630.968	546.419	2103.861	775.109	2878.970	0.9232	10.963	9.029	7.632

(TS2=top test section, TS3 =middle test section, TS4=bottom test section)

A7.3 Mass Balance Calculations across Test and Dump Condensers

Table A7.9. Material flows for test run number 1.

$\dot{M}_{v,in,TC}$	$\dot{M}_{v,out,TS}$ TS4	$\dot{M}_{v,out,TS}$ TS3	$\dot{M}_{v,out,TC}$	$\dot{M}_{f,out,TS}$ TS2	$\dot{M}_{f,out,TS}$ TS3	$\dot{M}_{f,out,TC}$	$\dot{M}_{f,out,DC}$
(kg/s)	*(kg/s)*	*(kg/s)*	*(kg/s)*	*(kg/s)*	*(kg/s)*	*(kg/s)*	*(kg/s)*
0.01447	0.01171	0.00819	0.00366	0.00453	0.00805	0.01081	0.00366
0.01457	0.01169	0.00830	0.00366	0.00464	0.00803	0.01090	0.00366
0.01462	0.01174	0.00836	0.00371	0.00465	0.00803	0.01091	0.00371
0.01462	0.01174	0.00835	0.00371	0.00465	0.00803	0.01091	0.00371
0.00160	0.00779	0.00646	0.00464	0.00304	0.00486	0.00620	0.00160
0.00160	0.00790	0.00645	0.00463	0.00303	0.00485	0.00630	0.00160
0.00154	0.00785	0.00652	0.00458	0.00304	0.00498	0.00631	0.00154
0.00160	0.00779	0.00645	0.00451	0.00291	0.00485	0.00619	0.00160

(TS2=top test section, TS3 =middle test section, TS4=bottom test section)

Table A7.10. Material flows for test run number 2.

$\dot{M}_{v,in,TC}$ (kg/s)	$\dot{M}_{v,out,TS}$ TS4 (kg/s)	$\dot{M}_{v,out,TS}$ TS3 (kg/s)	$\dot{M}_{v,out,TC}$ (kg/s)	$\dot{M}_{f,out,TS}$ TS2 (kg/s)	$\dot{M}_{f,out,TS}$ TS3 (kg/s)	$\dot{M}_{f,out,TC}$ (kg/s)	$\dot{M}_{f,out,DC}$ (kg/s)
0.01459	0.01221	0.00895	0.00430	0.00465	0.00791	0.01028	0.00430
0.01456	0.01218	0.00893	0.00429	0.00464	0.00789	0.01026	0.00429
0.01449	0.01210	0.00896	0.00431	0.00466	0.00780	0.01018	0.00431
0.01446	0.01221	0.00895	0.00430	0.00465	0.00791	0.01016	0.00430
0.00796	0.00700	0.00542	0.00252	0.00291	0.00448	0.00545	0.00252
0.00791	0.00694	0.00537	0.00246	0.00291	0.00448	0.00545	0.00246
0.00786	0.00690	0.00532	0.00241	0.00291	0.00449	0.00546	0.00241
0.00793	0.00696	0.00539	0.00247	0.00291	0.00449	0.00546	0.00247

(TS2=top test section, TS3 =middle test section, TS4=bottom test section)

Table A7.11. Material flows for test run number 3.

$\dot{M}_{v,in,TC}$ (kg/s)	$\dot{M}_{v,out,TS}$ TS4 (kg/s)	$\dot{M}_{v,out,TS}$ TS3 (kg/s)	$\dot{M}_{v,out,TC}$ (kg/s)	$\dot{M}_{f,out,TS}$ TS2 (kg/s)	$\dot{M}_{f,out,TS}$ TS3 (kg/s)	$\dot{M}_{f,out,TC}$ (kg/s)	$\dot{M}_{f,out,DC}$ (kg/s)
0.00752	0.00586	0.00432	0.00218	0.00214	0.00368	0.00534	0.00218
0.00753	0.00586	0.00420	0.00218	0.00202	0.00368	0.00535	0.00218
0.00759	0.00593	0.00426	0.00224	0.00202	0.00369	0.00535	0.00224
0.00754	0.00587	0.00421	0.00218	0.00203	0.00369	0.00536	0.00218
0.01490	0.01182	0.00849	0.00442	0.00407	0.00740	0.01048	0.00442
0.01472	0.01152	0.00832	0.00437	0.00395	0.00715	0.01035	0.00437
0.01478	0.01171	0.00838	0.00443	0.00395	0.00727	0.01035	0.00443
0.01492	0.01171	0.00838	0.00443	0.00395	0.00728	0.01048	0.00443

(TS2=top test section, TS3 =middle test section, TS4=bottom test section)

Table A7.12. Material flows for test run number 4.

$\dot{M}_{v,in,TC}$	$\dot{M}_{v,out,TS}$ TS4	$\dot{M}_{v,out,TS}$ TS3	$\dot{M}_{v,out,TC}$	$\dot{M}_{f,out,TS}$ TS2	$\dot{M}_{f,out,TS}$ TS3	$\dot{M}_{f,out,TC}$	$\dot{M}_{f,out,DC}$
(kg/s)	*(kg/s)*	*(kg/s)*	*(kg/s)*	*(kg/s)*	*(kg/s)*	*(kg/s)*	*(kg/s)*
0.01487	0.01218	0.00887	0.00434	0.00454	0.00784	0.01053	0.00434
0.01484	0.01214	0.00883	0.00428	0.00455	0.00786	0.01056	0.00428
0.01486	0.01218	0.00887	0.00434	0.00453	0.00784	0.01052	0.00434
0.01483	0.01213	0.00883	0.00429	0.00454	0.00785	0.01054	0.00429
0.00784	0.00642	0.00464	0.00192	0.00272	0.00450	0.00592	0.00192
0.00787	0.00646	0.00469	0.00197	0.00272	0.00449	0.00591	0.00197
0.00788	0.00646	0.00457	0.00197	0.00260	0.00449	0.00591	0.00197
0.00787	0.00634	0.00457	0.00197	0.00260	0.00437	0.00590	0.00197

(TS2=top test section, TS3 =middle test section, TS4=bottom test section)

A7.4 Calculated Mean Experimental Heat Transfer Coefficients

Table A7.13. Heat transfer coefficients for test run number 1.

$\overline{U}_{i,TS}$ TS2 (W/m²°C)	$\overline{U}_{i,TS}$ TS3 (W/m²°C)	$\overline{U}_{i,TS}$ TS4 (W/m²°C)	$\overline{\alpha}_{c,TS}$ TS2 (W/m²°C)	$\overline{\alpha}_{c,TS}$ TS3 (W/m²°C)	$\overline{\alpha}_{c,TS}$ TS4 (W/m²°C)	$\overline{\alpha}_{w,TS}$ TS2 (W/m²°C)	$\overline{\alpha}_{w,TS}$ TS3 (W/m²°C)	$\overline{\alpha}_{w,TS}$ TS4 (W/m²°C)	$\overline{\alpha}_{f,i,TS}$ TS2 (W/m²°C)	$\overline{\alpha}_{f,i,TS}$ TS3 (W/m²°C)	$\overline{\alpha}_{f,i,TS}$ TS4 (W/m²°C)
1084.06	1003.68	922.05	10765.57	11070.60	11303.30	84640.0	84697.8	84766.7	1169.95	1075.02	930.49
1113.70	967.54	964.53	10739.43	11052.09	11275.86	84640.0	84700.0	84766.7	1204.75	1033.77	973.76
1114.41	968.16	965.14	10744.93	11057.75	11281.64	84640.0	84697.8	84766.7	1205.54	1034.45	974.39
1114.41	962.49	965.14	10744.93	11057.75	11281.64	84642.2	84700.0	84768.9	1205.54	1027.98	974.39
1305.14	950.56	804.53	10333.82	10551.27	10680.20	84520.0	84548.9	84588.9	1436.67	1017.19	810.96
1301.99	948.28	881.09	10313.92	10530.94	10659.62	84520.0	84548.9	84588.9	1433.11	1014.69	888.81
1303.53	1007.72	803.50	10314.45	10531.80	10669.23	84520.0	84548.9	84588.9	1434.96	1083.05	809.91
1256.33	1007.72	813.26	10323.21	10531.80	10669.23	84520.0	84548.9	84588.9	1377.88	1083.05	819.83

(TS2=top test section, TS3 =middle test section, TS4=bottom test section)

Table A7.14. Heat transfer coefficients for test run number 2.

$\overline{U}_{i,TS}$ TS2 *(W/m² ℃)*	$\overline{U}_{i,TS}$ TS3 *(W/m² ℃)*	$\overline{U}_{i,TS}$ TS4 *(W/m² ℃)*	$\overline{\alpha}_{c,TS}$ TS2 *(W/m² ℃)*	$\overline{\alpha}_{c,TS}$ TS3 *(W/m² ℃)*	$\overline{\alpha}_{c,TS}$ TS4 *(W/m² ℃)*	$\overline{\alpha}_{w,TS}$ TS2 *(W/m² ℃)*	$\overline{\alpha}_{w,TS}$ TS3 *(W/m² ℃)*	$\overline{\alpha}_{w,TS}$ TS4 *(W/m² ℃)*	$\overline{\alpha}_{f,i,TS}$ TS2 *(W/m² ℃)*	$\overline{\alpha}_{f,i,TS}$ TS3 *(W/m² ℃)*	$\overline{\alpha}_{f,i,TS}$ TS4 *(W/m² ℃)*
1189.96	1005.44	861.51	10881.06	11190.87	11404.43	84677.8	84728.9	84791.1	1293.22	1076.33	868.86
1187.68	1003.50	853.48	10864.34	11173.67	11386.91	84677.8	84728.9	84791.1	1290.67	1074.21	860.70
1198.52	965.34	856.77	10906.25	11216.35	11421.95	84677.8	84728.9	84791.1	1303.11	1030.37	864.04
1189.90	1005.39	806.96	10889.53	11199.15	11412.58	84680.0	84731.1	84793.3	1293.08	1076.22	813.41
1465.35	970.08	693.87	10523.28	10728.18	10837.94	84575.6	84600.0	84633.3	1630.33	1038.51	698.64
1465.35	970.08	693.87	10523.28	10728.18	10837.94	84575.6	84600.0	84633.3	1630.33	1038.51	698.64
1468.18	971.96	695.21	10539.56	10744.77	10854.71	84575.6	84600.0	84633.3	1633.60	1040.56	700.00
1469.13	972.58	695.66	10544.98	10750.30	10860.29	84575.6	84597.8	84633.3	1634.69	1041.25	700.46

(TS2=top test section, TS3 =middle test section, TS4=bottom test section)

Table A7.15. Heat transfer coefficients for test run number 3.

$\overline{U}_{i,TS}$ TS2 *(W/m² ℃)*	$\overline{U}_{i,TS}$ TS3 *(W/m² ℃)*	$\overline{U}_{i,TS}$ TS4 *(W/m² ℃)*	$\overline{\alpha}_{c,TS}$ TS2 *(W/m² ℃)*	$\overline{\alpha}_{c,TS}$ TS3 *(W/m² ℃)*	$\overline{\alpha}_{c,TS}$ TS4 *(W/m² ℃)*	$\overline{\alpha}_{w,TS}$ TS2 *(W/m² ℃)*	$\overline{\alpha}_{w,TS}$ TS3 *(W/m² ℃)*	$\overline{\alpha}_{w,TS}$ TS4 *(W/m² ℃)*	$\overline{\alpha}_{f,i,TS}$ TS2 *(W/m² ℃)*	$\overline{\alpha}_{f,i,TS}$ TS3 *(W/m² ℃)*	$\overline{\alpha}_{f,i,TS}$ TS4 *(W/m² ℃)*
1128.95	970.70	1257.01	10206.24	10360.74	10471.31	84513.3	84546.7	84580.0	1227.19	1041.45	1272.77
1050.10	1039.98	1257.83	10211.58	10357.61	10476.78	84511.1	84544.4	84580.0	1134.54	1121.64	1273.62
1061.73	1040.66	1258.65	10216.91	10363.02	10482.25	84511.1	84544.4	84580.0	1148.08	1122.39	1274.46
1063.81	1042.69	1261.12	10232.90	10379.25	10498.66	84511.1	84544.4	84580.0	1150.39	1124.64	1276.98
1033.46	1006.08	1109.39	10685.66	10959.99	11180.39	84655.6	84717.8	84784.4	1111.76	1078.43	1121.62
1004.08	965.18	1149.26	10689.88	10955.72	11167.94	84655.6	84717.8	84784.4	1077.80	1031.59	1162.39
1004.08	1005.59	1108.85	10689.88	10955.72	11176.03	84655.6	84717.8	84784.4	1077.80	1077.89	1121.07
1005.22	1006.73	1159.09	10699.62	10965.69	11186.21	84657.8	84717.8	84784.4	1079.06	1079.14	1172.45

(TS2=top test section, TS3 =middle test section, TS4=bottom test section)

Table A7.16. Heat transfer coefficients for test run number 4.

$\overline{U}_{i,TS}$ TS2 ($W/m^2\,°C$)	$\overline{U}_{i,TS}$ TS3 ($W/m^2\,°C$)	$\overline{U}_{i,TS}$ TS4 ($W/m^2\,°C$)	$\overline{\alpha}_{c,TS}$ TS2 ($W/m^2\,°C$)	$\overline{\alpha}_{c,TS}$ TS3 ($W/m^2\,°C$)	$\overline{\alpha}_{c,TS}$ TS4 ($W/m^2\,°C$)	$\overline{\alpha}_{w,TS}$ TS2 ($W/m^2\,°C$)	$\overline{\alpha}_{w,TS}$ TS3 ($W/m^2\,°C$)	$\overline{\alpha}_{w,TS}$ TS4 ($W/m^2\,°C$)	$\overline{\alpha}_{f,i,TS}$ TS2 ($W/m^2\,°C$)	$\overline{\alpha}_{f,i,TS}$ TS3 ($W/m^2\,°C$)	$\overline{\alpha}_{f,i,TS}$ TS4 ($W/m^2\,°C$)
1125.58	984.65	942.30	10635.52	10940.02	11157.94	84671.1	84726.7	84793.3	1219.50	1053.96	951.10
1128.35	987.07	944.61	10656.45	10961.55	11179.90	84671.1	84726.7	84793.3	1222.58	1056.61	953.47
1124.84	984.00	941.68	10629.94	10934.28	11152.08	84671.1	84726.7	84793.3	1218.68	1053.25	950.47
1126.31	985.29	942.91	10641.11	10945.77	11163.80	84671.1	84726.7	84793.3	1220.32	1054.66	951.73
1253.90	997.97	939.22	10211.08	10405.77	10531.32	84544.4	84573.3	84611.1	1376.21	1072.61	947.99
1251.43	996.00	937.37	10194.92	10389.31	10514.66	84544.4	84573.3	84611.1	1373.40	1070.44	946.10
1191.95	1057.56	937.98	10200.31	10386.40	10520.22	84542.2	84573.3	84611.1	1302.04	1141.90	946.73
1189.59	983.69	1007.89	10184.15	10369.94	10495.24	84542.2	84573.3	84611.1	1299.39	1056.36	1018.00

(TS2=top test section, TS3 =middle test section, TS4=bottom test section)

A7.5 Condensate film Properties

Table A7.17. Condensate properties for test run number 1.

Test Condenser Measurements						Predictions of Nusselt Theory			Predictions of HTFS Method		
Ref	Ref	Ref	Prf	Prf	Prf	$\overline{\alpha}_{f,l,TS}$	$\overline{\alpha}_{f,l,TS}$	$\overline{\alpha}_{f,l,TS}$	$\overline{\alpha}_{f,l,TS}$	$\overline{\alpha}_{f,l,TS}$	$\overline{\alpha}_{f,l,TS}$
TS2	TS3	TS4	TS2	TS3	TS4	TS2	TS3	TS4	TS2	TS3	TS4
(-)	*(-)*	*(-)*	*(-)*	*(-)*	*(-)*	*(W/m^2 ℃)*	*(W/m^2 ℃)*	*(W/m^2 ℃)*	*(W/m^2 ℃)*	*(W/m^2 ℃)*	*(W/m^2 ℃)*
730.26	1297.20	1742.05	4.0642	4.0642	4.0642	829.06	559.07	487.45	1100.92	840.19	767.31
748.26	1293.28	1756.93	4.0642	4.0642	4.0642	822.35	557.63	486.89	1094.99	838.73	766.74
748.74	1294.11	1758.06	4.0642	4.0642	4.0642	822.18	557.51	486.79	1094.83	838.61	766.63
748.74	1294.11	1758.06	4.0642	4.0642	4.0642	822.18	557.51	486.79	1094.83	838.61	766.63
435.64	696.68	887.96	4.2410	4.2410	4.2410	969.77	667.84	596.20	1216.23	939.76	871.80
434.59	695.00	903.17	4.2410	4.2410	4.2410	970.55	668.38	594.57	1216.89	940.26	870.23
435.10	713.20	904.24	4.2410	4.2410	4.2410	970.17	664.87	592.13	1216.57	937.02	867.87
417.68	695.78	886.82	4.2410	4.2410	4.2410	983.48	671.83	596.46	1227.74	943.50	872.05

(TS2=top test section, TS3 =middle test section, TS4=bottom test section)

Table A7.18. Condensate properties for test run number 2.

Test Condenser Measurements						Predictions of Nusselt Theory			Predictions of HTFS Method		
Ref	*Ref*	*Ref*	*Prf*	*Prf*	*Prf*	$\overline{\alpha}_{f,i,TS}$	$\overline{\alpha}_{f,i,TS}$	$\overline{\alpha}_{f,i,TS}$	$\overline{\alpha}_{f,i,TS}$	$\overline{\alpha}_{f,i,TS}$	$\overline{\alpha}_{f,i,TS}$
TS2	TS3	TS4	TS2	TS3	TS4	TS2	TS3	TS4	TS2	TS3	TS4
(-)	*(-)*	*(-)*	*(-)*	*(-)*	*(-)*	*(W/m^2 ℃)*	*(W/m^2 ℃)*	*(W/m^2 ℃)*	*(W/m^2 ℃)*	*(W/m^2 ℃)*	*(W/m^2 ℃)*
750.59	1277.06	1661.30	4.0606	4.0606	4.0606	821.74	558.98	493.03	1094.55	840.14	773.16
749.15	1274.61	1658.11	4.0606	4.0606	4.0606	822.27	559.33	493.34	1095.02	840.50	773.48
752.82	1260.54	1645.94	4.0594	4.0594	4.0594	821.01	560.27	494.88	1093.94	841.44	775.10
751.37	1278.39	1642.79	4.0594	4.0594	4.0594	821.53	558.84	494.01	1094.40	840.03	774.20
419.53	646.50	786.08	4.2296	4.2296	4.2296	983.05	681.92	617.12	1227.81	953.10	892.17
419.53	646.50	786.08	4.2296	4.2296	4.2296	983.05	681.92	617.12	1227.81	953.10	892.18
420.34	647.75	787.60	4.2296	4.2296	4.2296	982.42	681.48	616.72	1227.28	952.70	891.80
420.61	648.16	788.10	4.2296	4.2296	4.2296	982.21	681.33	616.59	1227.11	952.56	891.67

(TS2=top test section, TS3 =middle test section, TS4=bottom test section)

Table A7.19. Condensate properties for test run number 3.

Test Condenser Measurements						Predictions of Nusselt Theory			Predictions of HTFS Method		
Re_f	Re_f	Re_f	Pr_f	Pr_f	Pr_f	$\overline{\alpha}_{f,i,TS}$	$\overline{\alpha}_{f,i,TS}$	$\overline{\alpha}_{f,i,TS}$	$\overline{\alpha}_{f,i,TS}$	$\overline{\alpha}_{f,i,TS}$	$\overline{\alpha}_{f,i,TS}$
TS2	TS3	TS4	TS2	TS3	TS4	TS2	TS3	TS4	TS2	TS3	TS4
(-)	(-)	(-)	(-)	(-)	(-)	(W/m^2 °C)	(W/m^2 °C)	(W/m^2 °C)	(W/m^2 °C)	(W/m^2 °C)	(W/m^2 °C)
300.39	517.13	750.39	4.2744	4.2744	4.2744	1094.23	742.57	640.71	1317.94	1006.92	913.33
283.89	517.47	750.88	4.2744	4.2744	4.2744	1115.03	747.96	640.57	1334.87	1011.80	913.20
284.07	517.80	751.37	4.2744	4.2744	4.2744	1114.79	747.79	640.43	1334.67	1011.65	913.07
284.63	518.82	752.84	4.2744	4.2744	4.2744	1114.07	747.31	640.01	1334.08	1011.22	912.68
654.16	1188.49	1682.59	4.0689	4.0689	4.0689	859.68	577.05	496.73	1127.69	857.84	776.84
633.30	1147.04	1660.11	4.0701	4.0701	4.0701	868.92	583.63	500.49	1135.72	864.24	780.71
633.99	1168.07	1661.93	4.0689	4.0689	4.0689	868.69	581.44	499.14	1135.56	862.14	779.33
634.72	1169.40	1683.60	4.0689	4.0689	4.0689	868.36	581.21	497.83	1135.27	861.93	777.99

(TS2=top test section, TS3 =middle test section, TS4=bottom test section)

Table A7.20. Condensate properties for test run number 4.

Test Condenser Measurements						Predictions of Nusselt Theory			Predictions of HTFS Method		
Ref	Ref	Ref	Prf	Prf	Prf	$\overline{\alpha}_{f,i,TS}$	$\overline{\alpha}_{f,i,TS}$	$\overline{\alpha}_{f,i,TS}$	$\overline{\alpha}_{f,i,TS}$	$\overline{\alpha}_{f,i,TS}$	$\overline{\alpha}_{f,i,TS}$
TS2	TS3	TS4	TS2	TS3	TS4	TS2	TS3	TS4	TS2	TS3	TS4
(-)	(-)	(-)	(-)	(-)	(-)	(W/m^2 °C)	(W/m^2 °C)	(W/m^2 °C)	(W/m^2 °C)	(W/m^2 °C)	(W/m^2 °C)
734.08	1268.77	1703.87	4.0583	4.0583	4.0583	828.01	561.46	491.29	1100.16	842.67	771.42
735.89	1271.89	1708.06	4.0583	4.0583	4.0583	827.33	561.00	490.89	1099.56	842.21	771.01
733.60	1267.94	1702.75	4.0583	4.0583	4.0583	828.18	561.58	491.40	1100.32	842.79	771.53
734.56	1269.60	1704.99	4.0583	4.0583	4.0583	827.82	561.33	491.18	1100.00	842.54	771.31
391.81	647.03	851.05	4.2353	4.2353	4.2353	1005.18	687.85	607.88	1246.09	958.45	883.21
391.03	645.75	849.37	4.2353	4.2353	4.2353	1005.85	688.30	608.28	1246.65	958.87	883.59
373.87	645.46	848.99	4.2367	4.2367	4.2367	1020.87	692.39	608.29	1259.09	962.63	883.56
373.13	627.24	847.30	4.2367	4.2367	4.2367	1021.54	696.57	611.10	1259.65	966.43	886.27

(TS2=top test section, TS3 =middle test section, TS4=bottom test section)

A7.6 Analysis over full Test Condenser Length

Table A7.21. Full length analysis for test run number 1.

$\dot{Q}_{c,TC}$ (W)	$\Delta T_{ln,TC}$ (°C)	$\overline{U}_{i,TC}$ (W/m²°C)	$\overline{\alpha}_{c,TC}$ (W/m²°C)	$\overline{\alpha}_{w,TC}$ (W/m²°C)	$T_{f,TC}$ (°C)	$\dot{M}_{f,out,TC}$ (kg/s)	Ref (-)	Prf (-)	Measured $\overline{\alpha}_{f,i,TC}$ (W/m²°C)	Nusselt $\overline{\alpha}_{f,i,TC}$ (W/m²°C)	HTFS $\overline{\alpha}_{f,i,TC}$ (W/m²°C)
3737.964	17.448	1008.58	11158.33	84701.5	43.61	0.01039	1614.430	4.1164	1080.12	633.50	919.47
3769.900	17.389	1020.67	11135.39	84702.2	43.61	0.01048	1628.223	4.1164	1094.14	631.70	917.74
3772.315	17.389	1021.32	11141.10	84701.5	43.61	0.01049	1629.266	4.1164	1094.86	631.57	917.61
3772.315	17.389	1021.32	11141.10	84703.7	43.64	0.01049	1630.180	4.1160	1094.86	631.47	917.53
2212.149	10.239	1017.12	10585.76	84552.6	31.80	0.00606	849.827	4.2773	1093.55	773.42	1044.57
2250.042	10.180	1040.60	10567.52	84552.6	31.80	0.00617	864.384	4.2773	1120.86	769.05	1040.64
2252.702	10.282	1031.48	10570.58	84552.6	31.80	0.00617	865.406	4.2773	1110.26	768.75	1040.37
2209.289	10.239	1015.81	10572.74	84552.6	31.80	0.00605	848.728	4.2773	1092.11	773.76	1044.87

Table A7.22. Full length analysis for test run number 2.

$\dot{Q}_{c,TC}$ (W)	$\Delta T_{ln,TC}$ (°C)	$\overline{U}_{i,TC}$ (W/m² °C)	$\overline{\alpha}_{c,TC}$ (W/m² °C)	$\overline{\alpha}_{w,TC}$ (W/m² °C)	$T_{f,TC}$ (°C)	$\dot{M}_{f,out,TC}$ (kg/s)	Ref (-)	Prf (-)	Measured $\overline{\alpha}_{f,i,TC}$ (W/m² °C)	Nusselt $\overline{\alpha}_{f,i,TC}$ (W/m² °C)	HTFS $\overline{\alpha}_{f,i,TC}$ (W/m² °C)
3553.045	16.359	1022.52	11261.06	84732.6	44.17	0.00991	1546.484	4.1094	1095.51	643.03	928.80
3546.221	16.359	1020.55	11243.76	84732.6	44.17	0.00989	1543.514	4.1094	1093.36	643.44	929.19
3516.345	16.418	1008.29	11282.49	84732.6	44.24	0.00980	1531.306	4.1086	1079.07	645.20	930.89
3509.620	16.418	1006.36	11267.24	84734.8	44.27	0.00979	1529.237	4.1082	1076.95	645.51	931.20
1941.079	8.758	1043.41	10749.35	84603.0	32.99	0.00535	757.374	4.2599	1122.85	805.01	1073.35
1941.079	8.758	1043.41	10749.35	84603.0	32.99	0.00535	757.374	4.2599	1122.85	805.02	1073.35
1944.833	8.758	1045.42	10765.98	84603.0	32.99	0.00536	758.838	4.2599	1125.08	804.50	1072.89
1946.085	8.758	1046.10	10771.52	84602.2	32.99	0.00536	759.327	4.2599	1125.82	804.33	1072.74

Table A7.23. Full length analysis for test run number 3.

$\dot{Q}_{c,TC}$ (W)	$\Delta T_{ln,TC}$ (°C)	$\overline{U}_{i,TC}$ (W/m²°C)	$\overline{\alpha}_{c,TC}$ (W/m²°C)	$\overline{\alpha}_{w,TC}$ (W/m²°C)	$T_{f,TC}$ (°C)	$\dot{M}_{f,out,TC}$ (kg/s)	Ref (-)	Prf (-)	Measured $\overline{\alpha}_{f,i,TC}$ (W/m²°C)	Nusselt $\overline{\alpha}_{f,i,TC}$ (W/m²°C)	HTFS $\overline{\alpha}_{f,i,TC}$ (W/m²°C)
1917.667	8.041	1122.73	10407.63	84546.7	30.11	0.00526	725.882	4.3027	1218.07	813.19	1079.13
1918.911	8.041	1123.46	10410.94	84545.2	30.11	0.00526	726.353	4.3027	1218.90	813.01	1078.98
1920.164	8.041	1124.19	10416.37	84545.2	30.11	0.00526	726.827	4.3027	1219.72	812.84	1078.82
1923.922	8.041	1126.39	10432.68	84545.2	30.11	0.00527	728.250	4.3027	1222.17	812.31	1078.35
3626.200	16.180	1055.14	11054.31	84719.3	43.60	0.01011	1569.933	4.1166	1134.37	639.42	925.14
3581.660	16.035	1051.57	11050.00	84719.3	43.53	0.00998	1549.841	4.1174	1130.28	642.12	927.70
3581.662	16.137	1044.91	11052.04	84719.3	43.60	0.00998	1550.650	4.1166	1122.57	642.05	927.66
3628.362	16.077	1062.48	11064.15	84720.0	43.60	0.01011	1570.869	4.1166	1142.80	639.28	925.01

Table A7.24. Full length analysis for test run number 4.

$\dot{Q}_{c,TC}$ (W)	$\Delta T_{ln,TC}$ (°C)	$\overline{U}_{i,TC}$ (W/m^2°C)	$\overline{\alpha}_{c,TC}$ (W/m^2°C)	$\overline{\alpha}_{w,TC}$ (W/m^2°C)	Tf,TC (°C)	$\dot{M}_{f,out,TC}$ (kg/s)	Ref (-)	Prf (-)	Measured $\overline{\alpha}_{f,i,TC}$ (W/m^2°C)	Nusselt $\overline{\alpha}_{f,i,TC}$ (W/m^2°C)	HTFS $\overline{\alpha}_{f,i,TC}$ (W/m^2°C)
3636.135	16.733	1023.02	11019.13	84730.4	44.34	0.01014	1585.187	4.1073	1097.54	637.86	923.89
3645.082	16.733	1025.53	11040.82	84730.4	44.34	0.01017	1589.088	4.1073	1100.31	637.34	923.39
3633.749	16.733	1022.34	11013.35	84730.4	44.34	0.01013	1584.147	4.1073	1096.81	638.00	924.02
3638.521	16.733	1023.69	11024.91	84730.4	44.34	0.01015	1586.227	4.1073	1098.28	637.72	923.76
2110.840	9.584	1036.93	10445.65	84576.3	32.40	0.00580	817.234	4.2686	1117.46	784.22	1054.53
2106.666	9.584	1034.88	10429.13	84576.3	32.40	0.00579	815.618	4.2686	1115.20	784.73	1055.00
2108.042	9.481	1046.73	10432.54	84575.6	32.33	0.00579	815.708	4.2696	1128.95	784.63	1054.87
2103.861	9.481	1044.66	10413.92	84575.6	32.33	0.00578	814.090	4.2696	1126.67	785.15	1055.33

A7.7 Vapour Flooding Velocities in the Test Condenser

Table A7.25. Flooding calculations for test run number 1.

			Predicted Flooding Velocity	
		Actual Vapour Velocity	Conservative	Non-conservative
$\dot{M}_{v,in,TC}$	Re_v	$\dot{u}_{v,in,TC}$	$\dot{v}_v$	
(kg/s)	*(-)*	*(m/s)*	*(m/s)*	
0.01405	53779.2	2.0603	1.5826	2.5322
0.01414	54131.5	2.0738	1.5797	2.5275
0.01420	54352.7	2.0823	1.5795	2.5271
0.01420	54348.4	2.0821	1.5794	2.5270
0.00766	30621.6	1.7118	2.2603	3.6165
0.00777	31038.8	1.7352	2.2519	3.6030
0.00772	30848.2	1.7245	2.2513	3.6020
0.00765	30587.7	1.7099	2.2609	3.6175

Table A7.26. Flooding calculations for test run number 2.

			Predicted Flooding Velocity	
		Actual Vapour Velocity	Conservative	Non-conservative
$\dot{M}_{v,in,TC}$	Re_V	$\dot{u}_{v,in,TC}$	$\dot{v}_v$	
(kg/s)	*(-)*	*(m/s)*	*(m/s)*	
0.01421	54347.3	2.0656	1.5913	2.5460
0.01418	54229.4	2.0612	1.5919	2.5471
0.01411	53950.5	2.0451	1.5922	2.5476
0.01409	53867.4	2.0420	1.5928	2.5485
0.00786	31346.9	1.7121	2.2903	3.6645
0.00781	31137.0	1.7006	2.2903	3.6645
0.00776	30951.3	1.6905	2.2893	3.6629
0.00783	31221.4	1.7052	2.2890	3.6624

Table A7.27. Flooding calculations for test run number 3.

			Predicted Flooding Velocity	
		Actual Vapour Velocity	Conservative	Non-conservative
$\dot{M}_{v,in,TC}$	Re_v	$\dot{u}_{v,in,TC}$	$\dot{v}_v$	
(kg/s)	*(-)*	*(m/s)*	*(m/s)*	
0.00743	29934.6	1.7907	2.4322	3.8915
0.00744	29954.7	1.7919	2.4318	3.8909
0.00750	30208.7	1.8071	2.4315	3.8904
0.00745	30018.7	1.7957	2.4304	3.8887
0.01453	55678.9	2.1558	1.6032	2.5651
0.01436	55036.9	2.1366	1.6102	2.5764
0.01441	55242.0	2.1389	1.6075	2.5721
0.01454	55740.6	2.1582	1.6030	2.5647

Table A7.28. Flooding calculations for test run number 4.

			Predicted Flooding Velocity	
		Actual Vapour Velocity	Conservative	Non-conservative
$\dot{M}_{v,in,TC}$	Re_V	$\dot{u}_{v,in,TC}$	$\dot{v}_v$	
(kg/s)	*(-)*	*(m/s)*	*(m/s)*	
0.01448	55336.3	2.0922	1.5778	2.5245
0.01445	55210.0	2.0874	1.5770	2.5231
0.01447	55322.0	2.0916	1.5780	2.5249
0.01444	55172.4	2.0860	1.5776	2.5241
0.00772	30814.4	1.7027	2.2660	3.6256
0.00776	30958.4	1.7106	2.2670	3.6272
0.00776	30996.4	1.7177	2.2707	3.6332
0.00775	30955.8	1.7155	2.2717	3.6347

Appendix A8 Iso-octane Experimental Data and Data Analysis Calculations

A8.1 Test Data

Table A8.1. Data for test run number 1

Boiler Measurements				Test Condenser Measurements										Dump Condenser Measurements			
$\dot{Q}$	T_v	P_v	$\dot{V}_c$	$T_{c,in}$ TS2	$T_{c,in}$ TS3	$T_{c,in}$ TS4	$T_{c,out}$	T_v TS2	T_v TS3	T_v TS4	$\overline{T}_w$ TS2	$\overline{T}_w$ TS3	$\overline{T}_w$ TS4	$\dot{V}_c$	$T_{c,in}$	$T_{c,out}$	T_f
(W)	*(°C)*	*(bara)*	*(l/min)*	*(°C)*	*(°C)*	*(°C)*	*(°C)*	*(°C)*	*(°C)*	*(°C)*	*(°C)*	*(°C)*	*(°C)*	*(l/min)*	*(°C)*	*(°C)*	*(°C)*
2054.7	35.7	0.120	5.016	21.8	24.2	25.6	26.7	35.6	35.5	35.5	23.7	25.1	26.8	3.010	18.0	18.2	14.5
2052.2	35.8	0.120	5.032	21.8	24.2	25.7	26.7	35.6	35.6	35.5	23.7	25.1	26.8	3.004	18.0	18.2	14.5
2056.7	35.8	0.120	5.040	21.7	24.1	25.6	26.7	35.6	35.5	35.5	23.7	25.1	26.8	3.007	18.0	18.1	14.4
2052.7	35.8	0.121	5.043	21.7	24.1	25.6	26.7	35.6	35.6	35.5	23.7	25.1	26.8	3.013	17.9	18.1	14.3

(TS2=top test section, TS3 =middle test section, TS4=bottom test section)

Table A8.2. Data for test run number 2.

Boiler Measurements				Test Condenser Measurements										Dump Condenser Measurements			
$\dot{Q}$	T_v	P_v	$\dot{V}_c$	$T_{c,in}$ TS2	$T_{c,in}$ TS3	$T_{c,in}$ TS4	$T_{c,out}$	T_v TS2	T_v TS3	T_v TS4	$\overline{T}_w$ TS2	$\overline{T}_w$ TS3	$\overline{T}_w$ TS4	$\dot{V}_c$	$T_{c,in}$	$T_{c,out}$	T_f
(W)	*(°C)*	*(bara)*	*(l/min)*	*(°C)*	*(°C)*	*(°C)*	*(°C)*	*(°C)*	*(°C)*	*(°C)*	*(°C)*	*(°C)*	*(°C)*	*(l/min)*	*(°C)*	*(°C)*	*(°C)*
2089.7	35.3	0.121	5.160	21.0	23.2	24.8	26.1	35.1	35.1	35.0	22.9	24.4	26.1	3.013	17.6	17.5	9.6
2087.5	35.3	0.121	5.157	21.1	23.3	24.8	26.1	35.2	35.1	35.0	22.9	24.4	26.2	3.010	17.6	17.5	9.6
2086.0	35.4	0.122	5.153	21.1	23.3	24.8	26.1	35.2	35.1	35.1	23.0	24.5	26.2	3.011	17.6	17.5	9.6
2084.1	35.4	0.122	5.160	21.1	23.3	24.8	26.2	35.2	35.2	35.1	23.0	24.5	26.2	3.011	17.6	17.6	9.6

(TS2=top test section, TS3 =middle test section, TS4=bottom test section)

Table A8.3. Data for test run number 3

Boiler Measurements				Test Condenser Measurements										Dump Condenser Measurements			
$\dot{Q}$	T_v	P_v	$\dot{V}_c$	$T_{c,in}$ TS2	$T_{c,in}$ TS3	$T_{c,in}$ TS4	$T_{c,out}$	T_v TS2	T_v TS3	T_v TS4	$\overline{T}_w$ TS2	$\overline{T}_w$ TS3	$\overline{T}_w$ TS4	$\dot{V}_c$	$T_{c,in}$	$T_{c,out}$	T_f
(W)	*(°C)*	*(bara)*	*(l/min)*	*(°C)*	*(°C)*	*(°C)*	*(°C)*	*(°C)*	*(°C)*	*(°C)*	*(°C)*	*(°C)*	*(°C)*	*(l/min)*	*(°C)*	*(°C)*	*(°C)*
2058.7	35.5	0.121	5.028	23.8	25.9	27.2	28.0	35.4	35.3	35.3	25.6	26.6	28.1	3.004	20.4	21.8	18.8
2054.9	35.5	0.122	5.020	23.8	25.9	27.2	28.0	35.4	35.3	35.3	25.6	26.6	28.1	2.997	20.3	21.8	18.8
2055.8	35.6	0.122	5.028	23.8	25.9	27.2	28.0	35.4	35.4	35.3	25.6	26.6	28.1	2.998	20.4	21.8	18.8
2058.5	35.6	0.121	5.032	23.8	25.9	27.2	28.0	35.6	35.5	35.4	25.6	26.6	28.1	3.001	20.3	21.8	18.8

(TS2=top test section, TS3 =middle test section, TS4=bottom test section)

Table A8.4. Data for test run number 4.

Boiler Measurements				Test Condenser Measurements										Dump Condenser Measurements			
$\dot{Q}$	T_v	P_v	$\dot{V}_c$	$T_{c,in}$ TS2	$T_{c,in}$ TS3	$T_{c,in}$ TS4	$T_{c,out}$	T_v TS2	T_v TS3	T_v TS4	$\overline{T}_w$ TS2	$\overline{T}_w$ TS3	$\overline{T}_w$ TS4	$\dot{V}_c$	$T_{c,in}$	$T_{c,out}$	T_f
(W)	*(°C)*	*(bara)*	*(l/min)*	*(°C)*	*(°C)*	*(°C)*	*(°C)*	*(°C)*	*(°C)*	*(°C)*	*(°C)*	*(°C)*	*(°C)*	*(l/min)*	*(°C)*	*(°C)*	*(°C)*
2081.5	38.0	0.134	5.016	23.6	26.1	27.6	28.6	37.9	37.8	37.7	25.6	27.0	28.7	2.994	20.0	20.2	16.8
2080.3	38.0	0.134	5.012	23.5	26.1	27.6	28.6	37.9	37.8	37.8	25.6	27.0	28.7	2.997	19.9	20.2	16.7
2079.4	38.0	0.134	5.016	23.5	26.1	27.6	28.6	37.9	37.8	37.8	25.6	27.0	28.7	2.998	20.0	20.1	16.7
2077.6	38.0	0.134	5.012	23.5	26.1	27.6	28.6	37.9	37.8	37.8	25.6	27.0	28.7	2.997	20.0	20.1	16.6

(TS2=top test section, TS3 =middle test section, TS4=bottom test section)

A8.2 Heat Transfer Calculations

Table A8.5. Heat transfer results for test run number 1.

$\dot{Q}_{c,TS}$ TS2 (W)	$\dot{Q}_{c,TS}$ TS3 (W)	$\dot{Q}_{c,TS}$ TS4 (W)	$\dot{Q}_{c,TC}$ (W)	$\dot{Q}_{c,DC}$ (W)	$\dot{Q}_{c,T}$ (W)	$\dot{Q}_{c,T}/\dot{Q}$ (-)	$\Delta T_{ln,TS}$ TS2 (°C)	$\Delta T_{ln,TS}$ TS3 (°C)	$\Delta T_{ln,TS}$ TS4 (°C)
838.363	488.436	383.495	1710.294	42.009	1752.303	0.8528	12.562	10.585	9.339
841.038	524.993	349.726	1715.757	41.925	1757.682	0.8565	12.562	10.632	9.291
842.419	525.855	385.330	1753.604	20.983	1774.587	0.8628	12.662	10.632	9.339
842.920	526.168	385.559	1754.648	42.053	1796.700	0.8753	12.662	10.733	9.339

(TS2=top test section, TS3 =middle test section, TS4=bottom test section)

Table A8.6. Heat transfer results for test run number 2.

$\dot{Q}_{c,TS}$ TS2 (W)	$\dot{Q}_{c,TS}$ TS3 (W)	$\dot{Q}_{c,TS}$ TS4 (W)	$\dot{Q}_{c,TC}$ (W)	$\dot{Q}_{c,DC}$ (W)	$\dot{Q}_{c,T}$ (W)	$\dot{Q}_{c,T}/\dot{Q}$ (-)	$\Delta T_{ln,TS}$ TS2 (°C)	$\Delta T_{ln,TS}$ TS3 (°C)	$\Delta T_{ln,TS}$ TS4 (°C)
790.895	574.534	466.424	1831.853	-21.030	1831.853	0.8766	12.969	11.081	9.535
790.393	538.285	466.153	1794.831	-21.009	1794.831	0.8598	12.969	11.033	9.535
789.780	537.867	465.791	1793.438	-21.016	1793.438	0.8597	12.969	11.033	9.635
790.853	538.598	502.303	1831.753	0.000	1831.753	0.8789	12.969	11.133	9.583

(TS2=top test section, TS3 =middle test section, TS4=bottom test section)

Table A8.7. Heat transfer results for test run number 3.

$\dot{Q}_{c,TS}$ TS2 (W)	$\dot{Q}_{c,TS}$ TS3 (W)	$\dot{Q}_{c,TS}$ TS4 (W)	$\dot{Q}_{c,TC}$ (W)	$\dot{Q}_{c,DC}$ (W)	$\dot{Q}_{c,T}$ (W)	$\dot{Q}_{c,T}/\dot{Q}$ (-)	$\Delta T_{ln,TS}$ TS2 (°C)	$\Delta T_{ln,TS}$ TS3 (°C)	$\Delta T_{ln,TS}$ TS4 (°C)
734.558	454.236	279.346	1468.140	293.097	1761.237	0.8555	10.515	8.734	7.693
733.389	453.514	278.901	1465.804	313.318	1779.122	0.8658	10.515	8.734	7.693
734.558	454.236	279.346	1468.140	292.512	1760.652	0.8564	10.515	8.834	7.693
735.142	454.598	279.568	1469.308	313.736	1783.044	0.8662	10.716	8.934	7.793

(TS2=top test section, TS3 =middle test section, TS4=bottom test section)

Table A8.8. Heat transfer results for test run number 4.

$\dot{Q}_{c,TS}$ TS2 (W)	$\dot{Q}_{c,TS}$ TS3 (W)	$\dot{Q}_{c,TS}$ TS4 (W)	$\dot{Q}_{c,TC}$ (W)	$\dot{Q}_{c,DC}$ (W)	$\dot{Q}_{c,T}$ (W)	$\dot{Q}_{c,T}/\dot{Q}$ (-)	$\Delta T_{ln,TS}$ TS2 (°C)	$\Delta T_{ln,TS}$ TS3 (°C)	$\Delta T_{ln,TS}$ TS4 (°C)
872.477	522.815	348.278	1743.570	41.741	1785.310	0.8577	13.010	10.933	9.591
906.699	522.398	348.001	1777.098	62.677	1839.775	0.8844	13.057	10.933	9.691
907.423	522.815	348.278	1778.516	20.898	1799.414	0.8654	13.057	10.933	9.691
906.699	522.398	348.001	1777.098	20.891	1797.989	0.8654	13.057	10.933	9.691

(TS2=top test section, TS3 =middle test section, TS4=bottom test section)

A8.3 Mass Balance Calculations across Test and Dump Condensers

Table A8.9. Material flows for test run number 1.

$\dot{M}_{v,in,TC}$	$\dot{M}_{v,out,TS}$ TS4	$\dot{M}_{v,out,TS}$ TS3	$\dot{M}_{v,out,TC}$	$\dot{M}_{f,out,TS}$ TS2	$\dot{M}_{f,out,TS}$ TS3	$\dot{M}_{f,out,TC}$	$\dot{M}_{f,out,DC}$
(kg/s)	*(kg/s)*	*(kg/s)*	*(kg/s)*	*(kg/s)*	*(kg/s)*	*(kg/s)*	*(kg/s)*
0.00588	0.00459	0.00295	0.00012	0.00282	0.00447	0.00576	0.00012
0.00590	0.00472	0.00295	0.00012	0.00283	0.00460	0.00578	0.00012
0.00597	0.00467	0.00290	0.00006	0.00284	0.00461	0.00590	0.00006
0.00603	0.00473	0.00296	0.00012	0.00284	0.00461	0.00591	0.00012

(TS2=top test section, TS3 =middle test section, TS4=bottom test section)

Table A8.10. Material flows for test run number 2.

$\dot{M}_{v,in,TC}$ (kg/s)	$\dot{M}_{v,out,TS}$ TS4 (kg/s)	$\dot{M}_{v,out,TS}$ TS3 (kg/s)	$\dot{M}_{v,out,TC}$ (kg/s)	$\dot{M}_{f,out,TS}$ TS2 (kg/s)	$\dot{M}_{f,out,TS}$ TS3 (kg/s)	$\dot{M}_{f,out,TC}$ (kg/s)	$\dot{M}_{f,out,DC}$ (kg/s)
0.00616	0.00459	0.00266	0.00000	0.00266	0.00459	0.00616	-0.00006
0.00604	0.00447	0.00266	0.00000	0.00266	0.00447	0.00604	-0.00006
0.00603	0.00447	0.00266	0.00000	0.00266	0.00447	0.00603	-0.00006
0.00616	0.00447	0.00266	0.00000	0.00266	0.00447	0.00616	0.00000

(TS2=top test section, TS3 =middle test section, TS4=bottom test section)

Table A8.11. Material flows for test run number 3.

$\dot{M}_{v,in,TC}$ (kg/s)	$\dot{M}_{v,out,TS}$ TS4 (kg/s)	$\dot{M}_{v,out,TS}$ TS3 (kg/s)	$\dot{M}_{v,out,TC}$ (kg/s)	$\dot{M}_{f,out,TS}$ TS2 (kg/s)	$\dot{M}_{f,out,TS}$ TS3 (kg/s)	$\dot{M}_{f,out,TC}$ (kg/s)	$\dot{M}_{f,out,DC}$ (kg/s)
0.00583	0.00489	0.00336	0.00089	0.00247	0.00400	0.00494	0.00089
0.00588	0.00494	0.00341	0.00095	0.00247	0.00399	0.00493	0.00095
0.00582	0.00488	0.00336	0.00088	0.00247	0.00400	0.00494	0.00088
0.00589	0.00495	0.00342	0.00095	0.00247	0.00400	0.00495	0.00095

(TS2=top test section, TS3 =middle test section, TS4=bottom test section)

Table A8.12. Material flows for test run number 4.

$\dot{M}_{v,in,TC}$ (kg/s)	$\dot{M}_{v,out,TS}$ TS4 (kg/s)	$\dot{M}_{v,out,TS}$ TS3 (kg/s)	$\dot{M}_{v,out,TC}$ (kg/s)	$\dot{M}_{f,out,TS}$ TS2 (kg/s)	$\dot{M}_{f,out,TS}$ TS3 (kg/s)	$\dot{M}_{f,out,TC}$ (kg/s)	$\dot{M}_{f,out,DC}$ (kg/s)
0.00601	0.00484	0.00307	0.00012	0.00295	0.00471	0.00589	0.00012
0.00619	0.00501	0.00325	0.00018	0.00306	0.00483	0.00600	0.00018
0.00607	0.00489	0.00313	0.00006	0.00307	0.00483	0.00601	0.00006
0.00607	0.00489	0.00313	0.00006	0.00306	0.00483	0.00600	0.00006

(TS2=top test section, TS3 =middle test section, TS4=bottom test section)

A8.4 Calculated Mean Experimental Heat Transfer Coefficients

Table A8.13. Heat transfer coefficients for test run number 1.

$\overline{U}_{i,TS}$ TS2 $(W/m^2 °C)$	$\overline{U}_{i,TS}$ TS3 $(W/m^2 °C)$	$\overline{U}_{i,TS}$ TS4 $(W/m^2 °C)$	$\overline{\alpha}_{c,TS}$ TS2 $(W/m^2 °C)$	$\overline{\alpha}_{c,TS}$ TS3 $(W/m^2 °C)$	$\overline{\alpha}_{c,TS}$ TS4 $(W/m^2 °C)$	$\overline{\alpha}_{w,TS}$ TS2 $(W/m^2 °C)$	$\overline{\alpha}_{w,TS}$ TS3 $(W/m^2 °C)$	$\overline{\alpha}_{w,TS}$ TS4 $(W/m^2 °C)$	$\overline{\alpha}_{f,i,TS}$ TS2 $(W/m^2 °C)$	$\overline{\alpha}_{f,i,TS}$ TS3 $(W/m^2 °C)$	$\overline{\alpha}_{f,i,TS}$ TS4 $(W/m^2 °C)$
939.47	649.58	578.03	8723.28	8898.28	8999.22	84526.7	84557.8	84595.6	1017.14	685.13	581.34
942.46	695.06	529.87	8745.53	8920.98	9029.37	84526.7	84557.8	84595.6	1020.46	735.82	532.65
936.53	696.21	580.80	8749.28	8925.05	9033.65	84526.7	84557.8	84595.6	1013.48	737.09	584.14
937.09	690.12	581.14	8753.44	8929.30	9037.95	84526.7	84557.8	84595.6	1014.10	730.25	584.49

(TS2=top test section, TS3 =middle test section, TS4=bottom test section)

Table A8.14. Heat transfer coefficients for test run number 2.

$\overline{U}_{i,TS}$ TS2 *(W/m² °C)*	$\overline{U}_{i,TS}$ TS3 *(W/m² °C)*	$\overline{U}_{i,TS}$ TS4 *(W/m² °C)*	$\overline{\alpha}_{c,TS}$ TS2 *(W/m² °C)*	$\overline{\alpha}_{c,TS}$ TS3 *(W/m² °C)*	$\overline{\alpha}_{c,TS}$ TS4 *(W/m² °C)*	$\overline{\alpha}_{w,TS}$ TS2 *(W/m² °C)*	$\overline{\alpha}_{w,TS}$ TS3 *(W/m² °C)*	$\overline{\alpha}_{w,TS}$ TS4 *(W/m² °C)*	$\overline{\alpha}_{f,i,TS}$ TS2 *(W/m² °C)*	$\overline{\alpha}_{f,i,TS}$ TS3 *(W/m² °C)*	$\overline{\alpha}_{f,i,TS}$ TS4 *(W/m² °C)*
858.45	729.88	688.57	8862.82	9027.78	9146.42	84508.9	84542.2	84580.0	921.89	774.46	693.28
857.91	686.78	688.17	8866.23	9031.03	9142.17	84508.9	84542.2	84582.2	921.24	726.10	692.87
857.24	686.25	680.49	8860.73	9025.42	9136.49	84511.1	84544.4	84582.2	920.51	725.53	685.09
858.41	681.00	737.85	8870.36	9035.23	9146.42	84511.1	84544.4	84582.2	921.79	719.63	743.25

(TS2=top test section, TS3 =middle test section, TS4=bottom test section)

Table A8.15. Heat transfer coefficients for test run number 3.

$\overline{U}_{i,TS}$ TS2 ($W/m^2\,°C$)	$\overline{U}_{i,TS}$ TS3 ($W/m^2\,°C$)	$\overline{U}_{i,TS}$ TS4 ($W/m^2\,°C$)	$\overline{\alpha}_{c,TS}$ TS2 ($W/m^2\,°C$)	$\overline{\alpha}_{c,TS}$ TS3 ($W/m^2\,°C$)	$\overline{\alpha}_{c,TS}$ TS4 ($W/m^2\,°C$)	$\overline{\alpha}_{w,TS}$ TS2 ($W/m^2\,°C$)	$\overline{\alpha}_{w,TS}$ TS3 ($W/m^2\,°C$)	$\overline{\alpha}_{w,TS}$ TS4 ($W/m^2\,°C$)	$\overline{\alpha}_{f,i,TS}$ TS2 ($W/m^2\,°C$)	$\overline{\alpha}_{f,i,TS}$ TS3 ($W/m^2\,°C$)	$\overline{\alpha}_{f,i,TS}$ TS4 ($W/m^2\,°C$)
983.37	732.11	511.15	8886.26	9038.00	9130.99	84568.9	84591.1	84624.4	1067.30	776.92	513.73
981.80	730.95	510.33	8874.94	9026.50	9119.37	84568.9	84591.1	84624.4	1065.55	775.67	512.91
983.37	723.81	511.15	8886.26	9038.00	9130.99	84568.9	84591.1	84624.4	1067.30	767.58	513.73
965.72	716.26	504.98	8891.91	9043.75	9136.80	84568.9	84591.1	84624.4	1046.49	759.07	507.51

(TS2=top test section, TS3 =middle test section, TS4=bottom test section)

Table A8.16. Heat transfer coefficients for test run number 4.

$\overline{U}_{i,TS}$ TS2 ($W/m^2 °C$)	$\overline{U}_{i,TS}$ TS3 ($W/m^2 °C$)	$\overline{U}_{i,TS}$ TS4 ($W/m^2 °C$)	$\overline{\alpha}_{c,TS}$ TS2 ($W/m^2 °C$)	$\overline{\alpha}_{c,TS}$ TS3 ($W/m^2 °C$)	$\overline{\alpha}_{c,TS}$ TS4 ($W/m^2 °C$)	$\overline{\alpha}_{w,TS}$ TS2 ($W/m^2 °C$)	$\overline{\alpha}_{w,TS}$ TS3 ($W/m^2 °C$)	$\overline{\alpha}_{w,TS}$ TS4 ($W/m^2 °C$)	$\overline{\alpha}_{f,i,TS}$ TS2 ($W/m^2 °C$)	$\overline{\alpha}_{f,i,TS}$ TS3 ($W/m^2 °C$)	$\overline{\alpha}_{f,i,TS}$ TS4 ($W/m^2 °C$)
944.01	673.16	511.15	8854.76	9035.07	9141.96	84568.9	84600.0	84637.8	1021.36	710.87	513.74
977.52	672.62	505.47	8841.85	9029.30	9136.13	84568.9	84600.0	84637.8	1060.81	710.29	508.00
978.30	673.16	505.87	8847.49	9035.07	9141.96	84568.9	84600.0	84637.8	1061.68	710.87	508.41
977.52	672.62	505.47	8841.85	9029.30	9136.13	84568.9	84600.0	84637.8	1060.81	710.29	508.00

(TS2=top test section, TS3 =middle test section, TS4=bottom test section)

A8.5 Condensate film Properties

Table A8.17. Condensate properties for test run number 1

Test Condenser Measurements						Predictions of Nusselt Theory			Predictions of HTFS Method		
Re_f	Re_f	Re_f	Pr_f	Pr_f	Pr_f	$\overline{\alpha}_{f,i,TS}$	$\overline{\alpha}_{f,i,TS}$	$\overline{\alpha}_{f,i,TS}$	$\overline{\alpha}_{f,i,TS}$	$\overline{\alpha}_{f,i,TS}$	$\overline{\alpha}_{f,i,TS}$
TS2	TS3	TS4	TS2	TS3	TS4	TS2	TS3	TS4	TS2	TS3	TS4
(-)	(-)	(-)	(-)	(-)	(-)	(W/m^2 °C)	(W/m^2 °C)	(W/m^2 °C)	(W/m^2 °C)	(W/m^2 °C)	(W/m^2 °C)
189.52	299.94	386.63	9.1854	9.1854	9.1854	729.87	503.66	449.35	837.29	644.49	597.64
190.37	309.20	388.36	9.1795	9.1795	9.1795	729.07	500.55	447.10	836.76	641.96	595.75
190.68	309.71	396.93	9.1795	9.1795	9.1795	728.67	500.28	445.22	836.45	641.73	594.09
190.80	309.89	397.17	9.1795	9.1795	9.1795	728.53	500.17	445.13	836.33	641.65	594.01

(TS2=top test section, TS3 =middle test section, TS4=bottom test section)

Table A8.18. Condensate properties for test run number 2.

Test Condenser Measurements						Predictions of Nusselt Theory			Predictions of HTFS Method		
Ref	*Ref*	*Ref*	*Prf*	*Prf*	*Prf*	$\overline{\alpha}_{f,i,TS}$	$\overline{\alpha}_{f,i,TS}$	$\overline{\alpha}_{f,i,TS}$	$\overline{\alpha}_{f,i,TS}$	$\overline{\alpha}_{f,i,TS}$	$\overline{\alpha}_{f,i,TS}$
TS2	TS3	TS4	TS2	TS3	TS4	TS2	TS3	TS4	TS2	TS3	TS4
(-)	*(-)*	*(-)*	*(-)*	*(-)*	*(-)*	*(W/m² °C)*	*(W/m² °C)*	*(W/m² °C)*	*(W/m² °C)*	*(W/m² °C)*	*(W/m² °C)*
177.88	307.10	412.00	9.2091	9.2091	9.2091	744.26	504.78	441.85	848.24	645.14	590.73
177.77	298.83	403.67	9.2091	9.2091	9.2091	744.41	507.60	445.31	848.36	647.50	593.79
177.86	298.98	403.88	9.2032	9.2032	9.2032	744.59	507.72	445.42	848.60	647.69	593.96
178.10	299.39	412.51	9.2032	9.2032	9.2032	744.25	507.49	443.57	848.34	647.49	592.35

(TS2=top test section, TS3 =middle test section, TS4=bottom test section)

Table A8.19. Condensate properties for test run number 3.

Test Condenser Measurements						Predictions of Nusselt Theory			Predictions of HTFS Method		
Ref	Ref	Ref	Prf	Prf	Prf	$\overline{\alpha}_{f,i,TS}$	$\overline{\alpha}_{f,i,TS}$	$\overline{\alpha}_{f,i,TS}$	$\overline{\alpha}_{f,i,TS}$	$\overline{\alpha}_{f,i,TS}$	$\overline{\alpha}_{f,i,TS}$
TS2	TS3	TS4	TS2	TS3	TS4	TS2	TS3	TS4	TS2	TS3	TS4
(-)	(-)	(-)	(-)	(-)	(-)	(W/m^2 °C)	(W/m^2 °C)	(W/m^2 °C)	(W/m^2 °C)	(W/m^2 °C)	(W/m^2 °C)
165.63	268.06	331.04	9.1973	9.1973	9.1973	762.78	524.06	469.77	863.04	661.44	615.25
165.37	267.63	330.52	9.1973	9.1973	9.1973	763.18	524.34	470.01	863.35	661.67	615.47
165.84	268.40	331.47	9.1914	9.1914	9.1914	762.76	524.05	469.75	863.13	661.52	615.33
165.98	268.61	331.73	9.1914	9.1914	9.1914	762.56	523.91	469.63	862.97	661.40	615.22

(TS2=top test section, TS3 =middle test section, TS4=bottom test section)

Table A8.20. Condensate properties for test run number 4.

Test Condenser Measurements						Predictions of Nusselt Theory			Predictions of HTFS Method		
Ref	*Ref*	*Ref*	*Prf*	*Prf*	*Prf*	$\bar{\alpha}_{f,i,TS}$	$\bar{\alpha}_{f,i,TS}$	$\bar{\alpha}_{f,i,TS}$	$\bar{\alpha}_{f,i,TS}$	$\bar{\alpha}_{f,i,TS}$	$\bar{\alpha}_{f,i,TS}$
TS2	TS3	TS4	TS2	TS3	TS4	TS2	TS3	TS4	TS2	TS3	TS4
(-)	*(-)*	*(-)*	*(-)*	*(-)*	*(-)*	*(W/m² °C)*	*(W/m² °C)*	*(W/m² °C)*	*(W/m² °C)*	*(W/m² °C)*	*(W/m² °C)*
203.08	324.77	405.83	9.0523	9.0523	9.0523	719.73	495.65	444.07	831.60	639.68	594.82
211.04	332.63	413.64	9.0523	9.0523	9.0523	710.56	490.73	440.93	824.31	635.47	592.04
211.21	332.90	413.97	9.0523	9.0523	9.0523	710.37	490.60	440.82	824.16	635.36	591.94
211.04	332.63	413.64	9.0523	9.0523	9.0523	710.56	490.73	440.93	824.31	635.47	592.04

(TS2=top test section, TS3 =middle test section, TS4=bottom test section)

A8.6 Analysis over full Test Condenser Length

Table A8.21. Full length analysis for test run number 1.

$\dot{Q}_{c,TC}$	$\Delta T_{ln,TC}$	$\overline{U}_{i,TC}$	$\overline{\alpha}_{c,TC}$	$\overline{\alpha}_{w,TC}$	$T_{f,TC}$	$\dot{M}_{f,out,TC}$	Ref	Prf	Measured $\overline{\alpha}_{f,i,TC}$	Nusselt $\overline{\alpha}_{f,i,TC}$	HTFS $\overline{\alpha}_{f,i,TC}$
(W)	*(°C)*	*(W/m² °C)*	*(W/m² °C)*	*(W/m² °C)*	*(°C)*	*(kg/s)*	*(-)*	*(-)*	*(W/m² °C)*	*(W/m² °C)*	*(W/m² °C)*
1710.294	11.273	714.25	8925.40	84560.0	32.85	0.00562	365.399	9.3579	757.34	579.67	713.14
1715.757	11.375	710.14	8949.98	84560.0	32.92	0.00564	366.806	9.3537	752.61	579.09	712.73
1753.604	11.418	723.04	8955.92	84560.0	32.92	0.00576	374.897	9.3537	767.09	574.89	709.25
1754.648	11.418	723.47	8960.19	84560.0	32.92	0.00576	375.120	9.3537	767.55	574.78	709.15

Table A8.22. Full length analysis for test run number 2.

$\dot{Q}_{c,TC}$ (W)	$\Delta T_{\ln,TC}$ (°C)	$\overline{U}_{i,TC}$ (W/m^2 °C)	$\overline{\alpha}_{c,TC}$ (W/m^2 °C)	$\overline{\alpha}_{w,TC}$ (W/m^2 °C)	$T_{f,TC}$ (°C)	$\dot{M}_{f,out,TC}$ (kg/s)	Re_f (-)	Pr_f (-)	Measured $\overline{\alpha}_{f,i,TC}$ (W/m^2 °C)	Nusselt $\overline{\alpha}_{f,i,TC}$ (W/m^2 °C)	HTFS $\overline{\alpha}_{f,i,TC}$ (W/m^2 °C)
1831.853	11.563	745.83	9070.55	84543.7	32.36	0.00601	388.618	9.3889	792.24	566.72	701.91
1794.831	11.520	733.51	9070.04	84544.4	32.39	0.00589	381.006	9.3869	778.35	570.54	705.12
1793.438	11.621	726.53	9064.41	84545.9	32.46	0.00588	380.960	9.3826	770.53	570.72	705.34
1831.753	11.563	745.79	9076.12	84545.9	32.46	0.00601	389.099	9.3826	792.16	566.72	702.00

Table A8.23. Full length analysis for test run number 3.

$\dot{Q}_{c,TC}$ (W)	$\Delta T_{ln,TC}$ (°C)	$\overline{U}_{i,TC}$ (W/m² °C)	$\overline{\alpha}_{c,TC}$ (W/m² °C)	$\overline{\alpha}_{w,TC}$ (W/m² °C)	$T_{f,TC}$ (°C)	$\dot{M}_{f,out,TC}$ (kg/s)	Ref (-)	Prf (-)	Measured $\overline{\alpha}_{f,i,TC}$ (W/m² °C)	Nusselt $\overline{\alpha}_{f,i,TC}$ (W/m² °C)	HTFS $\overline{\alpha}_{f,i,TC}$ (W/m² °C)
1468.140	9.445	731.80	9061.32	84594.8	33.13	0.00484	315.844	9.3406	776.47	609.23	737.75
1465.804	9.445	730.64	9049.78	84594.8	33.13	0.00483	315.341	9.3406	775.21	609.55	738.01
1468.140	9.547	724.01	9061.32	84594.8	33.20	0.00484	316.050	9.3364	767.71	609.26	737.85
1469.308	9.547	724.59	9067.08	84594.8	33.20	0.00484	316.301	9.3364	768.33	609.10	737.72

Table A8.24. Full length analysis for test run number 4.

$\dot{Q}_{c,TC}$ (W)	$\Delta T_{ln,TC}$ (°C)	$\overline{U}_{i,TC}$ (W/m²°C)	$\overline{\alpha}_{c,TC}$ (W/m²°C)	$\overline{\alpha}_{w,TC}$ (W/m²°C)	$T_{f,TC}$ (°C)	$\dot{M}_{f,out,TC}$ (kg/s)	Ref (-)	Prf (-)	Measured $\overline{\alpha}_{f,i,TC}$ (W/m²°C)	Nusselt $\overline{\alpha}_{f,i,TC}$ (W/m²°C)	HTFS $\overline{\alpha}_{f,i,TC}$ (W/m²°C)
1743.570	11.723	700.21	9061.88	84602.2	35.02	0.00574	382.668	9.2256	741.00	575.89	712.07
1777.098	11.766	711.04	9054.32	84602.2	35.02	0.00585	390.027	9.2256	753.16	572.25	709.04
1778.516	11.766	711.61	9060.10	84602.2	35.02	0.00586	390.338	9.2256	753.78	572.09	708.91
1777.098	11.766	711.04	9054.32	84602.2	35.02	0.00585	390.027	9.2256	753.16	572.25	709.04

A8.7 Vapour Flooding Velocities in the Test Condenser

Table A8.25. Flooding calculations for test run number 1.

			Predicted Flooding Velocity	
		Actual Vapour Velocity	Conservative	Non-conservative
$\dot{M}_{v,in,TC}$	Re_v	$\dot{u}_{v,in,TC}$	$\dot{v}_v$	
(kg/s)	*(-)*	*(m/s)*	*(m/s)*	
0.00574	25592.1	7.4602	5.8660	9.3855
0.00576	25659.9	7.4517	5.8494	9.3590
0.00582	25939.0	7.5327	5.8214	9.3142
0.00589	26230.1	7.6173	5.8206	9.3130

Table A8.26. Flooding calculations for test run number 2.

			Predicted Flooding Velocity	
		Actual Vapour Velocity	Conservative	Non-conservative
$\dot{M}_{v,in,TC}$	Re_v	$\dot{u}_{v,in,TC}$	$\dot{v}_v$	
(kg/s)	*(-)*	*(m/s)*	*(m/s)*	
0.00595	26547.6	7.8572	5.8299	9.3278
0.00583	26013.1	7.6991	5.8558	9.3693
0.00582	25981.2	7.6604	5.8443	9.3509
0.00601	26811.0	7.9051	5.8172	9.3075

Table A8.27. Flooding calculations for test run number 3.

			Predicted Flooding Velocity	
		Actual Vapour Velocity	Conservative	Non-conservative
$\dot{M}_{v,in,TC}$	Re_v	$\dot{u}_{v,in,TC}$	$\dot{v}_v$	
(kg/s)	*(-)*	*(m/s)*	*(m/s)*	
0.00573	25539.2	7.5015	6.0875	9.7400
0.00578	25777.3	7.5715	6.0896	9.7434
0.00572	25521.2	7.4678	6.0745	9.7193
0.00579	25819.0	7.5550	6.0735	9.7176

Table A8.28. Flooding calculations for test run number 4.

			Predicted Flooding Velocity	
		Actual Vapour Velocity	Conservative	Non-conservative
$\dot{M}_{v,in,TC}$	Re_v	$\dot{u}_{v,in,TC}$	$\dot{v}_v$	
(kg/s)	*(-)*	*(m/s)*	*(m/s)*	
0.00586	25948.7	6.9378	5.5580	8.8929
0.00604	26710.1	7.1414	5.5348	8.8557
0.00592	26185.5	7.0012	5.5338	8.8541
0.00591	26164.6	6.9956	5.5348	8.8557

Appendix A9 First Binary Hydrocarbon Mixture Experimental Data and Data Analysis Calculations

A9.1. Test Data

Table A9.1. Data for test run number 1.

Boiler Measurements				Test Condenser Measurements										Dump Condenser Measurements			
$\dot{Q}$	T_v	P_v	$\dot{V}_c$	$T_{c,in}$ TS2	$T_{c,in}$ TS3	$T_{c,in}$ TS4	$T_{c,out}$	T_v TS2	T_v TS3	T_v TS4	$\overline{T}_w$ TS2	$\overline{T}_w$ TS3	$\overline{T}_w$ TS4	$\dot{V}_c$	$T_{c,in}$	$T_{c,out}$	T_f
(W)	*(°C)*	*(bara)*	*(l/min)*	*(°C)*	*(°C)*	*(°C)*	*(°C)*	*(°C)*	*(°C)*	*(°C)*	*(°C)*	*(°C)*	*(°C)*	*(l/min)*	*(°C)*	*(°C)*	*(°C)*
3160.1	71.4	0.957	6.084	31.8	34.2	35.4	36.2	65.4	66.1	67.3	33.8	35.0	36.5	2.885	28.6	32.7	28.2
3164.6	71.2	0.956	6.108	31.8	34.2	35.4	36.1	65.3	66.0	66.8	33.7	34.9	36.5	2.894	28.6	32.5	28.2
3168.7	71.2	0.960	6.108	31.7	34.1	35.4	36.1	65.2	65.9	67.2	33.7	34.9	36.5	2.893	28.6	32.5	28.2
3172.0	71.3	0.963	6.096	31.7	34.1	35.4	36.1	65.1	65.9	67.1	33.7	34.9	36.5	2.895	28.6	32.5	28.1
5710.1	86.8	1.448	6.127	36.3	40.0	42.3	44.1	80.1	80.8	82.1	39.2	41.5	44.6	2.881	32.9	41.0	43.4
5714.8	86.9	1.450	6.131	36.3	40.0	42.3	44.1	80.2	81.1	82.3	39.2	41.5	44.6	2.881	33.1	41.1	43.5
5722.2	86.6	1.447	6.135	36.3	39.9	42.2	44.0	80.0	80.7	82.2	39.1	41.4	44.5	2.880	32.9	40.9	42.4
5716.5	86.8	1.452	6.135	36.3	39.9	42.2	44.1	80.0	80.8	82.0	39.1	41.4	44.6	2.880	32.9	41.0	42.8

(TS2=top test section, TS3=middle test section, TS4=bottom test section)

Table A9.2. Data for test run number 2.

Boiler Measurements				Test Condenser Measurements										Dump Condenser Measurements			
$\dot{Q}$	T_v	P_v	$\dot{V}_c$	$T_{c,in}$ TS2	$T_{c,in}$ TS3	$T_{c,in}$ TS4	$T_{c,out}$	T_v TS2	T_v TS3	T_v TS4	$\overline{T}_w$ TS2	$\overline{T}_w$ TS3	$\overline{T}_w$ TS4	$\dot{V}_c$	$T_{c,in}$	$T_{c,out}$	T_f
(W)	*(°C)*	*(bara)*	*(l/min)*	*(°C)*	*(°C)*	*(°C)*	*(°C)*	*(°C)*	*(°C)*	*(°C)*	*(°C)*	*(°C)*	*(°C)*	*(l/min)*	*(°C)*	*(°C)*	*(°C)*
5798.2	89.2	1.529	6.069	36.0	40.0	42.5	44.5	82.3	83.1	84.2	39.0	41.3	44.6	2.875	32.9	40.1	32.9
5806.8	89.4	1.533	6.049	36.0	40.0	42.5	44.6	82.3	83.0	84.5	39.0	41.4	44.6	2.882	32.9	40.0	32.9
5797.2	89.4	1.536	6.065	36.0	40.0	42.5	44.6	82.5	83.1	84.4	39.0	41.3	44.7	2.871	32.9	40.1	32.9
5799.3	88.9	1.524	6.049	36.0	39.9	42.4	44.4	81.9	82.8	83.9	38.9	41.3	44.5	2.877	32.8	39.8	32.8
3140.0	74.5	1.068	6.061	30.2	33.2	34.9	36.0	68.1	68.5	69.5	32.5	34.0	35.8	2.902	27.2	28.2	25.0
3140.5	74.5	1.073	6.072	30.1	33.2	34.8	36.0	67.9	68.6	69.9	32.5	34.0	36.6	2.903	27.0	27.8	24.9
3144.9	74.7	1.075	6.049	30.1	33.1	34.8	36.0	68.0	68.6	69.6	32.5	34.0	36.6	2.901	27.0	27.9	24.8
3135.2	74.8	1.073	6.057	30.1	33.2	34.9	36.0	68.0	68.8	69.7	32.5	34.0	36.6	2.888	27.0	27.9	24.7

(TS2=top test section, TS3=middle test section, TS4=bottom test section)

Table A9.3. Data for test run number 3.

Boiler Measurements				Test Condenser Measurements										Dump Condenser Measurements			
$\dot{Q}$	T_v	P_v	$\dot{V}_c$	$T_{c,in}$ TS2	$T_{c,in}$ TS3	$T_{c,in}$ TS4	$T_{c,out}$	T_v TS2	T_v TS3	T_v TS4	$\overline{T}_w$ TS2	$\overline{T}_w$ TS3	$\overline{T}_w$ TS4	$\dot{V}_c$	$T_{c,in}$	$T_{c,out}$	T_f
(W)	*(°C)*	*(bara)*	*(l/min)*	*(°C)*	*(°C)*	*(°C)*	*(°C)*	*(°C)*	*(°C)*	*(°C)*	*(°C)*	*(°C)*	*(°C)*	*(l/min)*	*(°C)*	*(°C)*	*(°C)*
3092.4	73.4	1.019	6.108	30.7	33.5	35.0	35.9	67.1	67.8	68.9	32.9	34.1	36.4	2.895	27.7	29.4	25.9
3097.7	73.4	1.021	6.096	30.7	33.6	35.0	36.0	67.2	67.9	68.8	32.9	34.3	36.4	2.897	27.7	29.5	25.9
3069.3	73.4	1.020	6.100	30.7	33.6	35.0	35.9	66.9	67.7	68.7	32.9	34.3	36.3	2.891	27.8	29.3	26.0
3070.1	73.5	1.023	6.092	30.8	33.6	35.1	36.0	67.0	68.0	69.1	33.0	34.5	36.4	2.894	27.9	29.4	26.0
5834.1	90.1	1.546	6.092	36.7	40.8	43.3	45.1	83.1	83.9	85.2	39.8	42.3	45.7	2.875	33.9	41.1	34.1
5825.0	90.1	1.546	6.119	36.7	40.8	43.3	45.1	83.1	83.9	85.2	39.7	42.2	45.7	2.873	33.8	41.1	34.2
5813.1	89.9	1.538	6.111	36.7	40.8	43.2	45.1	83.0	83.8	85.1	39.7	42.2	45.7	2.884	33.8	41.0	34.1
5795.8	89.9	1.545	6.115	36.6	40.7	43.2	45.1	83.1	83.7	84.9	39.7	42.2	45.7	2.886	33.8	41.0	34.0

(TS2=top test section, TS3=middle test section, TS4=bottom test section)

A9.2 Heat Transfer Calculations

Table A9.4. Heat transfer results for test run number 1.

$\dot{Q}_{c,TS}$ TS2 (W)	$\dot{Q}_{c,TS}$ TS3 (W)	$\dot{Q}_{c,TS}$ TS4 (W)	$\dot{Q}_{c,TC}$ (W)	$\dot{Q}_{c,DC}$ (W)	$\dot{Q}_{c,T}$ (W)	$\dot{Q}_{c,T}/\dot{Q}$ (-)	$\Delta T_{ln,TS}$ TS2 (°C)	$\Delta T_{ln,TS}$ TS3 (°C)	$\Delta T_{ln,TS}$ TS4 (°C)
1011.726	505.272	336.654	1853.652	820.882	2674.534	0.846	32.385	31.296	31.498
1015.717	507.266	295.734	1818.717	783.275	2601.991	0.822	32.285	31.196	31.049
1015.767	549.564	295.734	1861.065	783.004	2644.069	0.834	32.285	31.145	31.449
1013.771	548.485	295.153	1857.409	783.545	2640.954	0.833	32.185	31.145	31.349
1567.353	972.599	760.352	3300.304	1616.059	4916.363	0.861	41.923	39.639	38.893
1568.376	973.234	760.848	3302.459	1595.953	4898.411	0.857	42.023	39.939	39.093
1526.983	973.915	761.380	3262.278	1595.554	4857.832	0.849	41.874	39.639	39.093
1526.983	973.915	803.679	3304.577	1615.498	4920.075	0.861	41.874	39.739	38.842

(TS2=top test section, TS3=middle test section, TS4=bottom test section)

Table A9.5. Heat transfer results for test run number 2.

$\dot{Q}_{c,TS}$ TS2 (W)	$\dot{Q}_{c,TS}$ TS3 (W)	$\dot{Q}_{c,TS}$ TS4 (W)	$\dot{Q}_{c,TC}$ (W)	$\dot{Q}_{c,DC}$ (W)	$\dot{Q}_{c,T}$ (W)	$\dot{Q}_{c,T}/\dot{Q}$ (-)	$\Delta T_{ln,TS}$ TS2 (°C)	$\Delta T_{ln,TS}$ TS3 (°C)	$\Delta T_{ln,TS}$ TS4 (°C)
1678.636	1047.166	836.761	3562.562	1433.505	4996.068	0.862	44.270	41.838	40.692
1673.104	1043.715	875.704	3592.522	1417.037	5009.560	0.863	44.270	41.738	40.941
1677.529	1046.476	878.020	3602.025	1431.511	5033.536	0.868	44.470	41.838	40.841
1631.276	1043.764	834.042	3509.082	1394.723	4903.805	0.846	43.921	41.637	40.492
1260.871	713.442	461.260	2435.573	201.537	2637.109	0.840	36.379	34.443	34.047
1305.329	672.694	504.130	2482.153	161.301	2643.454	0.842	36.228	34.594	34.497
1258.437	712.064	502.220	2472.721	181.339	2654.060	0.844	36.379	34.643	34.196
1302.104	712.971	460.955	2476.031	180.526	2656.557	0.847	36.328	34.743	34.247

(TS2=top test section, TS3=middle test section, TS4=bottom test section)

Table A9.6. Heat transfer results for test run number 3.

$\dot{Q}_{c,TS}$ TS2 (W)	$\dot{Q}_{c,TS}$ TS3 (W)	$\dot{Q}_{c,TS}$ TS4 (W)	$\dot{Q}_{c,TC}$ (W)	$\dot{Q}_{c,DC}$ (W)	$\dot{Q}_{c,T}$ (W)	$\dot{Q}_{c,T}/\dot{Q}$ (-)	$\Delta T_{ln,TS}$ TS2 (°C)	$\Delta T_{ln,TS}$ TS3 (°C)	$\Delta T_{ln,TS}$ TS4 (°C)
1185.645	634.297	380.302	2200.244	341.700	2541.944	0.822	34.981	33.544	33.448
1225.577	590.819	421.728	2238.124	362.050	2600.173	0.839	35.030	33.595	33.297
1226.381	591.206	379.804	2197.392	301.068	2498.460	0.814	34.730	33.395	33.248
1182.481	632.605	379.288	2194.373	301.365	2495.739	0.813	34.781	33.644	33.548
1726.546	1050.742	755.661	3532.948	1432.810	4965.758	0.851	44.318	41.838	40.993
1734.198	1055.399	759.010	3548.606	1451.769	5000.376	0.858	44.318	41.838	40.993
1731.930	1011.858	800.166	3543.955	1437.364	4981.319	0.857	44.218	41.789	40.943
1733.147	1054.758	800.690	3588.595	1438.361	5026.956	0.867	44.418	41.738	40.743

(TS2=top test section, TS3=middle test section, TS4=bottom test section)

A9.3 Mean Experimental Heat Transfer Coefficients

Table A9.7. Heat transfer coefficients for test run number 1.

$\overline{U}_{i,TS}$ TS2 ($W/m^2\,°C$)	$\overline{U}_{i,TS}$ TS3 ($W/m^2\,°C$)	$\overline{U}_{i,TS}$ TS4 ($W/m^2\,°C$)	$\overline{\alpha}_{c,TS}$ TS2 ($W/m^2\,°C$)	$\overline{\alpha}_{c,TS}$ TS3 ($W/m^2\,°C$)	$\overline{\alpha}_{c,TS}$ TS4 ($W/m^2\,°C$)	$\overline{\alpha}_{w,TS}$ TS2 ($W/m^2\,°C$)	$\overline{\alpha}_{w,TS}$ TS3 ($W/m^2\,°C$)	$\overline{\alpha}_{w,TS}$ TS4 ($W/m^2\,°C$)	$\overline{\alpha}_{cs,i,TS}$ TS2 ($W/m^2\,°C$)	$\overline{\alpha}_{cs,i,TS}$ TS3 ($W/m^2\,°C$)	$\overline{\alpha}_{cs,i,TS}$ TS4 ($W/m^2\,°C$)
439.763	227.267	150.452	11011.87	11204.15	11299.23	84751.1	84777.8	84811.1	452.99	230.70	150.67
442.866	228.895	134.079	11046.60	11239.49	11334.87	84748.9	84775.6	84811.1	456.25	232.37	134.26
442.887	248.385	132.373	11038.51	11231.51	11334.87	84748.9	84775.6	84811.1	456.28	252.48	132.55
443.391	247.897	132.535	11021.15	11213.85	11317.05	84748.9	84775.6	84811.1	456.83	251.98	132.71
526.282	345.394	275.198	11434.32	11723.12	11899.33	84871.1	84922.2	84991.1	544.72	353.07	275.94
525.371	343.022	273.968	11440.30	11729.25	11905.55	84871.1	84922.2	84991.1	543.73	350.59	274.71
513.321	345.861	274.160	11446.27	11727.64	11904.14	84868.9	84920.0	84988.9	530.83	353.56	274.90
513.321	344.990	291.259	11446.27	11727.64	11904.14	84868.9	84920.0	84991.1	530.83	352.65	292.09

(TS2=top test section, TS3=middle test section, TS4=bottom test section)

Table A9.8. Heat transfer coefficients for test run number 2.

$\overline{U}_{i,TS}$ TS2 *(W/m² °C)*	$\overline{U}_{i,TS}$ TS3 *(W/m² °C)*	$\overline{U}_{i,TS}$ TS4 *(W/m² °C)*	$\overline{\alpha}_{c,TS}$ TS2 *(W/m² °C)*	$\overline{\alpha}_{c,TS}$ TS3 *(W/m² °C)*	$\overline{\alpha}_{c,TS}$ TS4 *(W/m² °C)*	$\overline{\alpha}_{w,TS}$ TS2 *(W/m² °C)*	$\overline{\alpha}_{w,TS}$ TS3 *(W/m² °C)*	$\overline{\alpha}_{w,TS}$ TS4 *(W/m² °C)*	$\overline{\alpha}_{cs,i,TS}$ TS2 *(W/m² °C)*	$\overline{\alpha}_{cs,i,TS}$ TS3 *(W/m² °C)*	$\overline{\alpha}_{cs,i,TS}$ TS4 *(W/m² °C)*
533.765	352.331	289.465	11324.12	11634.26	11824.22	84866.7	84917.8	84991.1	552.90	360.38	290.29
532.006	352.012	301.093	11294.26	11603.58	11793.04	84866.7	84920.0	84991.1	551.06	360.06	301.98
531.012	352.099	302.629	11318.15	11628.12	11817.99	84866.7	84917.8	84993.3	549.96	360.14	303.53
522.824	352.874	289.950	11294.26	11595.94	11785.52	84864.4	84917.8	84988.9	541.21	360.97	290.78
487.885	291.581	190.708	10849.18	11090.72	11225.63	84722.2	84755.6	84795.6	504.44	297.30	191.07
507.199	273.729	205.716	10856.79	11106.82	11234.02	84722.2	84755.6	84813.3	525.10	278.76	206.13
486.943	289.338	206.735	10823.88	11065.18	11199.96	84722.2	84755.6	84813.3	503.47	294.98	207.16
504.553	288.872	189.469	10835.33	11084.86	11219.70	84722.2	84755.6	84813.3	522.30	294.49	189.82

(TS2=top test section, TS3=middle test section, TS4=bottom test section)

Table A9.9. Heat transfer coefficients for test run number 3.

$\overline{U}_{i,TS}$ TS2 *(W/m² °C)*	$\overline{U}_{i,TS}$ TS3 *(W/m² °C)*	$\overline{U}_{i,TS}$ TS4 *(W/m² °C)*	$\overline{\alpha}_{c,TS}$ TS2 *(W/m² °C)*	$\overline{\alpha}_{c,TS}$ TS3 *(W/m² °C)*	$\overline{\alpha}_{c,TS}$ TS4 *(W/m² °C)*	$\overline{\alpha}_{w,TS}$ TS2 *(W/m² °C)*	$\overline{\alpha}_{w,TS}$ TS3 *(W/m² °C)*	$\overline{\alpha}_{w,TS}$ TS4 *(W/m² °C)*	$\overline{\alpha}_{cs,i,TS}$ TS2 *(W/m² °C)*	$\overline{\alpha}_{cs,i,TS}$ TS3 *(W/m² °C)*	$\overline{\alpha}_{cs,i,TS}$ TS4 *(W/m² °C)*
477.112	266.179	160.052	10957.25	11183.52	11303.16	84731.1	84757.8	84808.9	492.79	270.91	160.30
492.496	247.560	178.288	10940.02	11173.94	11285.39	84731.1	84762.2	84808.9	509.25	251.65	178.60
497.078	249.206	160.804	10945.77	11179.81	11291.31	84731.1	84762.2	84806.7	514.14	253.35	161.06
478.576	264.680	159.149	10942.41	11168.07	11287.38	84733.3	84766.7	84808.9	494.37	269.36	159.40
548.398	353.534	259.486	11413.44	11730.81	11920.41	84884.4	84940.0	85015.6	568.48	361.58	260.15
550.829	355.101	260.636	11453.89	11772.39	11962.65	84882.2	84937.8	85015.6	571.03	363.19	261.30
551.353	340.851	275.110	11441.91	11760.07	11942.59	84882.2	84937.8	85015.6	571.61	348.31	275.85
549.255	355.736	276.642	11440.03	11758.56	11948.85	84882.2	84937.8	85015.6	569.36	363.86	277.39

(TS2=top test section, TS3=middle test section, TS4=bottom test section)

A9.4 Mass Balance Calculations across Test and Dump Condensers

Table A9.10. Material flows for test run number 1.

							TASC Predictions	
$\dot{M}_{v,in,TC}$ (kg/s)	$\tilde{y}_{P,in,TC}$ (moles/mole)	$\dot{M}_{f,out,DC}$ (kg/s)	$\tilde{x}_{P,out,DC}$ (moles/mole)	$\dot{M}_{f,out,TC}$ (kg/s)	$\tilde{x}_{P,out,TC}$ (moles/mole)	$\tilde{y}^{*}_{P,out,TC}$ (moles/mole)	ε (-)	$\tilde{x}_{P,out,DC}$ (moles/mole)	$T_{v,out,TC}$ (°C)
0.00764	0.4939	0.00206	0.75047	0.00557	0.38109	0.8246	0.7758	0.8016	53.10
0.00743	0.4919	0.00197	0.75047	0.00546	0.38109	0.8251	0.7761	0.8021	52.80
0.00757	0.4900	0.00197	0.75047	0.00560	0.38109	0.8252	0.7770	0.8032	52.60
0.00755	0.4903	0.00197	0.75047	0.00558	0.38109	0.8251	0.7772	0.8033	52.70
0.01412	0.5121	0.00422	0.71895	0.00990	0.41016	0.8202	0.6714	0.7881	69.30
0.01408	0.5111	0.00417	0.71895	0.00991	0.41016	0.8202	0.6725	0.7874	69.40
0.01395	0.5115	0.00415	0.71895	0.00980	0.41016	0.8205	0.6712	0.7880	69.10
0.01412	0.5118	0.00421	0.71895	0.00991	0.41016	0.8202	0.6716	0.7881	69.30

Table A9.11. Material flows for test run number 2.

							TASC Predictions		
$\dot{M}_{v,in,TC}$ (kg/s)	$\tilde{y}_{P,in,TC}$ (moles/mole)	$\dot{M}_{f,out,DC}$ (kg/s)	$\tilde{x}_{P,out,DC}$ (moles/mole)	$\dot{M}_{f,out,TC}$ (kg/s)	$\tilde{x}_{P,out,TC}$ (moles/mole)	$\tilde{y}^{*}_{P,out,TC}$ (moles/mole)	ε (-)	$\tilde{x}_{P,out,DC}$ (moles/mole)	$T_{v,out,TC}$ (℃)
0.01411	0.5268	0.00353	0.71047	0.01057	0.45759	0.8461	0.5754	0.8142	70.00
0.01416	0.5257	0.00349	0.71047	0.01067	0.45759	0.8459	0.5771	0.8146	70.10
0.01422	0.5261	0.00353	0.71047	0.01069	0.45759	0.8459	0.5766	0.8146	70.10
0.01386	0.5262	0.00344	0.71047	0.01041	0.45759	0.8465	0.5753	0.8151	69.60
0.00761	0.5201	0.00050	0.74258	0.00712	0.50278	0.8871	0.6061	0.8793	49.80
0.00768	0.5166	0.00040	0.74258	0.00729	0.50278	0.8873	0.6096	0.8817	49.40
0.00768	0.5183	0.00045	0.74258	0.00724	0.50278	0.8870	0.6083	0.8803	49.80
0.00769	0.5182	0.00044	0.74258	0.00725	0.50278	0.8869	0.6086	0.8802	49.90

Table A9.12. Material flows for test run number 3.

							TASC Predictions		
$\dot{M}_{v,in,TC}$ (kg/s)	$\tilde{y}_{P,in,TC}$ (moles/mole)	$\dot{M}_{f,out,DC}$ (kg/s)	$\tilde{x}_{P,out,DC}$ (moles/mole)	$\dot{M}_{f,out,TC}$ (kg/s)	$\tilde{x}_{P,out,TC}$ (moles/mole)	$\tilde{y}^{*}_{P,out,TC}$ (moles/mole)	ε (-)	$\tilde{x}_{P,out,DC}$ (moles/mole)	$T_{v,out,TC}$ (°C)
0.00728	0.5787	0.00088	0.66434	0.00640	0.56639	0.9111	0.2577	0.8939	49.80
0.00744	0.5791	0.00093	0.66434	0.00651	0.56639	0.9111	0.2567	0.8932	49.90
0.00716	0.5774	0.00077	0.66434	0.00639	0.56639	0.9112	0.2604	0.8960	49.50
0.00716	0.5774	0.00077	0.66434	0.00639	0.56639	0.9111	0.2605	0.8959	49.60
0.01404	0.5387	0.00355	0.70588	0.01049	0.47558	0.8545	0.5295	0.8208	70.80
0.01413	0.5391	0.00360	0.70588	0.01053	0.47558	0.8544	0.5289	0.8211	70.80
0.01409	0.5387	0.00356	0.70588	0.01053	0.47558	0.8547	0.5291	0.8222	70.50
0.01421	*0.5381*	*0.00356*	*0.70588*	*0.01065*	*0.47558*	*0.8547*	*0.5298*	*0.8208*	70.60

A9.5 Analysis over full Test Condenser Length

Table A9.13. Full length analysis for test run number 1.

$\dot{Q}_{c,TC}$ (W)	$\Delta T_{ln,TC}$ (°C)	$\overline{U}_{i,TC}$ (W/m²°C)	$\overline{\alpha}_{c,TC}$ (W/m²°C)	$\overline{\alpha}_{w,TC}$ (W/m²°C)	$\overline{\alpha}_{cs,i,TC}$ (W/m²°C)	Ref (-)	Prf (-)	$\overline{\alpha}_{f,i,TC}$ By HTFS (W/m²°C)	Corrected $\overline{\alpha}_{f,i,TC}$ (W/m²°C)	$\overline{\alpha}_{v,eff,i,TC}$ (W/m²°C)
1853.652	34.394	252.888	11188.23	84811.1	257.149	549.446	6.9579	796.56	853.51	368.03
1818.717	34.294	248.846	11219.53	84811.1	252.960	536.512	6.9688	800.10	856.23	359.03
1861.065	34.294	254.640	11215.53	84811.1	258.951	551.723	6.9601	795.69	852.76	371.87
1857.409	34.292	254.152	11197.90	84811.1	258.452	549.580	6.9623	796.24	853.18	370.77
3300.304	43.248	358.073	11738.55	84991.1	366.321	1115.602	6.4960	708.51	800.77	675.20
3302.459	43.348	357.480	11744.68	84991.1	365.697	1118.255	6.4925	708.34	800.77	673.08
3262.278	43.148	354.768	11746.95	84988.9	362.858	1105.026	6.4951	710.05	801.74	662.86
3304.577	43.198	358.948	11750.81	84991.1	367.230	1115.688	6.4978	708.39	800.65	678.38

Table A9.14. Full length analysis for test run number 2.

$\dot{Q}_{c,TC}$ (W)	$\Delta T_{\ln,TC}$ (°C)	$\overline{U}_{i,TC}$ (W/m²°C)	$\overline{\alpha}_{c,TC}$ (W/m²°C)	$\overline{\alpha}_{w,TC}$ (W/m²°C)	$\overline{\alpha}_{cs,i,TC}$ (W/m²°C)	Ref (-)	Prf (-)	$\overline{\alpha}_{f,i,TC}$ By HTFS (W/m²°C)	Corrected $\overline{\alpha}_{f,i,TC}$ (W/m²°C)	$\overline{\alpha}_{v,eff,i,TC}$ (W/m²°C)
3562.562	45.495	367.432	11653.39	84991.1	376.177	1238.371	6.3009	706.85	807.90	703.95
3592.522	45.546	370.110	11626.47	84991.1	379.003	1251.557	6.2960	705.48	807.30	714.38
3602.025	45.645	370.286	11651.06	84993.3	379.170	1254.064	6.2969	705.12	807.07	715.16
3509.082	45.196	364.309	11618.84	84988.9	372.927	1217.244	6.3066	709.22	809.05	691.82
2435.573	38.199	299.176	11082.74	84795.6	305.207	760.783	6.4680	780.54	853.45	475.11
2482.153	38.149	305.300	11094.83	84813.3	311.576	782.722	6.4533	776.57	850.88	491.59
2472.721	38.299	302.951	11061.19	84813.3	309.147	775.834	6.4590	777.73	851.60	485.33
2476.031	38.348	302.964	11072.89	84813.3	309.155	777.291	6.4571	777.53	851.49	485.38

Table A9.15. Full length analysis for test run number 3.

$\dot{Q}_{c,TC}$ (W)	$\Delta T_{ln,TC}$ (°C)	$\overline{U}_{i,TC}$ (W/m² °C)	$\overline{\alpha}_{c,TC}$ (W/m² °C)	$\overline{\alpha}_{w,TC}$ (W/m² °C)	$\overline{\alpha}_{cs,i,TC}$ (W/m² °C)	Ref (-)	Prf (-)	$\overline{\alpha}_{f,i,TC}$ By HTFS (W/m² °C)	Corrected $\overline{\alpha}_{f,i,TC}$ (W/m² °C)	$\overline{\alpha}_{v,eff,i,TC}$ (W/m² °C)
2200.244	36.947	279.428	11167.49	84808.9	284.647	711.568	6.2176	815.19	887.18	419.12
2238.124	36.948	284.231	11153.94	84808.9	289.639	722.935	6.2193	812.20	884.89	430.57
2197.392	36.846	279.831	11155.79	84806.7	285.070	708.504	6.2219	815.67	887.44	419.98
2194.373	36.846	279.447	11152.08	84808.9	284.673	710.920	6.2140	815.59	887.56	419.09
3532.948	45.696	362.774	11738.45	85015.6	371.242	1252.629	6.2146	711.47	814.24	682.35
3548.606	45.696	364.381	11780.06	85015.6	372.900	1258.181	6.2146	710.78	813.85	688.25
3543.955	45.546	365.107	11767.73	85015.6	373.667	1256.795	6.2161	710.86	813.84	690.88
3588.595	45.645	368.905	11770.06	85015.6	377.645	1269.544	6.2193	709.09	812.75	705.42

A9.6 Measured and Calculated Gas-side Heat Transfer Coefficients

Table A9.16. Mean gas-side heat transfer coefficients for test run number 1.

Measured	Predicted dry-gas values		Using dry-gas values		Using dry-gas values with Silver's method		Using measured value with Silver's method	
$\overline{\alpha}_{v,i,TC}$	$\overline{\alpha}_{v,i,TC}$ Without θ	$\overline{\alpha}_{v,i,TC}$ With θ	$\overline{\alpha}_{v,eff,i,TC}$ Without θ	$\overline{\alpha}_{v,eff,i,TC}$ With θ	$\overline{\alpha}_{v,eff,i,TC}$ Without θ	$\overline{\alpha}_{v,eff,i,TC}$ With θ	$\overline{\alpha}_{v,eff,i,TC}$ Without θ	$\overline{\alpha}_{v,eff,i,TC}$ With θ
$(W/m^2 ℃)$	$(W/m^2 ℃)$	$(W/m^2 ℃)$	$(W/m^2 ℃)$	$(W/m^2 ℃)$	$(W/m^2 ℃)$	$(W/m^2 ℃)$	$(W/m^2 ℃)$	$(W/m^2 ℃)$
11.007	21.453	5.404	717.307	180.685	268.309	176.070	137.662	57.812
10.421	20.904	5.226	720.175	180.059	271.680	180.268	135.441	56.681
10.887	21.152	5.176	722.519	176.798	262.519	173.166	135.116	57.550
11.223	21.131	5.187	698.097	171.353	262.026	172.988	139.166	61.133
25.033	37.516	8.561	1011.891	230.898	365.409	223.507	243.825	113.814
24.819	37.376	8.454	1013.602	229.271	364.736	222.492	242.202	112.112
24.149	37.090	8.449	1018.073	231.918	361.925	221.262	235.647	107.639
25.466	37.483	8.530	998.514	227.234	365.315	223.264	248.191	117.440

Table A9.17. Mean gas-side heat transfer coefficients for test run number 2.

Measured	Predicted dry-gas values		Using dry-gas values		Using dry-gas values with Silver's method		Using measured value with Silver's method	
$\overline{\alpha}_{v,i,TC}$	$\overline{\alpha}_{v,i,TC}$ Without θ	$\overline{\alpha}_{v,i,TC}$ With θ	$\overline{\alpha}_{v,eff,i,TC}$ Without θ	$\overline{\alpha}_{v,eff,i,TC}$ With θ	$\overline{\alpha}_{v,eff,i,TC}$ Without θ	$\overline{\alpha}_{v,eff,i,TC}$ With θ	$\overline{\alpha}_{v,eff,i,TC}$ Without θ	$\overline{\alpha}_{v,eff,i,TC}$ With θ
(W/m^2 °C)	*(W/m^2 °C)*	*(W/m^2 °C)*	*(W/m^2 °C)*	*(W/m^2 °C)*	*(W/m^2 °C)*	*(W/m^2 °C)*	*(W/m^2 °C)*	*(W/m^2 °C)*
24.115	36.642	7.034	1069.599	205.315	438.347	266.514	288.496	131.825
25.003	36.683	6.932	1048.120	198.065	437.656	264.936	298.299	139.442
24.386	36.835	6.985	1080.250	204.846	439.001	266.007	290.632	132.747
23.914	36.036	6.909	1042.517	199.861	438.764	266.673	291.164	133.913
9.732	18.784	2.173	917.008	106.070	205.689	135.292	106.570	45.399
10.153	18.729	2.025	906.856	98.039	204.417	135.537	110.810	50.009
10.280	18.830	2.098	888.951	99.059	198.175	129.500	108.196	47.727
10.430	18.844	2.096	876.980	97.534	198.332	129.559	109.772	48.985

Table A9.18. Mean gas-side heat transfer coefficients for test run number 3.

Measured	Predicted dry-gas values		Using dry-gas values		Using dry-gas values with Silver's method		Using measured value with Silver's method	
$\overline{\alpha}_{v,i,TC}$	$\overline{\alpha}_{v,i,TC}$ Without θ	$\overline{\alpha}_{v,i,TC}$ With θ	$\overline{\alpha}_{v,eff,i,TC}$ Without θ	$\overline{\alpha}_{v,eff,i,TC}$ With θ	$\overline{\alpha}_{v,eff,i,TC}$ Without θ	$\overline{\alpha}_{v,eff,i,TC}$ With θ	$\overline{\alpha}_{v,eff,i,TC}$ Without θ	$\overline{\alpha}_{v,eff,i,TC}$ With θ
(W/m² °C)	*(W/m² °C)*	*(W/m² °C)*	*(W/m² °C)*	*(W/m² °C)*	*(W/m² °C)*	*(W/m² °C)*	*(W/m² °C)*	*(W/m² °C)*
9.391	18.831	2.831	840.435	126.367	213.805	142.319	106.623	44.952
9.575	19.219	2.915	864.279	131.065	209.876	139.936	104.557	44.201
9.454	18.415	2.650	818.067	117.734	208.774	137.791	107.180	45.595
9.455	18.430	2.652	816.878	117.546	208.875	137.854	107.161	45.556
23.912	36.668	7.120	1046.361	203.172	443.172	270.311	289.002	131.695
24.209	36.909	7.195	1049.285	204.546	436.541	266.561	286.338	131.372
23.867	36.756	7.124	1063.978	206.217	435.625	265.573	282.866	128.314
23.877	36.954	7.082	1091.758	209.219	436.461	265.244	282.010	126.712

A9.7 Vapour Flooding Velocities in the Test Condenser

Table A9.19. Flooding calculations for test run number 1.

			Predicted Flooding Velocity	
		Actual Vapour Velocity	Conservative	Non-conservative
$\dot{M}_{v,in,TC}$	Re_V	$\dot{u}_{v,in,TC}$	$\dot{v}_v$	
(kg/s)	*(-)*	*(m/s)*	*(m/s)*	
0.00764	28950.5	1.8120	1.9149	3.0639
0.00743	28189.6	1.7777	1.9329	3.0927
0.00757	28728.3	1.8176	1.9246	3.0793
0.00755	28653.7	1.8065	1.9225	3.0760
0.01412	50929.3	2.0589	1.3055	2.0887
0.01408	50773.0	2.0493	1.3036	2.0857
0.01395	50345.0	2.0461	1.3122	2.0994
0.01412	50906.7	2.0577	1.3054	2.0886

Table A9.20. Flooding calculations for test run number 2.

			Predicted Flooding Velocity	
		Actual Vapour Velocity	Conservative	Non-conservative
$\dot{M}_{v,in,TC}$	Re_V	$\dot{u}_{v,in,TC}$	$\dot{v}_v$	
(kg/s)	*(-)*	*(m/s)*	*(m/s)*	
0.01411	50397.6	1.8855	1.2507	2.0012
0.01416	50559.9	1.8839	1.2450	1.9920
0.01422	50765.1	1.8920	1.2445	1.9913
0.01386	49552.3	1.8703	1.2617	2.0188
0.00761	28496.3	1.5902	1.7795	2.8472
0.00768	28771.3	1.6122	1.7727	2.8363
0.00768	28742.3	1.5983	1.7685	2.8297
0.00769	28758.7	1.5943	1.7648	2.8237

Table A9.21. Flooding calculations for test run number 3.

			Predicted Flooding Velocity	
		Actual Vapour Velocity	Conservative	Non-conservative
$\dot{M}_{v,in,TC}$	Re_V	$\dot{u}_{v,in,TC}$	$\dot{v}_v$	
(kg/s)	*(-)*	*(m/s)*	*(m/s)*	
0.00728	27143.2	1.4625	1.8239	2.9183
0.00744	27731.9	1.4929	1.8167	2.9067
0.00716	26696.6	1.4407	1.8272	2.9235
0.00716	26703.2	1.4370	1.8230	2.9168
0.01404	49938.1	1.8039	1.2336	1.9738
0.01413	50274.1	1.8152	1.2321	1.9714
0.01409	50160.7	1.8206	1.2361	1.9778
0.01421	50588.6	1.8370	1.2337	1.9739

Appendix A10 Second Binary Hydrocarbon Mixture Experimental Data and Data Analysis Calculations

A10.1. Test Data

Table A10.1. Data for test run number 1.

Boiler Measurements				Test Condenser Measurements										Dump Condenser Measurements			
$\dot{Q}$	T_v	P_v	$\dot{V}_c$	$T_{c,in}$ TS2	$T_{c,in}$ TS3	$T_{c,in}$ TS4	$T_{c,out}$	T_v TS2	T_v TS3	T_v TS4	$\overline{T}_w$ TS2	$\overline{T}_w$ TS3	$\overline{T}_w$ TS4	$\dot{V}_c$	$T_{c,in}$	$T_{c,out}$	T_f
(W)	*(°C)*	*(bara)*	*(l/min)*	*(°C)*	*(°C)*	*(°C)*	*(°C)*	*(°C)*	*(°C)*	*(°C)*	*(°C)*	*(°C)*	*(°C)*	*(l/min)*	*(°C)*	*(°C)*	*(°C)*
3063.2	66.0	1.069	6.154	31.5	33.8	35.1	35.9	60.3	61.0	62.1	33.7	34.6	36.1	2.876	28.6	32.0	27.9
3063.6	65.9	1.069	6.166	31.5	33.8	35.0	35.8	60.2	60.8	61.9	33.7	34.6	36.1	2.880	28.5	31.9	27.9
3070.3	66.1	1.072	6.178	31.5	33.8	35.1	35.9	60.4	61.1	62.0	33.7	34.6	36.1	2.889	28.5	31.9	27.8
3062.9	66.1	1.073	6.189	31.5	33.8	35.1	35.9	60.4	61.1	62.2	33.7	34.6	36.1	2.869	28.5	32.0	27.8
5707.4	81.9	1.621	6.174	36.4	40.0	42.3	44.2	76.1	76.6	78.1	39.8	41.3	44.4	2.866	33.5	41.1	41.1
5713.1	81.9	1.625	6.154	36.4	40.0	42.3	44.2	76.1	76.7	78.0	39.8	41.4	44.4	2.867	33.3	41.1	41.1
5719.1	82.0	1.628	6.158	36.4	40.0	42.4	44.3	76.2	76.7	76.7	39.8	41.4	44.4	2.871	33.5	41.2	41.2
5710.6	81.8	1.625	6.174	36.4	40.0	42.3	44.2	76.1	76.6	77.8	39.8	41.4	44.4	2.867	33.4	41.0	40.4

(TS2=top test section, TS3=middle test section, TS4=bottom test section)

Table A10.2. Data for test run number 2.

Boiler Measurements				Test Condenser Measurements										Dump Condenser Measurements			
$\dot{Q}$	T_v	P_v	$\dot{V}_c$	$T_{c,in}$ TS2	$T_{c,in}$ TS3	$T_{c,in}$ TS4	$T_{c,out}$	T_v TS2	T_v TS3	T_v TS4	$\overline{T}_w$ TS2	$\overline{T}_w$ TS3	$\overline{T}_w$ TS4	$\dot{V}_c$	$T_{c,in}$	$T_{c,out}$	T_f
(W)	*(°C)*	*(bara)*	*(l/min)*	*(°C)*	*(°C)*	*(°C)*	*(°C)*	*(°C)*	*(°C)*	*(°C)*	*(°C)*	*(°C)*	*(°C)*	*(l/min)*	*(°C)*	*(°C)*	*(°C)*
3105.6	66.5	1.066	6.131	31.9	34.3	35.6	36.3	60.7	61.4	62.6	34.2	35.0	36.4	2.881	29.0	32.9	28.6
3103.5	66.3	1.063	6.135	31.9	34.3	35.5	36.2	60.3	61.1	62.2	34.1	34.9	36.4	2.879	28.9	32.8	28.5
3100.3	66.5	1.065	6.127	31.8	34.2	35.4	36.2	60.6	61.2	62.3	34.1	34.9	36.3	2.880	28.9	32.7	28.4
3104.3	66.4	1.065	6.139	31.8	34.1	35.4	36.1	60.5	61.4	62.6	34.0	34.9	36.3	2.876	28.8	32.7	28.3
5702.8	84.4	1.698	6.143	38.5	42.3	44.6	46.3	78.2	78.9	80.2	41.7	44.0	46.5	2.871	35.8	43.7	49.6
5708.7	84.5	1.699	6.135	38.5	42.2	44.5	46.3	78.4	78.9	80.4	41.7	43.9	46.5	2.862	35.9	43.6	49.7
5699.0	84.1	1.687	6.131	38.5	42.2	44.5	46.2	78.0	78.2	79.9	41.6	43.9	46.4	2.866	35.5	43.4	48.7
5685.5	84.3	1.695	6.123	38.4	42.1	44.4	46.2	78.2	78.3	79.7	41.6	43.9	46.4	2.855	35.5	43.5	48.9

(TS2=top test section, TS3=middle test section, TS4=bottom test section)

Table A10.3. Data for test run number 3.

Boiler Measurements				Test Condenser Measurements										Dump Condenser Measurements			
$\dot{Q}$	T_v	P_v	$\dot{V}_c$	$T_{c,in}$ TS2	$T_{c,in}$ TS3	$T_{c,in}$ TS4	$T_{c,out}$	T_v TS2	T_v TS3	T_v TS4	$\overline{T}_w$ TS2	$\overline{T}_w$ TS3	$\overline{T}_w$ TS4	$\dot{V}_c$	$T_{c,in}$	$T_{c,out}$	T_f
(W)	*(°C)*	*(bara)*	*(l/min)*	*(°C)*	*(°C)*	*(°C)*	*(°C)*	*(°C)*	*(°C)*	*(°C)*	*(°C)*	*(°C)*	*(°C)*	*(l/min)*	*(°C)*	*(°C)*	*(°C)*
3089.4	67.0	1.068	6.111	32.2	34.6	35.8	36.6	61.6	62.3	63.4	34.5	35.4	36.8	2.879	29.3	32.8	28.2
3087.4	67.1	1.069	6.100	32.2	34.6	35.8	36.6	61.9	62.5	63.7	34.5	35.4	36.8	2.879	29.2	32.8	28.2
3085.2	67.1	1.068	6.108	32.2	34.6	35.9	36.6	61.9	62.5	63.6	34.5	35.4	36.8	2.884	29.3	32.8	28.2
3083.9	67.0	1.067	6.108	32.3	34.6	35.8	36.5	61.7	62.3	63.4	34.5	35.4	36.8	2.882	29.3	32.8	28.3
5688.6	84.1	1.664	6.096	37.8	41.5	43.9	45.7	77.9	78.2	79.8	41.3	43.3	45.9	2.849	34.8	42.8	46.1
5697.4	83.9	1.664	6.100	37.8	41.5	43.8	45.7	78.0	78.7	80.0	41.2	43.3	45.9	2.851	34.9	42.8	46.0
5709.6	83.9	1.651	6.096	37.7	41.4	43.8	45.5	77.9	78.2	79.7	41.2	43.2	45.7	2.858	34.9	42.7	45.5
5721.1	83.7	1.658	6.100	37.7	41.4	43.7	45.5	77.7	78.0	79.6	41.1	43.2	45.7	2.854	34.9	42.5	45.1

(TS2=top test section, TS3=middle test section, TS4=bottom test section)

A10.2 Heat Transfer Calculations

Table A10.4. Heat transfer results for test run number 1.

$\dot{Q}_{c,TS}$ TS2 (W)	$\dot{Q}_{c,TS}$ TS3 (W)	$\dot{Q}_{c,TS}$ TS4 (W)	$\dot{Q}_{c,TC}$ (W)	$\dot{Q}_{c,DC}$ (W)	$\dot{Q}_{c,T}$ (W)	$\dot{Q}_{c,T}/\dot{Q}$ (-)	$\Delta T_{ln,TS}$ TS2 (°C)	$\Delta T_{ln,TS}$ TS3 (°C)	$\Delta T_{ln,TS}$ TS4 (°C)
980.871	553.783	340.576	1875.230	678.608	2553.838	0.8337	27.634	26.545	26.598
982.783	512.182	341.257	1836.222	679.586	2515.807	0.8212	27.534	26.395	26.498
984.696	555.943	341.904	1882.544	681.709	2564.253	0.8352	27.734	26.645	26.498
986.449	556.933	342.513	1885.895	696.901	2582.797	0.8433	27.734	26.645	26.698
1536.617	980.060	808.750	3325.427	1507.968	4833.395	0.8469	37.871	35.438	34.841
1531.639	976.885	806.131	3314.655	1548.342	4862.996	0.8512	37.871	35.538	34.741
1532.634	1020.021	806.617	3359.273	1530.475	4889.748	0.8550	37.972	35.486	33.341
1536.617	980.060	808.750	3325.427	1508.567	4833.994	0.8465	37.871	35.438	34.541

(TS2=top test section, TS3=middle test section, TS4=bottom test section)

Table A10.5. Heat transfer results for test run number 2.

$\dot{Q}_{c,TS}$ TS2 (W)	$\dot{Q}_{c,TS}$ TS3 (W)	$\dot{Q}_{c,TS}$ TS4 (W)	$\dot{Q}_{c,TC}$ (W)	$\dot{Q}_{c,DC}$ (W)	$\dot{Q}_{c,T}$ (W)	$\dot{Q}_{c,T}/\dot{Q}$ (-)	$\Delta T_{ln,TS}$ TS2 (°C)	$\Delta T_{ln,TS}$ TS3 (°C)	$\Delta T_{ln,TS}$ TS4 (°C)
1019.492	551.580	296.819	1867.891	779.600	2647.492	0.8525	27.583	26.445	26.648
1020.157	509.483	297.027	1826.667	779.098	2605.765	0.8396	27.182	26.195	26.348
1018.877	508.843	339.033	1866.753	759.385	2626.138	0.8471	27.583	26.395	26.498
978.336	552.353	297.235	1827.924	778.325	2606.249	0.8396	27.534	26.645	26.848
1612.234	974.098	719.226	3305.558	1568.488	4874.046	0.8547	37.768	35.438	34.743
1567.763	972.874	760.576	3301.213	1523.914	4825.127	0.8452	38.020	35.538	34.992
1566.740	972.240	717.854	3256.834	1565.981	4822.816	0.8463	37.620	34.837	34.543
1564.770	971.016	759.123	3294.909	1579.717	4874.627	0.8574	37.920	35.037	34.392

(TS2=top test section, TS3=middle test section, TS4=bottom test section)

Table A10.6. Heat transfer results for test run number 3.

$\dot{Q}_{c,TS}$ TS2 (W)	$\dot{Q}_{c,TS}$ TS3 (W)	$\dot{Q}_{c,TS}$ TS4 (W)	$\dot{Q}_{c,TC}$ (W)	$\dot{Q}_{c,DC}$ (W)	$\dot{Q}_{c,T}$ (W)	$\dot{Q}_{c,T}/\dot{Q}$ (-)	$\Delta T_{ln,TS}$ TS2 (°C)	$\Delta T_{ln,TS}$ TS3 (°C)	$\Delta T_{ln,TS}$ TS4 (°C)
1016.017	507.417	338.083	1861.517	699.051	2560.568	0.8288	28.183	27.096	27.198
1014.188	506.503	337.474	1858.166	719.060	2577.226	0.8348	28.483	27.296	27.498
1015.518	549.432	295.663	1860.613	700.265	2560.878	0.8301	28.483	27.245	27.349
973.157	507.168	295.677	1776.002	699.780	2475.782	0.8028	28.234	27.096	27.249
1558.311	1009.047	755.949	3323.307	1576.928	4900.235	0.8614	38.220	35.486	34.992
1559.334	967.638	798.506	3325.477	1558.234	4883.712	0.8572	38.320	36.038	35.241
1558.385	*1009.093*	*713.984*	*3281.463*	*1542.287*	*4823.750*	*0.8448*	38.320	35.587	35.043
1559.408	967.682	756.514	3283.604	1500.638	4784.243	0.8362	38.120	35.438	34.992

(TS2=top test section, TS3=middle test section, TS4=bottom test section)

A10.3 Calculated Mean Experimental Heat Transfer Coefficients

Table A10.7. Heat transfer coefficients for test run number 1.

$\overline{U}_{i,TS}$ TS2 ($W/m^2\,°C$)	$\overline{U}_{i,TS}$ TS3 ($W/m^2\,°C$)	$\overline{U}_{i,TS}$ TS4 ($W/m^2\,°C$)	$\overline{\alpha}_{c,TS}$ TS2 ($W/m^2\,°C$)	$\overline{\alpha}_{c,TS}$ TS3 ($W/m^2\,°C$)	$\overline{\alpha}_{c,TS}$ TS4 ($W/m^2\,°C$)	$\overline{\alpha}_{w,TS}$ TS2 ($W/m^2\,°C$)	$\overline{\alpha}_{w,TS}$ TS3 ($W/m^2\,°C$)	$\overline{\alpha}_{w,TS}$ TS4 ($W/m^2\,°C$)	$\overline{\alpha}_{cs,i,TS}$ TS2 ($W/m^2\,°C$)	$\overline{\alpha}_{cs,i,TS}$ TS3 ($W/m^2\,°C$)	$\overline{\alpha}_{cs,i,TS}$ TS4 ($W/m^2\,°C$)
499.654	293.673	180.247	11088.65	11275.01	11379.19	84748.9	84768.9	84802.2	516.698	299.396	180.566
502.447	273.147	181.288	11105.95	11292.60	11388.94	84748.9	84768.9	84802.2	519.663	278.085	181.612
499.793	293.712	181.633	11123.23	11310.18	11414.68	84748.9	84768.9	84802.2	516.800	299.421	181.957
500.683	294.235	180.593	11139.08	11326.28	11430.93	84748.9	84768.9	84802.2	517.730	299.957	180.914
571.156	389.306	326.754	11512.38	11795.01	11972.30	84884.4	84917.8	84986.7	592.804	399.036	327.805
569.306	386.952	326.634	11482.54	11764.43	11941.27	84884.4	84920.0	84986.7	590.861	396.585	327.683
568.175	404.621	340.558	11488.51	11770.55	11955.11	84884.4	84920.0	84986.7	589.632	415.161	341.699
571.156	389.306	329.593	11512.38	11795.01	11972.30	84884.4	84920.0	84986.7	592.804	399.036	330.662

(TS2=top test section, TS3=middle test section, TS4=bottom test section)

Table A10.8. Heat transfer coefficients for test run number 2.

$\overline{U}_{i,TS}$ TS2 (W/m²°C)	$\overline{U}_{i,TS}$ TS3 (W/m²°C)	$\overline{U}_{i,TS}$ TS4 (W/m²°C)	$\overline{\alpha}_{c,TS}$ TS2 (W/m²°C)	$\overline{\alpha}_{c,TS}$ TS3 (W/m²°C)	$\overline{\alpha}_{c,TS}$ TS4 (W/m²°C)	$\overline{\alpha}_{w,TS}$ TS2 (W/m²°C)	$\overline{\alpha}_{w,TS}$ TS3 (W/m²°C)	$\overline{\alpha}_{w,TS}$ TS4 (W/m²°C)	$\overline{\alpha}_{cs,i,TS}$ TS2 (W/m²°C)	$\overline{\alpha}_{cs,i,TS}$ TS3 (W/m²°C)	$\overline{\alpha}_{cs,i,TS}$ TS4 (W/m²°C)
520.296	293.611	156.791	11087.99	11281.34	11384.88	84760.0	84777.8	84808.9	538.805	299.329	157.033
528.302	273.783	158.688	11093.77	11287.22	11382.88	84757.8	84775.6	84808.9	547.386	278.746	158.935
519.982	271.367	180.107	11074.09	11267.45	11363.07	84757.8	84775.6	84806.7	538.489	276.249	180.426
500.174	291.815	155.841	11091.43	11277.09	11380.87	84755.6	84775.6	84806.7	517.250	297.464	156.080
600.903	386.937	291.406	11631.08	11924.19	12098.25	84926.7	84977.8	85033.3	624.695	396.457	292.241
580.457	385.364	305.966	11618.96	11904.14	12078.14	84926.7	84975.6	85033.3	602.648	394.819	306.886
586.251	392.853	292.535	11612.90	11897.94	12071.84	84924.4	84975.6	85031.1	608.906	402.689	293.376
580.878	390.118	310.710	11592.99	11877.90	12051.74	84924.4	84975.6	85031.1	603.145	399.830	311.659

(TS2=top test section, TS3=middle test section, TS4=bottom test section)

Table A10.9. Heat transfer coefficients for test run number 3.

$\overline{U}_{i,TS}$ TS2 $(W/m^2 °C)$	$\overline{U}_{i,TS}$ TS3 $(W/m^2 °C)$	$\overline{U}_{i,TS}$ TS4 $(W/m^2 °C)$	$\overline{\alpha}_{c,TS}$ TS2 $(W/m^2 °C)$	$\overline{\alpha}_{c,TS}$ TS3 $(W/m^2 °C)$	$\overline{\alpha}_{c,TS}$ TS4 $(W/m^2 °C)$	$\overline{\alpha}_{w,TS}$ TS2 $(W/m^2 °C)$	$\overline{\alpha}_{w,TS}$ TS3 $(W/m^2 °C)$	$\overline{\alpha}_{w,TS}$ TS4 $(W/m^2 °C)$	$\overline{\alpha}_{cs,i,TS}$ TS2 $(W/m^2 °C)$	$\overline{\alpha}_{cs,i,TS}$ TS3 $(W/m^2 °C)$	$\overline{\alpha}_{cs,i,TS}$ TS4 $(W/m^2 °C)$
507.477	263.614	174.980	11083.30	11275.79	11370.98	84766.7	84786.7	84817.8	525.075	268.216	175.281
501.225	261.211	172.759	11067.34	11259.55	11354.60	84766.7	84786.7	84817.8	518.407	265.734	173.053
501.882	283.878	152.183	11078.95	11271.36	11374.41	84766.7	84786.7	84817.8	519.094	289.223	152.411
485.184	263.485	152.749	11087.02	11271.36	11366.51	84766.7	84786.7	84817.8	501.241	268.083	152.978
573.936	400.267	304.104	11505.42	11790.39	11971.76	84917.8	84962.2	85020.0	595.810	410.563	305.013
572.813	377.969	318.953	11511.46	11796.58	11970.53	84915.6	84962.2	85020.0	594.589	387.133	319.953
572.464	399.161	286.806	11497.63	11782.77	11964.25	84915.6	84960.0	85015.6	594.237	409.405	287.614
575.848	384.389	304.331	11503.66	11788.96	11963.02	84913.3	84960.0	85015.6	597.873	393.876	305.242

(TS2=top test section, TS3=middle test section, TS4=bottom test section)

A10.4 Mass Balance Calculations across Test and Dump Condensers

Table A10.10. Material flows for test run number 1.

							TASC Predictions		
$\dot{M}_{v,in,TC}$ (kg/s)	$\tilde{y}_{P,in,TC}$ (moles/mole)	$\dot{M}_{f,out,DC}$ (kg/s)	$\tilde{x}_{P,out,DC}$ (moles/mole)	$\dot{M}_{f,out,TC}$ (kg/s)	$\tilde{x}_{P,out,TC}$ (moles/mole)	$\tilde{y}^{*}_{P,out,TC}$ (moles/mole)	ε (-)	$\tilde{x}_{P,out,DC}$ (moles/mole)	$T_{v,out,TC}$ (°C)
0.00711	0.6886	0.00167	0.8473	0.00545	0.6345	0.9341	0.6463	0.9234	45.20
0.00700	0.6895	0.00167	0.8473	0.00533	0.6345	0.9341	0.6448	0.9232	45.20
0.00713	0.6886	0.00167	0.8473	0.00546	0.6345	0.9340	0.6464	0.9233	45.30
0.00719	0.6894	0.00171	0.8473	0.00548	0.6345	0.9340	0.6453	0.9233	45.30
0.01362	0.6496	0.00378	0.8184	0.00984	0.5765	0.9038	0.6637	0.8872	62.30
0.01368	0.6512	0.00388	0.8184	0.00980	0.5765	0.9038	0.6619	0.8872	62.40
0.01369	0.6503	0.00384	0.8184	0.00985	0.5765	0.9037	0.6631	0.8875	62.40
0.01360	0.6495	0.00377	0.8184	0.00983	0.5765	0.9039	0.6636	0.8880	62.10

Table A10.11. Material flows for test run number 2.

							TASC Predictions		
$\dot{M}_{v,in,TC}$ (kg/s)	$\tilde{y}_{P,in,TC}$ (moles/mole)	$\dot{M}_{f,out,DC}$ (kg/s)	$\tilde{x}_{P,out,DC}$ (moles/mole)	$\dot{M}_{f,out,TC}$ (kg/s)	$\tilde{x}_{P,out,TC}$ (moles/mole)	$\tilde{y}^{*}_{P,out,TC}$ (moles/mole)	ε (-)	$\tilde{x}_{P,out,DC}$ (moles/mole)	$T_{v,out,TC}$ (°C)
0.00734	0.6997	0.00192	0.8462	0.00542	0.6422	0.9355	0.6210	0.9237	46.30
0.00722	0.7007	0.00192	0.8462	0.00530	0.6422	0.9356	0.6192	0.9235	46.20
0.00728	0.6987	0.00187	0.8462	0.00541	0.6422	0.9356	0.6225	0.9240	46.20
0.00722	0.7005	0.00191	0.8462	0.00531	0.6422	0.9355	0.6197	0.9235	46.30
0.01385	0.6760	0.00412	0.8125	0.00974	0.6123	0.9138	0.5742	0.8946	65.40
0.01373	0.6748	0.00400	0.8125	0.00973	0.6123	0.9138	0.5764	0.8948	65.40
0.01368	0.6764	0.00409	0.8125	0.00959	0.6123	0.9140	0.5730	0.8949	65.10
0.01381	0.6764	0.00413	0.8125	0.00968	0.6123	0.9138	0.5734	0.8948	65.30

Table A10.12. Material flows for test run number 3.

							TASC Predictions		
$\dot{M}_{v,in,TC}$ (kg/s)	$\tilde{y}_{P,in,TC}$ (moles/mole)	$\dot{M}_{f,out,DC}$ (kg/s)	$\tilde{x}_{P,out,DC}$ (moles/mole)	$\dot{M}_{f,out,TC}$ (kg/s)	$\tilde{x}_{P,out,TC}$ (moles/mole)	$\tilde{y}^{*}_{P,out,TC}$ (moles/mole)	ε (-)	$\tilde{x}_{P,out,DC}$ (moles/mole)	$T_{v,out,TC}$ (°C)
0.00709	0.7230	0.00172	0.8379	0.00538	0.6833	0.9454	0.5164	0.9341	46.80
0.00714	0.7238	0.00176	0.8379	0.00537	0.6833	0.9453	0.5148	0.9332	47.10
0.00709	0.7230	0.00172	0.8379	0.00538	0.6833	0.9453	0.5165	0.9335	47.00
0.00685	0.7244	0.00172	0.8379	0.00513	0.6833	0.9453	0.5134	0.9335	47.00
0.01380	0.6867	0.00406	0.8108	0.00974	0.6302	0.9198	0.5321	0.9002	65.10
0.01378	0.6861	0.00400	0.8108	0.00978	0.6302	0.9200	0.5329	0.9008	64.80
0.01358	0.6862	0.00395	0.8108	0.00962	0.6302	0.9200	0.5327	0.9009	64.80
0.01348	0.6851	0.00384	0.8108	0.00964	0.6302	0.9202	0.5346	0.9011	64.50

A10.5 Analysis over full Test Condenser Length

Table A10.13. Full length analysis for test run number 1.

$\dot{Q}_{c,TC}$ (W)	$\Delta T_{ln,TC}$ (°C)	$\overline{U}_{i,TC}$ (W/m² °C)	$\overline{\alpha}_{c,TC}$ (W/m² °C)	$\overline{\alpha}_{w,TC}$ (W/m² °C)	$\overline{\alpha}_{cs,i,TC}$ (W/m² °C)	*Ref* (-)	*Prf* (-)	$\overline{\alpha}_{f,i,TC}$ By HTFS (W/m² °C)	Corrected $\overline{\alpha}_{f,i,TC}$ (W/m² °C)	$\overline{\alpha}_{v,eff,i,TC}$ (W/m² °C)
1875.230	29.445	298.83	11266.96	84773.3	304.76	608.297	6.0417	865.048	932.175	452.791
1836.222	29.394	293.12	11280.50	84773.3	298.82	594.582	6.0452	869.188	935.399	439.081
1882.544	29.545	298.98	11302.10	84773.3	304.90	609.504	6.0435	864.538	931.733	453.204
1885.895	29.545	299.51	11318.20	84773.3	305.44	612.094	6.0400	863.980	931.364	454.500
3325.427	38.691	403.29	11818.28	84929.6	413.72	1194.143	5.9628	743.552	846.436	809.277
3314.655	38.691	401.98	11787.64	84930.4	412.37	1188.819	5.9643	744.191	846.753	803.836
3359.273	38.741	406.87	11797.64	84930.4	417.51	1185.015	5.9845	743.470	845.639	824.675
3325.427	38.640	403.82	11818.28	84930.4	414.28	1190.609	5.9674	743.753	846.392	811.459

Table A10.14. Full length analysis for test run number 2.

$\dot{Q}_{c,TC}$ (W)	$\Delta T_{\ln,TC}$ (°C)	$\overline{U}_{i,TC}$ (W/m^2 °C)	$\overline{\alpha}_{c,TC}$ (W/m^2 °C)	$\overline{\alpha}_{w,TC}$ (W/m^2 °C)	$\overline{\alpha}_{cs,i,TC}$ (W/m^2 °C)	Ref (-)	Prf (-)	$\overline{\alpha}_{f,i,TC}$ By HTFS (W/m^2 °C)	Corrected $\overline{\alpha}_{f,i,TC}$ (W/m^2 °C)	$\overline{\alpha}_{v,eff,i,TC}$ (W/m^2 °C)
1867.891	29.494	297.16	11265.33	84782.2	303.03	611.455	5.9952	868.527	936.208	448.048
1826.667	29.242	293.11	11267.20	84780.7	298.82	595.834	6.0021	873.028	939.645	438.158
1866.753	29.544	296.49	11251.45	84780.0	302.33	608.479	6.0011	869.027	936.479	446.466
1827.924	29.493	290.82	11265.06	84779.3	296.43	598.432	5.9960	872.635	939.457	433.092
3305.558	38.895	398.78	11931.81	84979.3	408.90	1234.771	5.7746	753.743	861.214	778.543
3301.213	39.044	396.74	11919.37	84978.5	406.75	1235.287	5.7717	753.853	861.380	770.677
3256.834	38.694	394.94	11909.35	84977.0	404.87	1214.008	5.7795	756.259	862.460	763.093
3294.909	38.944	397.00	11893.12	84977.0	407.05	1223.466	5.7824	754.782	861.516	771.616

Table A10.15. Full length analysis for test run number 3.

$\dot{Q}_{c,TC}$ (W)	$\Delta T_{ln,TC}$ (°C)	$\overline{U}_{i,TC}$ (W/m^2 °C)	$\overline{\alpha}_{c,TC}$ (W/m^2 °C)	$\overline{\alpha}_{w,TC}$ (W/m^2 °C)	$\overline{\alpha}_{cs,i,TC}$ (W/m^2 °C)	*Ref* (-)	*Prf* (-)	$\overline{\alpha}_{f,i,TC}$ By HTFS (W/m^2 °C)	Corrected $\overline{\alpha}_{f,i,TC}$ (W/m^2 °C)	$\overline{\alpha}_{v,eff,i,TC}$ (W/m^2 °C)
1861.517	29.897	292.16	11259.86	84790.4	297.83	630.792	5.7858	884.196	954.872	432.827
1858.166	30.098	289.68	11243.64	84790.4	295.26	631.549	5.7810	884.326	955.081	427.393
1860.613	30.098	290.07	11255.44	84790.4	295.66	631.605	5.7826	884.187	954.936	428.242
1776.002	29.947	278.28	11255.44	84790.4	283.42	601.815	5.7858	893.489	962.222	401.751
3323.307	39.244	397.36	11809.41	84966.7	407.49	1246.428	5.7113	758.339	867.382	768.535
3325.477	39.191	398.15	11815.61	84965.9	408.31	1252.069	5.7085	757.761	867.164	771.655
3281.463	39.293	391.86	11798.00	84963.7	401.72	1229.563	5.7140	760.452	868.468	747.463
3283.604	39.093	394.12	11804.19	84963.0	404.09	1230.608	5.7154	760.219	868.285	755.860

A10.6 Measured and Calculated Gas-side Heat Transfer Coefficients

Table A10.16. Mean gas-side heat transfer coefficients for test run number 1.

Measured	Predicted dry-gas values		Using dry-gas values		Using dry-gas values with Silver's method		Using measured value with Silver's method	
$\overline{\alpha}_{v,l,TC}$	$\overline{\alpha}_{v,l,TC}$ Without θ	$\overline{\alpha}_{v,l,TC}$ With θ	$\overline{\alpha}_{v,eff,l,TC}$ Without θ	$\overline{\alpha}_{v,eff,l,TC}$ With θ	$\overline{\alpha}_{v,eff,l,TC}$ Without θ	$\overline{\alpha}_{v,eff,l,TC}$ With θ	$\overline{\alpha}_{v,eff,l,TC}$ Without θ	$\overline{\alpha}_{v,eff,l,TC}$ With θ
(W/m² °C)	*(W/m² °C)*	*(W/m² °C)*	*(W/m² °C)*	*(W/m² °C)*	*(W/m² °C)*	*(W/m² °C)*	*(W/m² °C)*	*(W/m² °C)*
11.374	19.552	4.481	778.353	178.389	233.038	168.587	135.565	76.228
11.120	19.350	4.521	764.052	178.502	240.647	174.763	138.294	77.724
11.377	19.605	4.491	780.953	178.918	233.570	168.959	135.546	76.092
11.507	19.766	4.569	780.749	180.459	234.839	170.178	136.707	77.143
24.193	35.535	7.600	1188.644	254.218	331.067	219.900	225.404	121.553
24.338	35.805	7.813	1182.557	258.029	326.731	214.987	222.093	117.909
24.586	35.748	7.709	1199.070	258.591	325.297	216.507	223.727	121.840
23.779	35.459	7.574	1210.029	258.466	328.920	218.407	220.577	117.684

Table A10.17. Mean gas-side heat transfer coefficients for test run number 2.

Measured	Predicted dry-gas values		Using dry-gas values		Using dry-gas values with Silver's method		Using measured value with Silver's method	
$\overline{\alpha}_{v,i,TC}$	$\overline{\alpha}_{v,i,TC}$ Without θ	$\overline{\alpha}_{v,i,TC}$ With θ	$\overline{\alpha}_{v,eff,i,TC}$ Without θ	$\overline{\alpha}_{v,eff,i,TC}$ With θ	$\overline{\alpha}_{v,eff,i,TC}$ Without θ	$\overline{\alpha}_{v,eff,i,TC}$ With θ	$\overline{\alpha}_{v,eff,i,TC}$ Without θ	$\overline{\alpha}_{v,eff,i,TC}$ With θ
(W/m^2 °C)	*(W/m^2 °C)*	*(W/m^2 °C)*	*(W/m^2 °C)*	*(W/m^2 °C)*	*(W/m^2 °C)*	*(W/m^2 °C)*	*(W/m^2 °C)*	*(W/m^2 °C)*
12.147	20.443	5.067	754.016	186.878	245.035	177.767	145.603	83.366
12.393	20.213	5.110	714.650	180.678	242.728	176.834	148.819	87.424
12.165	20.236	4.956	742.665	181.871	242.265	175.315	145.642	83.596
12.039	20.218	5.094	727.296	183.262	242.913	174.592	144.650	81.559
26.063	36.779	8.382	1098.635	250.368	331.189	217.283	234.695	127.577
25.078	36.389	8.151	1118.263	250.483	334.183	221.356	230.310	124.680
25.209	36.423	8.385	1102.543	253.830	334.659	220.149	231.624	124.440
25.440	36.710	8.427	1113.468	255.598	330.213	217.057	228.832	122.900

Table A10.18. Mean gas-side heat transfer coefficients for test run number 3.

Measured	Predicted dry-gas values		Using dry-gas values		Using dry-gas values with Silver's method		Using measured value with Silver's method	
$\overline{\alpha}_{v,i,TC}$	$\overline{\alpha}_{v,i,TC}$ Without θ	$\overline{\alpha}_{v,i,TC}$ With θ	$\overline{\alpha}_{v,eff,i,TC}$ Without θ	$\overline{\alpha}_{v,eff,i,TC}$ With θ	$\overline{\alpha}_{v,eff,i,TC}$ Without θ	$\overline{\alpha}_{v,eff,i,TC}$ With θ	$\overline{\alpha}_{v,eff,i,TC}$ Without θ	$\overline{\alpha}_{v,eff,i,TC}$ With θ
$(W/m^2 °C)$	$(W/m^2 °C)$	$(W/m^2 °C)$	$(W/m^2 °C)$	$(W/m^2 °C)$	$(W/m^2 °C)$	$(W/m^2 °C)$	$(W/m^2 °C)$	$(W/m^2 °C)$
10.453	19.690	4.638	815.319	192.067	239.184	169.395	126.975	64.397
10.062	19.857	4.746	843.456	201.608	242.553	172.328	122.906	60.579
9.969	19.699	4.642	846.256	199.401	240.399	170.264	121.652	59.496
9.706	19.255	4.722	796.976	195.452	244.310	174.556	123.155	61.198
25.416	36.569	8.255	1105.786	249.619	330.253	216.130	229.530	122.699
24.155	36.427	8.131	1163.678	259.740	328.299	217.265	217.701	114.644
23.767	36.008	8.095	1132.414	254.582	331.133	216.472	218.569	112.502
23.714	35.636	7.859	1135.877	250.488	327.800	216.271	218.132	114.593

A10.7 Vapour Flooding Velocities in the Test Condenser

Table A10.19. Flooding calculations for test run number 1.

			Predicted Flooding Velocity	
		Actual Vapour Velocity	Conservative	Non-conservative
$\dot{M}_{v,in,TC}$	Re_V	$\dot{u}_{v,in,TC}$	$\dot{v}_v$	
(kg/s)	*(-)*	*(m/s)*	*(m/s)*	
0.00711	26749.8	1.5337	2.0152	3.2243
0.00700	26330.3	1.5115	2.0267	3.2428
0.00713	26817.0	1.5331	2.0110	3.2176
0.00719	27014.9	1.5434	2.0084	3.2135
0.01362	48965.8	1.9115	1.3658	2.1853
0.01368	49182.7	1.9159	1.3656	2.1849
0.01369	49184.0	1.9131	1.3655	2.1847
0.01360	48891.6	1.9148	1.3692	2.1907

Table A10.20. Flooding calculations for test run number 2.

			Predicted Flooding Velocity	
		Actual Vapour Velocity	Conservative	Non-conservative
$\dot{M}_{v,in,TC}$	Re_V	$\dot{u}_{v,in,TC}$	$\dot{v}_v$	
(kg/s)	*(-)*	*(m/s)*	*(m/s)*	
0.00734	27514.3	1.5291	1.9854	3.1767
0.00722	27063.5	1.5101	2.0012	3.2020
0.00728	27272.8	1.5181	1.9892	3.1827
0.00722	27074.8	1.5063	1.9961	3.1938
0.01385	49221.8	1.7351	1.3004	2.0806
0.01373	48767.7	1.7175	1.2995	2.0792
0.01368	48662.2	1.7283	1.3108	2.0973
0.01381	49071.4	1.7341	1.3049	2.0878

Table A10.21. Flooding calculations for test run number 3.

			Predicted Flooding Velocity	
		Actual Vapour Velocity	Conservative	Non-conservative
$\dot{M}_{v,in,TC}$	Re_V	$\dot{u}_{v,in,TC}$	$\dot{v}_v$	
(kg/s)	*(-)*	*(m/s)*	*(m/s)*	
0.00709	26453.5	1.3952	1.9514	3.1223
0.00714	26601.8	1.3958	1.9454	3.1127
0.00709	26447.8	1.3898	1.9470	3.1152
0.00685	25534.2	1.3424	1.9683	3.1493
0.01380	48995.1	1.7143	1.3026	2.0841
0.01378	48959.1	1.7232	1.3056	2.0890
0.01358	48233.4	1.6978	1.3109	2.0975
0.01348	47921.8	1.6986	1.3159	2.1054